UNIVERSIDAD DE CÓRDOBA

Eidgenössische Technische Hochschule Zürich
Swiss Federal Institute of Technology Zurich

TESIS DOCTORAL

PROGRAMA DE DOCTORADO DE QUÍMICA FINA

Determinación de vapores en tiempo real mediante ionización secundaria por electrospray (SESI) acoplada a espectrometría de masas: estudios mecanísticos y aplicaciones bioquímicas

Real-time determination of vapors by means of secondary electrospray ionization (SESI) coupled to mass spectrometry: mechanistic studies and biochemical applications

ALBERTO TEJERO RIOSERAS

Directores: Pablo Martínez-Lozano Sinues y Diego García Gómez

Tutora: Soledad Rubio Bravo

En Córdoba, a 11 de diciembre de 2018

TITULO: *Real-time determination of vapors by means of secondary electrospray ionization (SESI) coupled to mass spectrometry: mechanistic studies and biochemical applications*

AUTOR: *Alberto Tejero Rioseras*

© Edita: UCOPress. 2019
Campus de Rabanales
Ctra. Nacional IV, Km. 396 A
14071 Córdoba

https://www.uco.es/ucopress/index.php/es/
ucopress@uco.es

Tesis doctoral

Determinación de vapores en tiempo real mediante ionización secundaria por electrospray (SESI) acoplada a espectrometría de masas: estudios mecanísticos y aplicaciones bioquímicas

Trabajo presentado para obtener el grado de Doctor por:

Alberto Tejero Rioseras,

que lo firma en Córdoba, a 11 de diciembre de 2018

Y con el VºBº de:

el Director,
Pablo Martínez-Lozano Sinues,
Assistant Professor at the Department
of Biomedical Engineering,
University of Basel

el Codirector,
Diego García Gómez,
Profesor Ayudante Doctor
en el Dpto. de Química Analítica
de la Universidad de Salamanca

y la Tutora,
Soledad Rubio Bravo
Catedrática del Departamento
de Química Analítica
de la Universidad de Córdoba

Mediante la defensa de esta memoria se opta a la obtención de "**Doctorado Internacional**" dado que se reúnen los siguientes requisitos:

1) El doctorando ha realizado una estancia de 2 años en la *Eidgenössische Technische Hochschule Zürich* (ETH Zürich) en Suiza donde se ha realizado la formación participando en cursos y conferencias.
2) La Tesis doctoral está escrita en inglés, una de las lenguas oficiales de la Unión Europea y distinta a cualquiera de las lenguas oficiales en España.
3) Cuenta con informes favorables de dos doctores pertenecientes a instituciones de enseñanza superior o institutos de investigación de países europeos distintos a España.
4) Uno de los miembros del tribunal de evaluación de la Tesis pertenece a un centro de enseñanza superior de otro país europeo.

Título: Determinación de vapores en tiempo real mediante ionización secundaria por electrospray (SESI) acoplada a espectrometría de masas: estudios mecanísticos y aplicaciones bioquímicas

Autor: Alberto Tejero Rioseras

Ingeniero Industrial. Universidad de Valladolid
Máster de instrumentación en física. Universidad de Valladolid

Este trabajo de tesis ha dado lugar a tres publicaciones científicas:

- A. Tejero Rioseras et al. (2017), Secondary electrospray ionization proceeds via gas-phase chemical ionization. *Anal. Methods*, 9 (34), 5052–5057.
- A. Tejero Rioseras et al. (2017), Comprehensive Real-Time Analysis of the Yeast Volatilome. *Sci. Rep.*, 7 (1) 14236.
- A. Tejero Rioseras et al. (2018), Real-Time Monitoring of Tricarboxylic Acid Metabolites in Exhaled Breath. *Anal. Chem.*, 90 (11) 6453–6460.

Se ha realizado la siguiente comunicación, presentada en un congreso nacional:

Poster: "In-vivo mass spectrometric analysis of yeast growth metabolism"; Swiss Chemical Society Fall Meeting 2016, University of Zurich. September 15th.

A mis Padres,

sin su apoyo no hubiera sido posible.

TÍTULO DE LA TESIS: DETERMINACIÓN DE VAPORES EN TIEMPO REAL MEDIANTE IONIZACIÓN SECUNDARIA POR ELECTROSPRAY (SESI) ACOPLADA A ESPECTROMETRÍA DE MASAS: ESTUDIOS MECANÍSTICOS Y APLICACIONES BIOQUÍMICAS

DOCTORANDO/A: ALBERTO TEJERO RIOSERAS

INFORME RAZONADO DEL/DE LOS DIRECTOR/ES DE LA TESIS

(se hará mención a la evolución y desarrollo de la tesis, así como a trabajos y publicaciones derivados de la misma).

En este Tesis Doctoral se ha evaluado la capacidad de la ionización secundaria por Electrospray (SESI) acoplada a espectrometría de masas de alta resolución para ser aplicada en novedosos estudios dentro del campo de la bioquímica. Asimismo, se han abordado estudios mecanísticos que han permitido ahondar en el proceso mediante el cual se ionizan los vapores en SESI.

En primer lugar, se afrontaron los estudios mecanísticos destinados a dilucidar cuál de los dos posibles procesos que se han propuesto en el pasado tiene lugar, al menos de forma mayoritaria, cuando se produce la ionización de vapores en SESI. Dichos estudios, basados en la utilización de disolventes deuterados, han permitido dar una clara respuesta a dicha pregunta científica.

En una segunda etapa, se exploró la utilidad de SESI en el campo de la microbiología como herramienta para caracterizar los volátiles emitidos por *S. cerevisiae*. Los resultados obtenidos, tanto con cepas naturales como mutantes, demostraron fehacientemente la capacidad de SESI como alternativa viable para el estudio de los procesos en los que están envueltos estos microorganismos.

Finalmente, se exploró SESI como técnica para la explotación del análisis de aliento en el estudio metabólico del ciclo de los ácidos tricarboxílicos. Este estudio puso de manifiesto la gran capacidad de SESI para analizar en tiempo real diversos metabolitos presentes en el torrente sanguíneo, que alcanzan el aliento en concentraciones de hasta partes por cuatrillón (ppq), y las posibles respuestas a diversas preguntas bioquímicas que SESI puede ofrecer.

Los avances desarrollados en el curso de esta Tesis han propiciado un conocimiento más profundo de la técnica estudiada y su difusión en diferentes áreas científicas.

Adicionalmente, los resultados de las investigaciones realizadas se han materializado en 3 artículos científicos, publicados en revistas científicas indexadas. Los resultados obtenidos también han sido presentados por el doctorando como contribución en formato póster a un congreso nacional.

Por lo tanto, en base a la originalidad de las investigaciones desarrolladas y expuestas en esta Memoria así como a la amplia formación científica adquirida por el doctorando Alberto Tejero Rioseras, autorizamos la presentación de esta Tesis Doctoral.

Córdoba, a 11 de diciembre de 2018

Firma de los directores:

Fdo.: Pablo Martínez-Lozano Sinues

Fdo.: Diego García Gómez

Acknowledgements

My deepest gratitude is to my supervisor Prof. Dr. Pablo Martinez-Lozano Sinues. This PhD project would not have been possible without his guidance, support and infinite patient teaching me, from the very basics, everything about SESI, MS and writing skills.

I also would like to thank my supervisor Prof. Dr. Diego García Gómez for advice and support both personally and professionally. When I started this project, he showed me how to use the scientific instruments and to set up the experiments. Close to the end, his guidance and insightful comments have helped me to improve this work.

I wish to acknowledge the help provided by Prof. Dr. Soledad Rubio tutoring this PhD project at the university of Córdoba.

I owe my gratitude to Prof. Dr. Renato Zenobi for hosting me and letting me use the old LTQ Orbitrap for my experiments. Especially during our group meetings, I got to understand research strategies and how to clearly express scientific ideas. Thanks to all members of Zenobi's group whose lectures helped me to think more like a chemist, and thanks for the great atmosphere during lunch time and other activities.

I am also in debt to all my collaborators regarding my three published papers, distinguished scientists like Prof. Dr. Alfredo Ibañez or prominent scientists like Martin Gaugg, for sharing their time discussing about our scientific results.

I gratefully thank Dr Juan Zhang (Novartis AG) for the donation of the LTQ Orbitrap instrument, and I thank the EU for funding the ACID project (609691) through the European Community's Seventh Framework Programme (FP7-2013-IAPP).

I appreciate the great work done by Christoph Bärtschi and Christian Marro, from the ETHZ mechanical shop, manufacturing the LFSESI and all the modifications required to set up new experiments. I thank Brigitte Bräm for being always friendly and cheery and for taking care of all the administrative work.

Table of contents

Resumen

La Tesis que se presenta se centra en la aplicación de la técnica de ionización secundaria por electrospray (SESI), acoplada a un espectrómetro de masas de alta resolución. El principal objetivo puede definirse como la monitorización de variaciones en las concentraciones de ciertos metabolitos de interés de forma *on-line* y no invasiva y sus aplicaciones en el campo de la bioquímica.

En primer lugar, se llevaron a cabo estudios sobre el mecanismo por el cual los compuestos volátiles se ionizan en SESI al interactuar con el electrospray. Una mejor comprensión de este fenómeno permitiría una mejor optimización de los parámetros claves en SESI y una mejora sustancial en las eficiencias de ionización. Los experimentos realizados con agua pesada tanto como disolvente del electrospray como en el gas de muestra apuntan a que en la etapa final de SESI las reacciones ion-molécula en fase vapor gobiernan el mecanismo mediante el cual se ionizan los compuestos volátiles.

Seguidamente, se demostró el potencial de la técnica SESI-HRMS para medir volátiles en diferentes cepas de levadura *Saccharomyces cerevisiae* durante las fases de crecimiento exponencial y muerte. Se demostró la posibilidad de monitorizar la concentración de hasta 263 metabolitos volátiles, producidos por la levadura alimentada con glucosa marcada isotópicamente, hasta durante 48 horas. La identificación de los metabolitos según su fórmula molecular resultó en 111 metabolitos señalados como candidatos en la "*yeast metabolome database*", y otros 101 metabolitos en la "*human metabolome database*". Estos resultados demuestran como muchos metabolitos producidos por la levadura, y que pueden ser analizados mediante SESI, son aún desconocidos por la comunidad científica. Adicionalmente, repitiendo el experimento con distintas cepas mutantes de levaduras alimentadas con $^{13}C_1$-glucosa, se obtuvo información relevante para entender la cinética y rutas metabólicas involucradas en la fermentación alcohólica.

El ciclo de los ácidos tricarboxílicos (TCA) es una de las rutas metabólicas más importantes involucradas en la respiración celular de los organismos aeróbicos. TCA provee y recoge subproductos de muchas otras rutas metabólicas interconectándolas y actuando como centro de actividad del metabolismo de carbohidratos, ácidos grasos y aminoácidos. En esta tesis doctoral se ha evaluado la posibilidad de que los compuestos más volátiles del TCA puedan ser detectados en el aliento mediante SESI. Los resultados apuntan a que el

TCA podría ser convenientemente monitorizado a través de esta técnica, lo que abre nuevas oportunidades para el estudio de esta importante ruta metabólica de forma no invasiva, en vivo y a tiempo real.

Abstract

This Doctoral Thesis focuses on the application of Secondary ElectroSpray Ionization (SESI) coupled to High Resolution Mass Spectrometry (HRMS) for the online and non-invasive monitoring of fluctuations in metabolite levels of interest for biochemical applications.

Our studies started by getting insights into the mechanism by which volatiles are ionized in their interaction with plumes of electrospray solvents (i.e., SESI). This knowledge could help in the optimization of key parameters in SESI, leading to an enhancement in ionization efficiency. Our observations, using protonated water in the ESI solvent and in the carrier gas, revealed that, in the final stage of SESI, gas-phase ion–molecule reactions lead the mechanism by which electrosprays ionize vapor species.

The power of SESI-HRMS technique to measure volatiles was shown for different strains of baker's yeast during growth to starvation. It was demonstrated that the concentration profiles of 263 volatile metabolites, produced by yeast consuming labeled glucose, can be monitored for at least 48 hours. 111 of these metabolites could be matched by molecular formula in the yeast metabolome database, and 101 additional metabolites were found in the human metabolome database. These results suggest that a large number of these metabolites were not previously reported in the literature nor are their biochemical origin deciphered. Additionally, it was shown how, by replicating the experiment with different strains of yeast, useful information to understand the kinetics and pathways followed by each mutant when processing $^{13}C_1$-glucose can be obtained.

The tricarboxylic acid (TCA) cycle is one of the most important metabolic pathways for cellular respiration in aerobic organisms. It provides and collects intermediates for many other interconnecting pathways and acts as a hub connecting the metabolism of carbohydrates, fatty acids, and amino acids. In this Doctoral Thesis, we evaluated whether at least the most volatile metabolites of the TCA cycle could be detected *in vivo* and in real time in exhaled breath. The results provided the first evidence that the TCA cycle can conveniently be monitored in breath, opening new opportunities to study this important metabolic pathway, as stated previously, *in vivo* and in real time.

Aim & Content

The content of this PhD Thesis, whose aim is the chemical analysis of Volatile Organic Compounds (VOCs) by means of Mass Spectrometry (MS) Coupled to a Secondary ElectroSpray Ionization (SESI) source, is organized in three main chapters headed by an introduction and followed by a conclusion section and two annexes. The content and main aim of each of these sections is summarized below.

In the introduction chapter, the most popular applications where the study of volatiles is most frequently carried out and the analytical techniques applied for this purpose are shown. Then, a brief history of the development of mass spectrometry and its ionization methods is given. Finally, an explanation of how an electrospray works and the ionization mechanisms involved in ESI and SESI is presented.

In chapter A, the ionization mechanism by which volatiles are ionized in Secondary Electrospray Ionization is studied. The scientific community have commonly and historically accepted two possible scenarios for SESI: vapors dissolving into the electrospray charged droplet and then being re-ejected in their ionized form in the gas-phase; or primary ions, ejected from the electrospray charged droplets, interacting with the vapors in gas-phase. Several experiments were carried out with heavy water in the ESI solvent and in the carrier gas in order to elucidate this issue. It is the aim of this chapter to advance towards a better understanding of how our ionization source works, which may help to enhance the ionization efficiencies by choosing the optimum ESI solvent, temperature, etc.

In chapter B, SESI-MS is applied for the monitoring of volatile metabolites in baker's yeast fermentation during growth to starvation. Well-known end products like ethanol and acetic acid are tracked to confirm the agreement of our results with previous studies. The results reveal that 263 compounds are produced by yeast during the fermentation of labeled glucose. It is suggested that a large number of metabolites produced by yeast from glucose neither are reported in the literature nor are their biochemical origins deciphered. To show the real potential of SESI combine to a high-resolution MS, the experiments were repeated in a medium with $^{13}C_1$-glucose with two mutants of *Saccharomyces cerevisiae*: *pfk1* and *zwf1*. The PFK1 gene is involved in glycolysis, indispensable for anaerobic growth. The ZWF1 gene is involved in adaptation to oxidative stress, as it catalyzes the first step of the pentose phosphate pathway. The results show clear differences of the metabolites produced by the mutants. Additionally, thanks to high-resolution mass spectrometry, it is possible to resolve isotopic distributions useful to understand the kinetics and pathways of each mutant.

In chapter C, SESI-HRMS is applied in the field of breath analysis to assess its suitability to detect fumaric, succinic, malic, keto-glutaric, oxaloacetic and aconitic acids in breath *in vivo* and in real-time. These metabolites are intermediates of the citric acid cycle that collects intermediates for many other interconnecting pathways and acts as a hub connecting metabolism of carbohydrates, fatty acids, and amino acids. These molecules are difficult to ionize by other techniques due to their low concentration in breath. Thanks to the high resolving power of the LTQ Orbitrap, these metabolites can be unequivocally identified by its molecular formula. In order to validate the overall procedure, the reproducibility of measurements was checked to elucidate whether it is possible or not to detect differences between individuals and its variability during a day. These metabolites were identified by tandem MS by comparing their fragmentation pattern with standards. Additionally, the analysis of Exhaled Breath Condensate (EBC) by Ultra High-Performance Liquid Chromatography (UHPLC) coupled to tandem MS (MS/MS) was pursued in order to check, for these compounds, whether retention times and MS/MS spectra matched with the corresponding standards.

1. Introduction

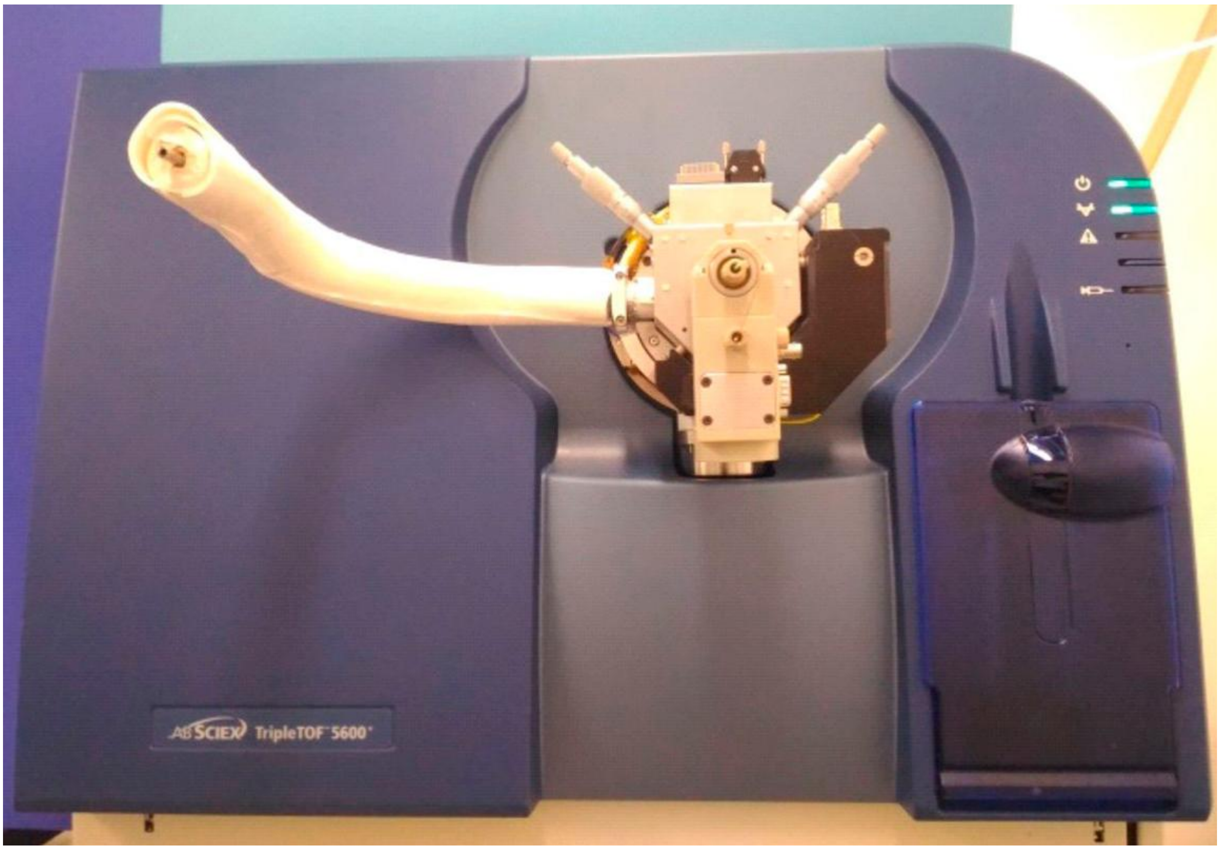

LFSESI source (SEADM®) coupled to a TripleTOF 5600 from ABSciex®

1.1. "Analytical Chemistry Instrumentation Development" project

The research studies carried out on this PhD Thesis were run at ETH Zürich (Switzerland) under the umbrella of the "Analytical Chemistry Instrumentation Development" (ACID) project. This project, led by Dr. Pablo Martínez-Lozano Sinues, was financed by the European Union through the FP7 program and its goals were as follows:

1) To develop a commercial Secondary ElectroSpray Ionization (SESI) source to be interfered to a High-Resolution Mass Spectrometer (HRMS).
2) To extend the ability of this analytical technique for measuring Volatile Organic Compounds (VOCs) into unexplored fields such as biology, pharmacy, medicine or environmental sciences.

ACID started in 2014 when engineers from "Sociedad Europea de Análisis Diferencial de Movilidad" (SEADM, España) developed a novel SESI source with an ionization efficiency ten-fold higher than previous state-of-the-art SESI sources. This ionization source was initially design for a specific mass spectrometer, the LTQ Orbitrap Classic from Thermo Fischer Scientific, and later adapted to the TripleTOF 5600 from AB Sciex.

This SESI source was, in collaboration with scientists of ETH Zürich, further applied in projects from fields as distant as chemistry, biology and medicine. These successful research projects helped getting an unparalleled insight into those fields. These studies are summarized in:

- D. García-Gómez et al. (2015), "Identification of 2-Alkenals, 4-Hydroxy-2-alkenals, and 4-Hydroxy-2,6-alkadienals in Exhaled Breath Condensate by UHPLC-HRMS and in Breath by Real-Time HRMS" *Anal. Chem.* 87, 3087–3093.
- D. García-Gómez et al. (2015), "Real-Time High-Resolution Tandem Mass Spectrometry Identifies Furan Derivatives in Exhaled Breath" *Anal. Chem.* 87, 6919–6924.
- D. García-Gómez et al. (2015), "Detection and Quantification of Benzothiazoles in Exhaled Breath and Exhaled Breath Condensate by Real-Time Secondary Electrospray Ionization–High-Resolution Mass Spectrometry and Ultra-High-Performance Liquid Chromatography" *Envi. Sci. & Tech.* 49, 12519–12524.
- L. Bregy et al. (2015), "Differentiation of oral bacteria in in vitro cultures and human saliva by secondary electrospray ionization – mass spectrometry" *Sci. Rep.* 5, 15163.

- D. García-Gómez et al. (2016), “Real-Time Quantification of Amino Acids in the Exhalome by Secondary Electrospray Ionization-Mass Spectrometry: A Proof-of-Principle Study” *Clin. Chem.* 62, 1230–1237.
- D. García-Gómez et al. (2016), “Secondary electrospray ionization coupled to high-resolution mass spectrometry reveals tryptophan pathway metabolites in exhaled human breath” *Chem. Comm.* 52, 8526–8528.
- M. Gaugg et al. (2016), “Expanding metabolite coverage of real-time breath analysis by coupling a universal secondary electrospray ionization source and high-resolution mass spectrometry – a pilot study on tobacco smokers” *J. Breath Res.*10, 016010.
- C. Barrios-Collado et al. (2016), “Capturing in Vivo Plant Metabolism by Real-Time Analysis of Low to High Molecular Weight Volatiles” *Anal. Chem.* 88, 2406-2412.
- D. García-Gómez et al. (2016), “Real-Time Chemical Analysis of E-Cigarette Aerosols By Means Of Secondary Electrospray Ionization Mass Spectrometry” *Chem. Eur. J.* 22, 2452-2457.
- A. Tejero Rioseras et al. (2017), “Secondary electrospray ionization proceeds via gas-phase chemical ionization” *Anal. Methods* 9, 5052–5057.
- A. Tejero Rioseras et al. (2017), “Comprehensive Real-Time Analysis of the Yeast Volatilome” *Sci. Rep.* 7, 14236.
- A. Tejero Rioseras et al. (2018), “Real-Time Monitoring of Tricarboxylic Acid Metabolites in Exhaled Breath” *Anal. Chem.* 90, 6453–6460.

The last three publications are the main core of this PhD Thesis. Finally, it should be highlighted that, due to its success in those fields, the new SESI source is still used by breath analysis researchers at ETH Zürich and abroad.

1.2. The importance of gas and Volatile Organic Compound analysis

1.2.1. Air pollution

The importance of gas analysis can be illustrated by CO_2, the most significant long-lived greenhouse gas in Earth's atmosphere. The anthropogenic CO_2 emissions have grown exponentially since the beginning of the industrial revolution. As seen in Figure 1, this fact was first noticed by the scientist Charles David Keeling, who took long-term CO_2 measurements by an IR gas analyzer invented by himself in the South Pole and Manua Loa, far from major CO_2 sinks and sources.

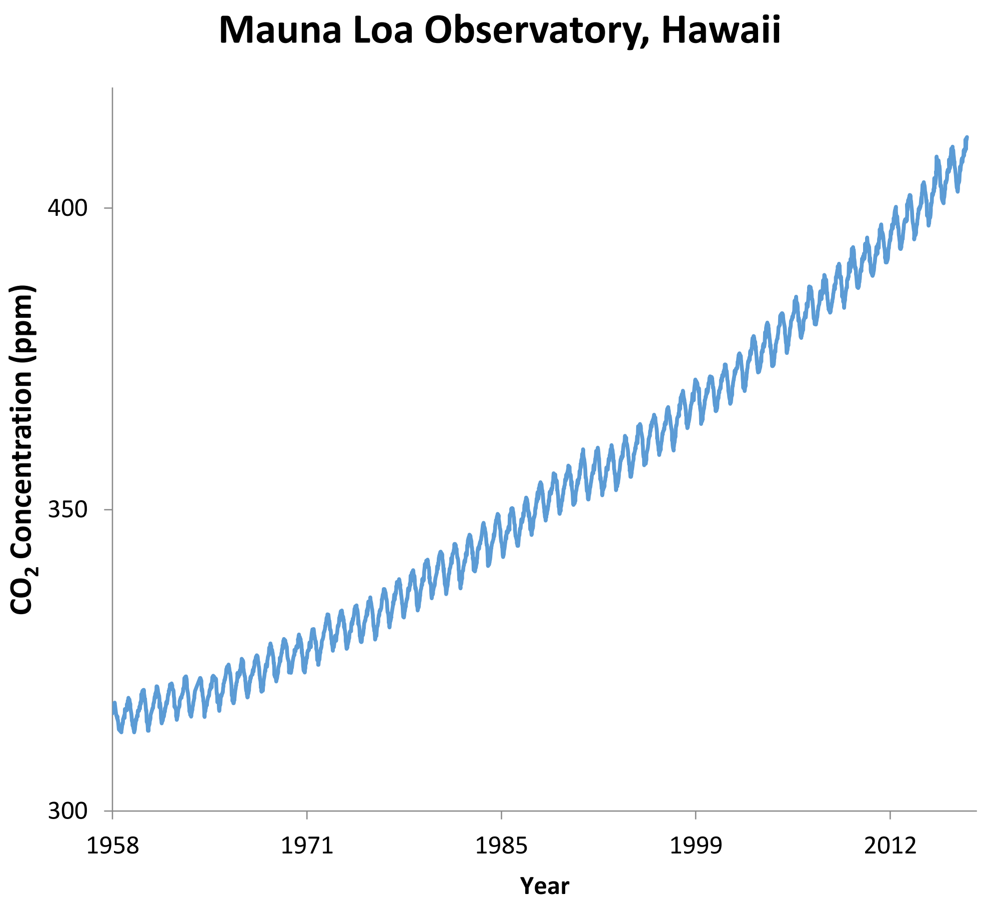

Figure 1 CO_2 concentration is been monitored regularly in the Mauna Loa Observatory since 1958 thanks to the development of more accurate measurement techniques. As shown by the long-term measurements, the CO_2 emissions have grown exponentially since the industrial revolution. Additionally, CO_2 concentration shows seasonal cycles [1] *due to photosynthetic activity. Data from the [Mauna Loa CO_2 records]* [2]

Thanks to this data, it was possible to show enough evidences to correlate the anthropogenic CO_2 emissions with the global warming, a fact that Svante Arrhenius [3] had predicted in 1896. In the 90s, the growing concern about the global warming was fueled by the media. Since then, scientific models combining the effect of the biogenic and anthropogenic emissions in the global warming have been developed to support this theory. In 2001, 186 countries joined the Kyoto protocol that commits state parties to reduce greenhouse gas emissions. This goal is being achieved by limiting the use of greenhouse gases and fostering the energetic efficiency in sectors like transport or energy production. The results of these efforts are shown in Figure 2, which shows how the main emissions in the EU have proportionally dropped considerable since 1990.

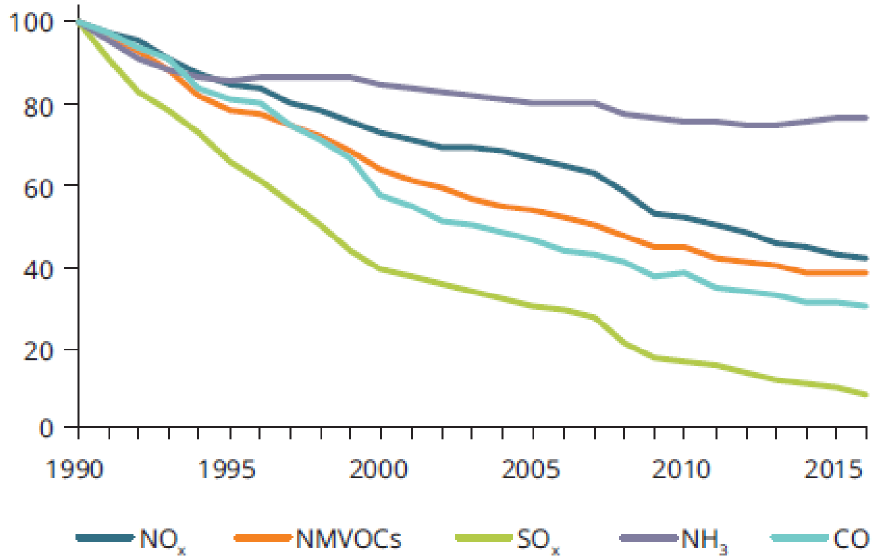

Figure 2 The graph shows the main air pollutants emissions compared to those in 1990 (100 %). NMVOCs refers to Non-Methane Volatile Organic Compounds. Figure reproduced from European Union emission inventory report 1990-2016 [4]

Carbon dioxide is not the only gas that may carry on an environmental hazard (Figure 2). Plants and aquatic environments can also be severely damaged as a side effect of SO_2 and NO_X emissions. A phenomenon known as acid rain occurs when these gases react with water, oxygen, and other chemicals to form sulfuric and nitric acids before reaching the ground. The aim of environmental policies is to prevent its harmful effects by, for example, penalizing the use of poor-quality coal and fuel. However, strict policies can result in losing competitiveness, jobs, and offshoring as shown for the steel industry. Therefore, the development of new policies must be justified by solid research studies, precise analytical measurements, and a broad consensus. It should also be noted that one third of these emissions come from biogenic sources such as wildfires, volcanic eruptions or thunderstorms.

Air pollution has been acknowledge to be the largest single environmental risk for health by the World Health Organization (WHO) [5]. The worst example happened during the Great Smog of London in 1952 when the combustion of poor-quality coal contaminated the air with big amounts of sulphur dioxide. London fog turned this contaminant into concentrated acid droplets killing around 4.000 people. Unfortunately, smog is still today a serious problem especially in winter when anticyclones can trap pollution at low atmospheric levels for several days. Therefore, it is important to monitor these gases in large population centers. WHO air quality guidelines [6] can be used to assess when city managers are forced to take timely corrective action to reduce the harmful impact of air pollution on health. For example, new initiatives taken in many European cities ban the most pollutant cars to reach the city center and encourage citizens to use public transportation. Simultaneously, in order to prevent air pollution, the acceptable limits for exhaust emissions of new vehicles have been reduced in Europe since 1990. This information is sum up in Table 1 and Table 2.

Table 1 Acceptable limits for exhaust emissions of new vehicles defined by European policies from Euro 1 to Euro 6

Directive		Directive 91/441/EC Euro 1	Directive 96/69/EC Euro 2	Directive 98/69/EC Euro 3	Directive 98/69/EC Euro 4	Regulation 715/2007 Euro 5	Regulation 715/2007 Euro 6
Implementation		1992	1996	2000	2005	2009	2014
CO	Petrol	2,72g/km	2,20g/km	2,30g/km	1,00g/km	1,00g/km	1,00g/km
	Diesel	2,72g/km	1,00g/km	0,64g/km	0,50g/km	0,50g/km	0,50g/km
HC or THC	Petrol	-	-	0,20g/km	0,10g/km	0,10g/km	0,10g/km
	Diesel	-	-	-	-	-	-
HC+NOx or THC+NOx	Petrol	0,97g/km	0,50g/km	-	-	0,068g/km	0,068g/km
	Diesel	0,97g/km	0,70g/km	0,56g/km	0,30g/km	0,23g/km	0,17g/km
NOx	Petrol	-	-	0,15g/km	0,08g/km	0,06g/km	0,06g/km
	Diesel	-	-	0,50g/km	0,25g/km	0,18g/km	0,08g/km
PM	Petrol	-	-	-	-	0,005g/km	0,005g/km
	Diesel	0,14g/km	0,08g/km	0,05g/km	0,025g/km	0,005g/km	0,005g/km

Table 2 EU air pollution trends due to transport activities. Data from "National emissions reported to the Convention on Long-range Transboundary Air Pollution" (LRTAP Convention), Published 12 Jul 2018. NMVOC means Non-Methane Volatile Organic Compounds. PM2.5 means fine particles that measure less than 2.5 μm

Year	CO	NMVOC	NOx	PM2.5	SOx
1990	100,0	100,0 %	100,0		100,0
1991	97,1 %	94,5 %	98,7 %		95,6 %
1992	93,0 %	92,9 %	99,8 %		95,7 %
1993	88,8 %	88,1 %	98,4 %		99,1 %

Year	CO	NMVOC	NOx	PM2.5	SOx
1994	81,2 %	82,1 %	95,1 %		95,0 %
1995	77,4 %	77,9 %	93,7 %		89,6 %
1996	74,8 %	75,6 %	93,9 %		89,5 %
1997	68,8 %	71,0 %	92,9 %		87,0 %
1998	64,4 %	66,5 %	92,7 %		92,4 %
1999	59,5 %	61,8 %	90,8 %		88,2 %
2000	53,7 %	54,3 %	86,5 %	100,0	82,3 %
2001	50,1 %	49,7 %	84,8 %	98,6 %	85,3 %
2002	46,0 %	44,8 %	82,0 %	96,7 %	81,8 %
2003	42,5 %	41,1 %	82,0 %	98,2 %	87,9 %
2004	39,4 %	37,1 %	82,8 %	99,6 %	90,7 %
2005	34,7 %	33,1 %	80,9 %	97,4 %	88,2 %
2006	31,7 %	29,9 %	81,3 %	92,1 %	89,9 %
2007	28,5 %	26,6 %	80,7 %	91,9 %	90,2 %
2008	25,6 %	23,8 %	76,8 %	88,2 %	85,6 %
2009	23,4 %	21,3 %	71,5 %	82,5 %	81,3 %
2010	21,0 %	19,1 %	68,9 %	76,6 %	72,5 %
2011	19,5 %	18,0 %	67,9 %	74,0 %	73,3 %
2012	17,9 %	16,4 %	64,2 %	69,3 %	70,9 %
2013	16,4 %	15,1 %	60,9 %	63,0 %	58,3 %
2014	15,3 %	14,3 %	59,9 %	60,8 %	58,6 %
2015	14,8 %	14,2 %	59,4 %	57,7 %	51,3 %

As a result, the transport sector has significantly reduced emissions of the main air pollutants. Unfortunately, the reduction was lower than previously anticipated as the sector has grown more than expected. This information is shown in Table 2.

As can be seen in Table 2, fine particles may suppose a new hazard. It should be noted that a large proportion of the particles emitted from direct injection engines are below 23 nm. Recent studies [7][8][9][10] show that inhaled nanoparticles penetrate deep into the lungs and translocate into the arterial blood contributing to cardiovascular diseases. Although the EU aims to regulate those emissions and impose limits, this is not yet possible due to the absence of accurate quantification methods. The European Union, through the SUREAL-23 project, is currently developing the necessary analytical techniques and protocols to deliver systematic characterization and to facilitate future particle emission regulations.

Air pollution also takes place inside buildings, mainly in the form of Volatile Organic Compounds (VOCs). It is especially harmful at the workplace as people usually spend there between eight to ten hours per day. In an office, VOCs sources are printers and cleaning agents. In the industry, VOCs come from the industrial activity itself and their concentration can be very high. In the past, canaries were regularly used by coal miners as an early warning system. Nowadays, standardized measurement techniques must be used to evaluate whether the exposition to dangerous chemical substances is below the limit defined by the Occupational Safety and Health Administration (OSHA). Additionally, according to the Spanish law on the prevention of risk in the workplace, companies must evaluate and identify the health risks. If any, the exposition of the workers should be reduced or, when not possible, individual protection equipment must be facilitated.

The purpose of this PhD Thesis is the chemical analysis of VOCs by means of Mass Spectrometry (MS) Coupled to a brand-new Secondary ElectroSpray Ionization (SESI) source. VOCs are organic compounds released into the environment as gases at normal conditions of pressure and temperature. These compounds generally contain no more than twelve carbon atoms and their boiling points are lower than 250 °C. They can be classified according to their boiling point as stated in Table 3.

Table 3 Classification of Volatile Organic Compounds (VOCs) according to their boiling points

Description	Acronym	Boiling Point (ºC)
Very volatile (gaseous) organic compounds	VVOC	from <0 to 50-100
Volatile organic compounds	VOC	from 50-100 to 240-260
Semi volatile organic compounds	SVOC	from 240-260 to 380-400

VOCs can be emitted by biogenic or anthropogenic sources. Biogenic substances are produced by living organism or by natural sources. The most abundant biogenic VOCs are isoterpenes and monoterpenes released by plants. On the other hand, anthropogenic substances are produced by human activities, for example by burning fuel.

1.2.2. Breath analysis

As a result of the equilibrium reached in the alveoli driven by Henry's law, exhaled breath contains biochemical information about the most volatile metabolites in blood. Since ancient times, healers have used their nose as a tool to diagnose a patient health status. Halitosis or chronic bad breath can ruin some one's social life as it is a sign of poor oral hygiene, but in 5-10% of cases its cause is elsewhere. For example, when exhaled breath smells like…:

- Rotten eggs, it may be caused by oral problems
- Fruity odors, it is associated with ketoacidosis which is common in diabetic patients

- Fishy odors, it is associated with patients with chronic kidney failure
- Acidic odors, it is associated with asthma or cystic fibrosis
- Musty odor, it may signal liver cirrhosis
- Fecal odor, it is related to bowel obstruction

Exhaled breath analysis has the potential to detect diseases non-invasively and painlessly. For example, hydrogen breath test has been successfully implemented as a method for clinical diagnosis of Small Intestinal Bacterial Overgrowth (SIBO) [11]. The method is based on the measurement though the breath of the hydrogen and methane produced by bacteria in the small intestine after eating carbohydrates. It is simple, fast, cheap and non-invasive whilst the direct method is very invasively and expensive as it consists on the aspiration and culture of the bacteria from the small intestine.

However, in most cases VOC biomarkers are usually found at trace levels in breath and, therefore, its reliable detection poses a challenge. Breath analysis implementation as a routine clinical practice is been delayed by the existence of several disadvantages: 1) different breath sampling protocols (single-breath or multiple breath, its duration, etc); 2) different collection containers (SPME, Tedlar, etc), 3) different pre-concentration methods [12][13]; 4) collection of different breath fractions (end-tidal or alveolar breath) and 5) different measuring techniques (GC-MS, LC-MS, PTR-MS, SIFT-MS, SESI-MS) [14]. Only by using standardized instrumentation and protocols, the difficulty in comparing and combining data from different sources can be overcome. Only then, breath analysis could fulfill its potential.

1.2.3. Bacteria and fungi identification

Breath analysis could, in the near future, revolutionize healthcare allowing doctors to identify which infectious pathogen is being carried by each patient [15][16]. Accurate and rapid bacterial identification can be theoretically achieved by measuring the unique fingerprint VOC for each bacterium [17][18][19][20]. Thus, personalized medicine would avoid the misuse of antibiotics that results in the development of resistant bacteria, untreatable infections and increased mortality in some patients.

In the pharmaceutical industry, bacteria are used to produce antibiotics. Interestingly enough, the first true antibiotic was accidentally discover by Alexander Fleming [21] in 1928 when he found that the bacteria culture in a petri dish had been killed around a mold caused by Penicillin fungi. A replication of Fleming discovery is shown in Figure 3.

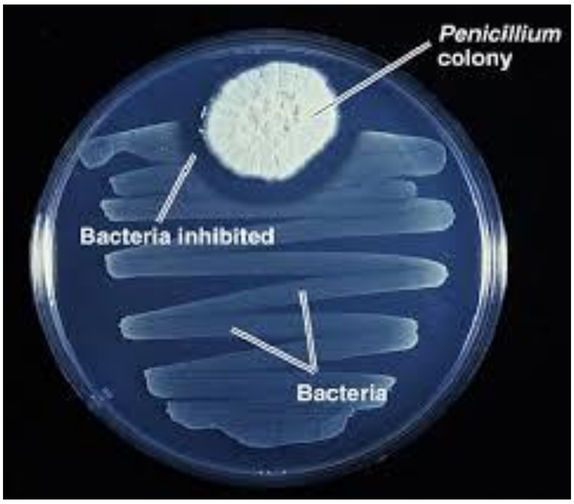

Figure 3 Replicated experiment of bacteria growth inhibited by antibiotic produce by the fungi: penicillin. Copyright © 2004 Pearson Education, Inc., publishing as Benjamin Cummings.

Beyond pharmaceutical interest, many biotechnological processes use bacteria and fungi microorganisms to produce goods and services like:

- Bacterial cultures of *Lactobacillus bulgaricus* and *Streptococcus thermophilus* are used to produce Yogurt as they ferment sugar milk to produce lactic acid.
- Bacteria, yeast and mold are used to make cheese defining its smell and taste. Lactic acid bacteria are very early added to the milk while fungi are responsible for the mold in white and blue cheese.
- Bread is a baked product made of baked dough previously growth in a mix of flour and water.
- Yeast is used by the beverage industry to transform sugar into alcohol and CO_2. The flavor and aroma of beer is usually defined by the different yeast strains that participate in the production process.
- Other fungi microbes are used to produce biofuel, most commonly ethanol [22], made from food crops and biomass, or biogas like methane from biodegradable waste.
- Biotechnology is also looking for solutions to unmet environmental problems like for example: bio-pesticides, bio-fertilizer, restoration of degraded lands and pollution control.

The control in real time of VOCs released by microbes during the microbial fermentation process could help the industry to maximize the production and researchers to get insights about the metabolic pathways followed by different microorganisms.

1.3. Analytical techniques to measure VOCs

Nowadays, there are many analytical techniques in the market to measure VOCs: starting from simple and cheap microsensors sensible to a specific gas, to spectrometry techniques that can be used for almost any substance providing information about its structure and improving its identification and quantification.

Microsensors

Microsensors are sensors with a size between 1-100 μm. Microsensors measure indirectly parameters like temperature, humidity or the concentration of a vapor by detecting changes in the resistance of a semiconductor or in the current through an electrochemical cell exposed to a specific gas. The main advantage of these sensors is their size, power consumption and price. Theoretically, the integration of nanomaterials in a semiconductor layer could make them sensible to a specific gas at very low price, which makes them very attractive for target applications. However, although their limits of detection are good enough to be used, for example, to monitor air pollution, further efforts need to be made to make them more robust and to improve the reproducibility and selectivity.

1.3.1. Spectroscopy techniques

Spectroscopy is the study of the interaction between matter and electromagnetic radiation. For obvious reasons, visible light was the first type of electromagnetic radiation used to study the structure, identify and quantify chemical substances, including VOCs.

Absorption spectroscopy

Absorption spectrophotometry is a technique that measures the number of photons absorbed by a chemical substance in a solution in order to determine its concentration. The general Beer-Lambert law that governs the absorption is written as:

where "A(λ)" is the wavelength-dependent absorbance measured, "I" is the light intensity after it passes through the sample and "I_o" is the intensity of the incident light. The absorbance depends on: "ε(λ)", the wavelength-dependent absorptivity coefficient of the chemical substance, "L", the path length of the light through the solution and "c", the concentration.

This method is widely used for identification and quantification of organic compounds. For identification, full absorption spectra may be recorded. As an example, Figure 4 shows the Infrared spectra of formaldehyde in gas-phase. The molecular bond C=O absorbs light at 1750 cm^{-1} transforming the electromagnetic radiation into motion, while CH_2 bond shows more than one absorbing frequency, each of them corresponds to a different vibrational transition. Unfortunately, the same chemical bonds in different environments will absorb varying intensities and at different frequencies. Therefore, the interpretation of the spectra can be very challenging especially in unknown complex mixtures. This method is more widely known as Ultraviolet (UV) spectroscopy or Infrared (IR) spectroscopy depending on the range of the spectra observed. It is a direct, non-contact, non-destructive, optical technique that can be successfully applied to monitor typical air pollutants [23] and other gases.

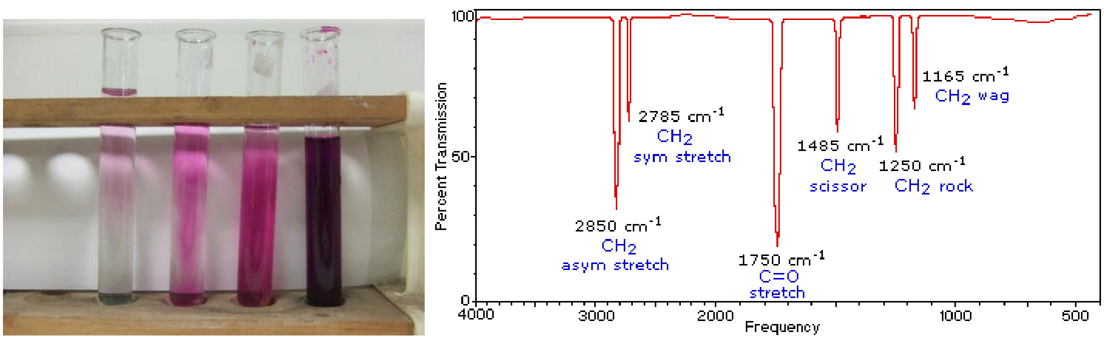

Figure 4. The left image shows an example of an application of a spectrophotometer using Beer-Lambert law to quantify the concentration in a solution of a substance that absorbs violet light. The darker the solution, the higher the concentration. Image from *Flickr* by *tjmwatson*, Copyright: Attribution 2.0 Generic (CC BY 2.0). *The right image shows an Infrared spectrum of gas-phase Formaldehyde $H_2C=O$. Each molecular bond may absorb light of a specific frequency transforming the electromagnetic radiation in motion (stretching or bending vibration, symmetrical or asymmetrical vibration). Image from tutorial pages of "Infrared Spectroscopy" by Department of Chemistry at Michigan State University, USA contributed by William Reusch and license Attribution-NonCommercial-ShareAlike 3.0 United States (CC BY-NC-SA 3.0 US)*

Emission spectroscopy

Another light-matter interaction occurs when the electromagnetic radiation is absorbed by the molecule and then a photon is re-emitted at the same or different frequency. When the energy of the incident light absorbed is high enough, an electron may go from its normal ground-energy orbital to a semi-stable higher-energy one. Then, photons with different energies are emitted as the molecule may drop down into any of several vibrational states in its way to the stable ground state. This phenomenon is known as fluorescence (or phosphorescence if the quantum transition is "forbidden") and it usually lasts from 1 ms to 1 second (up to 100 seconds for phosphorescence). Pulsed UV fluorescence is currently used to determine the concentration in gas-phase of sulfur compounds like H_2S and SO_2 [24][25].

Raman spectroscopy

When the energy of the incident light matches the energy required for the transition of an electron to a virtual energy orbital, the incident photon may be absorbed and another one may be emitted as the electron goes back to its stable orbital. In most cases, elastic or Rayleigh scattering occurs, which means that the incident and the emitted photon have the same frequency. On the other hand, inelastic or Raman scattering occurs only one in a million photons, when a photon finds a different vibrational energy state before reaching the ground state or when it starts from a vibrational energy state different than the ground state. In Raman spectroscopy, the unit of measurement is inverse centimeters, representing the difference in frequency between the incident light "v_0" and the emitted photon "$v_0 \pm v_r$". The Raman shift is independent of frequency of the incident light, providing information about the chemical bonds in the molecules being examined.

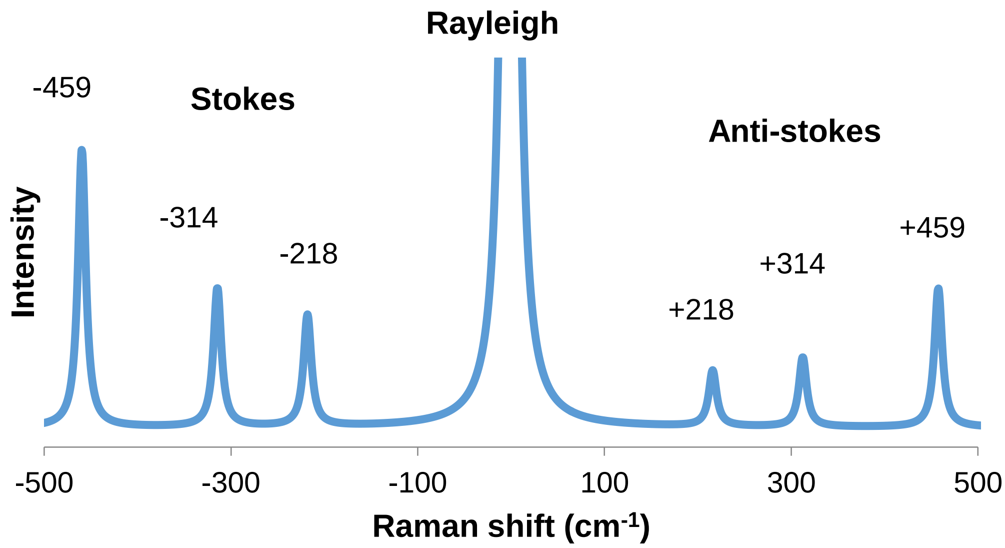

Figure 5. This shows a typical Raman spectrum of CCl_4 using 488 nm laser source. The Rayleigh scattering is much more intense, and its frequency matches the frequency of the incident light. Raman scattering intensity is much lower and the shift between the incident light frequency and the photons emitted by stokes or anti-stokes Raman scattering depends on the chemical bonds and no on the incident light frequency. Therefore, it provides structural information of the sample.

Raman spectroscopy is a direct, non-contact, non-destructive, optical technique that detects intrinsic vibrational, rotational and other low-frequency modes in molecules. It provides useful information about the structure of the molecule for its identification and quantification. As Infrared spectroscopy, Raman spectra may be difficult to interpret, especially in complex mixtures. Nevertheless, it has been successfully applied to monitor typical air pollutants [27] and other gases.

1.3.2. Mass spectrometry

Mass spectrometry uses electric and magnetic fields to accelerate and separate ions according to their mass to charge ratio (m/z). This technique has got very popular as the molecular formula of any chemical substance can be retrieved directly from its exact mass. The latest High-Resolution Mass Spectrometers (HRMS), like the LTQ Orbitrap, achieve an accuracy of 1 ppm and a resolution of 1.000.000 FWHM at m/z 200. Therefore, the molecular formula of most VOCs can be unambiguously identified even in a complex matrix. However, its structure must be further elucidated. This information can be retrieved by tandem MS that breaks the compound into fragments, which allows comparing the results with a standard reference.

Gas Chromatography Mass Spectrometry (GC-MS)

In analytical chemistry, the combination of different techniques is one of the most powerful tools to produce quality scientific results. Thus, Gas Chromatography - Tandem

Mass Spectrometry (GC-MS/MS) is the gold standard technique for compound separation, identification and quantification of volatile compounds. It is routinely used in forensic analysis that required the highest degree of confidence in the identification of drugs and toxic substances [28][29][30][31][32]. However, it should be noted that, for these setups, as selectivity increases, sensibility deteriorates. To overcome sensibility problems, many pre-concentration methods have been proposed. For example, in breath analysis, the most broadly used pre-concentration methods involve collecting Exhaled Breath condensate (EBC) for water-soluble compounds and Solid Phase Micro-Extraction (SPME) for non-soluble volatiles. Nevertheless, there are some disadvantages: the volume of sample needed is much higher; the protocol to pre-concentrate samples is usually very complex; and the time required increases significantly when compared to a direct measurement.

Proton Transfer Reaction Mass Spectrometry (PTR-MS)

Proton Transfer Reaction Mass Spectrometry (PTR-MS) is an analytical technique to measure VOCs in real time. It has become very popular because of its simplicity, since it is a soft ionization method that produces almost no fragmentation, just protonating the sample according to the equation:

ec 2

$$H_3O^+ + R \rightarrow RH^+ + H_2O$$

This reaction only takes place when the proton affinity of the molecule R is higher than the proton affinity of water (691 kJ/mol [33]). Nonetheless, as the proton affinity of most carrier gases like He, N_2, Ar, etc. is lower than water, only VOCs get ionized. In this sense, Table 4 shows the main compounds in dry air with their proton affinities.

The main advantage of this technique is its great sensitivity and the achievement of absolute quantification without need for calibration, as a result of reaction rate constants being well known for most compounds [34]. However, only compounds with higher proton affinity than water can be determined, it can only be used to ionize in positive mode, it is only capable of analyzing volatile compounds up to 150–200 u and, regarding MS detection, it is usually limited to low resolution and without tandem capabilities.

Table 4. List of main compounds in dry air with their proton affinities

Components in dry air	Formula	Concentration mol/mol$_{[dry\ air]}$	Proton affinity
Nitrogen	N_2	78.084 % [33]	493.8 KJ/mol [33]
Oxygen	O_2	20.9476 % [33]	421.0 KJ/mol [33]
Argon	Ar	0.934 % [33]	369.2 KJ/mol [33]
Carbon dioxide	CO_2	0.0314 % [33]	540.5 KJ/mol [33]
Neon	Ne	18.18 ppmv [33]	198.8 KJ/mol [33]
Helium	He	5.24 ppmv [33]	177.8 KJ/mol [33]
Methane	CH_4	2 ppmv [33]	543.5 KJ/mol [33]
Krypton	Kr	1.14 ppmv [33]	424.6 KJ/mol [33]
Hydrogen	H_2	0.5 ppmv [33]	422.3 KJ/mol [33]
Xenon	Xe	0.087 ppmv [33]	499.6 KJ/mol [33]
Ozone	O_3	trace to 0.07 % [33]	625.5 KJ/mol [33]
Carbon monoxide	CO	trace to 25 ppmv [35]	594.0 KJ/mol [33]
Sulfur dioxide	SO_2	trace to 10 ppmv [35]	672.3 KJ/mol [33]
Nitrogen Dioxide	NO_2	trace to 0.02 ppmv [33]	549.8 KJ/mol [33]
Ammonia	NH_3	trace to 0.3 ppmv [35]	853.6 KJ/mol [33]
Iodine	I_2	0.01 ppmv [33]	608.2 KJ/mol [33]

Selected Ion Flow Tube Mass Spectrometry (SIFT-MS)

Selected Ion Flow Tube Mass Spectrometry (SIFT-MS) is an analytical technique very similar to PTR-MS in which the reagent gas, that can be rapidly exchanged, most commonly involves H_3O^+, NO^+, O_2^+, O^-, O_2^-, OH^-, NO_2^-, and NO_3^-. These precursor ions react with VOCs following well-known gas-phase ion-molecule reactions, so absolute quantification is also possible. Additionally, its capability to change the reagent ion provides useful information for identification and interpretation of data. However, it is only capable of analyzing volatile compounds up to 150–200 u, and it shows a poor sensitivity when compared to other techniques. Table 5 shows a comparison of SESI-MS, SIFT-MS, PTR-MS and GC-MS, in terms of analytical capabilities, for the analysis of VOCs.

Table 5. Comparison of LFSESI-MS, SIFT-MS, PTR-MS and GC-MS for the analysis of VOCs [36]

System	Mode of operation	Number of compounds	LOD	MS/MS capability	HRMS capability	Automated operation
SESI-MS	Direct real time	100 – 1000	Sub-pptv	YES	YES	YES
SIFT-MS	Direct real time	~100	ppbv	NO	NO	YES
PTR-MS	Direct real time	~100	pptv	NO	NO	YES
GC-MS	Pre-concentration	100 – 1000	Sub-pptv	YES	YES	NO

It can be concluded from this section that the growth and popularity of MS is linked to the development of new, soft and efficient ionization sources. The next chapter provides a brief history of the development of mass spectrometry before explaining the measuring principles of the Secondary electrospray ionization source (SESI) used in this PhD to ionize volatile compounds.

1.4. Mass spectrometry: a brief history

In this PhD thesis, Secondary Electrospray ionization (SESI) is used to ionized VOCs prior being measured by a High-Resolution Mass Spectrometer (HRMS). However, before showing how a SESI source works, a brief explain of how mass spectrometry has been developed and popularized since its discovery is offered. Afterwards, electrospray ionization (ESI) is explained, as SESI has been developed from ESI and both techniques share a lot of working principles. Finally, the main ionization mechanism for SESI is explained in conjunction with a brief description of the nature of the SESI source used in this PhD thesis and how it was developed by the ACID project.

Mass spectrometry is a powerful analytical technique to determine the abundance and mass to charge ratio of ionized compounds. Additionally, tandem MS can also provide structural information according to fragmentation patterns. To simplify, this technique consists of three major components:

- An ionization source: Responsible of generating ions from the sample
- A mass analyzer: Responsible of separating ions according to their mass-charge ratio
- A detector: Responsible of measuring and quantifying the ions

The first instrument capable of separating ions according to their mass to charge ratio was built in 1897 by the British physicist J. J. Thomson [37] while studying the transmission of electricity through gases to elucidate the nature of cathode rays –particle vs. wave controversy-. In this instrument, the cathode rays or the beam of electrons were generated by gas discharge tubes, accelerated by an electric field and deflected into parabolic trajectories by a magnetic field. With this device, it was possible to measure the charge to mass ratio of ions. Lately, Thomson realized that the mass of some particles was much smaller than the mass of the atom, leading to the discovery of the electron. Thomson was awarded the Nobel Prize in Physics in 1906.

Some years later, Francis Aston [38] built the first mass spectrometer thought to measure mass to charge ratios, which resulted in the first evidence of the existence of Helium and Hydrogen isotopes. He was awarded the Nobel Prize in Chemistry in 1922.

The fist ionization method developed for mass spectrometry was Electron impact (EI) in 1918 by the physicist A. J. Dempster [39]. In his experiments, an electron beam was directed to a heated cylindrical anode made of the material of interest. In 1929, Walker Bleakney [40] modified this technique by using a heated tungsten wire filament to generate a mono-energetic electron beam for the ionization of volatiles. For many years, EI was the gold standard ionization technique.

Mass spectrometers were finally popularized by Alfred Nier (1911 – 1994), father of modern mass spectrometry, by, for example, helping biologist [41][42] to produce ^{13}C and geochemist [43][44] to determine the age of the earth by measuring $^{207}Pb/^{206}Pb$ ratios. The separation of uranium isotopes contributed to establish the nuclear fission era [45][46][47][48].

Until 1940, mass spectrometers were used mainly by physicists researching about the nature of the atom and by chemists in the industry as a way of measuring concentrations in mixtures of known compounds, mostly because the fragmentation arising inside the mass spectrometer was not understood.

In the meantime, scientists like Klaus Biemann, Carl Djerassi and Fred Warren McLafferty focused their efforts on decrypting the fragmentation mechanism of organic molecules, while others pursued the development of softer ionization sources.

The first soft ionization method, known as Field ionization [49] (FI), was described by R. Gomer and M.G. Inghram in 1955. It involved attaching a field emission microscope to a mass spectrometer. The analyte was ionized gently in the proximity of the tungsten tip of the field emission microscope by using a very high electric field. As it produced no fragmentation, the mass spectra contained typically only one peak corresponding to the radical ion of the analyte.

In 1969, Hans Beckey developed Field desorption (FD) [50] increasing considerably the sensitivity of the FI method. In his experiments, a very high voltage was applied to a tungsten stranded conductor cover with a tiny film of the analyte.

In 1966, Munson and Field [51] developed chemical ionization (CI) that relies on chemical gas-phase reactions rather than in beam impact to ionize the analytes. CI used methane ionized by electron impact as reagent ions to interact with the analytes. They realized that, depending on the reagent gas used, different reactions took place. For example, using CH_5^+, proton transfer is the main reaction ionizing the analytes. However, if N_2^+ is used, then electron transfer occurs. CI usually needs high partial pressures of the reagent gas in order to increase the number of collisions with the analyte and to enhance the sensitivity.

In 1975, Carroll and Horning [52][53] developed the first atmospheric pressure ionization source in order to be coupled to high performance liquid chromatography (HPLC). This ionization method replaced the CI source, based on radioactive ^{63}Ni, by a corona discharge source, decoupling the high vacuum entrance of the MS and the ionization of the sample. However, the presence of clusters generated complex spectra, so the method was not developed further at that time.

Until 1980s, the success of mass spectrometry was very limited when analyzing large molecules as there was still no method capable of ionizing macromolecules without fragmentation or decomposition. In 1981, Michael Barber developed a new ionization method called fast atom bombardment, capable of ionizing long peptides by aiming a beam of neutral argon atoms to the analyte, placed on a copper plate mixed with a low-volatile organic matrix. However, its success would be eclipsed by the appearance of electrospray (ESI) and MALDI [54]. These techniques have become the reference techniques to ionize macromolecules.

Electrospray ionization (ESI) was invented by Malcolm Dole [55] in 1968. He generated a spray of charged droplets by feeding a high voltage needle with a polymer solution. Analyte ions were released from the charge droplets after evaporation and electrostatic repulsion. Unfortunately, by that time the mass spectrometers were not able to detect single charged ions of macromolecules (>2000 Da). Almost 20 years later, Fenn [56][57][58] and colleagues resumed Dole's research overcoming some of the problems he had found and popularizing the technique. Fenn and Koichi Tanaka were awarded with the Nobel Prize in Chemistry in 2002.

Secondary electrospray ionization (SESI) is a technique based on ESI to ionize vapors. It was first reported by Fenn as an undesirable effect in ESI [59][60]. He found out that the ionization of some target drugs in the electrospray solvent were suppressed by volatiles before reaching the mass spectrometer. Its real potential was shown by H. Hill [61] that demonstrated that even molecules with low volatility could be ionized. SESI has been successfully applied for explosive, drug and illicit substances detection [62], [61], [63], [64], human breath and skin metabolite analysis [65], [66], [67], [68], food analysis [69], [70] and bacterial identification [71], [72], [73]. SESI is capable of ionizing compounds with low volatility, in low concentrations [74], and with molecular weights far beyond 300 Da.

1.5. Electrospray ionization: How it works

Electrospray ionization is a soft ionization technique that produces intact ions by applying a high voltage to the analyte in a conductive solution going out though a capillary.

1.5.1. Liquid through a capillary

One of the main properties in order to characterize an electrospray is how much liquid is going out through the capillary. The flow is generally controlled by the pressure drop through the capillary. This can be easily determined by the Poiseuille equation. It states that the flow through a long cylindrical pipe with constant cross section depends on the dynamic viscosity (μ) of the fluid, the pressure gradient inside the tubing (ΔP), its radius (r) and its length (L). It assumes that the tube is long enough so an incompressible and Newtonian fluid in laminar flow shows a fully developed velocity profile.

ec 3

$$Q = \frac{\pi \cdot R^4 \cdot \Delta P}{8 \cdot L \cdot \mu}$$

Typically, in a SESI setup, a minimum drop pressure of 0.050 bar is used with a 50 µm silica capillary:

ec 4

$$Q = \frac{\pi \cdot (25 \cdot 10^{-6}m)^4 \cdot 5{,}000Pa}{8 \cdot (50 \cdot 10^{-2}m) \cdot 0.001N \cdot s \cdot m^{-2}} \approx \ 1.5\mathrm{pm}^3/s \ = 90\mathrm{nL/min}$$

Or if using a 20 µm silica capillary, a drop pressure of 0.200 bar is preferred to keep a good stability:

ec 5

$$Q = \frac{\pi \cdot (10 \cdot 10^{-6}m)^4 \cdot 20{,}000Pa}{8 \cdot (50 \cdot 10^{-2}m) \cdot 0.001N \cdot s \cdot m^{-2}} \approx \ 0.15\mathrm{pm}^3/s \ = 9\mathrm{nL/min}$$

Therefore, for these conditions, the flow rates are in the range of nano-electrosprays.

Additionally, if the ESI solvent is assumed to be to usual solution of 0.1% formic acid in water:

ec 6

$$Molar\ (M) = \frac{moles\ of\ solute}{Volume\ solution\ (liters)} = \frac{\%(v/v)}{100} \cdot \rho \cdot \frac{1}{Molecular\ weight}$$

ec 7

$$Molar\ (M) = \left(\frac{1}{100} \cdot \frac{0.1L\ formic\ acid}{1L\ solution}\right) \cdot \left(1.22\frac{g}{mL} \cdot \frac{1000mL}{L}\right) \cdot \frac{1mol}{46.025\mathrm{g}} \approx 26.5mM$$

Then the molar flow of formic acid is:

ec 8

$$\dot{n}_{Formic\ acid} = Q \cdot M = 90nL/min \cdot 26.5mM \approx 2.39 \cdot 10^{-9}moles/min$$

It has been observed multiple times, when starting electrospray ionization, that using the minimum flow necessary to have a stable electrospray gives the best ionization efficiencies in SESI. A simple explanation could be that the electrospray solution goes to the gas phase and mixed with the sample competing for the ions. Therefore the higher the flow of ESI solvent, the higher the suppression [75][76] in the ionization of the target species due to a higher concentration of formic acid from the electrospray in the sample gas.

The concentration of formic acid injected into the sample gas can be calculated as follows:

First, the molar flow from a gas flow is calculated by applying the ideal gas law:

ec 9

$$P \cdot V = n \cdot R \cdot T$$

Considering a typical vapor sample flow of 0.5 lpm:

ec 10

$$\dot{n}_{sample} = \frac{P \cdot \dot{V}}{R \cdot T} = \frac{101{,}325Pa \cdot (0.5 \cdot 10^{-3} m^3/min)}{8.314472 J \cdot K^{-1} \cdot mol^{-1} \cdot 293K} \approx 20.8 \cdot 10^{-3} mol/min$$

Therefore, the concentration of formic acid injected by the electrospray in the vapor sample is:

ec 11

$$ppmv = 10^6 \cdot \frac{\dot{n}_{Formic\ acid}}{\dot{n}_{sample}} = 10^6 \cdot \frac{2.39 \cdot 10^{-9} moles/min}{20.8 \cdot 10^{-3} moles/min} \approx 0.115\ ppmv$$

It is well known that low flow rates achieve higher ionization efficiencies [77][78] in ESI (nano-ESI) since smaller primary droplets from the electrospray turn more easily into gas-phase ions [79][80][81]. It should be noted that as the ionization efficiency increases, the signal intensity decreases [82] after a maximum [83], since it is flow dependent at very low flow rates.

Gañán-Calvo et al [84] studied the absolute minimal flow rate to produce a steady Taylor cone-jet. It depends on the liquid properties (density ρ, surface tension σ, viscosity μ, electrical conductivity K and electrical permittivity ε_i), assuming stable environmental parameters and a fixed voltage. In addition, they found that this flow matches the natural flow that is extracted only by voltage on a liquid interface to form a Taylor cone. The lowest flow rates for a given emitter geometry and applied voltage are obtained without backpressure, which is called self-fed electrosprays. However, its determination is difficult as it depends on the balance between the capillary forces, surface tension and shear stress[84][85]. In addition, self-fed electrosprays offer little reproducibility as the narrow emitters needed for low flow rates get dirty or clogged easily.

Table 6 Image of a PicoTip™ TaperTip™ emitter from PicoTip Brochure and datasheet information

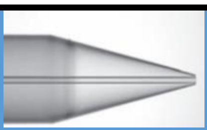	**Outside diameter**	**Internal diameter**	**Flow range**	**Length**
Reference	OD (μm)	ID (μm)	Q (μL/min)	L (cm)
TT360-50-50	360	50	0.2 – 1	50
TT360-20-50	360	20	0.2 – 0.5	50

Specifically, when little or no backpressure is applied, the flow rate and the electrospray mode strongly depend on the applied voltage and the emitters' geometry. The geometry of the ESI emitter [86] is a crucial parameter to determine the operational flow rates and stability range of the electrospray. Sharp emitters give the most stable electrosprays at the lowest flow rates. In our experiments, PicoTip™ TaperTip™ Emitters (Table 6) are used since, after being manufactured, they undergo a visual inspection, which is recommended to improve reproducibility.

The performance of the electrospray inevitable changes during normal operation due to problems in the capillary:

- Microscopic depositions can modify the geometry of the emitter, therefore the electric field.
- Capillary clogs can increase the backpressure needed to keep a stable flow rate.
- Air bubbles in the eluent can change the conductivity through the capillary and increase the backpressure needed to keep a stable flow rate.
- Emitter aging changes the geometry of the emitter, therefore the electric field.

In addition, the electrospray geometry is continuously changing as droplets escape from its surface disturbing the electrostatic forces. At frequent intervals, the electrospray becomes unstable and then it stabilizes again with a different shape which finally determines the ionization efficiency and the ion transmission through the electrode inlet to the mass spectrometer. Diagnosis of the shape of the spray cone can be accomplished by using a high-speed camera. In addition, as fluctuations in the meniscus of the spray occur due to variations in the electric field [87][88], the applied voltage [88] can be controlled, manually or by advance control algorithms, in order to improve the stability and reproducibility of the measurements. In addition, cone-jet geometry control loops have been developed using only the electrospray current as a feedback variable. According to Asep Suhendi et al. [89], the cone-jet length (L) follows a power law with the flow rate (Q) and the electrospray current (I).

ec 12

$$\log(L) = C_1 \cdot \log\left(\frac{Q}{I}\right) + C_3$$

Therefore, a stable cone-jet geometry can be obtained during the experiment keeping the current constant for a given flow rate. In addition, it is possible to keep constant the size of the emitted droplets as it is correlated with volume charge density (I/Q) [90].

However, they also found that constants C_1 and C_3 had to be determined independently for each flow rate. They hypothesized that it was due to the high evaporation rate of the solvent. Therefore, temperature in the electrospray also needs to be controlled for a better reproducibility.

1.5.2. Electrospray mode: steady cone–jet

It should be noted that there are 3 different modes of electrospray [88][91][92] according to its geometry: dripping, cone-jet and multi-jet mode. Taylor cone-jet mode is the most popular and better understood. Therefore, it is the one we pursue in our experiments. It happens in a narrow voltage between dripping and multi-jet mode.

Initially, when no voltage is applied, a droplet of ESI solvent with spherical shape goes out the capillary. Its size depends only in the balance between the liquid flow rate through the capillary and its evaporation rate. When a small voltage is applied, the liquid gets charged. As the voltage is increased, the droplet changes its shape into a conical geometry according to the balance between electrical repulsion and surface tension. When the voltage is high enough, the apex is so pointed that it breaks (by coulomb explosion) ejecting elongated single droplets that moves towards the electrode. This is known as dripping mode. In this mode, each time a droplet is released its shape changes. An onset voltage needs to be reached in order to get a stable jet emission in Taylor cone-jet mode. Smith et al [93] found out in 1986 that this voltage depends on the surface tension of the liquid (γ), distance to the electrode (d), radius of the capillary (r_c), half angle of the Taylor cone ($\theta = 49.3°$) and permittivity of vacuum ($\varepsilon_0 = 8.8 \times 10^{-12} J^{-1}C^2$):

ec 13

$$V_{on} = \left(\frac{r_c \cdot \gamma \cdot \cos\theta}{2 \cdot \varepsilon_0}\right)^{1/2} \cdot \ln\left(\frac{4 \cdot d}{r_c}\right)$$

In our setup, the capillary can be positioned freely between 4 mm and 12 mm distance from the electrode, so typically at 8 mm:

ec 14

$$V_{on} = \left(\frac{(25 \cdot 10^{-6} m) \cdot (0.073 N/m) \cdot \cos(49.3°)}{2 \cdot (8.8 \cdot 10^{-12} \mathrm{J}^{-1} \cdot \mathrm{C}^2)}\right)^{1/2} \cdot \ln\left(\frac{4 \cdot (8 \cdot 10^{-3} m)}{25 \cdot 10^{-6} m}\right) = 1860V$$

The voltage range at which the Taylor cone is stable is narrow. For higher voltages, two or more jets can appear. This is known as the multi-jet mode. This geometry is also effective for ionization. However, it requires higher voltages which can lead to small electric discharges, especially when using metallic tips or in negative mode, reducing ionization performance [94][95].

The charge state and size of the first droplets ejected by the Taylor cone-jet mode can be determined by the universal scaling laws [96][97] under steady conditions. Gañán-Calvo et al. [98] studied the unsteady electro-hydrodynamic behavior of the electrospray including numerical and experimental simulations. They examined the response in time of a step change in the electric field in the Taylor cone-jet and droplet ejection.

After the ejection of the droplet from the cone-jet, it undergoes evaporation until it is no longer stable due to a high charge concentration close to the Rayleigh limit[99]. Thus, electrostatic repulsion is balance by the surface tension and the droplet splits into multiple droplets whose diameter is about 1/10th of the parent. The Rayleigh stability limit states that the maximum number of surface charges (Q_R) in a droplet of radius R_R depends on the permittivity of free space (ϵ_0) and the liquid surface tension (γ).

ec 15

$$Q_R = 8 \cdot \pi \cdot \left(\epsilon_0 \cdot \gamma \cdot {R_R}^3\right)^{1/2}$$

1.5.3. Ionization mechanism in ESI

Immediately after the discovery and popularization of ESI, researchers began to hypothesize about the ionization mechanism gathering data to support one or the other. 30 years later, 2 models: i) ion evaporation model and ii) charge residue model are favored to explain the experimental result, with some limitations.

Ion evaporation model

In 1976, Iribarne et al. [100][101] proposed this model which states that the droplets containing the ions undergo evaporation until the field strength at their surface is high enough so that the ions can leave the droplet. In this case, the evaporation rate depends on the reaction free enthalpy needed to enlarge the droplet surface so that the ion is expelled. However experimental results show that some ions with very similar solvation energies have very different reaction rate constants and vice versa [101].

Charge residue model

In 1968, Dole et al. [55] proposed this model to explain its results. Later authors like Wilm et al. [81] supported this mechanism for the ionization of large molecules. The model states that the droplet evaporates until only the charged ion is left. Therefore, the ionization rate depends not on the ion, but on the initial droplet size and solvent evaporation efficiency.

1.5.4. Ionization mechanism in SESI

In secondary electrospray ionization, an electrospray is used as primary source of ions to ionize gas-phase molecules. Therefore, it is hypothesized that the target molecules, initially in gas phase, could get immerse in the droplet and then get ionized as in ESI or that ions from ESI and the target vapors are interacting directly in gas-phase via a chemical ionization mechanism. Again, researchers gather data to support one or the other ionization mechanism. Dillon et al. [102] reviewed these models and compared them with experimental data in order to optimized the ionization efficiencies of different compounds, according to parameters like drying-gas flow rate, nebulizing-gas flow rate and voltage. They found that for very soluble compounds, like 2,3-butanediol, the ionization was suppressed by higher dry-gas flow rates, whilst for the rest of compounds tested it was enhanced. These results evidenced that a single optimization can be accomplished only for a limited range of compounds.

A research study to find out which is the most important ionization mechanism for our SESI source has been carried out in this thesis.

1.6. Low-Flow Secondary Electrospray ionization (LFSESI)

The ionization source used in this PhD thesis was developed under the umbrella of the project "Analytical Chemistry Instrumentation Development" (ACID). Its main goal was to develop novel instrumentation for the characterization of gas-phase analytes with high sensitivity and in real time. State of the art secondary electrospray ionization sources typically use high sample flow rates (~ 5 lpm) to achieve higher signal intensities. However, the ionization efficiency decreases at these high flow rates. In addition, in most state-of-the-art SESIs the sample is mixed with the counter flow from the MS. This counter flow is needed to reduce cluster formation and to keep the MS inlet clean. However, if the sample is mixed prior ionization, this dilution reduces the ionization efficiency of the target molecules.

In the ACID project, a new concept of SESI source was designed specifically for working at low flow rates. As seen in Figure 6 and in Figure 7, an independent ionization chamber was initially proposed to avoid dilution with the counter flow from the MS prior the ionization of the target vapors. The ions from the electrospray chamber needed then to be guided to the MS inlet by high electric fields. One limitation of this design is that this electrospray chamber is no longer flushed by the clean counter flow from the MS. Therefore, it is much more susceptible to contamination that other state-of-the-art SESI sources. This weakness is best dealt by heating the SESI source up to temperatures between 100 and 200 °C. It should be noted that the temperature in the electrospray chamber is limited by the electrospray solvent used. For example, using 0.1 % formic acid in water, the temperature should not be higher than 100 °C whilst for 1 % HCl in DMSO and Octanol (1:10 v:v) the temperature can reach up to 200 °C. Unfortunately, according to our experience, electrosprays based on water solutions carry out the best ionization efficiencies even though they are more difficult to control, especially at higher temperatures.

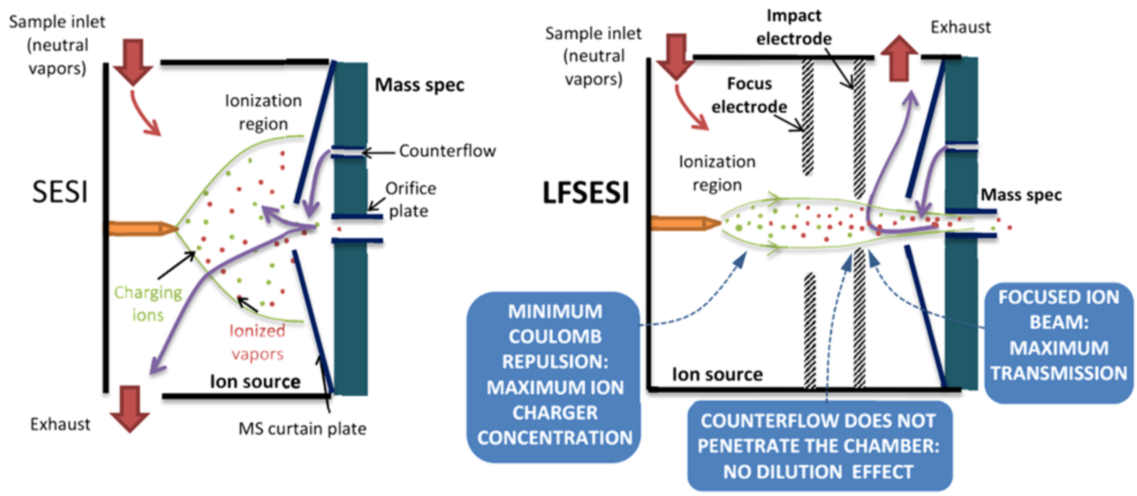

Figure 6. The left image shows a classic model of Secondary ElectroSpray Ionization source in which the sample vapors get diluted when mixing with the counterflow from the Mass Spectrometer prior being ionized by the electrospray. The right image shows the new design of the LFSESI in which the sample vapors get ionized by the electrospray in an independent chamber before reaching the mass spectrometer inlet. Image from LFSESI Technical brochure at [SEADM website]

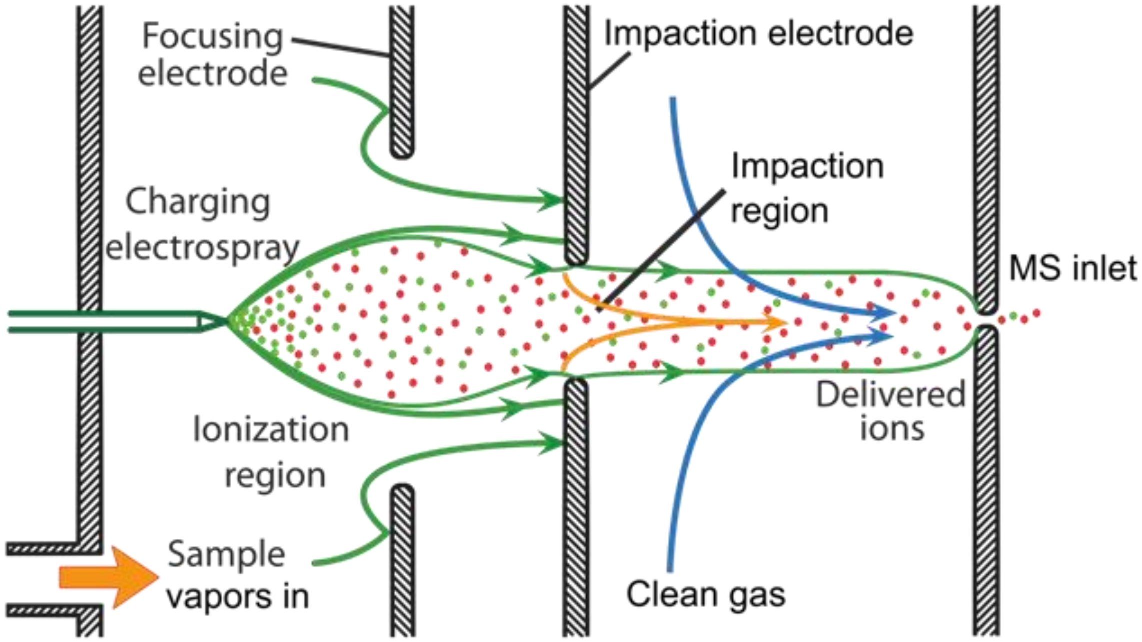

Figure 7.This image shows in detail how the ions are guide to the MS inlet and the flow paths of the sample, electrospray and counterflow after the optimization. Taken from Vidal-de-Miguel, G.; "Add-on Secondary Electrospray Ionizer for pre-existing MS and for high sensitivity volatile analysis" BIT's 4th Conference and EXPO of AnalytIX-2015; Nanjing, China, Apr 2015

One of the key steps to design the LFSESI was running numerical simulations. Models of fluid mechanics, electrostatics and the transport of diluted species were combined in a Finite Element Method algorithm to simulate the SESI phenomena. The key parameters to optimize the ionization efficiencies in the electrospray chamber and the highest ion transmission to the MS are:

- Distance of the capillary tip to the electrode
- Shape of the electrospray chamber
- Distance between electrodes
- Orifice diameter of the electrodes
- Distance between the electrode and the MS inlet
- Sample flow rate and counter flow from the MS

The results of these studies were published in the follow scientific paper:

- Barrios-Collado, C.; Vidal-de-Miguel, G.; Martínez-Lozano Sinues, P. "Numerical Modeling and Experimental Validation of a Universal SESI Source for Mass Spectrometric Gas Analysis in Real-Time." *Sensor Actuat. B-Chem.* 2016, 223, 217-225.

Figure 8 shows the results of the simulations for the concentrations of charging ions (c_c), neutral vapors (c_v), and ionized vapor (c_i). As expected, the concentration of ions is higher in the electrospray tip decreasing with distance. The ionization region has the shape of the electrospray plume, as was first validated by a model from J. F. De la Mora [103]. The neutral vapor concentration is constant in all the electrospray area outside the electrospray plume where neutral vapors get ionized. The simulations suggest that the best ionization efficiencies occur in the periphery of the plume. Unfortunately, these ions are driven against the electrode, losing their charge.

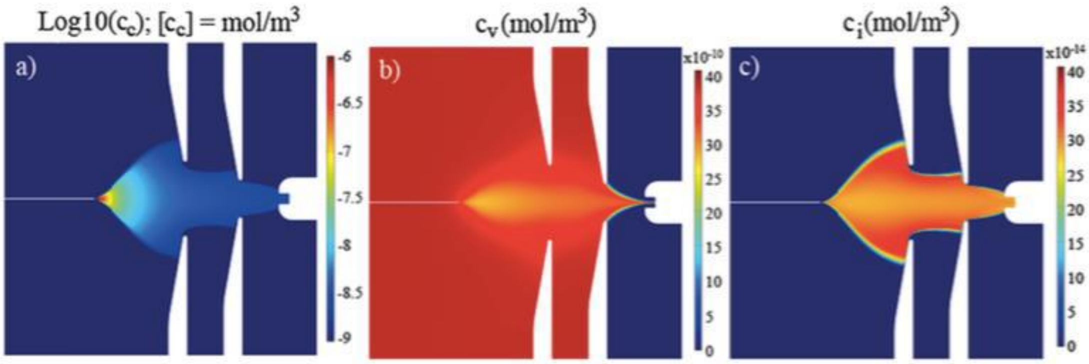

Figure 8. a) shows the concentration of charging ions coming from the electrospray; b) The concentration of neutral vapors drops inside the electrospray plume as neutral vapors gets ionized; c) concentration of ionized vapors. Image from "Numerical Modeling and Experimental Validation of a Universal SESI Source for Mass Spectrometric Gas Analysis in Real-Time" [104]. *Copyright © 2015 The Authors. Published by Elsevier B.V.*

Figure 9 shows the optimization of the ion transmission to the MS depending on the sample flow rate. The key parameters, i.e., the diameter of the orifice of the electrode and the distance from the electrode to the MS, were adjusted to enhance ion transmission and to avoid turbulences or dilution with the counter flow from the MS. The graph represents the optimum parameters for a counter flow from the MS of 1.6 lpm and sample flows of 0.01, 0.02 or 0.05 lpm. When the electrode is far from the MS inlet or the orifice diameter of the electrode is too big, then some ions do not reach the MS inlet (C1). On the other hand, when the electrode is too close to the MS inlet or the orifice diameter is too small, then there are turbulences inside the electrospray chamber leading to undesirable memory effects (C2).

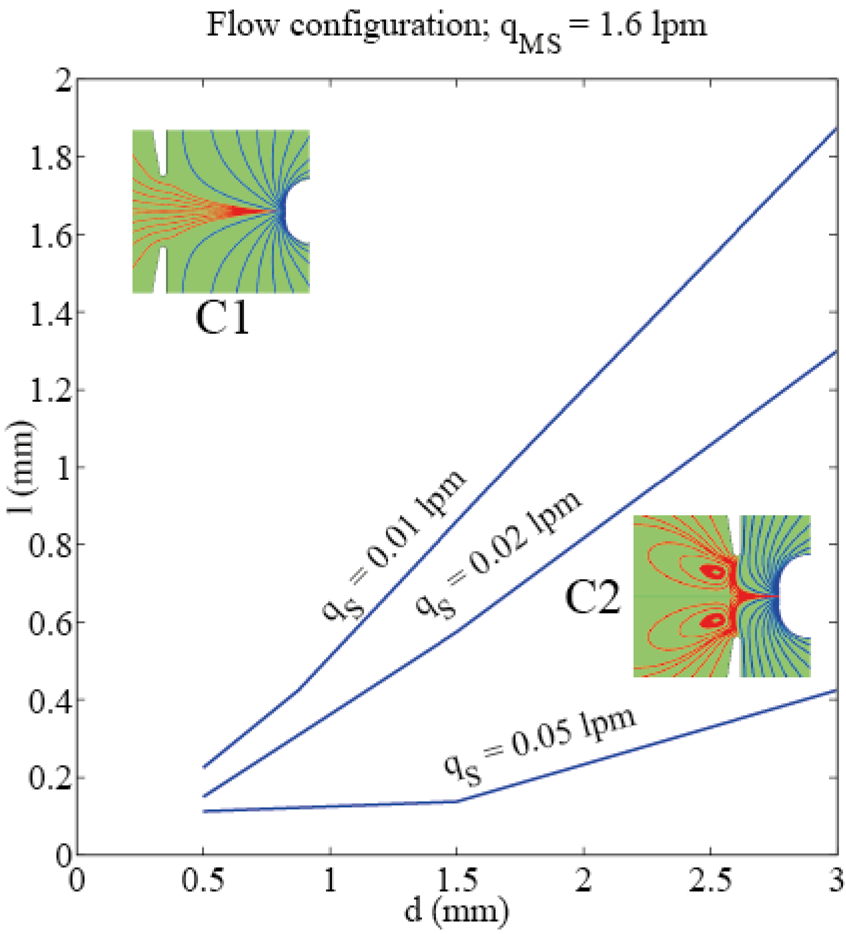

Figure 9. The lines represent the optimum L and d parameter calculated for a specific flow rate to improve the ion transmission to the MS avoiding memory effects. L means length from the electrode to the MS and d means diameter of the orifice in the electrode. Image from "Numerical Modeling and Experimental Validation of a Universal SESI Source for Mass Spectrometric Gas Analysis in Real-Time" [104]. *Copyright © 2015 The Authors. Published by Elsevier B.V.*

Additionally, one of the main goals of the ACID projects was to develop a robust and reproducible commercially available ionization source for pre-existing mass spectrometers. The LFSESI provided:

- A voltage splitter for the electrospray and the electrodes
- Control of the temperatures in the sample transfer line and in the electrospray area
- Mechanical alignment to optimize the ion transmission to the MS
- Precise capillary positioning in the electrospray chamber for good reproducibility
- Control of the electrospray pressure with a leak free vial holder where the electrospray solution can be kept safe while applying the high voltage
- An electrospray current display to check the stability

After optimization by means of numerical methods, the LFSESI was build and tested for the detection of volatiles and other applications like, for example, measuring plant metabolism [36]. A photograph of these first-generation LFSESI is shown in Figure 10. Additionally, this revolutionary design got patented:

- G. Vidal de Miguel, “Ionizer for vapor analysis decoupling the ionization region from the analyzer,” USPTO 8,461,523 B2, 2013.

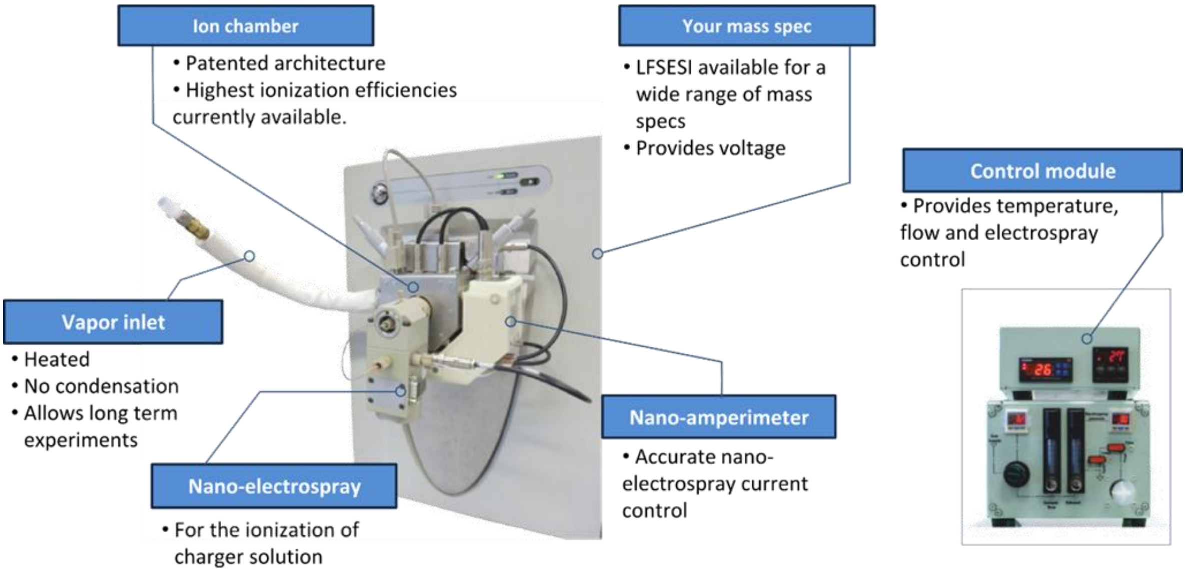

Figure 10. Photos of the LFSESI source coupled to an LTQ Orbitrap from Thermo and the external control module. In the figure, the main characteristics are highlighted. Image from LFSESI Technical brochure at [SEADM website]

1.6.1. Second generation of LFESI: Super SESI

The second generation of LFSESI simplifies the design eliminating one electrode, therefore reducing the surface susceptible to contamination. Additionally, the electrospray chamber can be taken apart and cleaned easily by ultrasonic cleaning while the rest of the ionization source can be cleaned with a wiper or just flushing ethanol though the sample line. The whole cleaning process can be accomplished in just 30 minutes. Finally, a specific vendor’s software helps post-processing the results, for example normalizing the data, and acknowledges contamination levels, warning the operator.

1.7. SESI: Applications

Several applications have been developed for the LFSESI source under the umbrella of the "ACID" project (see section 1.1). They are mainly focused on clinical breath analysis (Table 7), but also a few focuses on other biochemical subfields such as botany or microbiology. In this section, we highlight three innovative examples, previous to those developed in this Thesis.

Table 7. Breath Analysis by means of LFSESI focused on clinical breath analysis

Area	Object of the study	Samples size	Publication
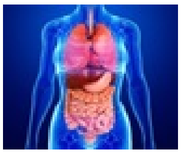 PHYSIOLOGY	Circadian clocks	3 individuals	Circadian Variation of the Human Metabolome Captured by Real-Time Breath Analysis [105]
	Aminoacids in blood	37 individuals	Real-Time Quantification of Amino Acids in the Exhalome by Secondary Electrospray Ionization-Mass Spectrometry: A Proof-of-Principle Study [106]
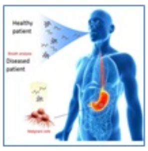 DISEASE DIAGNOSIS	Pulmonary fibrosis disease	21 patients 21 healthy individuals	Exhaled breath analysis by real-time mass spectrometry in patients with pulmonary fibrosis [107]
	Chronic Obstructive Pulmonary disease	22 patients 14 healthy individuals	Breath analysis in real time by mass spectrometry in chronic obstructive pulmonary disease [108]
 PHARMACOKYNETICS	Salbutamol effects	98 individuals	Metabolic effects of inhaled salbutamol determined by exhaled breath analysis [109]

1.7.1. Capturing in Vivo Plant Metabolism

The LFSESI source has been successfully applied to monitor, non-stop and in real time, the metabolism of a *Begonia semperflorens* for three days. The ionization source was capable of ionizing around 1200 different VOCs that might be released by the plant. 166 of these metabolites clearly followed day-night patterns. Monoterpenes like β-caryophyllene, that was identified by MSMS, were used to validate the results, as they are well known to be related to photosynthesis.

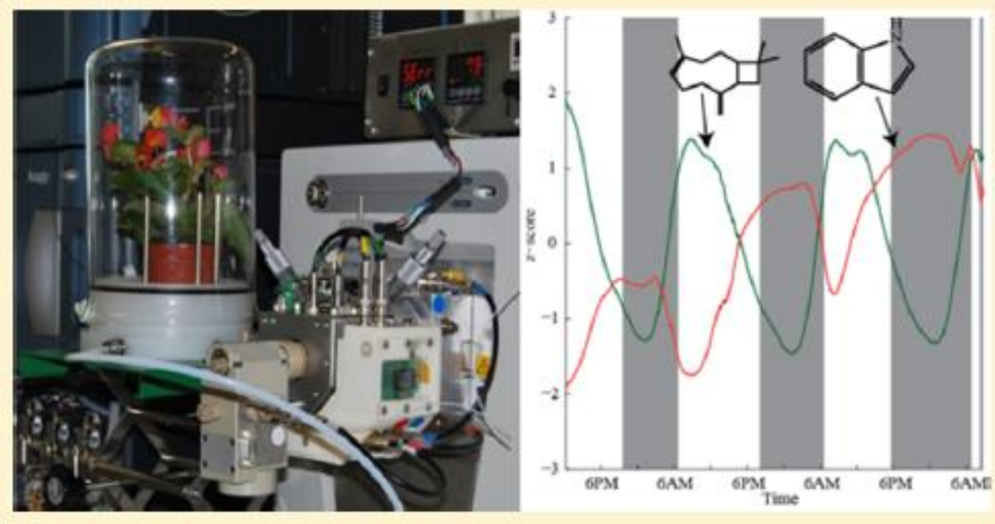

Figure 11 The image on the left shows the experimental set up. The image on the right shows the time traces of β-caryophyllene and indole during 3 consecutive days. These compounds are released by the plants following diurnal and nocturnal patterns. Image from: "[Capturing in vivo plant metabolism by real-time analysis of low to high molecular weight volatiles](#)" [36]. *Copyright © 2016, American Chemical Society*

Further results of this study can be found in the following scientific paper:

- Barrios-Collado, C.; García-Gómez, D.; Zenobi, R.; Vidal-de-Miguel, G.; Ibáñez, A. J.; Martínez-Lozano Sinues, P. "Capturing in vivo plant metabolism by real-time analysis of low to high molecular weight volatiles." *Anal Chem* 2016 88(4):2406-12.

1.7.2. Breath analysis

Blood and urine tests are commonly ordered by doctors for routine checks-ups or to help diagnose a patient health condition. Exhaled breath is another biofluid that contains biochemical information about the most volatile metabolites in blood. Actually, online breath analysis is a very promising technique as it is fast and completely non-invasive. However, its real potential remains to be exploited, as so far only a few breath tests have been approved for clinical assessment. The main limitation is that exhaled breath contains thousands of VOCs, most of them unknown. Therefore, most biomarkers discovery strategies rely on multivariate statistical comparison of breathprints between a healthy and a non-healthy control groups. Regardless of the efforts by several research groups, and as stated by Xia et al., *"Biomarkers must consist of positively identified compounds. Unknowns or tentatively identified features cannot (and never will) be approved for clinical laboratory testing*". Online breath analysis combined with high resolution mass spectrometry and MSMS capabilities could overcome these issues. Additionally, offline breath analysis techniques like GC-MS and LC-MS of EBC can help to fully identify the target compounds.

The LFSESI was tested on breath analysis studies in a pilot study to discriminate between tobacco smokers vs. non-smokers. The SESI-HRMS was capable of resolving about 1000 features in the breathprint of exhaled breath with masses up to 900 Da. The results of this study suggest that the smoking frequency can be determined by monitoring 4-hydroxy-2-alkenals and 4-hydroxy-alkadienals in exhaled breath. This is in agreement with previous studies associating cigarette smoking and products of lipid peroxidation [110]. Additionally, exogenous compounds like (trimethylsilyl)acetonitrile or 1,1-dioxide-tetrahydrothiophene (sulfolan) from the smoke of the cigarette were also found in exhaled breath of smokers. Using statistical methods, it is possible to predict smoking vs. non-smoking status with 100 % accuracy from the breathprint.

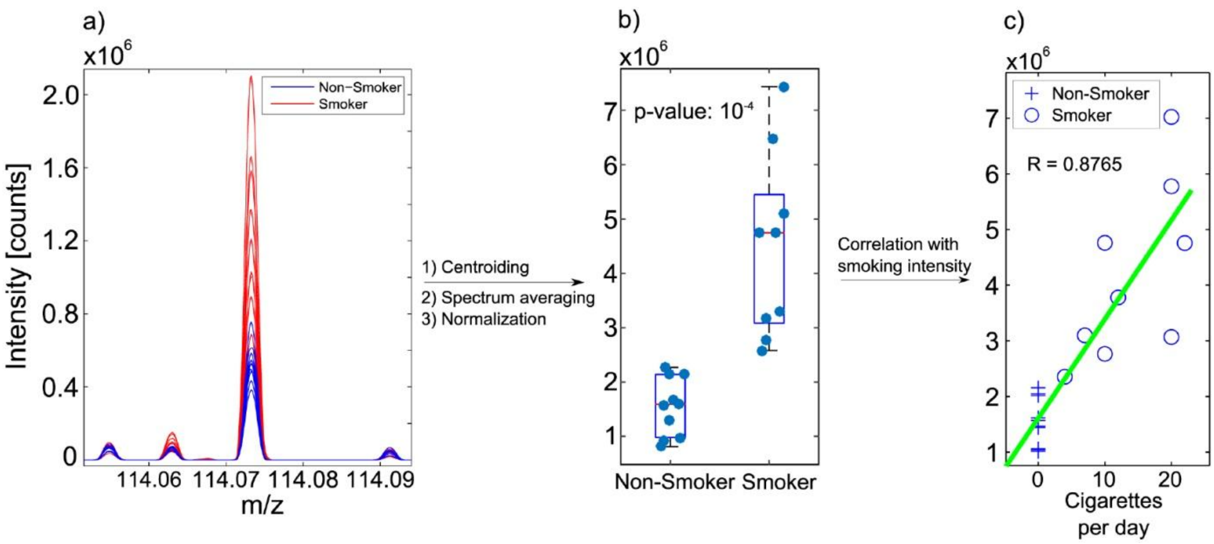

Figure 12. Differences between smokers and non-smokers: (a) overlaid breath mass spectra of all subjects in the region around the feature at m/z *114.0733; (b) box-plot of the average intensities per subject, split into smokers and non-smokers—this compound was significantly increased in smokers; (c) linear regression between the peak intensities of the feature at* m/z *114.0733 and smoking frequency. Image and citation from "Expanding metabolite coverage of real-time breath analysis by coupling a universal secondary electrospray ionization source and high-resolution mass spectrometry – a pilot study on tobacco smokers,"* [111]. Copyright: Attribution 3.0 Unported (CC BY 3.0)..

Further results of this study were published in the following scientific paper:

P. Gaugg, M. T.; Garcia Gomez, D.; Barrios Collado, C.; Vidal de Miguel, G.; Kohler, M.; Zenobi, R.; Martinez-Lozano Sinues, "Expanding metabolite coverage of real-time breath analysis by coupling a universal secondary electrospray ionization source and high-

resolution mass spectrometry – a pilot study on tobacco smokers," *J. Breath Res.*, vol. 10, 016010, 2016.

1.7.3. Bacterial identification

Secondary electrospray ionization can be used to identify the bacterial specific volatile metabolites and predict infections like periodontitis in saliva. Using our SESI source coupled to a HRMS, Lukas Breggy et al. found 120 bacteria specific compounds in pure bacterial culture of four oral bacteria strains: 13 for *A. actinomycetemcomitans*, 70 for *P. gingivalis*, 7 for *T. denticola* and 30 for *T. forsythia*. Therefore, in pure cultures, the bacteria strain could be identified by its volatile fingerprint using SESI-MS. Out of the 120 bacteria-specific compounds identified in vitro, 94 were found to be present in saliva of one patient suffering periodontitis. The concentration of 18 of the volatile compounds was found significantly higher in the saliva of that patient vs. two healthy controls. These results support the hypothesis that pathogen-related volatiles could be used as indicators of periodontitis development.

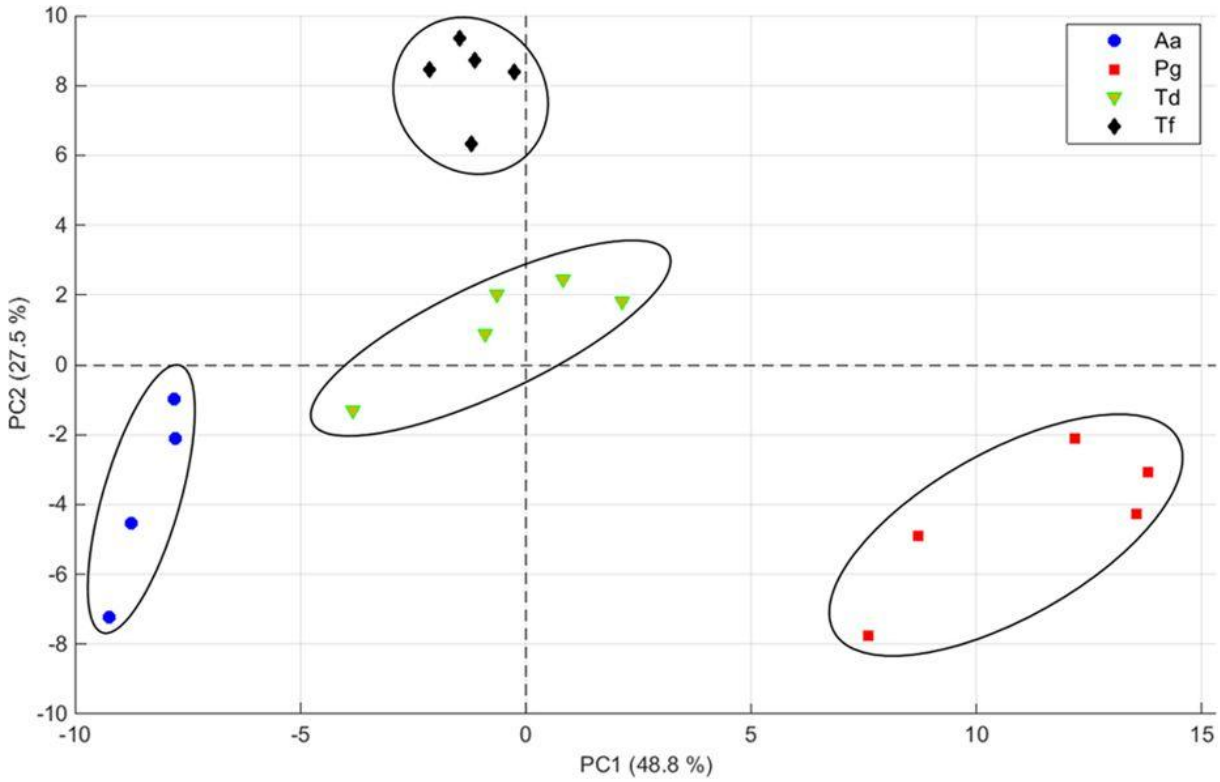

Figure 13. This image shows how the volatiles metabolites produced by pure bacteria cultures of each strain can be differentiated using statistical methods like PCA. Projection of the mass spectra from the biological replicates of the four different bacteria strains A. actinomycetemcomitans (circles), P. gingivalis (squares), T. denticola (triangles) and T. forsythia (rhomboids) onto a two-dimensional PCA subspace. Image from: "Differentiation of oral bacteria in in vitro cultures and human saliva by secondary electrospray ionization – mass spectrometry" [112]. *Copyright: Attribution 4.0 International (CC BY 4.0)*

The results of this study were published in the following scientific paper:

- L. Bregy *et al.*, “Differentiation of oral bacteria in in vitro cultures and human saliva by secondary electrospray ionization – mass spectrometry,” *Sci. Rep.* 5, 15163, 2015.

Chapter A - Secondary electrospray ionization proceeds via gas-phase chemical ionization

Analytical Methods

PAPER

View Article Online
View Journal | View Issue

Check for updates

Cite this: *Anal. Methods*, 2017, **9**, 5052

Secondary electrospray ionization proceeds *via* gas-phase chemical ionization

Alberto Tejero Rioseras,[abc] Martin Thomas Gaugg[a] and Pablo Martinez-Lozano Sinues[*ad]

Received 30th April 2017
Accepted 20th June 2017

DOI: 10.1039/c7ay01121k

rsc.li/methods

Our main goal was to gain further insights into the mechanism by which gas-phase analytes are ionized by interaction with plumes of electrospray solvents. We exposed target vapors to electrosprays of either water or deuterated water and mass analyzed them. Regardless of the solvent used, the analytes were detected in protonated form. In contrast, when the ionization chamber was humidified with deuterated water, the target vapors were detected in deuterated form. These observations suggest that either there is no interaction between analytes and electrospray charged droplets, or if there is any, a subsequent gas-phase ion–molecule reaction governs the process. Implications in practical examples such as breath analysis are discussed.

[a]*Department of Chemistry and Applied Biosciences, ETH Zurich, Zurich, Switzerland. E-mail: pablo.mlsinues@ukbb.ch*

[b]*SEADM, S.L., Spain*

[c]*Department of Analytical Chemistry, University of Cordoba, Spain*

[d]*University Children's Hospital Basel, University of Basel, Switzerland*

A.1. Secondary electrospray ionization proceeds via gas-phase chemical ionization

Alberto Tejero Rioseras [abc], Martin Thomas Gaugg [a] and Pablo Martinez-Lozano Sinues [*ad]

a Department of Chemistry and Applied Biosciences, ETH Zurich, Zurich, Switzerland. E-mail: pablo.mlsinues@ukbb.ch

b SEADM, S.L., Spain

c Department of Analytical Chemistry, University of Cordoba, Spain

d University Children's Hospital Basel, University of Basel, Switzerland

Received 30th April 2017, Accepted 20th June 2017

First published on 3rd July 2017

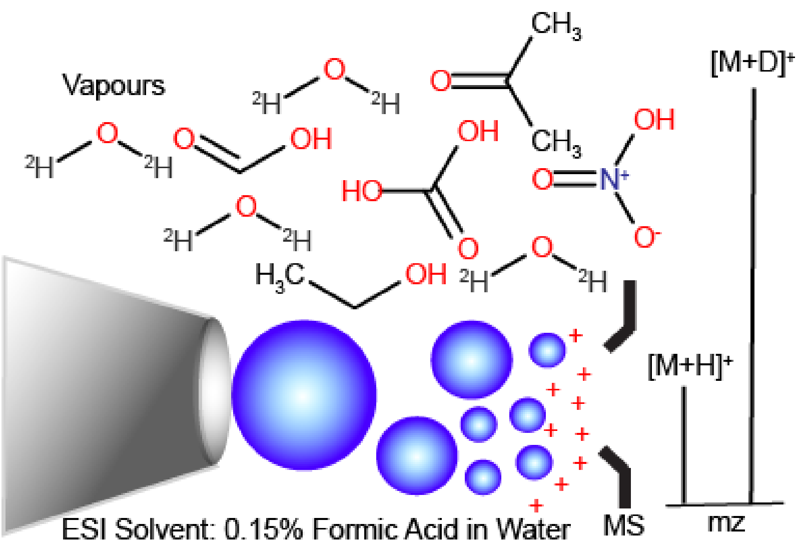

Figure 14. TOC. Table of contents: Secondary electrospray ionization proceeds via gas-phase chemical ionization

A.2. Abstract

Our main goal was to gain further insights into the mechanism by which gas-phase analytes are ionized by interaction with plumes of electrospray solvents. We exposed target vapors to electrosprays of either water or deuterated water and mass analyzed them. Regardless of the solvent used, the analytes were detected in protonated form. In contrast, when the ionization chamber was humidified with deuterated water, the target vapors were detected in deuterated form. These observations suggest that either there is no interaction

between analytes and electrospray charged droplets, or if there is any, a subsequent gas-phase ion–molecule reaction governs the process. Implications in practical examples such as breath analysis are discussed.

A.3. Introduction

The concept of “ambient ionization-mass spectrometry” essentially involves the exciting possibility of direct analysis with minimal sample preparation. [113][114] Well before a plethora of acronyms describing ambient ionization methods emerged during the second half of the 2000's, a number of pioneering papers describing similar concepts were presented. We feel that this pioneering work should be acknowledged in this special issue. For example, back in the 70's and early 80's Sciex's Trace Atmospheric Gas Analyzer (TAGA) was used to investigate human breath metabolites in real-time [115][116][117][118] and for environmental monitoring. [119] In these cases, chemical ionization coupled to atmospheric pressure ionization-mass spectrometry was at the core of such impressive early examples of the potential of what we call today ambient mass spectrometry. Similarly, during the early days of electrospray ionization development, John B. Fenn and co-workers noted the remarkable ability of electrosprays to ionize not only analytes in the liquid-phase, [58] but also pre-existing species in the gas-phase. [60][120][59] Similar observations on the potential of electrospray to ionize vapors were noted contemporarily by other groups. [121][122][123] Eventually, this technique was referred to as Secondary Electrospray Ionization (SESI) by Hill and co-workers to describe the use of a pure solvent electrospray to efficiently ionize gas-phase analytes. [64][61] Ever since, SESI has been used to detect trace vapors in a wide range of applications by different groups. [102][124][125][126][127][128][18][129] While it is generally accepted that SESI coupled to modern atmospheric pressure mass spectrometry is a sensitive method to detect gases at trace concentrations in real-time, the lack of full understanding of the SESI mechanism prevents making rational choices for the optimal parameters. In addition, with the advent of several ambient mass spectrometry techniques with overlapping features, fundamental aspects of such techniques have been blurred or confused. [130] Our goal in this study was to further previous work on the mechanism by which strictly vapor species are ionized in contact with electrospray plumes of pure solvents. [131][132]

A.4. Methods

A.4.1. SESI-MS

A commercially available SESI source (SEADM, Spain) was used in all experiments.[104] It was interfaced with an Orbitrap mass spectrometer (Thermo) and on one occasion (data shown in Figure 19) with a TripleTOF 5600+ (Sciex). The SESI was operated in the nanoliter range (~100 nL min^{-1}). We flushed the electrospray region with compressed air at a flow rate of 1 L min^{-1}. Compressed air contained around 5% relative humidity. Between the mass flow controller (Bronkhorst) and the ionization chamber, we placed a three-neck flask with rubber stoppers. Different liquids were injected into the flask to seed the carrier air with their corresponding vapors. Injected ambient vapors included water (H_2O), deuterated water (D_2O), ethanol (EtOH) and deuterated ethanol (EtOD). Relative humidity within the flask was recorded with a sensor (Alborn Almemo 2590A).

A.4.2. Breath analysis

SESI-MS breath analysis was accomplished by exhaling through the sampling tube of the ion source at a constant exhalation pressure of 10 mbar, as measured by a digital manometer.

The study was approved by the local ethical committee (EK 2012-N-49) and the subject gave written informed consent to participate.

A.5. Results and discussion

A.5.1. Deuterated spray solvent

Two (simplified) ionization scenarios are plausible in SESI: (i) the neutral species dissolve into the charged electrospray droplets to eventually be re-ejected in ionized form into the gas phase; (ii) electrospray droplets eject primary reactant ions that undergo an ion–molecule reaction with neutral species. Obviously, both mechanisms lead to very different scenarios to optimize the ionization efficiency. For the former mechanism, solubility of the analyte on the charging spray solvent would be crucial to maximize ionization efficiency. In the latter mechanistic scenario, analyte detection would be ultimately governed by thermochemistry. In order to determine which of the two potential scenarios apply in SESI we exposed neutral vapors to electrosprays of water and deuterated water. The exchange of hydrogen/deuterium has provided very valuable mechanistic insights since the initial developments of chemical ionization/mass spectrometry. [133][134][135][136] We hypothesized that, if the neutral vapors interact with the electrospray charged droplets to be re-emitted as gas-phase ions, they should be detected as $[M + D]^+$ ions.

Typical SESI-MS spectra has a rich chemical background in the range 50–500 Da.[137][138] For example, volatile polydimethylcyclosiloxanes in ambient laboratory air are well known interfering species in mass spectrometry. [139][140] Similarly, phthalates have also been reported to off-gas from vacuum O-rings. [141] Thus, we took advantage of the presence of these ubiquitous gas-phase contaminants to gain insights into how nano-electrosprays of solvent eventually lead to the ionization of such species. Figure 15 shows the mass spectra resulting of flushing the electrospray chamber with compressed air and using as spray solvent either 0.15% formic acid in H_2O (a) or 0.15% deuterated acetic acid (i.e. CD3-COOD) in D_2O (b). The resulting spectra are identical, including the known polysiloxanes and phthalates volatile species. Thus, regardless of the use of protonated or deuterated solvents, all species were detected in protonated form. This suggests that, even if the gas-phase species interact with the droplets to acquire a deuterium, eventually they exchange the deuterium with a proton in the gas-phase. In this case, with ambient water vapor, as the carrier gas contained ~5% of relative humidity.

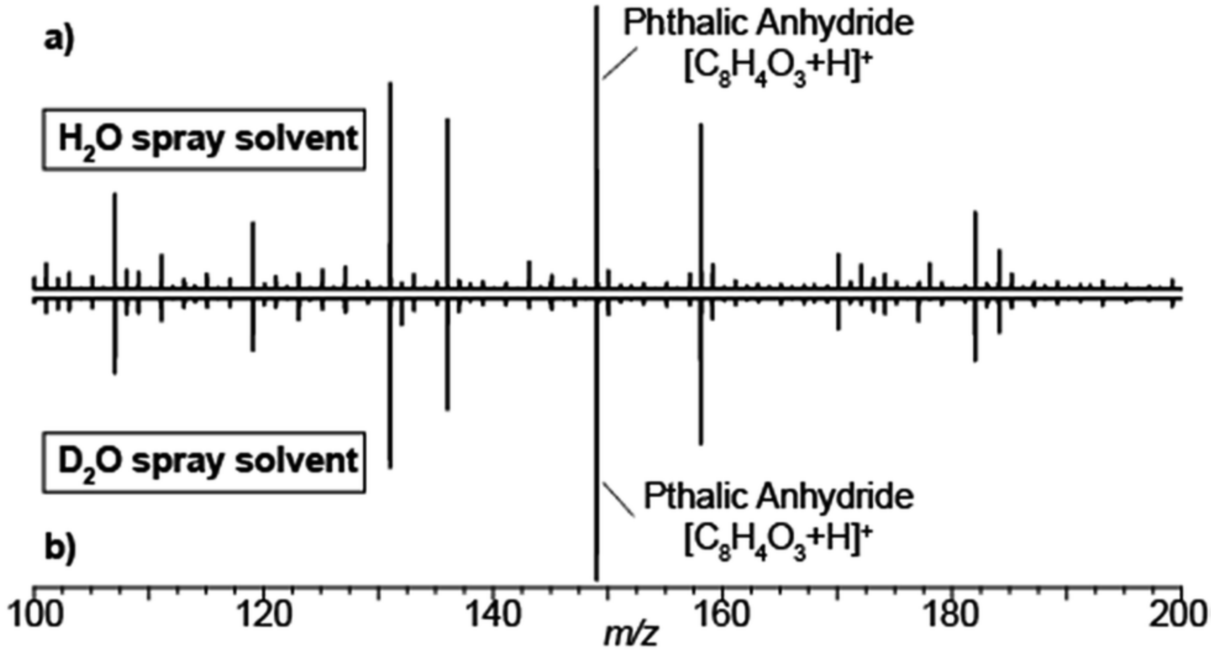

Figure 15 SESI mass spectra are independent of whether electrospray solvent is water or deuterated water. SESI chemical noise mass spectra with different electrospray solutions: (a) 0.15% formic acid in H2O; (b) 0.15% deuterated acetic in D_2O. In both cases, the analytes were detected in protonated form. For reference, the dominating peak of phthalic anhydride is labelled

A.5.2. Doping carrier gas with deuterated vapors

The data shown in Figure 15 b) strongly suggest that a gas-phase proton reaction takes place in SESI. To further confirm this hypothesis, we humidified the carrier air with either water or deuterated water. As a result of humidifying with deuterated water, the entire chemical background mass spectrum shifted by 1 Da. Figure 16 shows a zoomed view of the mass spectrum in the region of one representative example of a phthalate ($C_{16}H_{22}O_4$) and a polysiloxane ($C_{12}H_{36}Si_6O_6$) with H_2O-humidified air (bottom) and D_2O-humidified air (top). The fact that these species deuterate when the air is seeded with deuterated water vapor, but not when deuterated water is used in the spray solvent, strongly indicates that gas-phase ion chemistry plays a critical role in SESI, if not the only one.

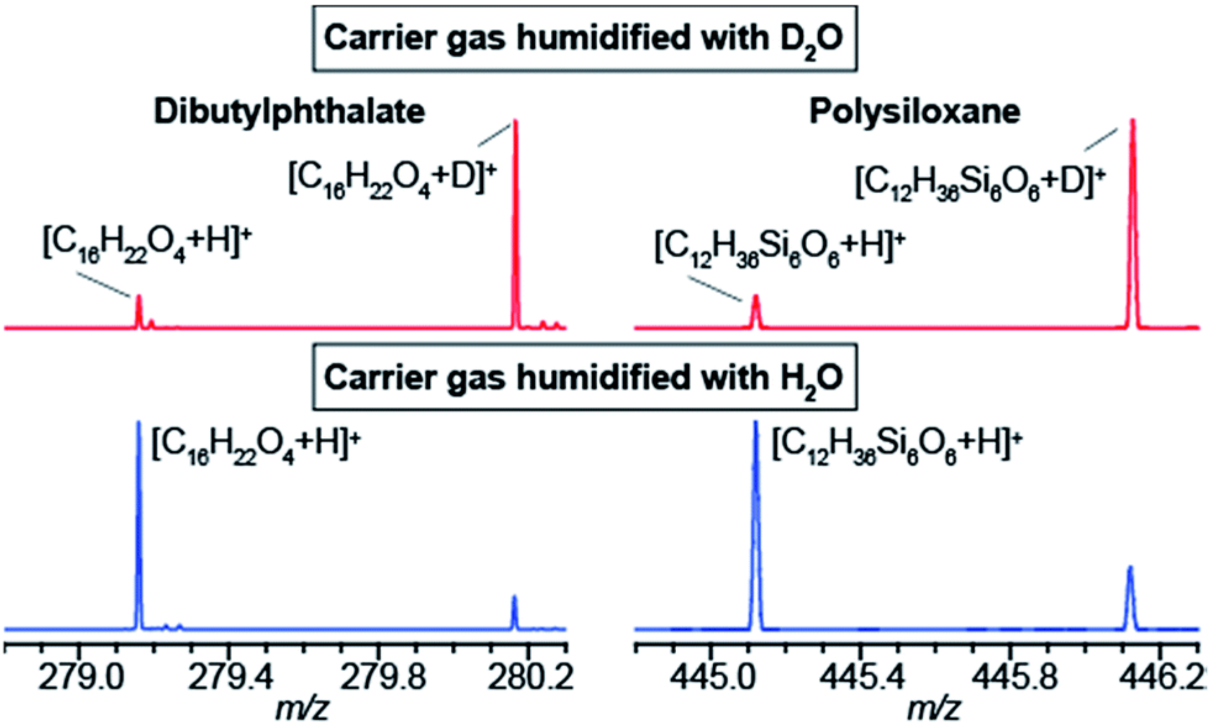

Figure 16. Humidifiying the carrier air with deuterated water leads to deuterated ions in SESI-MS. Electrospray solvent was 0.15% formic acid in H_2O. Mass spectra of dibutylphthalate (left) and a polysiloxane (right). As expected, humidifying with H_2O leads to protonated species (i.e. $[M + H]^+$; bottom) and humidifying with D_2O leads to deuterated species (i.e. $[M + D]^+$; top)

Further insight was gained by seeding the carrier gas with ethanol instead of water. Ethanol has a greater gas-phase proton affinity than water (776.4 vs. 691 kJ mol^{-1}). Thus, it would be expected that, if SESI is governed by thermochemistry of the water and ethanol proton transfer reaction, it would be detected in the presence of the former but not the latter. Figure 17 a) and b illustrate the behavior of another representative compound (benzothiazole; C_7H_5NS).[141] Figure 17 a) shows the $[M + D]^+/[M + H]^+$ ratio before and after humidifying with D_2O. Clearly, at the time point of D_2O injection, the protonated species decays, while simultaneously the deuterated adduct rises. Figure 17 b) shows the result of a similar experiment, but instead of D_2O, we seeded the SESI chamber with vapors of EtOD. Likewise, the deuterated adduct rose sharply in parallel with the relative EtOD concentration in air, suggesting a direct correlation between EtOD levels and $[C_7H_4NS + D]^+$ signal intensity. In contrast, the polysiloxanes experienced the same response upon exposure to D_2O vapors (Figure 17 c), but the signal dropped abruptly to 0 after introducing EtOD (Figure 17 d). Hence, Figure 17 c) and d suggests that the polysiloxane has a gas-phase proton affinity greater than water, but lower than ethanol.

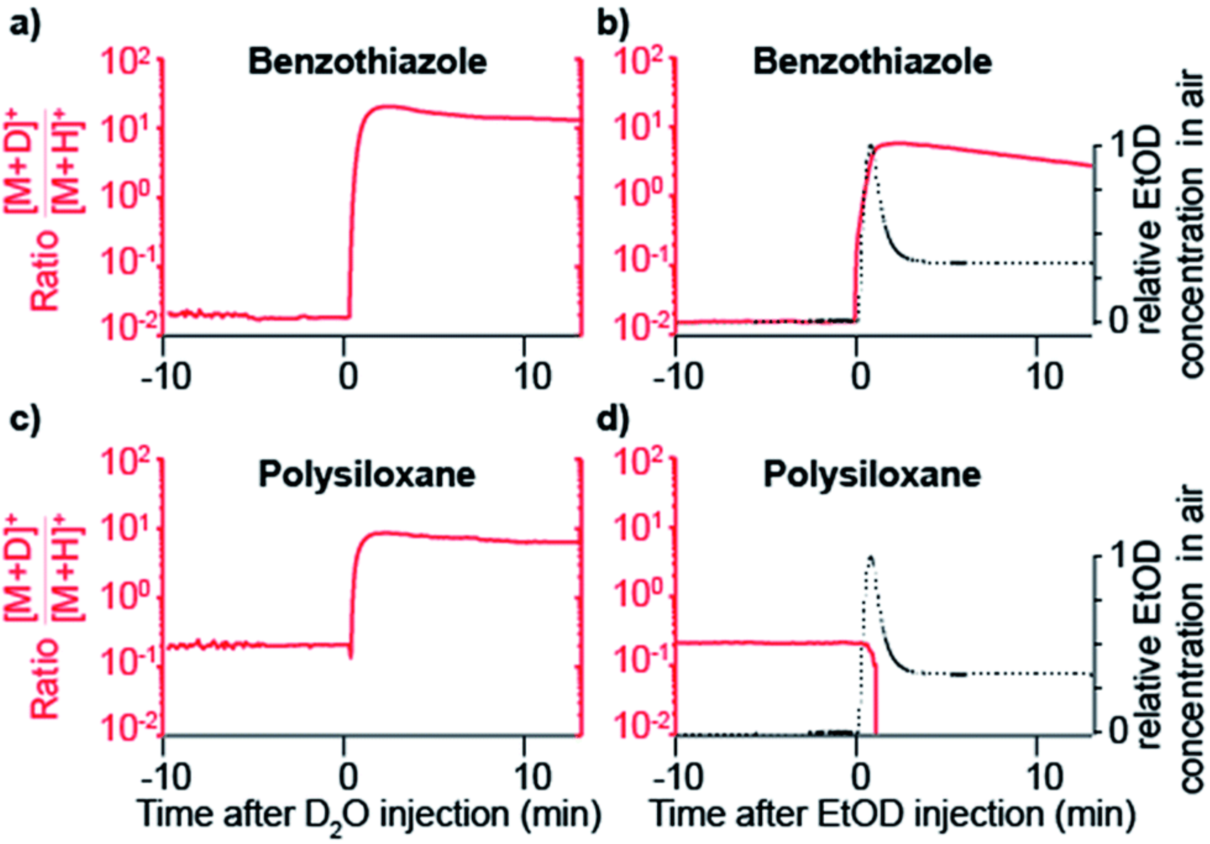

Figure 17 Gas-phase proton affinity of seeding vapors have an effect in SESI analyte detection. Benzothiazole deuterates after adding vapors of D_2O (a) and EtOD (b) in the carrier gas. In contrast, the deuterated form of the polysiloxane was detected with D_2O (c), but depleted upon exposure to EtOD vapors (d). Relative concentrations of EtOD in the carrier gas are shown for reference

To confirm that gas-phase thermochemistry ultimately dictates which analytes are detectable by SESI, we chose 2,2,2-trifluoroethanol as target analyte vapor. This particular compound has gas-phase proton affinity of 700.2 kJ mol^{-1}, [142] which is in between that of water and ethanol. As expected, this compound was detected as deuterated ion upon doping the carrier gas with D_2O, but not when EtOD was used.

Figure 18 a) shows how the $[M + D]^+/[M + H]^+$ ratio rises sharply immediately after injecting D_2O. For reference, relative humidity levels, as measured with the sensor, are overlaid. When the same experiment is performed but instead of D_2O, EtOD is injected in the carrier gas, 2,2,2-trifluoroethanol is no longer detected (Figure 18 b).

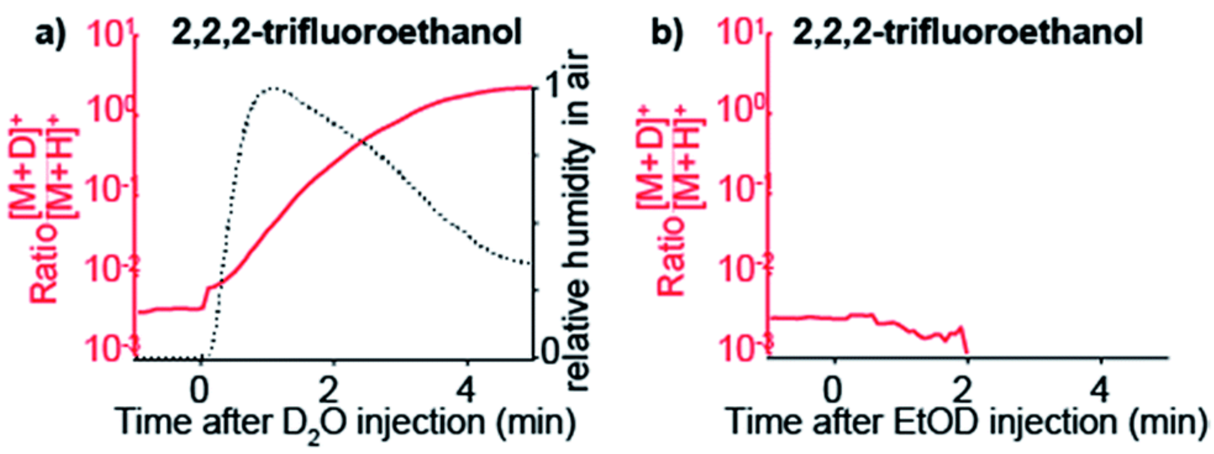

Figure 18. SESI selectivity towards target vapors is governed by the proton affinity of the dopant seeded in the carrier gas. Response of 2,2,2-trifluoroethanol vapors in the presence of D_2O (a) and EtOD (b) in the carrier gas. When D_2O is introduced in the system the protonated ion declines in favor of the deuterated species (a). In contrast, when EtOD is introduced in excess in the carrier gas the signal of $[C_2H_3F_3O + H]^+$ drops quickly to zero, but the $[C_2H_3F_3O + D]^+$ ion is not formed (b). This is explained by the fact that the gas-phase proton affinity of 2,2,2-trifluoroethanol is greater than water, but smaller than ethanol

We have just shown compelling evidence indicating that SESI leads to protonated species, even if the spray solvent is deuterated, as long as some water vapor is present in the carrier gas of the sample (in our case ~5% relative humidity). This directly leads to a gas-phase chemical ionization scenario, at least in the final step of the process. Our hypothesis to explain this observation is that, initially, $[(D_2O)_n + D]^+$ clusters are ejected from the electrospray droplets by ion evaporation. [100][101][143][144][145] These primary ions rapidly exchange deuterium by protons with ambient water, which is in excess in ambient air, leading to eventually dominating $[(H_2O)_n + H]^+$ clusters. These water clusters would then undergo a proton transfer reaction with neutral vapor species, provided the reaction is thermodynamically favorable. Of course, kinetically-controlled reactions are also conceivable for slow proton transfer, which indeed is known to be the case for many reactions in chemical ionization. [145][146][147] For example, under our particular experimental conditions in Figure 15 b), we formed the electrospray by infusing D_2O at ~100 nL min^{-1}. If we assume that all D_2O is immediately vaporized and considering that the ambient air flushing the SESI chamber at 1 L min^{-1} contained 5% relative humidity, the expected ratio H_2O/D_2O in the ionization chamber is in the order of 10. This excess of H_2O would then shift the equilibrium of reactant ions from $[(D_2O)_n + D]^+$ towards $[(H_2O)_n + H]^+$. This hypothesis is supported by the data shown in Figure 19. It shows a SESI mass spectrum using water–formic acid as electrospray solvent and the carrier gas bathing the SESI chamber humidified with a 50/50 mixture of H_2O and D_2O. It shows two binomial distributions for the water trimer and tetramer with all possible combinations of hydrogen and deuterium atoms.

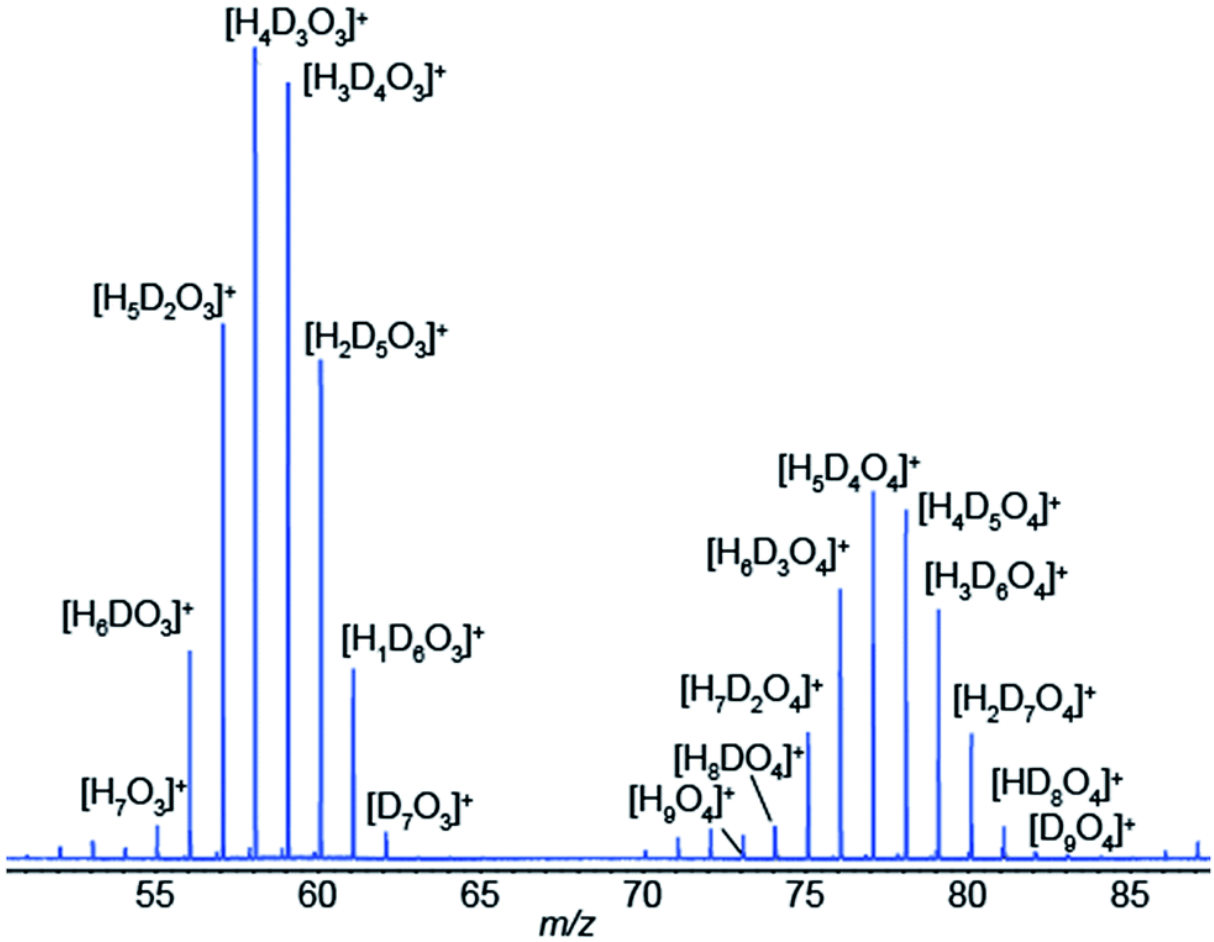

Figure 19. SESI gas-phase reactant ions in the presence of humidity are water clusters. Example of an electrospray of 0.15% formic acid in water flushed with a 50/50 mixture of H_2O/D_2O vapors, leading to all possible $[H_xD_yO_3]^+$ (x + y = 7) combinations for the trimer (left-hand-side) and $[H_xD_yO_4]^+$ (x + y = 9) for the tetramer (right-hand-side)

Warnings about the importance of gas-phase ion chemistry in the standard electrospray process have been given in the literature. [148] For example, Enke and co-workers convincingly showed that analytes present in solution are very likely to be ultimately depleted in the gas phase by the presence of molecules that are stronger gas-phase bases, resulting in ion suppression. [142] Our data support this view and extend it to SESI. Hence, we have advocated that one should be cautious when distinguishing the real-time analysis of gas- vs. condensed phase analytes with sprays of pure solvent. [131] The main reason is that a number of studies have suggested that for samples delivered in aerosol form (i.e. extractive electrospray ionization), solubility of the analytes and interaction with the charging spray solvent is the limiting factor to be considered. [149][150] We argue here that, in the case of vapor samples (i.e. secondary electrospray ionization), gas-phase ion chemistry considerations are ultimately governing the detection of such analytes. For this reason, we claim that water electrosprays operated in the cone-jet mode [151] are preferred in positive ion mode SESI over widely used H_2O/MeOH mixtures, as MeOH will probably deplete species detectable otherwise.

A.5.3. Breath analysis

The analysis of exhaled metabolites in breath is an attractive approach to monitor health status and therapeutic intervention. [152] Selected ion flow tube mass spectrometry (SIFT-MS) [153] and proton transfer reaction mass spectrometry (PTR-MS) [154] are two well established methods for real-time detection of volatiles in breath. One of the main strengths of SIFT-MS is its capability to provide absolute quantifications of trace gases in the parts-per-million to parts-per-billion range. [155] PTR-MS provides semi-quantitative information with limits of detection down to parts-per-trillion. Exhaling onto an electrospray plume in front of an atmospheric pressure ionization MS is another highly efficient way to perform such analyses. A wide range of species have been reported using this method; however chemical identification and absolute quantification of the species detected remain a challenge. Given that, low-volatility species such as urea have been detected using this approach, [156][157] there has been some debate regarding whether the metabolites detected in breath following this approach come in aerosol form or simply the method is sensitive enough to detect low-volatility vapors. [124][156][157] The debate is of importance because aerosols and volatiles have different physiological origins and therefore offer different diagnostic opportunities. Aerosols in breath are thought to be generated by the turbulence-induced aerosolization mechanism of the fluid film in the respiratory tract. [158] This leads to a high variability on particle size distribution and number depending on the inhalation and exhalation maneuvers [158] and hence difficulties in reproducibility. In contrast, the origin of gas-phase species is predominantly blood borne and therefore enable monitoring different metabolic processes. [159] We argue that breath analysis by SESI-MS detects volatile and non-volatile gas-phase species following that: (i) truly nonvolatile macromolecules such as cytokines have been reported in exhaled breath condensate,59 but are not detectable by SESI- SESIMS; (ii) exhaling through a particle filter leads to essentially the same mass spectrum as without such a filter; [156] (iii) analytical [132] and numerical [104] models capture experimental observations with reasonable accuracy in systematic mechanistic studies [131] and (iv) we have shown how small amounts of injected drugs in mice can be detected in breath shortly afterwards and correlate with plasma levels. [67][160] For example, ketamine and its main metabolites, which have molecular weights in the range of 250 Da and a relatively low estimated vapor pressure in the order of 8.5×10^{-5} mmHg at 25 C (SPARC online calculator). [161]

To further shed light on this mechanistic issue we performed SESI-MS breath analysis using H_2O and D_2O as spray solvents. Aerosolized samples have been shown to interact in the liquid-phase between charged electrospray droplets and neutral sample aerosols. [149] Hence we hypothesized that, if the detected compounds would come in aerosol form, they would necessarily pick up a deuterium from the D_2O charged droplets and a proton from H_2O sprays. Figure 20 shows the breath mass spectrum of one subject exhaling onto a spray of 0.15% formic acid in water (a) and 0.15% acetic acid-d_4 in D_2O (b). In both cases, the spectra were identical, with the vast majority of the species detected in protonated form. This may also explain the noted sensitivity enhancement of SESI in the presence of water vapor in breath. [156][66] Admittedly, these data cannot completely exclude the possibility of exhaled aerosols and vapors dissolving in the charged droplets, generation of $[M + D]^+$ gas-phase ions and subsequently exchanging H–D in the gas phase with ubiquitous water vapor. However, it clearly shows that, even if this is the case, gas-phase ion chemistry ultimately plays a critical role in the ionization of breath metabolites.

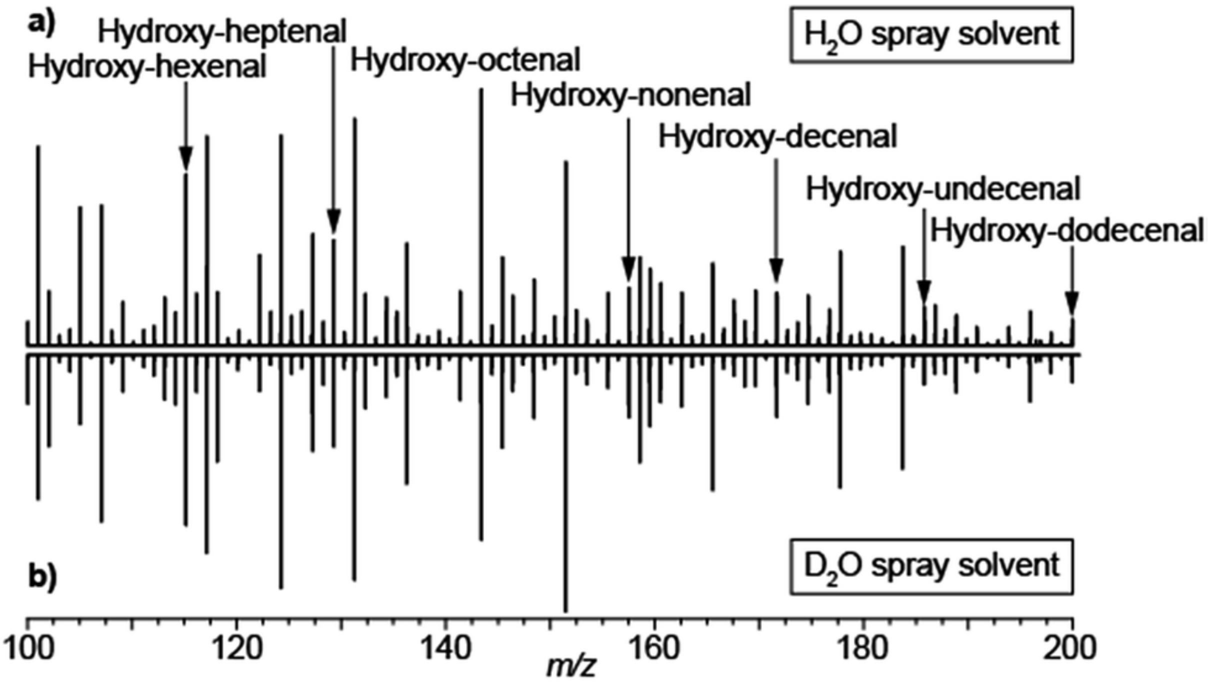

Figure 20 Breath metabolites are ultimately protonated via gas-phase ion–molecule reactions in SESI: (a) breath mass spectrum using 0.15% formic acid in water; (b) breath mass spectrum using 0.15% acetic acid-d_4 in heavy water. Breath metabolites were detected in protonated form regardless of the solvent used to generate the electrospray. For reference, a series of hydroxy-alkenals previously identified by García-Gómez [162] *are indicated*

A.6. Conclusions

We conclude that (i) neutral vapors carried in an air stream (5% relative humidity) and exposed to an electrospray of deuterated water leads to protonated ions; (ii) inversely, neutral vapors carried in an air stream seeded with deuterated solvents (e.g. D_2O), and exposed to an electrospray of water leads to deuterated ions; (iii) gas-phase proton affinity of the target analytes plays a crucial role in whether or not they are finally detected in SESI; (iv) breath metabolites are detected in protonated form regardless of whether the solvent used is H_2O or D_2O. These observations lead us to conclude that, in the final stage of SESI, gas-phase ion–molecule reactions govern the mechanism by which electrosprays ionize vapor species.

A.7. Acknowledgements

We are thankful to Prof. Renato Zenobi for hosting the ACID project at ETH Zurich and for critically reading this manuscript. We gratefully thank Dr Juan Zhang (Novartis AG) for the donation of the LTQ Orbitrap instrument used in this study and Prof. Malcolm Kohler (University Hospital Zurich) for giving access to the Sciex mass spectrometer. The research leading to these results has received funding from the European Community's Seventh Framework Programme (FP7-2013-IAPP) within the project “Analytical Chemistry Instrumentation Development” (609691). This work is dedicated to Prof. John B. Fenn (1917–2010) on the occasion of the centennial celebration of his birth.

Chapter B - Comprehensive Real-Time Analysis of the Yeast Volatilome

www.nature.com/scientificreports

SCIENTIFIC REPORTS

OPEN

Comprehensive Real-Time Analysis of the Yeast Volatilome

Alberto Tejero Rioseras[1,2,3], Diego Garcia Gomez[1,3], Birgitta E. Ebert[4], Lars M. Blank[4], Alfredo J. Ibáñez[1,5] & Pablo M-L Sinues[1,6]

Received: 30 May 2017

Accepted: 12 October 2017

Published online: 27 October 2017

While yeast is one of the most studied organisms, its intricate biology remains to be fully mapped and understood. This is especially the case when it comes to capture rapid, *in vivo* fluctuations of metabolite levels. Secondary electrospray ionization-high resolution mass spectrometry SESI-HRMS is introduced here as a sensitive and noninvasive analytical technique for online monitoring of microbial metabolic activity. The power of this technique is exemplarily shown for baker's yeast fermentation, for which the time-resolved abundance of about 300 metabolites is demonstrated. The results suggest that a large number of metabolites produced by yeast from glucose neither are reported in the literature nor are their biochemical origins deciphered. With the technique demonstrated here, researchers interested in distant disciplines such as yeast physiology and food quality will gain new insights into the biochemical capability of this simple eukaryote.

B.1. Comprehensive Real-Time Analysis of the Yeast Volatilome

Alberto Tejero Rioseras[1,2,3], Diego Garcia Gomez[1,3], Birgitta E. Ebert[4], Lars M. Blank[4], Alfredo J. Ibáñez[1,5] & Pablo M-L Sinues[1,6]

1 Department of Chemistry and Applied Biosciences, ETH Zurich, 8093, Zurich, Switzerland.

2 SEADM S.L., C\ José Lázaro Galdiano, 1, Madrid, 28036, Spain.

3 Department of Analytical Chemistry, University of Cordoba, Cordoba, Spain.

4 Institute of Applied Microbiology – iAMB, Aachen Biology and Biotechnology – ABBt, RWTH Aachen University, Worringerweg 1, Aachen, 52074, Germany.

5 Instituto de Ciencias Ómicas y Biotecnología Aplicada - Pontificia Universidad Católica del Perú (ICOBA-PUCP), Lima, Peru.

6 University Children's Hospital Basel, Department of Biomedical Engineering, University of Basel, Basel, Switzerland. Correspondence and requests for materials should be addressed to A.J.I. (email: aibanez@pucp.edu.pe) or P.M.-L.S. (email: pablo.mlsinues@ukbb.ch)

Received: 30 May 2017

Accepted: 12 October 2017

Published: 27 October 2017

B.2. Abstract

While yeast is one of the most studied organisms, its intricate biology remains to be fully mapped and understood. This is especially the case when it comes to capture rapid, in vivo fluctuations of metabolite levels. Secondary electrospray ionization-high resolution mass spectrometry SESI-HRMS is introduced here as a sensitive and noninvasive analytical technique for online monitoring of microbial metabolic activity. The power of this technique is exemplarily shown for baker's yeast fermentation, for which the time-resolved abundance of about 300 metabolites is demonstrated. The results suggest that a large number of metabolites produced by yeast from glucose neither are reported in the literature nor are their biochemical origins deciphered. With the technique demonstrated here, researchers interested in distant disciplines such as yeast physiology and food quality will gain new insights into the biochemical capability of this simple eukaryote.

B.3. Introduction

Metabolites are small molecules that provide a direct readout of organisms' phenotypes and cellular activity [163]. During metabolic processes [164], a subset of the metabolites, the so-called volatile organic compounds (VOCs) are released to the ambient at normal pressure and temperature. VOCs are organic compounds typically C_5-C_{20} [165] with molecular weights up to 500 Da [166], boiling point up to 250 °C [167] and high vapor pressure. Many living organisms including humans, animals, plants, and even microorganisms, produce large varieties of VOCs [168]. The sum of all VOCs produced by an organism has been termed the volatilome [169][170][171]. While some VOCs have dedicated pathways, many are intermediates of anabolic pathways or are synthesized by moonlighting activities of enzymes [172], hence reflect promiscuous enzymatic activities in the underlying metabolic network [173][174]. Although generally produced in small concentrations (parts-per-million to parts-per-trillion range) [175], VOCs reflect the metabolic state of a cell and, thus, can be used to understand many biological processes such as, e.g., oxidative stress [176][177][178]. VOCs are also at the core of the flavor and fragrance manufacturing, an industry with a focus on plant-derived VOCs. Volatile metabolites are also of importance in the food industry as taste and smell is informing the consumer on the quality of a product. A volatile metabolite, industrially produced in large quantities, is alcohol (i.e., ethanol), synthesized by yeast from glucose during fermentation. Interestingly, since ethanol is neutral-flavored, the taste of fermented drinks originates from minor compounds, such as higher alcohols, aldehydes, esters, and acids. Most of these metabolites are volatile and intensely flavored. Indeed, monitoring VOCs (i.e., diacetyl, 2,3-pentanedione) abundance in beer is industrial standard, since it has a strong effect on the product quality [179]. The economic impact of monitoring such compounds is thus vast[180].

Gas chromatography-mass spectrometry (GC-MS)-based methods have been the workhorse to analyze VOC profiles. The main limitation of such methods is that it requires sample manipulation, resulting in laborious procedures [181][182]. A more recently deployed approach is ion mobility spectrometry, which provides near real-time analysis, but its poor resolution compared to mass spectrometry compromises metabolite coverage and compound identification capabilities [183][184][185][186]. Real-time mass spectrometric methods used for on-line quantification of a handful of VOCs include proton transfer reaction (PTR) [175] and selected ion flow tube (SIFT) [187]. A recent mass spectrometric method based on direct flow injection, has shown to monitor metabolite dynamics in the 15–30 second range and was used to gain insights into cellular responses to environmental changes [188].

In line with such efforts to develop instrumentation capable of monitoring time-resolved metabolic information, we show here how secondary electrospray ionization (SESI) [123][61][60][59][124][18][67][112][189][190][111][36][191] coupled to high resolution mass spectrometry (HRMS) captures on-line an unprecedented wealth of volatile analytes emitted in vivo by growing baker's yeast (*Saccharomyces cerevisiae*).

B.4. Results and discussion

B.4.1. Volatiles emitted by wild type *Saccharomyces cerevisiae* during growth in $^{13}C_6$-glucose

Initially, to confirm that SESI-HRMS is indeed suitable to track growth-related metabolites in real-time, we grew the yeast in glucose minimal medium and monitored well-known end products [192] like ethanol or acetic acid. As expected, we observed the production of ethanol despite full aeration because baker's yeast is Crabtree positive. Figure 21 a) shows such an example, in which ethanol production kicked off shortly after the start of the growth experiment. The concentration increased exponentially to then level off, presumably concomitant with glucose depletion. Eventually, ethanol started to decrease again. Such a diauxic growth is expected for yeast fermentation on glucose. The depletion kinetic, however, seems too fast to be solely explained by metabolization. Evaporation of this volatile metabolite might have been enforced by the vigorous aeration (25 gas volume flow per unit of liquid volume per minute; vvm) of the bioreactor. When ethanol was almost completely depleted, we spiked glucose into the medium (~27 h; see Methods section for experimental details). The cells immediately re-started glucose consumption as evidenced by the instantaneous production of ethanol and acetic acid.

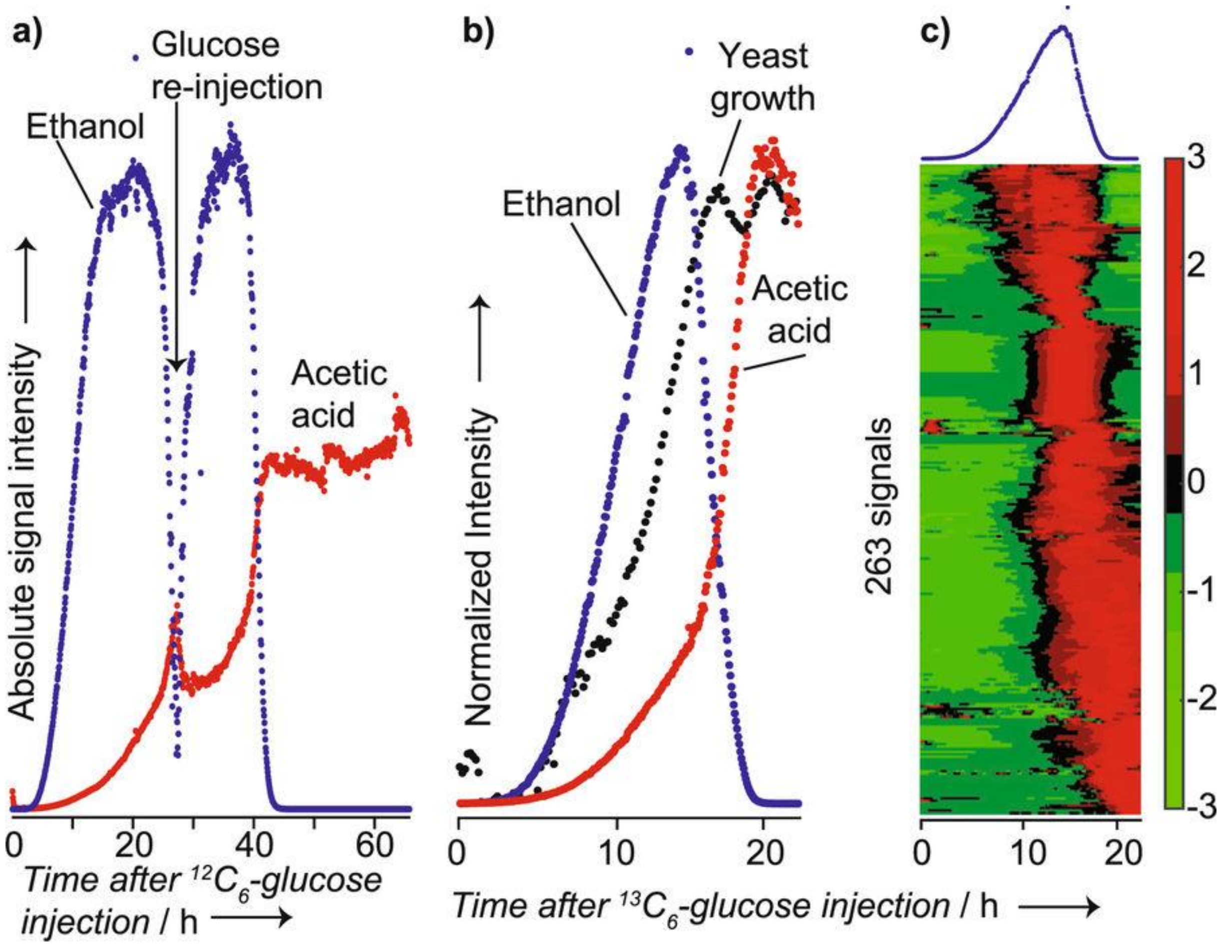

Figure 21 Real-time monitoring of volatile metabolites during yeast growth; (a) raw time profiles of ethanol (detected as the dimer) and acetic acid during growth on $^{12}C_6$-glucose and re-injection of glucose after ~27 h; (b) normalized raw time profiles of ethanol (detected as the dimer), acetic acid and the image signal captured by a time-lapse camera during growth on $^{13}C_6$-glucose; c) heatmap showing 263 time-dependent signals during yeast growth. All the signals in the heatmap were labeled with ^{13}C. For reference, the ethanol signal is shown on the top

One of the advantages of SESI coupled to high-resolution mass spectrometry (HRMS) is that it can detect a wide range of analytes, including species of low vapor pressure at concentrations in the low parts-per-trillion range [62]. Indeed, along with the well-known volatile metabolites ethanol and acetic acid, numerous other volatile metabolites were detected during yeast growth. Thus, we replicated the experiment independently; however, we administered glucose labelled with ^{13}C in all six carbon atoms. ^{13}C label incorporation into metabolites synthesized from glucose allowed differentiating analytes of biological origin from environmental contaminants or media components. Figure 21 b shows the resulting time profiles of ethanol, acetic acid, and yeast biomass estimated from image grayscale levels in a time-lapse video. The observed correlation between increase of ethanol and production of biomass confirmed that the analytical setup allowed capturing biological events soundly. ^{13}C-label incorporation confirmed that 263 signals observed in the previous experiment originated from the yeast's metabolism. In addition, we conducted a negative control experiment whereby a bioreactor was run under the very same conditions but without inoculation with yeast (monitored for ~17 hours). As expected, neither ethanol nor acetic acid were produced (Figure S 1).

The time-resolved dataset of the yeast fermentation enabled a comprehensive overview of the volatilome dynamics (Figure 21 c). The heatmap is ordered by a cluster analysis, easing the visualization of the different time-profiles. Note that these metabolites were captured simultaneously and in real-time without any sample manipulation. “Table S 1” lists the 263 signals detected in both experiments (i.e., labeled and non-labeled glucose) as they appear in the heatmap of Figure 21 c. Interestingly, homologous series of compounds tend to cluster together, suggesting similar kinetics for closely related metabolites. For example, one cluster comprised the homologous series C_6H_{10}, C_7H_{12}, C_8H_{14} and C_9H_{16}. This bouquet of volatile metabolites remains to be annotated, but the chemical formula suggests that these compounds could well be alkadienes. Several olefinic compounds have been reported for diverse organisms [16][193][194][195][196]. 1,3-octadiene (C_8H_{14}), for example, is produced by several fungi and predicted to be a degradation product of linoleic acid, but the responsible enzymes and encoding genes are yet to be identified [197]. None of the potential alkadienes detected here were previously identified in the headspace of yeast fermentations.

B.4.2. Volatiles emitted by wild type and mutants of *Saccharomyces cerevisiae* during growth in $^{13}C_1$-glucose

To demonstrate that the detected series of hydrocarbons were produced by the baker’s yeast and not by a biological contamination of the bioreactor, we repeated the measurements. Specifically, we performed a comparison of two baker’s yeast mutants (i) devoid of the oxidative pentose phosphate pathway (*zwf*1), which is associated with oxidative stress response or (ii) limited in glycolysis (*pfk*1); and compared them with a wild type (WT) strain. To discriminate in vivo pathway usage, we fed WT, *zwf*1, and *pfk*1 with $^{13}C_1$-glucose. Figure 22 a) shows a zoom of the m/z range 200–215 of a typical mass spectrum acquired during such measurements for WT during the stationary phase. It shows two distinct bell-shaped isotopic distributions. The first one assigned to a series of $C_x(^{13}C)_yH_{25}O_2$ with x ranging 11 to 7 and y 1 to 5 (i.e., molecular formula $C_{12}H_{25}O_2$). Similarly, another more abundant distribution of $C_{15}H_{25}$ (^{13}C ranging from 2 to 9) was clearly observed. Apart from high resolution (~ 30,000) enabling the discrimination of complete ^{13}C isotopic envelopes, MS/MS capability is just another advantage of our proposed technique over other common on-line technologies used to monitor volatiles in industrial processes [198]. Thus, further insights in this respect were gained by identifying some of the detected compounds. For example, the two compounds in Figure 22 a) were assigned to ethyl decanoate and farnesene based on the MS/MS spectrum (Figs 2b and S2). Ethyl esters have fruity and floral flavor and constitute important aroma compounds in wine or beer [199]. It is hypothesized that fatty acid ethyl esters are formed to prevent accumulation of medium chain fatty acid under anaerobic conditions during which fatty acid synthesis is inhibited and these fatty acids are prematurely released from the fatty acid synthase [200]. The sesquiterpene farnesene is synthesized from farnesyl diphosphate, an intermediate of the mevalonate pathway.

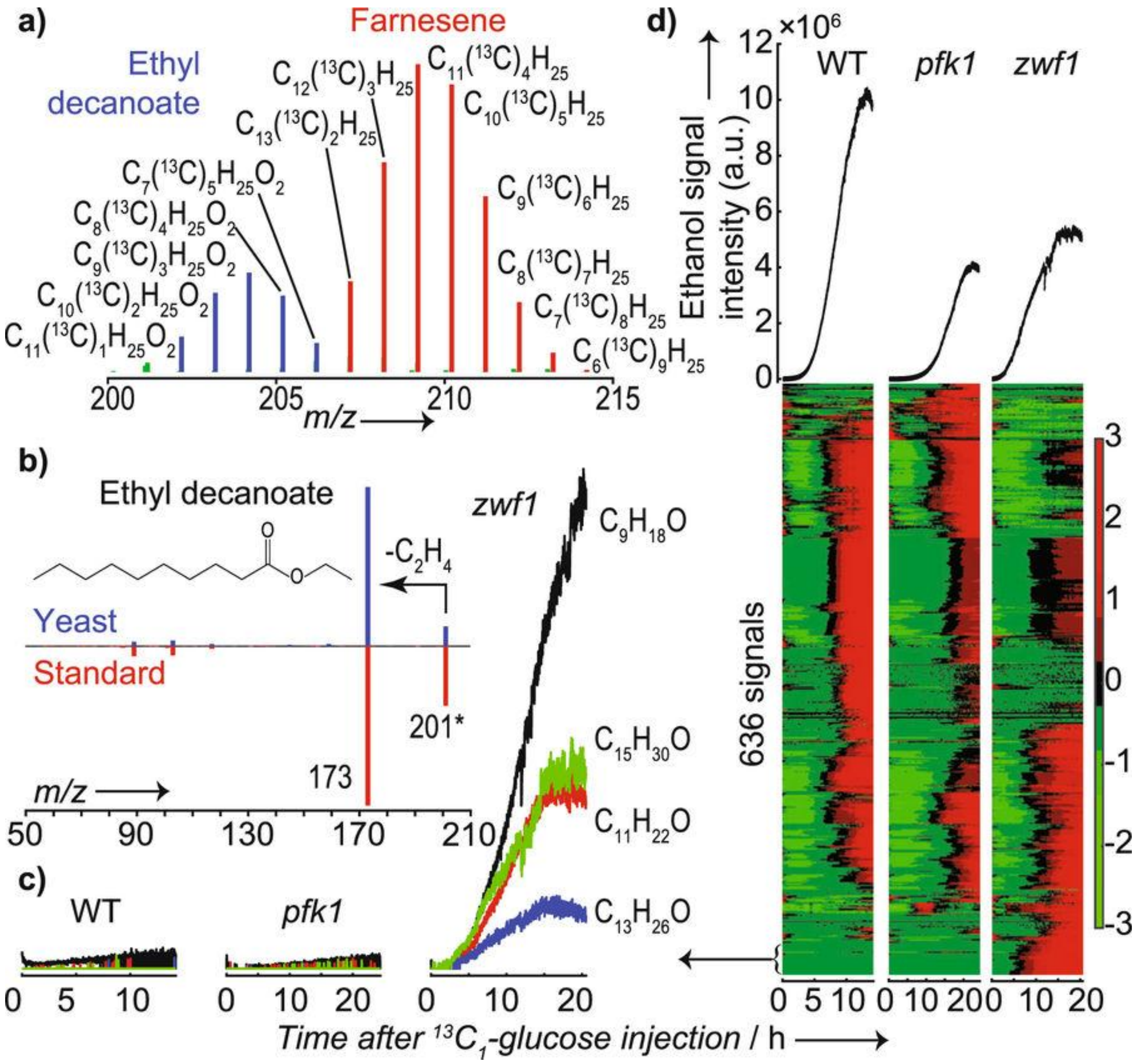

Figure 22. Growth of WT and mutants on $^{13}C_1$-glucose led to complex mass spectra that revealed a unique in vivo metabolic response; (a) Centroided mass spectrum of the region m/z 200–215 during the stationary phase of WT yeast growth upon injection of $^{13}C_1$-glucose into the system. Two isotopic envelopes for $C_{12}H_{25}O_2$ and $C_{15}H_{25}$ were clearly resolved. The incorporation of ^{13}C into ethyl decanoate and farnesene reflects the metabolism of the yeast; (b) Fragmentation (SESI MS/MS) spectrum produced using m/z 201 as the precursor ion from a yeast sample (top) and ethyl decanoate standard (bottom); (c) Set of odd-numbered carbon molecules built up during growth of the zwf1 mutant but absent in WT and pfk1; (d) Heatmap for the 636 signals detected for the three strains. For reference, ethanol profiles are shown on the top

Figure 22 c) shows an example of some representative time profiles for a set of metabolites present in the *zwf*1 mutant but absent in WT and *pfk*1. Notably, this set of metabolites is a homologous series of odd-numbered carbons ranging from C_7 to C_{15}. This observation was replicated in an independent experiment (Figure S 3). We hypothesize that these compounds are methyl ketones, which can be derived from β-oxidation of fatty acids, but their identity remains to be fully elucidated [201]. Likewise, some analytes were characteristic for *pfk*1 (see example in Figure S 4).

Figure 22 d) (top) shows the time traces for ethanol. We found that the WT produced approximately twice as much ethanol as the mutants under the same experimental conditions. The same results were obtained in a replicate experiment (Figure S3). This is consistent with previous work, where similar, reduced glucose uptake and growth rate —and as a consequence, a low ethanol formation rate— was found for the *zwf*1 mutant [202]. As for Fig. 1c, we subjected the time traces for all detected signals of the three strains to a cluster analysis and visualized them in heatmaps. Figure 22 d) (bottom) shows the results, providing an overview of the differences in volatile profiles between the strains. While the general picture seems relatively similar for WT and *pfk*1, the *zwf*1 mutant showed marked differences for some compounds. For example, at the bottom of the heatmap one can observe the cluster of molecules from Fig. 2b. “Table S 2” lists all the peaks detected in this experiment. Overall, this initial assessment illustrates the potential of SESI-HRMS to provide a comprehensive overview of VOC production by baker’s yeast in real-time.

Although the *pfk*1 cells showed a different metabolic profile than WT and *zwf*1 cells, our study showed an unexpected result. The *pfk*1 strain was able to undergo glycolysis (apparent from lower than expected loss of ^{13}C) after an extended time of lag-phase growth. It is not entirely clear to us, how the *C*1 strain was able to accomplish this. However, *S. cerevisiae*’s phosphofructokinase is a heterooctameric enzyme with an alpha subunit encoded by PFK1 and a beta subunit encoded by PFK2. Thus, a single gene deletion mutant deficient in either of these genes might retain phosphofructokinase activity, which may explain the observed labeling pattern [203][204].

Another common approach to visualize multivariate data is principal component analysis (PCA). The score plot of the mass spectra during the exponential phase (Fig. 3a) clearly shows a separation between the three strains, confirming the existence of a distinct volatile profile for each strain. Please note that we have excluded ethanol and acetic acid from the analysis in order to show that even without these major end-products, the less abundant volatile compounds suggest a very distinct profile. As expected, a similar result was obtained when we included ethanol and acetic acid in the PCA matrix (Figure S 5). To understand which metabolites contributed mostly to the separation shown in the score plot,

Fig. 3b displays the loadings for the first PC, which separate WT from the mutants. Some other highly discriminating molecules were identified via MS/MS and by comparison with standards (Figure S 2). The esters ethyl octanoate and ethyl decanoate were major contributors, along with farnesene and octanoic acid. Tables S3 and S4 list the major contributions for PC1 and PC2, respectively. When ethanol was included in the analysis, it was by far the major contributor to the separation shown in the score plot (Figure S5).

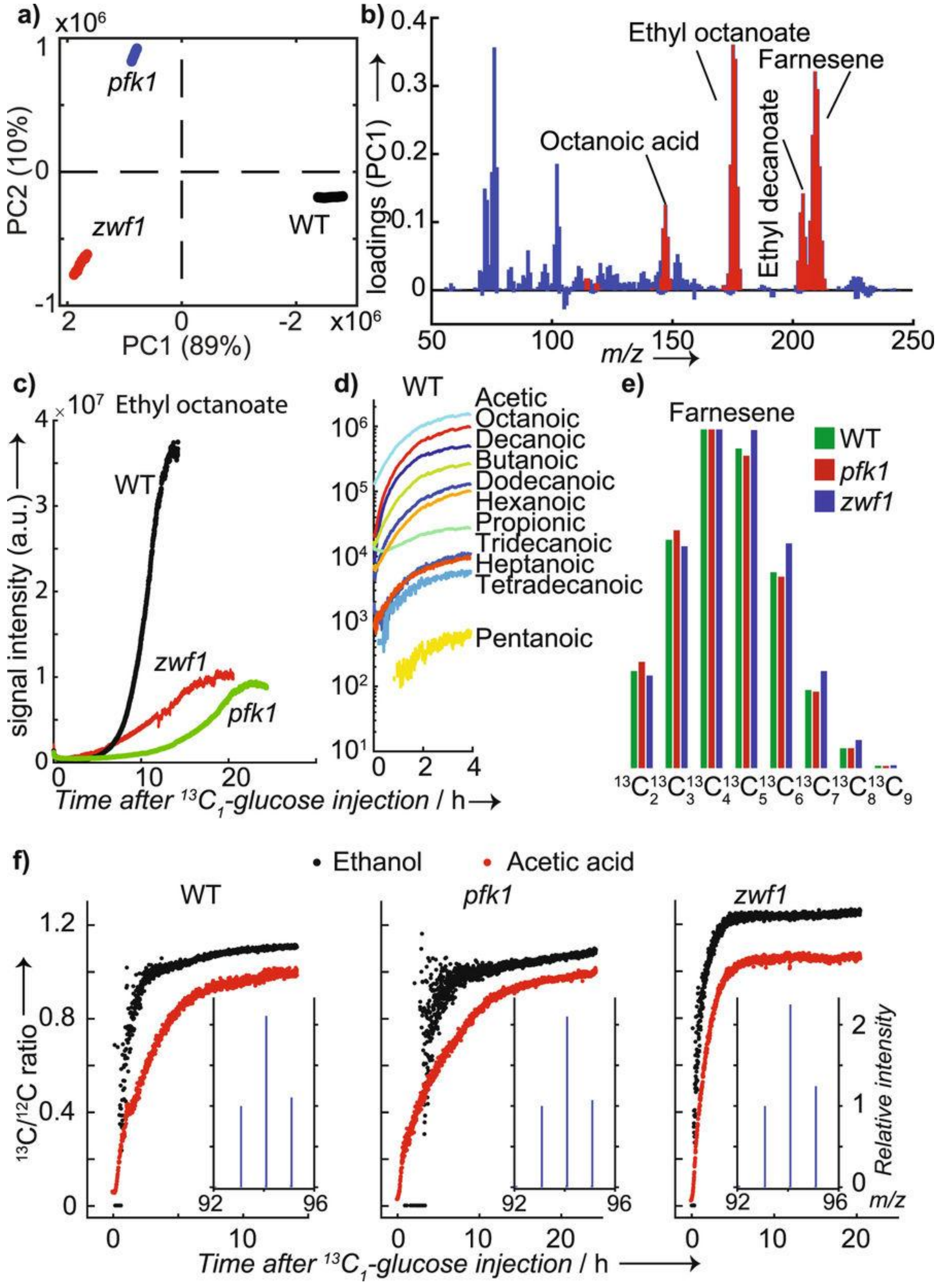

Figure 23. Distinct volatile metabolic profiles and production kinetics for yeast WT and mutants; (a) PCA score plot of average spectra in the exponential phase for WT and mutants suggests a clear distinction based on the volatile metabolic profile; (b) the corresponding loading plot for score 1 shows that esters, acids, and sesquiterpenes are major contributors to the separation between WT and mutants. Identified compounds are highlighted in red. Note that ethanol and acetic acid were excluded from the PCA analysis; (c) Kinetic profiles of the food-relevant metabolite ethyl octanoate for WT, pfk1 and zwf1 illustrates the potential to monitor industrial processes; (d) series of fatty acids detected in negative ion mode during WT growth in $^{13}C_1$-glucose; (e) isotopic distribution for farnesene obtained during the stationary phase. As expected, it shows a greater accumulation of ^{13}C for zwf1; (f) Time profiles of $^{13}C/^{12}C$ ratios for ethanol dimer (i.e., m/z 95/93; black) and acetic acid (red) for the three strains investigated. Note the different kinetic profiles. The average spectra during the stationary phase for the ethanol dimer is shown in the insets

Some of the identified compounds are not only relevant biologically, but also industrially. For example, ethyl octanoate is a yeast-based food product with sour apple aroma [205]. Figure 23 c) shows the time traces for ethyl octanoate for the three strains investigated. It clearly shows that the levels produced by WT were about four times as much as that of the mutants, reinforcing the potential to monitor industrial processes. Interestingly, ethyl hexanoate showed a very similar trend (this and additional relevant examples are shown in Figure S 6). Fatty acids such as hexanoic, octanoic, and decanoic acids are just some other examples of relevant metabolites for the food and cosmetic industry. To demonstrate that these products can also be conveniently monitored, we switched the polarity to negative ion mode. SESI-HRMS spectra in negative ion mode are dominated by deprotonated fatty acids [66][65]. Therefore, isomeric interferences such as esters could be excluded. Figure 23 d) shows the time traces of a complete series of 11 fatty acids detected in WT after injecting $^{13}C_1$-glucose. Acetic, octanoic, and decanoic acids were the major products. The complete list of all 43 compounds detected in this experiment is given in supplementary "Table S 5".

Thus, in total, 8 compounds were identified with a high degree of confidence by real-time MS/MS, although isomeric structures cannot be excluded. 11 fatty acids were also confirmed in negative ion mode with a high degree of confidence based on prior studies[66][65]. Additional hints of potential compounds were sought by querying publicly available databases. Of the 263 peaks associated to glucose metabolism in positive ion mode, 111 formulae matched at least one compound present in the yeast metabolome database ("Table S 1") [206].

By injecting $^{13}C_1$-glucose, we also aimed to confirm the validity of our approach to capture well-known biological processes. For example, while the contribution of the oxidative pentose phosphate pathway is rather small in baker's yeast grown on glucose, this little contribution should be detectable [207]. This is indeed suggested in Fig. 3c, which shows the normalized isotopic distributions for farnesene for the three strains. The maximum isotope accumulation for all three strains was found at $^{13}C_4$, but clearly, the relative abundance of C_5 to C_9 is greater in the culture of the *zwf*1 knockout strain as no $^{13}CO_2$ is released during breakdown of glucose to acetyl-CoA. The same trend was observed for acetic acid, ethanol, ethyl octanoate, ethyl decanoate, and octanoic acid. All these observations were reproduced in a replicate experiment (Figure S 7).

As metabolic systems are highly plastic, the ability to monitor metabolite dynamics is crucial for understanding cellular processes. Here, our time-resolved data was pivotal for understanding the metabolic pathways involved in the metabolism of glucose that are favored by each yeast strain. Figure 23 f) shows the $^{13}C/^{12}C$ ratio for ethanol and acetic acid.

Note that, in the case of ethanol, we monitored the dimer, which lead to a triplet-like isotopic distribution (i.e., m/z 93 for C_2H_6O-C_2H_6O; m/z 94 for $C(^{13}C)H_6O$-C_2H_6O and m/z 95 for $C(^{13}C)H_6O$-$C(^{13}C)H_6O$; inset in Fig. 3f). Both, the kinetic and isotopic ratios were different for the three strains. Mutant *zwf*1 incorporated ^{13}C into ethanol steeply to reach a plateau of $^{13}C/^{12}C$ ratio of ~1.2 after 5 h. The label incorporation in ethanol formed by the WT was similar but reached lower final fractional labeling. In contrast, no labeled ethanol was observed for *pfk*1 in the first 4 h after the ^{13}C tracer injection and did not reach a steady labeling within the 25 h of the experiment. This is explained by a slowed-down glucose metabolism and the delayed ethanol formation in this mutant. Interestingly, the ^{13}C in acetic acid built up immediately upon glucose injection in all strains. Other compounds showed different kinetics (Figure S 8). The time resolution capability allowed to exquisitely capture fine details of kinetic profiles, which is crucial to adjust industrial parameters to tune in real-time the desired volatile profile.

In conclusion, we deployed a sensitive and selective, yet, real-time mass spectrometric technique to investigate the production of volatile metabolites during yeast growth. The technique gently tracks biological processes at the metabolic level in vivo with a time resolution of less than one minute. Thus, we benchmarked the technique by observing well-known processes such as production of ethanol from glucose. However, despite being one of the most widely studied organisms, the rich volatile profiles (~300 metabolites combining positive and negative mode) of *S. cerevisiae* detected in these analyses, including non-reported analytes suggests that much work remains to be accomplished to fully map the metabolism of yeast. Such comprehensive metabolic coverage may also have potential to tune industrial processes where yeast fermentation is involved.

B.5. Methods

B.5.1. Secondary Electrospray Ionization-High Resolution Mass Spectrometry (SESI-HRMS)

SESI-HRMS experiments were carried out using a commercial ion source (SEADM S.L.)[104] plugged onto a Thermo-Fisher LTQ Orbitrap mass spectrometer. The SESI solvent was 0.1% formic acid in water infused at ~100 nL/min through a 20 µm ID silica capillary. The electrospray voltage was set to 5.4 kV in positive mode (i.e., focusing electrode 2.59 kV and impact electrode 1.6 kV) and to 5 kV in negative mode. The sweep gas used for cleaning the electrospray region was set to 2 a.u. All other internal Orbitrap parameters were optimized during calibration. Orbitrap scan parameters: scan type: FTMS full MS [50–500 Da]; source fragmentation: off; resolution: 30.000; polarity: positive and negative; Typical mass accuracies were within 2 ppm by using common chemical noise encountered in SESI-HRMS background as lock masses (i.e. m/z 149.0233, 279.1591 and 445.1200) [137][138].

AGC target: 30.000; Maximum injection time: 150 ms; micro scans: 30, which led to acquire a profile mass spectrum every ~49 seconds to prevent the generation of intractable large files during several hours of volatiles monitoring. The system was properly calibrated in the respective polarities prior to the analysis. MS/MS fragmentation spectra for both, yeast and standards, were obtained under identical conditions: Same collision energies; 5 microscans; Isolation width: 1 Da; Activation Q: 0.25 and Activation time: 30 ms.

B.5.2. Yeast cell cultures

The bioreactor consisted of an autoclaved 100 mL three-neck flask filled with 20 mL of medium, stirred at 800 rpm with a Teflon magnet and uniformly heated at 40 °C in a water bath. The metabolites produced during yeast growth were dragged downstream towards the SESI source by a continuous flow of compressed air at 0.5 L/min. The compressed air was filtered and humidified upstream the bioreactor. The bioreactor was connected to the ion source through a stainless-steel tube (OD 6 mm) heated at 130 °C to minimize metabolite adsorption onto the tube walls.

All the described experiments in this study were performed with *Saccharomyces cerevisiae*, prototrophic, YSBN.6 (wild-type) strain. Cells were grown in minimal defined medium: BD (DIFCO) yeast nitrogen base (#233520); and 2% glucose (as only carbon-source). For each experiment, pre-cultures were inoculated from SD plates and grown at 30 °C while shaking with 300 rpm for 8 to 10 hours in 1 mL pre-culture tubes. Then, the cells were inoculated (starting optical density; OD ~0.1) in 500 mL Erlenmeyer flasks with 50 mL of growth medium. Cultivation was performed at 30 °C with stirrer bar at 300 rpm until an OD of 1.2. The YSBN.6 strains *zwf*1Δ (Δzwf::Kan) and *pfk*1Δ (ΔPFK1::Kan), were grown in a similar minimal defined medium with the addition of 0.02% (v/v) of kanamycin and under the same time, temperature, and mixing conditions. To start the experiment, 1 mL of inoculum with an OD (between 0.8 to 1.0) was injected into the bioreactor for obtaining a starting OD of 0.1. When the ethanol signal decayed, 0.8 mL of 50% glucose was injected to prolong the exponential growth phase.

During the experiment, a time-lapse camera took a picture of the bioreactor every minute. Using ImageJ, an open platform for scientific image analysis [208], yeast concentrations of relative values were obtained by averaging grayscale level in a region of interest of the image in a video. Absolute OD values were also obtained at the beginning and at the end of each experiment with a Thermo electron corporation GENESYS 10 UV spectrophotometer.

Figure 24 shows a schematic of the experimental set-up (photograph in Figure S 9).

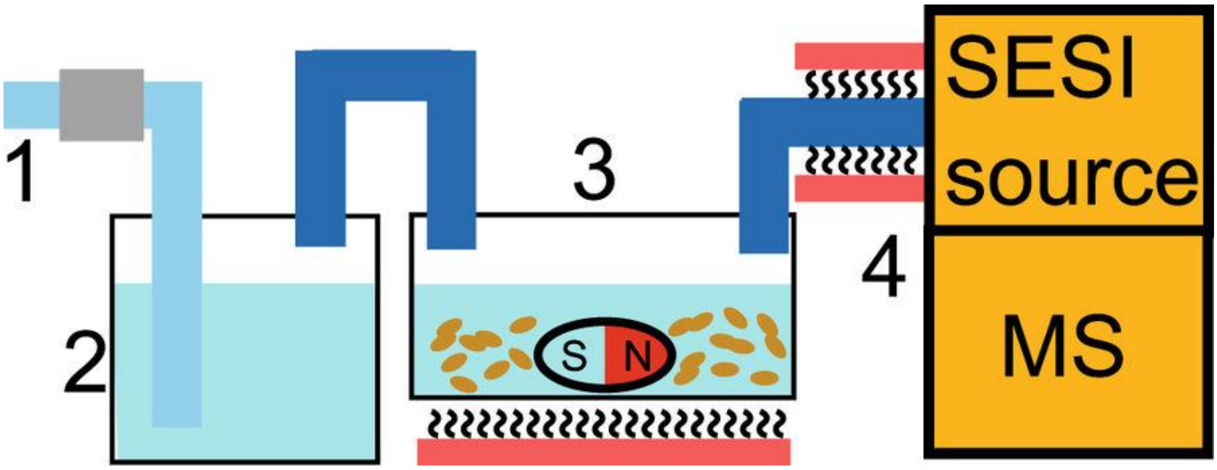

Figure 24 Experimental set-up: 0.5 L/min of compressed air flowed constantly through an active carbon filter (1); it was humidified in a gas washing bottle (2) before entering the bioreactor (3), a three-neck bottle with rubber stoppers filled with 50 mL of medium, heated to 30 °C and stirred at 800 rpm. The gas-phase metabolites were dragged to the SESI source (4) to be analyzed in the mass spectrometer

B.5.3. Data analysis

The raw mass spectra were transformed into mzXML format via MSConvert (Proteowizard)[209] and imported to MATLAB (R2016b). Each sample file was interpolated linearly (106 points in the range 50–500 Da). These interpolated profile mass spectra were then centroided (intensity threshold of 50 a.u.), resulting in ~4,400 mass spectral features (number of peaks dependent of course on the experiment performed). Subsequently, we computed the time traces for each of these peaks by adding the signal intensities ± 2, 5 mDa around the peaks. The resulting time traces (i.e., signal intensity for each m/z value as a function of time) were subjected to an agglomerative hierarchical cluster tree (Ward method; Euclidean distance; Figs 1c and 2d). To ease visualization, the time traces were smoothed (moving mean; span = 25). The 263 features finally considered (Table S 1) were retained as they raised upon the ^{12}C-glucose and ^{13}C-glucose injection but did not experience any temporal change in a blank experiment were glucose was spiked in sterile fermentation medium. The signal to noise ratios were determined as the ratio of the variances of the signals of the experiment with yeast and the negative control where we spiked glucose into sterile medium (Figure S 1).

The generation of molecular formulae from accurate mass was performed assuming protonated ions in the positive ion mode and deprotonated ions in negative mode. The following rules [210] were taken into account: Masses up to 500 Da; considered elements were restricted to C, H, N and O; restricted maximum number of each of these elements, bounded H/C ratio and heteroatom/C ratio and limited number of double-bond equivalent.

Principal component analysis (PCA) was also used for dimensionality reduction and visualization of the mass spectra (Fig. 3a,b). The matrix subjected for PCA consisted of 30 rows (i.e., ten time points during the exponential growth for each of the three strains investigated) and 636 variables (i.e., peaks listed in Table S 2). The data was mean-centered prior PCA. No further transformation of the matrix was applied.

B.6. Additional Information

Publisher's note: Springer Nature remains neutral with regard to jurisdictional claims in published maps and institutional affiliations.

B.7. Supporting information

It can be downloaded from:

https://static-content.springer.com/esm/art%3A10.1038%2Fs41598-017-14554-y/MediaObjects/41598_2017_14554_MOESM1_ESM.pdf

Chapter C - Real-Time Monitoring of Tricarboxylic Acid Metabolites in Exhaled Breath

analytical chemistry

Article

Cite This: Anal. Chem. 2018, 90, 6453−6460

pubs.acs.org/ac

Real-Time Monitoring of Tricarboxylic Acid Metabolites in Exhaled Breath

Alberto Tejero Rioseras,[†,‡,§] Kapil Dev Singh,[∥,⊥] Nora Nowak,[†] Martin T. Gaugg,[†] Tobias Bruderer,[†] Renato Zenobi,[†] and Pablo M.-L. Sinues*[,†,∥,⊥]

[†]Department of Chemistry and Applied Biosciences, ETH Zurich, 8093 Zurich, Switzerland

[‡]SEADM, S.L., 28036 Madrid, Spain

[§]Department of Analytical Chemistry, University of Cordoba, 14005 Cordoba, Spain

[∥]University Children's Hospital Basel, University of Basel, 4056 Basel, Switzerland

[⊥]Department of Biomedical Engineering, University of Basel, 4123 Allschwil, Switzerland

Supporting Information

ABSTRACT: The tricarboxylic acid (TCA) cycle is one of the most important metabolic pathway for cellular respiration in aerobic organisms. It provides and collects intermediates for many other interconnecting pathways and acts as a hub connecting metabolism of carbohydrates, fatty acids, and amino acids. Alteration in intracellular levels of its intermediates has been linked with a wide range of illnesses ranging from cancer to cellular necrosis or liver cirrhosis. Therefore, there exists an intrinsic interest in monitoring such metabolites. Our goal in this study was to evaluate whether, at least the most volatile metabolites of the TCA cycle, could be detected in breath *in vivo* and in real time. We used secondary electrospray ionization coupled with high-resolution mass spectrometry

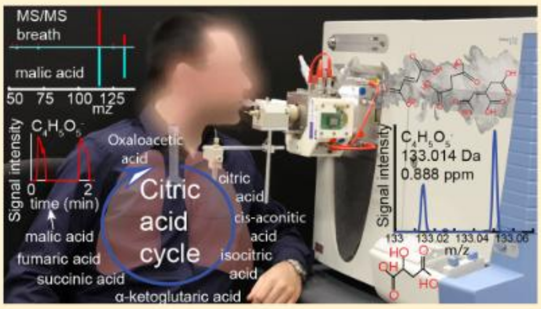

(SESI-HRMS) to conduct this targeted analysis. We enrolled six healthy individuals who provided full exhalations into the SESI-HRMS system at different times during 3 days. For the first time, we observed exhaled compounds that appertain to the TCA cycle: fumaric, succinic, malic, keto-glutaric, oxaloacetic, and aconitic acids. We found high intraindividual variability and a significant overall difference between morning and afternoon levels for malic acid, oxaloacetic acid, and aconitic acid, supporting previous studies suggesting circadian fluctuations of these metabolites in humans. This study provides first evidence that TCA cycle could conveniently be monitored in breath, opening new opportunities to study *in vivo* this important metabolic pathway.

C.1. Real-Time Monitoring of Tricarboxylic Acid Metabolites in Exhaled Breath

Alberto Tejero Rioseras[1,2,3], Kapil Dev Singh[4,5], Nora Nowak[1], Martin T. Gaugg[1], Tobias Bruderer[1], Renato Zenobi[1] and Pablo M-L Sinues[1,4,5*]

[1] Department of Chemistry and Applied Biosciences, ETH Zurich, 8093 Zurich (Switzerland)

[2] SEADM, S.L., 28036 Madrid (Spain)

[3] Department of Analytical Chemistry, University of Cordoba, 14005 Cordoba (Spain)

[4] University Children's Hospital Basel, University of Basel, 4056 Basel (Switzerland)

[5] Department of Biomedical Engineering, University of Basel, 4123 Allschwil (Switzerland)

* pablo.mlsinues@ukbb.ch

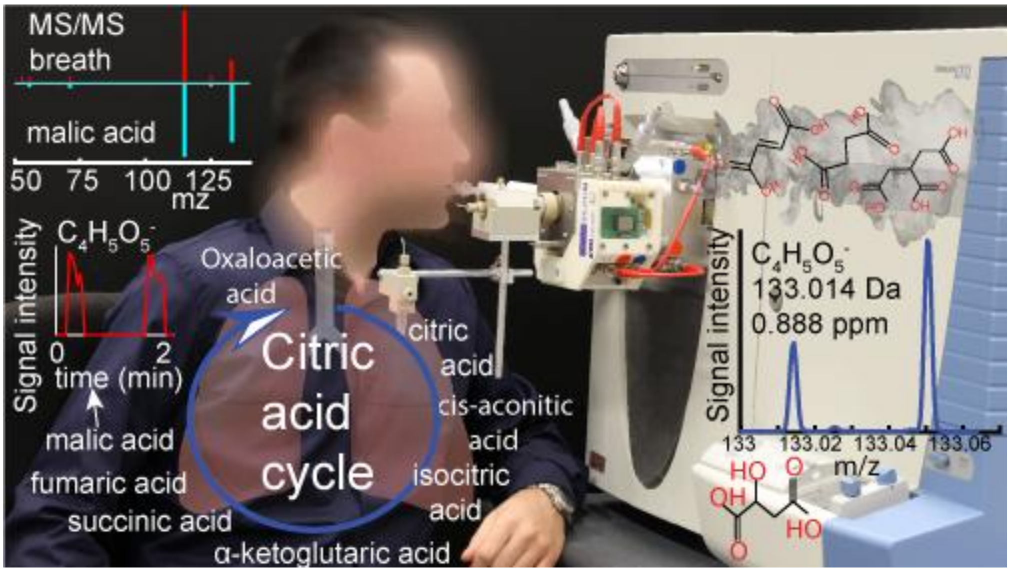

Figure 25. TOC. Table of Contents graphic: Real-Time Monitoring of Tricarboxylic Acid Metabolites in Exhaled Breath. Article's copyright © 2018, American Chemical Society

C.2. Abstract

The tricarboxylic acid (TCA) cycle is one of the most important metabolic pathway for cellular respiration in aerobic organisms. It provides and collects intermediates for many other interconnecting pathways and acts as a hub connecting metabolism of carbohydrates, fatty acids, and amino acids. Alteration in intracellular levels of its intermediates has been linked with a wide range of illnesses ranging from cancer to cellular necrosis or liver cirrhosis.

Therefore, there exists an intrinsic interest in monitoring such metabolites. Our goal in this study was to evaluate whether, at least the most volatile metabolites of the TCA cycle, could be detected in breath *in vivo* and in real time. We used secondary electrospray ionization coupled with high resolution mass spectrometry (SESI-HRMS) to conduct this targeted analysis. We enrolled six healthy individuals who provided full exhalations into the SESI-HRMS system at different times during three days. For the first time, we observed exhaled compounds that appertain to the TCA cycle: fumaric, succinic, malic, keto-glutaric, oxaloacetic and aconitic acids. We found high intra-individual variability and a significant overall difference between morning and afternoon levels for malic acid, oxaloacetic and aconitic acid, supporting previous studies suggesting circadian fluctuations of these metabolites in humans. This study provides first evidence that TCA cycle could conveniently be monitored in breath, opening new opportunities to study *in vivo* this important metabolic pathway.

C.3. Introduction

The tricarboxylic acid (TCA) cycle, also known as citric acid cycle or Krebs cycle, is a series of chemical reactions which combine the metabolism of different energy sources (such as carbohydrates, fatty acids, and amino acids) in the cell. [211] Metabolic disorders leading to abnormal concentrations of intermediates from the TCA cycle are the cause or the consequence of many illnesses. [212][213][214] In addition, fumaric acid has been reported as a reliable biomarker of cellular necrosis [215] (*i.e.* tumors or acute kidney disease); and reduced concentrations in plasma of α-ketoglutaric and cis-aconitic acids have been found for patients with aconitase deficiency. [216] Malic acid and succinic acid have been proposed as markers for liver cirrhosis. [217][218] Bipolar disorder has also been associated with abnormalities of the TCA cycle. [219]

Routine clinical assays traditionally monitor these metabolites in plasma, urine and tissues. [220][221] Alternatively, breath represents a non-invasive window to monitor certain metabolic processes. [152] Mass spectrometry-based breath analysis platforms can be categorized into off-line (*e.g.*, gas chromatography-mass spectrometry, GC-MS) and on-line methods, where proton transfer reaction-mass spectrometry (PTR-MS), [222][223] selected ion flow tube-mass spectrometry (SIFT-MS) [224][225][226][227] and secondary electrospray ionization-mass spectrometry (SESI-MS) [218][127][102][126][73][228][62][61] are the most common on-line techniques. Despite the attractiveness of breath as an alternative matrix, and the importance of the TCA cycle, few studies have reported on these metabolites in breath. For example, succinic and citric acid have been detected in exhaled breath condensate (EBC) by liquid chromatography-mass spectrometry (LC-MS). [229] Here, we present first evidence for the feasibility of monitoring the TCA cycle by real-time SESI-HRMS breath analysis.

C.4. Materials and Methods

C.4.1. Subjects

The exhaled breath of six healthy non-smokers volunteers (five males, one female), aged 30.7 ± 4.53 (mean ± SD) was measured over three consecutive days at different time points. The order of the measurements was randomized. The total number of samples collected per subject ranged from 7 to 29, depending on their availability. The measurements took place during working hours. The volunteers were asked not to eat, drink (anything except water), or brush their teeth for at least 30 minutes prior to the breath measurement. They retained their dietary habits and lifestyle. The study was approved by the local ethical committee (EK 2012-N-49), and all subjects gave written informed consent to participate.

C.4.2. SESI-HRMS real-time breath analyses

A numerically optimized commercial SESI source (SEADM, Spain) [104][74] was interfaced with a high resolution mass spectrometer (Orbitrap, Thermo Scientific, Bremen, Germany). The SESI source was operated at a flow rate of ~ 150 nL/min, using 0.1 % ammonium formate in water as SESI solvent. Water-based SESI solvents have been found to be optimal, as SESI is thought to operate via gas-phase ion-molecule reactions. [230][131]

We followed a standardized sampling protocol, similar to that used in previous studies, [230][109][111] to minimize confounding effects due the exhalation maneuvers. [231][232] The participants sat comfortably in an office chair in front of the MS prior the experiment. The subjects provided full exhalations through a disposable mouthpiece featuring a non-return valve (ACE AL5500). The disposable mouthpiece was attached to a heated sampling line (⌀: 6mm; length: 50 cm; stainless steel) heated at 160 ^{0}C to minimize adsorption of metabolites onto the line. The other end of the tube was attached to the core of the SESI chamber, which was filled with exhaled breath. The core was kept at 80 ^{0}C, dictated by the boiling point of the electrospray solvent. The SESI chamber featured an exhaust port through which excess breath could escape via an exhaust line into a laboratory fume hood. A digital manometer was placed at the exhaust port in order to fix the exhalation pressure across all measurements by biofeedback of the subjects. The exhalation flow rate under these conditions was on the order of 1.2 L/min. A typical full exhalation for each volunteer lasted on the order of twenty seconds. Thus, we recorded dead space volume (~ 150 mL) followed by tidal volume. [233] To minimize carryover effects, the ion source and the sampling line were flushed with clean nitrogen between exhalation maneuvers. “Figure S 10” shows a schematic of the set-up.

The mass spectrometer was operated in negative mode in the spectral range of *m/z* 50 – 1000, with an accumulation time of 3 seconds. The mass resolution across the entire mass range was on the order of 60,000. Commonly detected fatty acids [62][66] were used as lock masses to achieve mass accuracies typically within 1 ppm. The lock masses used are listed in Table S 6.

C.4.3. SESI-HRMS-MS real-time breath and standards analyses

Real-time SESI-MS/MS fragmentation experiments of exhaled breath and chemical standards were also carried out for compound identification purposes. In the case of breath, the exhalation maneuver was the same as in full MS mode. For the standards, we placed the chemicals in a clean three-neck flask (DURAN), which was connected to the sampling tube. The flask was flushed with 1 L/min of humidified air, dragging as a result the standard's vapors into the SESI core. Each standard was analyzed separately in individual experiments. Real-time MS/MS of exhaled breath and the standards were obtained under identical mass spectrometric conditions: 3 microscans; isolation width: 1 Da; activation Q: 0.25 and activation time: 30 ms. The full list of chemicals and collision energies used for MS/MS experiments are listed in Table S 7.

UPLC-MS/MS analysis of Exhaled Breath Condensate (EBC)

Further experiments to confirm compound identification were carried out by measuring EBC. The procedures were identical to those described recently in an investigation of aliphatic acids in EBC. [234] Shortly, EBC from 15 subjects was pooled and up-concentrated by lyophilization. [235]

An ACQUITY UPLC system (I-Class, Waters, Milford, MA, USA) with an ACQUITY UPLC BEH C18 column (1.7 µm, 2.1 × 150 mm, Waters) featuring a pre-column filter was used for EBC analyses. The UPLC was coupled to a quadrupole time-of-flight mass spectrometer (AB Sciex, Triple TOF 5600+, Concord, ON, Canada). The MS was operated in negative ion mode and its mass accuracy was within 5 ppm. The flow rate was set to 240 µL/min using a binary mixture of solvent A (water with 0.1% formic acid) and solvent B (methanol with 0.1% formic acid). The used gradient was: 5% B (1 min), 5−95% B (9 min), 100% B (2 min), and 5% B (2 min). Product ion scans and data dependent acquisitions were used for acquiring fragment spectra. The total cycle time was kept at 450 ms to obtain at least 12 points/peak (minimal LC peak width = 6 s) with 80 ms for TOF MS and 320 ms for four product ion scans acquired with a collision energy CE = 10/20/30 eV.

C.4.4. Data analysis

Raw files from both the Orbitrap and Triple TOF 5600+ instruments were converted to mzXML format using MSConvert (Proteowizard) [236] and imported into MATLAB (R2016a, Mathworks Inc.), to then read and extract the spectral information. The real-time traces for *m/z* feature were extracted. Afterwards, the median at the plateau of each single exhalation of each subject was computed. These plateau intensity values were then used for analysis without further normalization. To assess whether there existed any association among the TCA cycle metabolites, we computed Pearson's correlation. Differences in the mean values between morning and afternoon TCA compounds signal intensities were tested using a two-tailed unpaired t-test. For compound identification purposes, real-time fragmentation spectra, as well as retention times and fragmentation spectra from UPLC-MS/MS analyses, were extracted from mzXML files. For comparison between breath samples and standards, we generated head-to-tail plots of the pairs of spectra, normalizing the maximum signal intensity to one.

C.5. Results and discussion

Real-time detection in human breath

We initially confirmed that the overall procedure provided robust results by simply inspecting the total ion current (TIC) during the exhalation maneuvers. We confirmed that replicate exhalations for a single subject resulted in repeatable traces. In addition, obvious differences were clearly observed at the TIC level between different subjects, as expected [237] (Figure S 11). We subsequently checked whether the expected signals corresponding to the deprotonated (*i.e.* $[M\text{-}H]^-$) TCA cycle metabolites were detected in breath. The center of Figure 26 illustrates a simplified scheme of the TCA cycle, showing the chemical structures of the compounds detected in this study. Moreover, the figure shows a typical breath mass spectrum for one subject (zooming into the *m/z* regions of interest). The corresponding mass spectral peaks for the TCA metabolites are indicated with an arrow and neighboring peaks are also shown. Despite the fact that breath is a relatively simple body fluid, a high resolving power of the mass analyzer is crucial for its real-time analysis to discriminate isobaric species, as evidenced by the mass spectra shown in Figure 26. Well-defined neighboring peaks to those of interest were always present in breath. For example, a minimum resolution of ~25,000 would be needed to fully resolve alpha-ketoglutaric acid (*m/z* 145.0142) from the interference at m/z 145.0255. We operated the instrument at a resolution on the order of 60,000, allowing for complete separation of the TCA peaks from nearby interferences. High resolution is a key advantage of the SESI-Orbitrap [124][190] platform used here, as compared with alternative real-time gas mass analyzers. For example, the single quadrupole of SIFT-MS [238][239][240] achieves unit mass resolution and the top

PTR-MS instrument reaches a resolution on the order of 8,000. [241] In addition, the high mass accuracy (within 1 ppm using the lock mass feature) enabled direct assignment of unambiguous molecular formulae. In total, we detected seven signals whose molecular formulae would in principle fit with the expected metabolites from the TCA cycle.

Succinic and citric acid have been reported in EBC by LC-MS analysis, [229] which provides strong evidence that breath could indeed be exploited as an easily accessible matrix to monitor TCA metabolism. However, in order to continuously monitor these metabolites, it would be highly desirable to accomplish this by real-time analysis, rather than off-line. In order to do so, it is instructive to estimate the expected concentration in breath and therefore the required sensitivity. Hence, we estimated expected gas-phase concentrations in exhaled breath assuming that the only contributor is the exchange in the blood-air barrier. Firstly, we computed the blood:air partition coefficient by implementing a simple model based on vapor pressure, the octanol:water partition coefficient and molecular weight. [242] Since typical blood concentrations for these compounds in healthy individuals are in the range of 1-10 µM, the expected gas-phase concentrations are in the low to high parts-per-quadrillion (ppq) level (Table S 8). This required high sensitivity is compatible with previous SESI-MS studies, where sub-ppt limits of detection for gas-phase analytes were achieved. [62][243] We note that contributions from other sources like saliva, which is known to contain these metabolites [244], cannot be excluded. This would result in higher gas-phase concentrations.

The data in Figure 26 demonstrates that indeed SESI-HRMS is sensitive enough to track these metabolites in breath in real-time. It shows the time traces for the TCA cycle metabolites —along with their neighboring interferences— for two consecutive exhalations for one subject. One can clearly observe how the signal intensities rise during the exhalation maneuver (~0.2 min), reach a stable phase (plateau) and drop again to baseline level when the subject finishes the exhalation. When the exhalation maneuver was replicated by the same subject (~1.8 min), essentially the same result is obtained, as evidenced by the similar signal intensity and trace profiles. A closer look to the time profiles and intensity scales for the metabolites of interest is shown in Figure S 12, which displays the overlaid time traces for the six compounds during two consecutive exhalations for another subject.

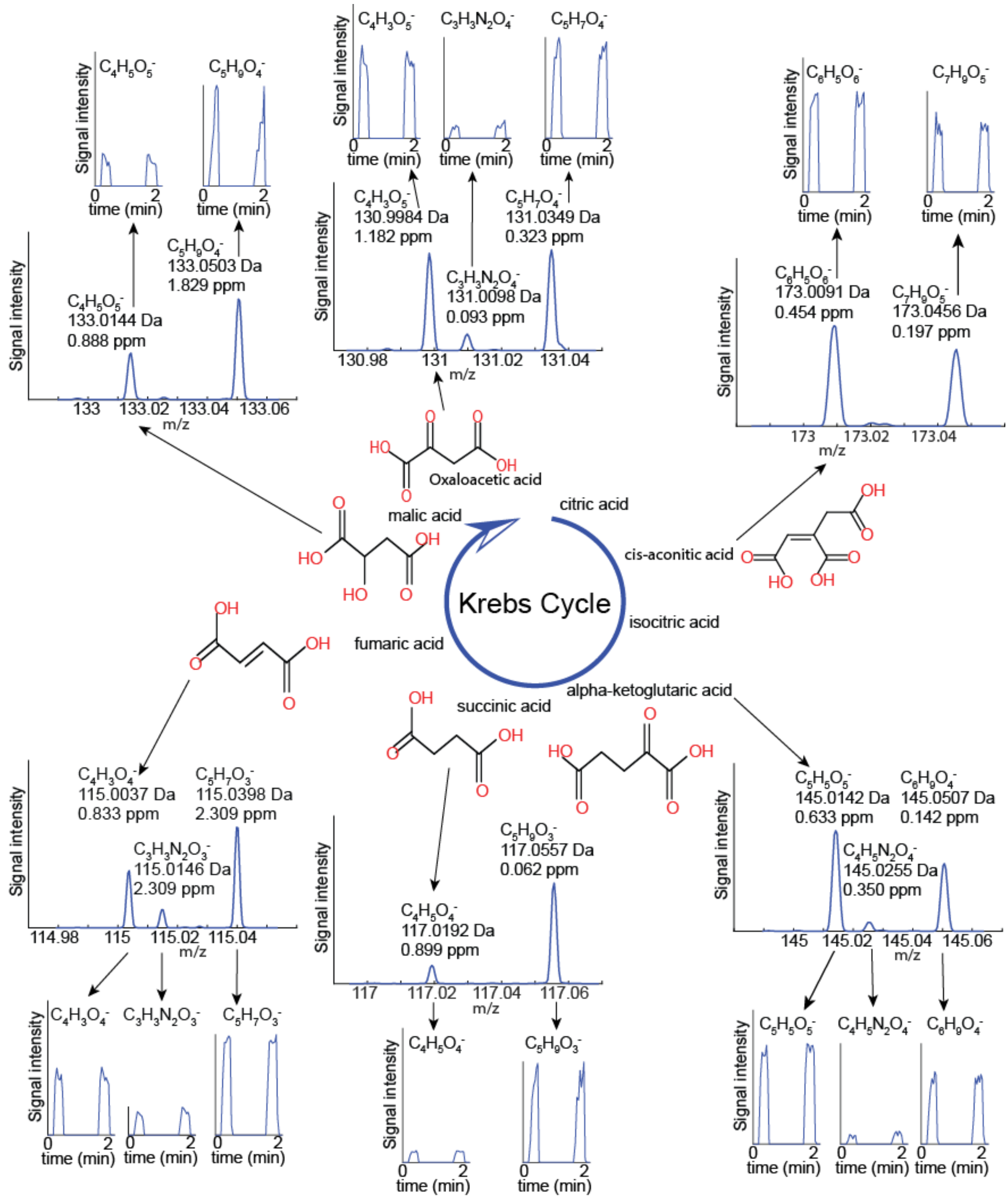

Figure 26. Real-time detection of the tricarboxylic acid (TCA) cycle metabolites in exhaled breath. The center of the figure shows a simplified schematic of TCA cycle, along with chemical structure of metabolites observed in exhaled breath. The mass spectra show the nominal m/z window for the deprotonated species. The chemical structures of the metabolites and their corresponding mass spectral peaks are linked with an arrow. The remaining peaks are isobaric structures that highlight the importance of high mass resolution for real-time breath analysis. The signal intensity as a function of time for each of the mass spectrum peaks is shown at the bottom and the top of the figure. The time traces show the signal intensities rising during two consecutives exhalations within two minutes for one subject, illustrating the concept of real-time analysis. Article's copyright © 2018, American Chemical Society

Compound identification

To further confirm whether these molecules were indeed the expected metabolites, we carried out real-time tandem mass spectrometry experiments both in breath and with chemical standards. Figure 27 shows the fragmentation spectra for both breath and the standards of six TCA cycle compounds. Not surprisingly, because the MS/MS isolation window was 1 Da, other isobaric species (see Figure 26) also produced fragments. For this reason, the top spectra corresponding to the breath samples show a greater number of fragments than the standards (bottom). Nevertheless, we found that all the diagnostic fragmentation peaks were present in the breath spectra, providing reassuring evidence on the presence of these TCA cycle metabolites in breath. In contrast, positive identification of citric acid could not be confirmed as both fragmentation patterns did not match (Figure S 13). A reasonable explanation would be that this peak may correspond to a more abundant isomeric structure. For example, a potential candidate is diketogulonic acid, according to the human metabolome database. [220] Overall, these experiments reinforce the notion that the ability of carrying out SESI-MS/MS experiments is a key advantage for compound identification purposes over SIFT and PTR systems, which rely solely on full MS information.

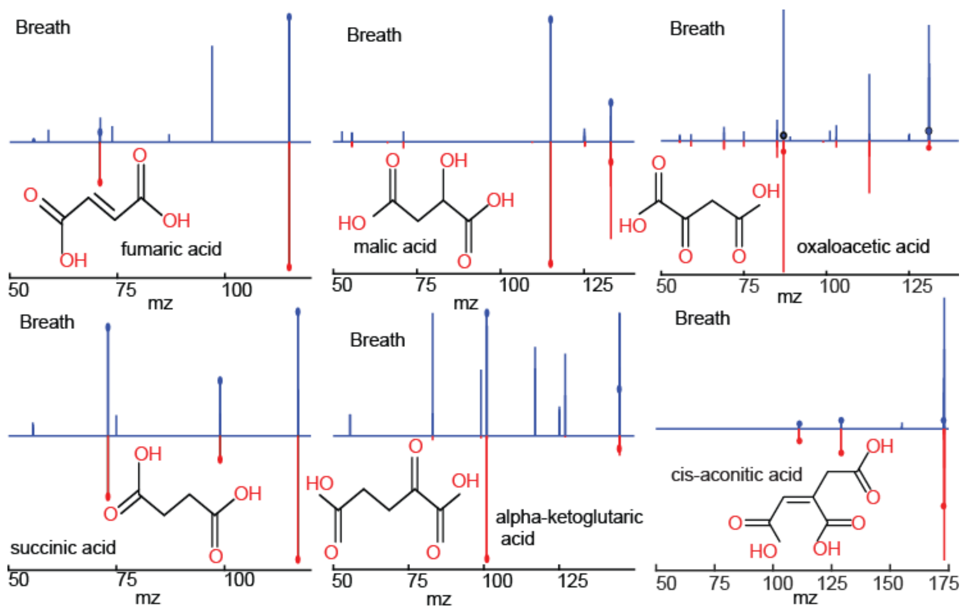

Figure 27. Real-time SESI-MS/MS confirms the identification of six metabolites appertaining to the TCA cycle in exhaled breath. The figure shows the MS/MS spectra for six TCA cycle metabolites measured in exhaled breath (blue) and using chemical standards (red). The y-axis is in normalized relative abundance (not shown here). The diagnostic peaks are labelled with a dot. The exhaled breath spectra tend to show additional fragments due to co-fragmentation of possibly other interfering ions present in 1 Da precursor mass isolation window. [Article's](#) copyright © 2018, American Chemical Society

To gain further evidence on the identification of these compounds in breath, we pursued analysis of EBC by UPLC-MS/MS. [234][245] The underlying assumption is that the same compounds detected in real time are also present in EBC. For clarity, EBC analyses were meant only for compound identification confirmation and the data was not used for subjects' comparison. We obtained enough EBC signal intensities for fumaric, succinic and malic acids. Figure 28 (top) shows the extracted ion chromatograms of EBC at *m/z* 115.0037. It shows four main chromatographic peaks, indicating the presence of four isomeric structures, which obviously would be detected simultaneously in real-time measurements. When we ran UPLC-MS/MS on the chemical standard, we found that indeed one of the four compounds corresponds to fumaric acid. The retention time and MS/MS matched (*i.e.* main loss of CO_2 at *m/z* 71.0128). Similarly, we confirmed succinic (Figure 28; middle panels) and malic acid (Figure 28; bottom panels). A minor isomeric compound was observed for succininc acid, whereas for the case of malic acid, no other compounds were detected. "Table S 9" lists the retention times, and *m/z* and intensity values for the fragmentation spectra for EBC. As expected, the fragmentation spectra obtained from EBC match with those from our real-time data (Figure 27). Overall, our real-time SESI-MS/MS strategy (Figure 27) provided strong evidence that fumaric, succinic, malic, keto-glutaric, oxaloacetic and aconitic acids are detectable in real time. The off-line EBC analysis provided an even higher degree of confidence for fumaric, succinic and malic acids.

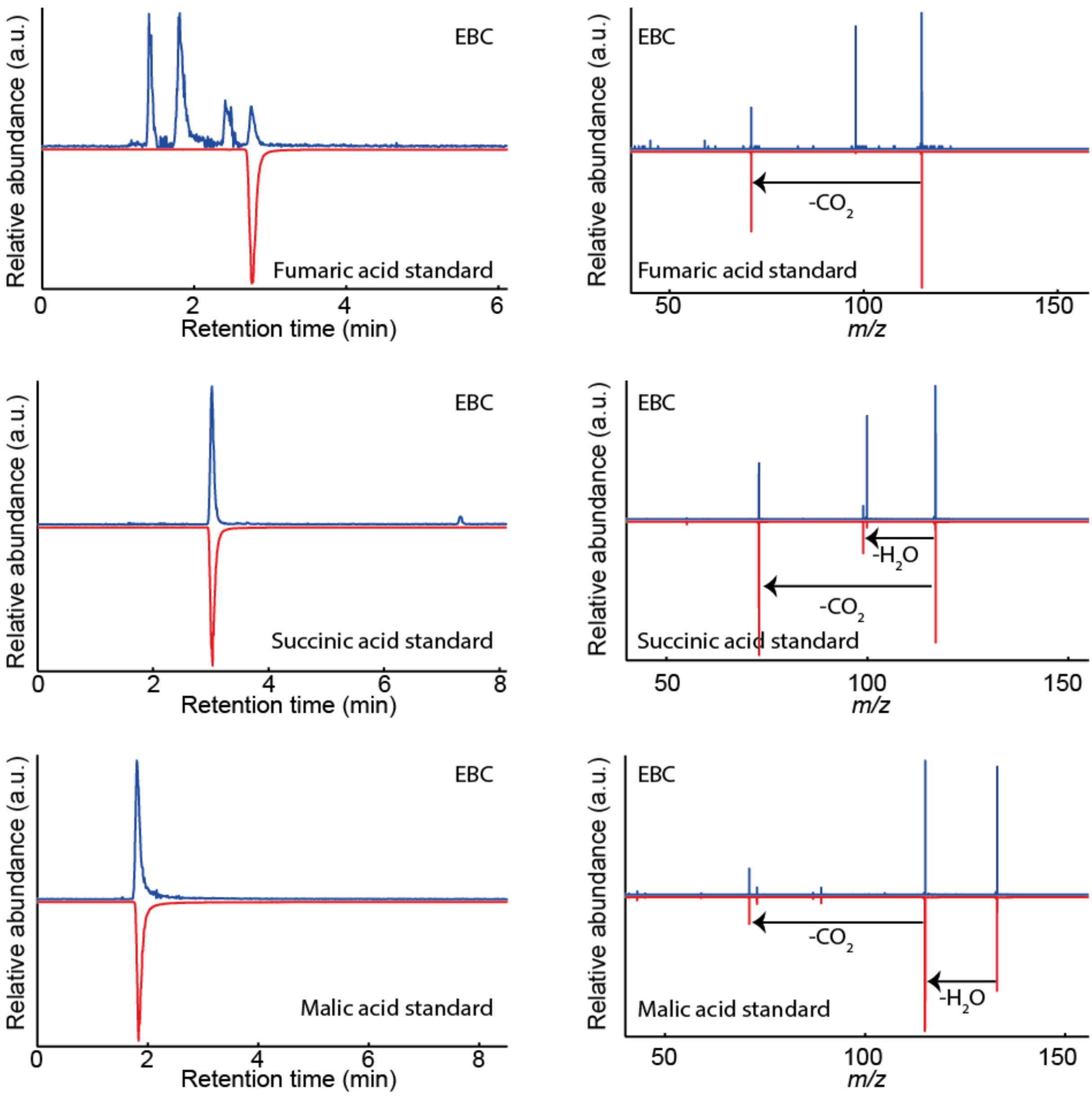

Figure 28 Overlap between retention time and MS/MS spectra for TCA cycle metabolites between EBC and standards further confirm compound identification. The figure shows the UPLC chromatogram (left side) and UPLC-MS/MS spectra (right side) for fumaric, succinic, and malic acid in EBC (blue) and standards (red). Apart from fumaric acid, three additional isomers were observed in EBC (top-left). Succinic acid showed a small isomeric peak (RT = 7.3 min) while malic acid was found to be the only one species. Article's copyright © 2018, American Chemical Society

TCA cycle metabolites variability in exhaled breath

The signal intensity of fumaric, succinic, malic, keto-glutaric, oxaloacetic and aconitic acid for the six subjects collected during three days is summarized in Figure 29. It shows obvious intra-individual differences. For example, subject #1 consistently showed the lowest signal intensities. These observations are in line with a previous study suggesting high individual-specific breathprints. [245] This notion is reinforced by inspection of Figure 30, which shows the pairwise correlation for the six compounds detected for all the subjects.

With the exception of some artificially high correlations that are driven by outliers (*e.g.* α-ketoglutaric acid), the overall picture shows a high correlation between the metabolites of the TCA cycle, which is to be expected [246][247] as these metabolites are intimately interconnected, although some of them are generated/re-routed from/to other cycles. For example, fumaric acid is also produced from the urea cycle. The strongest correlation without the contribution of outliers (r = 0.91) was found between malic and oxaloacetic acid, which are located in consecutive positions downstream the TCA cycle.

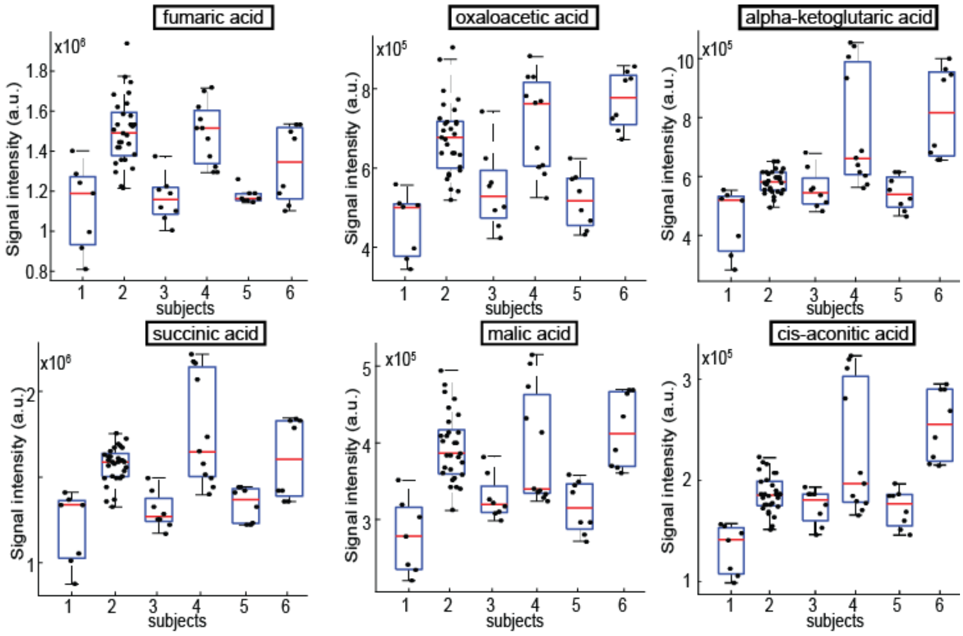

Figure 29. Measured TCA cycle metabolites show high inter-individual variability in exhaled breath. Box plots representing intra- and inter-individual variability in exhaled breath abundance of the six TCA cycle metabolites. Each data point (overlaid) represents a single exhalation. Article's copyright © 2018, American Chemical Society

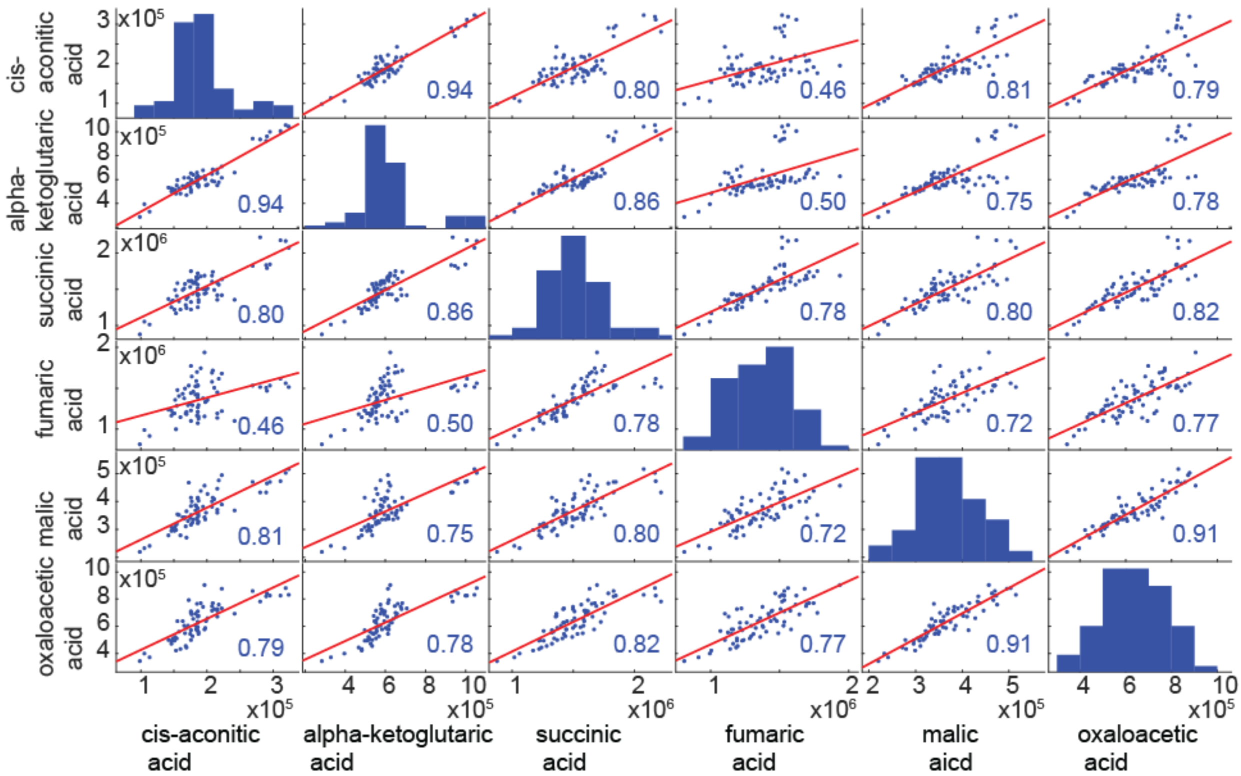

Figure 30 TCA cycle metabolites measured in exhaled breath show high pairwise correlation. Correlation matrix plot for the six TCA cycle metabolites. The diagonal shows the histograms of exhaled breath abundance for each metabolite. Scatter plots between different metabolites are shown above and below the diagonal, along with least-squares fitted line (in red) and Pearson correlation coefficients. Despite the presence of some outliers, the overall picture suggests a high interdependence of the metabolites, as it would be expected from this metabolic cycle. Copyright © 2018, American Chemical Society

Subsequently, we analyzed our data from a different perspective. Following previous observations that suggested a time-of-day dependence on certain breath metabolite levels, [248] resembling in some cases circadian fluctuations, [105] we further investigated whether these TCA metabolites would show such a temporal behavior. Our initial hypothesis was that these metabolites would indeed show such behavior as this energy metabolic pathway has been identified to be circadian, with the highest concentrations of metabolites during the morning. [244] We thus pooled all the measurements into two different categories: before 12:00 (*i.e.* AM) and after 12:00 (*i.e.* PM). We found that malic acid, oxaloacetic and cis-aconitic acid were significantly decreased during the course of the day (Figure 31 and Table S 10), whereas we did not find significant differences for fumaric, succinic and α-ketoglutaric acid for the time span studied here (Figure S 13).

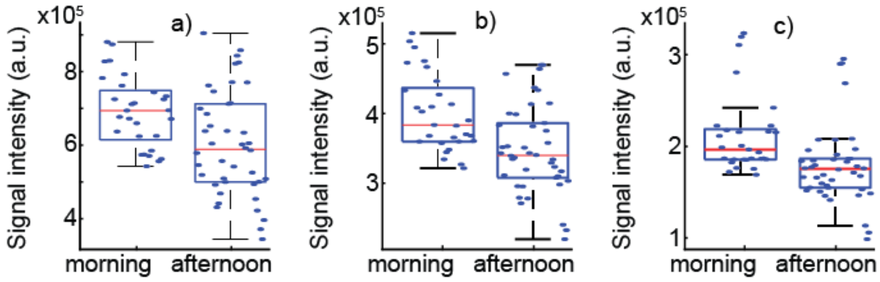

Figure 31 Three out of six measured TCA cycle metabolites show time-of-day dependence in exhaled breath abundance. Box plots representing significant decrease in exhaled breath abundance during the afternoon for a) oxaloacetic acid; b) malic acid and c) cis-aconitic acid. Article's copyright © 2018, American Chemical Society

Overall, this study shows compelling evidence that these important metabolites are detectable in real time in exhaled breath, hence opening new opportunities to measure them non-invasively. However, this work has also limitations that need to be flagged. For example, given the limited sample size, the concentration fluctuations (AM vs PM) and inter-individual differences observed are likely not representative for such a small group. Another limitation of this study is that we did not quantify absolute gas-phase concentrations, therefore the signal intensities shown are relative. [249] Further calibration studies (*i.e.* infusing known concentrations of vapors [62]) will be required to translate signal intensity into gas-phase concentration. Finally, another important aspect that will need to be addressed is to confirm that these breath compounds do actually mirror systemic concentrations of other body fluids. Blood concentrations should be measured using standard methods and compared with simultaneous measurements in breath to confirm whether a correlation exists between blood and breath levels.

C.6. Conclusion

We conclude that SEMI-HRMS breath analysis offers an attractive approach to monitor *in vivo* the TCA cycle. Hence, opening new opportunities to investigate in a patient-friendly way the energy metabolism, as well as its circadian behavior.

C.7. ASSOCIATED CONTENT

Supporting Information Available at:

https://pubs.acs.org/doi/suppl/10.1021/acs.analchem.7b04600

Contents of the supporting information:

Figure S 10 Schematic description of the experimental set-up.

Figure S 11 Total ion current (TIC) as a function of time during the exhalation maneuvers.

Figure S 12 Signal intensities vs time during two consecutives exhalations from the same subject.

Figure S 13 SESI-MS/MS fragmentation spectra of citric acid standard (bottom) and breath (top).

Figure S 14 TCA cycle metabolites a) fumaric acid; b) succinic acid and c) alpha-ketoglutaric acid showed no significant time-of-day dependence in exhaled breath abundance.

Table S 6 Lock masses employed in negative ion mode to ensure high mass accuracy during the experiments.

Table S 7 List of chemicals used for running MS/MS experiments and collision energies used to compare the fragmentation pattern of the standards and the exhaled breath.

Table S 8 Estimation of gas-phase concentrations in breath for healthy humans.

Table S 9. Retention times and fragmentation spectra data from Figure 28 for EBC.

Table S 10 Mean values, mean differences, corresponding 95% confidence interval and p-value resulting from running an unpaired t-test to compare morning vs afternoon levels of the TCA cycle metabolites identified in exhaled breath.

C.8. Acknowledgements

We gratefully thank Dr. Juan Zhang (Novartis AG) for the donation of the LTQ Orbitrap instrument used in this study. This research has received funding from the European Community's Seventh Framework Programme (FP7-2013-IAPP) within the project “Analytical Chemistry Instrumentation Development” (609691). This work is part of the Zurich Exhalomics project under the umbrella of University Medicine Zurich/Hochschulmedizin Zürich.

C.9. Conflict of Interest Disclosure

The authors declare the following competing financial interest(s): Alberto Tejero Rioseras and Pablo M-L Sinues work in the framework of a project (Analytical Chemistry Instrumentation Development, FP7-2013-IAPP, 609691), one of whose main objectives is to develop the commercial ion source used in this study

2. Conclusiones generales

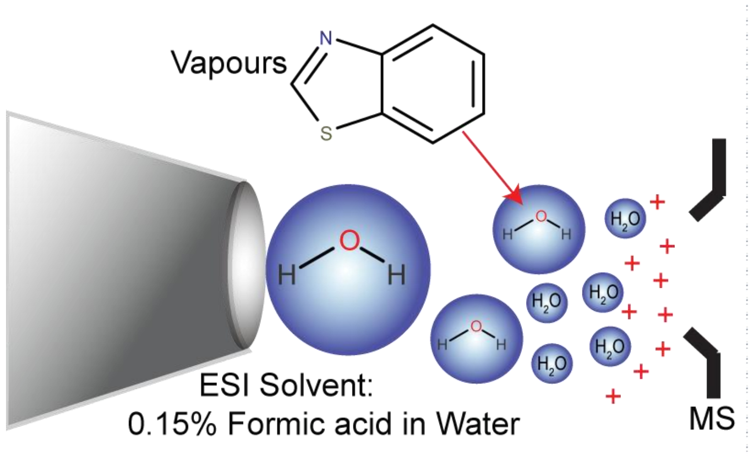

VS

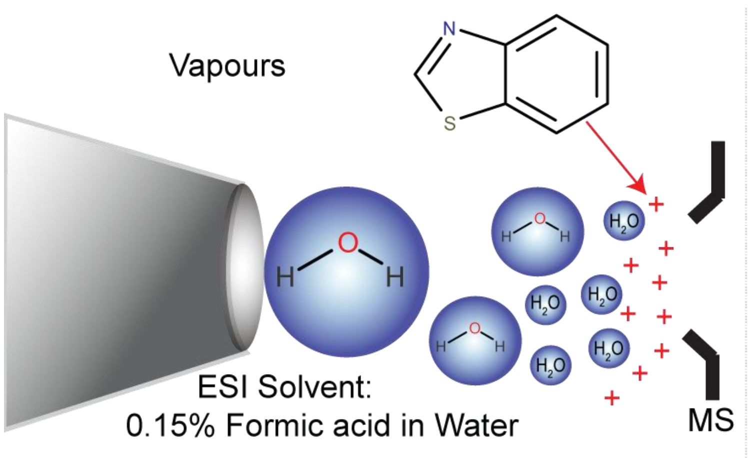

Two possible ionization mechanisms proposed for Secondary ElectroSpray Ionization (SESI)

A partir de esta Memoria de Tesis pueden alcanzarse las siguientes conclusiones:

- En ionización secundaria por electrospray (SESI), el mecanismo de ionización por el cual los vapores neutros adquieren carga al interactuar con el electrospray está gobernado por reacciones de ionización química en fase gaseosa. Por lo tanto, la afinidad protónica en fase vapor tanto del disolvente utilizado en el electrospray como de la propia muestra determinan que moléculas son ionizadas.
- La ionización secundaria por electrospray acoplada a espectrometría de masas de alta resolución (SESI-HRMS) es una técnica analítica sensible y selectiva, adecuada para medir en tiempo real metabolitos volátiles producidos por *S. cerevisiae* durante su fase de crecimiento. Esta capacidad de SESI para ionizar metabolitos, hasta entonces desconocidos en las bases de datos sobre levaduras, puede ayudar a completar el mapa metabólico de estos microorganismos. Además, los perfiles en tiempo real de metabolitos volátiles aportan información clave para entender la cinética y rutas metabólicas seguidas por las cepas de las levaduras WT, *pfk1* y *zwf1* al procesar $^{13}C_1$-glucosa. Esta técnica analítica, que ha demostrado así su potencial para medir VOCs producidos por levaduras, podría extender su aplicación a otros microorganismos tanto en el campo de la investigación como en la optimización de procesos biológicos en la industria.
- SESI-HRMS permite detectar y monitorizar, en tiempo real y en aliento humano, los ácidos fumárico, succínico, málico, cetoglutarico, oxaloacético y aconítico, identificándolos mediante MS/MS. Además, el análisis *off-line* de condensado de aliento (EBC) por UPLC-MS/MS permitió confirmar la identificación del ácido fumárico, succínico y málico. A pesar de que no fue posible cuantificar las concentraciones en valores absolutos, sí pudieron encontrarse diferencias entre individuos. Estos resultados abren una nueva vía para investigar el metabolismo del ciclo de los ácidos tricarboxílicos de forma no invasiva y en tiempo real.

Las conclusiones que se derivan de este trabajo de investigación han de ser consideradas junto con las limitaciones que se citan a continuación:

- SESI está considerada una técnica de ionización suave. Esto significa que la gran mayoría de los compuestos volátiles se ionizan sin fragmentarse. Sin embargo, debe destacarse que una minoría de compuestos podrían fragmentarse o disociarse en el muestreo o durante la ionización, antes de alcanzar la entrada del espectrómetro de masas.

- Se ha considerado que la mayoría de los compuestos se ionizan en modo positivo a través de una reacción de transferencia protónica $[M+H]^+$ dado que se utiliza una solución de electrospray basada en 0.1% de ácido fórmico en agua. Sin embargo, se debe destacarse que es posible que algunos aductos pudieran ionizar las moléculas más eficientemente. Por ejemplo, usando un electrospray de formiato de amonio algunas moléculas se ionizarían muy eficientemente como $[M+NH_4]^+$, como ya se ha demostrado en otros estudios de ionización química.
- La identificación de compuestos por MS/MS nos permite confirmar que la molécula analizada tiene el mismo patrón de fragmentación que un estándar. Sin embargo, se debe tener en cuenta que otros compuestos químicos de la misma familia podrían tener rutas de fragmentación aparentemente iguales. Se conseguiría una mayor confianza en la identificación mediante una confirmación completa por LC-MS/MS o GC-MS/MS.

En base a los resultados obtenidos se proponen las siguientes líneas de investigación:

- En el estudio sobre el metabolismo de la levadura se han encontrado alrededor de 300 metabolitos producidos durante la fermentación de la glucosa. Nótese que la mayoría de estos compuestos tan solo se identificaron por formula molecular y de algunos se desconoce su origen metabólico. Sería muy interesante que se aplicaran otras técnicas analíticas con el fin de confirmar nuestros resultados e identificar completamente estos compuestos, descifrando su origen metabólico.
- SESI podría aplicarse también para la identificación bacteriana, así como para obtener más información en tiempo real sobre su metabolismo.
- En el estudio de los ácidos tricarboxílicos en el aliento, se afirma que los compuestos detectados provienen del aliento. En el futuro, serán necesarios estudios que combinen los análisis de sangre y de aliento para corroborar esta hipótesis. Además, estos estudios permitirían realizar estimaciones sobre cuál es la concentración en sangre por correlación con la correspondiente señal en el aliento. Finalmente, nuevos experimentos, realizados con una población más grande y controlando parámetros como la dieta, permitirían reducir la variabilidad de los resultados.

- La técnica SESI podría ser aplicada en el campo del diagnóstico clínico, avanzando en la búsqueda de biomarcadores de ciertas enfermedades y permitiendo un acercamiento a la ansiada meta de la medicina personalizada.

3. General Conclusions

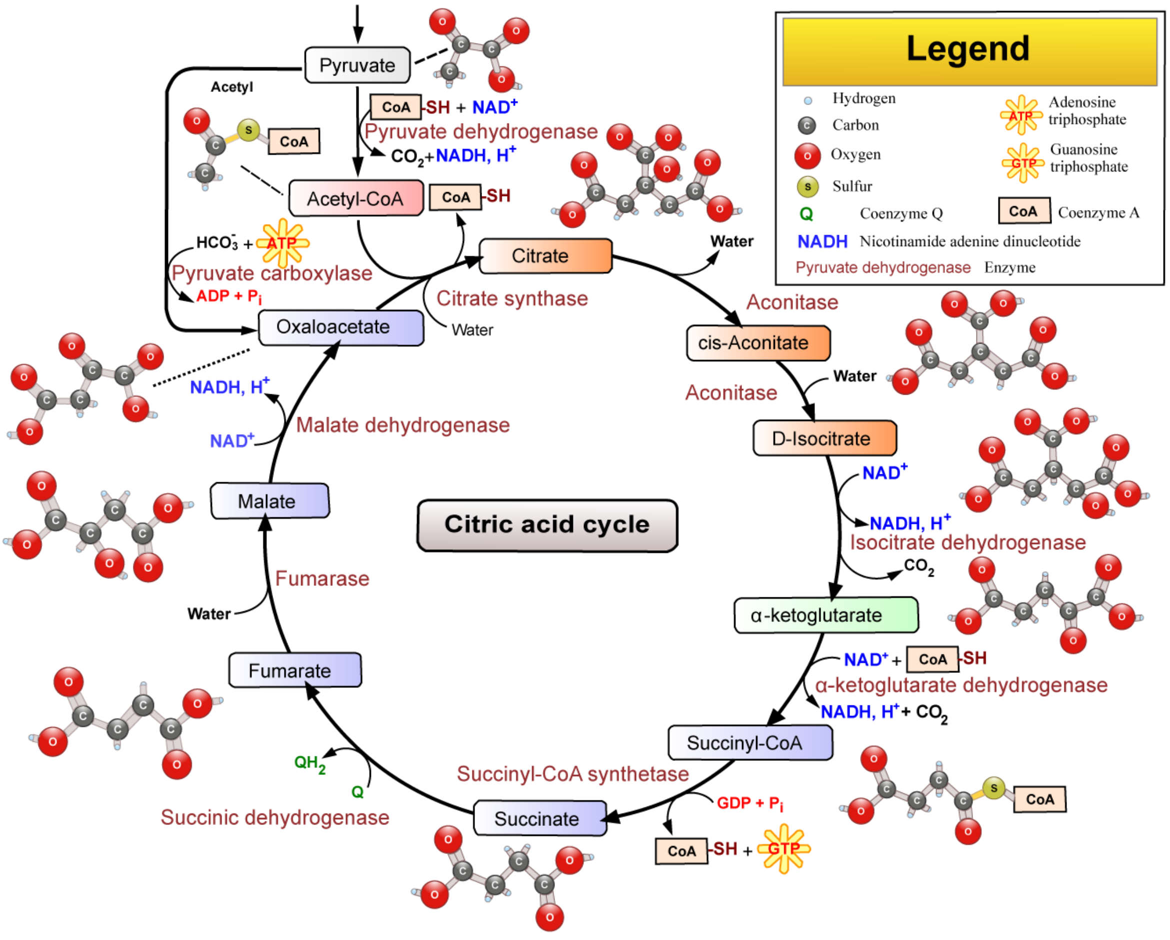

Image of the TCA cycle by Narayanese, WikiUserPedia, YassineMrabet, TotoBaggins released under Creative Commons Attribution ShareAlike 3.0 license

The research here presented enables the following conclusions to be drawn:

- In Secondary ElectroSpray Ionization (SESI), gas-phase chemical ionization governs the ionization mechanism by which neutral vapors carried in an air stream get ionized when interacting with an electrospray plume. Therefore, gas-phase proton affinity of the ESI solvent and of the sample itself determined which molecules get finally protonated.
- Secondary electrospray ionization couple to high resolution mass spectrometry (SESI-HRMS) is a sensitive and selective analytical technique suitable to measure in real-time volatile metabolites produced by *S. cerevisiae* during yeast growth. The capability of SESI to ionize volatile metabolites not previously reported in yeast metabolome databases can help biologist to fully map its metabolism. Additionally, real-time profiles of the volatile metabolites provided key information to get further insights into kinetics and metabolic pathways of WT, *pfk1* and *zwf1* yeast when processing $^{13}C_1$-glucose. We believe that the potential of SESI already demonstrated for yeast could be apply to other microorganism as a tool for research or to optimize industrial processes.
- In breath analysis studies, fumaric, succinic, malic, keto-glutaric, oxaloacetic and aconitic acid can be conveniently detected and monitored in exhaled breath of individuals by real-time SESI-HRMS. The identification of these compounds was accomplished by tandem MS while the analysis of off-line EBC samples by UPLC-MS/MS provided a higher degree of confidence for fumaric, succinic and malic acids. Although absolute quantification was not achieved in real-time measurements, inter-individual differences could be obtained, opening new opportunities to explore the metabolism in a patient-friendly way.

The conclusions drawn from these research project must be considered taking into account the following limitations:

- SESI is treated as a soft ionization technique, which means that most of the volatile molecules get ionized without fragmentation. However, it should be noted that a minority of molecules could fragment or disassociate in the sample procedure or during the ionization, before reaching the mass spectrometer inlet.
- It has been considered that most compounds get ionized in positive mode by proton transfer reaction $[M+H]^+$ since an electrospray solution of 0.1% Formic

Acid in Water was used. However, it should be highlighted that other adducts could ionize some molecules more efficiently. For example, using an electrospray of ammonium formate some molecules would get efficiently ionized in the form of $[M + NH_4]^+$, as it has been already demonstrated in chemical ionization studies.

- Compound identification by means of MS/MS confirms that the molecule being analyzed have the same fragmentation pattern than a chemical standard. However, other compounds from the same family could also show similar fragmentation patterns. A higher degree of confidence in the identification could be achieved by a comprehensive LC-MS/MS or GC-MS/MS identification.

The results presented in this dissertation provide a good starting point for further research. For example:

- In the study regarding yeast metabolism, about 300 compounds were related experimentally with glucose fermentation. However, most of these compounds were identified just by molecular formula and their origin was not decrypted. Further research efforts should continue this study in order to confirm the results by different analytical techniques, achieving a full identification of these compounds, and to get insight about the metabolic pathway by which they are produced.
- SESI technique could be applied to identify other microbial cultures and to get insight about their real-time metabolism.
- In the study regarding the TCA cycle, it is stated that the compounds detected arise from the blood stream. As an extension, blood analysis in parallel with breath analysis would further corroborate this hypothesis. It could also provide an estimation of blood concentrations, by correlating known blood concentrations with exhaled breath signals. Finally, a higher population would result in a reduction of variability in the average signal intensities detected in breath, especially if dietary habits are controlled.
- SESI technique could be applied to find novel biomarkers in breath analysis studies and to achieve, in the near future, the golden aim of personalized medicine.

ANNEXES

Photo of the research group of Renazo Zenoni at ETH Zürich in 2017. Image taken from: http://www.zenobi.ethz.ch/people/group-photos.html. Starting from left of the upper row: Nora Nowak, Katharina Root, Martin köhler, Professor Dr. Renato Zenobi, Dr. Martin Czár, Alberto Tejero, Agni F.M. Gavriilidou, Prince Tiwari and Dominika Strzelecka. In the middle row: Brigitte Bräm, Martin Gaugg, - Ulrike Anders, Luzia Gyr, Timo Niepel, Sahar Ghiasikhou, Jacek Szczerbinski, -, -, Dr. Anna K. Huba, Dr. Guillaume Goubert, -, Mario F. Mirabelli. In the botton row: Jonas Bastian Metternich, Feng Shao, Giovanni Luca Bartolomeo, Dr. Adrien Marchand, and Liqing Zheng.

ANNEX 1. Scientific publications derived from this Thesis

- A. Tejero Rioseras, M. T. Gaugg, P. Martinez-Lozano Sinues, (2017). “Secondary electrospray ionization proceeds via gas-phase chemical ionization” *Anal. Methods*, 9 (34), 5052–5057.

Category: CHEMISTRY, ANALYTICAL

  - Impact factor (2017): 2.073
    - Ranking (2017), (CHEMISTRY, ANALYTICAL) 41/80 Q3
    - Ranking (2017), (FOOD SCIENCE & TECH) 52/133 Q2
    - Ranking (2017), (SPECTROSCOPY) 18/42 Q2

- A. Tejero Rioseras, D. Garcia Gomez, B. E. Ebert, L. M. Blank, A. J. Ibáñez, P. M.-L. Sinues, (2017). “Comprehensive Real-Time Analysis of the Yeast Volatilome” *Sci. Rep.*, 7 (1), 14236.

Category: MULTIDISCIPLINARY SCIENCES

  - Impact factor (2017): 4.122
    - Ranking (2017), (MULTIDISCIPLINARY SCI) 12/64 Q1

- A. Tejero Rioseras, K. D. Singh, N. Novak, M. T. Gaugg, T. Bruderer, R. Zenobi, P. Martinez-Lozano Sinues, (2018). “Real-Time Monitoring of Tricarboxylic Acid Metabolites in Exhaled Breath” *Anal. Chem.*, 90 (11), 6453–6460.

Category: CHEMISTRY, ANALYTICAL

  - Impact factor (2017): 6.042
    - Ranking (2017), (CHEMISTRY, ANALYTICAL) 4/80 Q1

ANNEX 2. Supporting information – "Comprehensive Real-Time Analysis of the Yeast Volatilome"

Experimental Section

Secondary Electrospray Ionization-Mass Spectrometry

Secondary Electrospray Ionization-Mass Spectrometry (SESI-MS) experiments were carried out using a commercial ion source (SEADM S.L.) [104] plugged onto a Thermo-Fisher LTQ Orbitrap mass spectrometer. The SESI solvent was 0.1% formic acid in water infused at ~100 nL/min through a 20 µm ID silica capillary. The electrospray voltage was set to 5.4 kV (i.e., focusing electrode 2.59 kV and impact electrode 1.6 kV). The sweep gas used for cleaning the electrospray region was set to 2 a.u. All other internal Orbitrap parameters were optimized during calibration. The m/z range was set to 50 – 500 Da. Accumulation time was 1 minute to prevent the generation of intractable large files during several hours of volatiles monitoring. Pre-set resolution was 30,000 and typical mass accuracies were within 2 ppm by using common chemical noise encountered in SESI-MS background as lock masses. [137][138]

The bioreactor consisted of an autoclaved 100 mL three-neck flask filled with 20 mL of medium, stirred at 800 rpm with a Teflon magnet and uniformly heated at 40 °C in a water bath. The metabolites produced during yeast growth were dragged downstream towards the SESI source by a continuous flow of compressed air at 0.5 L/min. The compressed air was filtered and humidified upstream the bioreactor. The bioreactor was connected to the ion source through a stainless-steel tube (OD 6 mm) heated at 130 °C to minimize metabolite adsorption onto the tube walls. "Figure S 10" shows the experimental set-up.

Yeast cell cultures

All the described experiments in this study were performed with *Saccharomyces cerevisiae*, prototrophic, YSBN.6 (wild-type) strain. Cells were grown in minimal defined medium: BD (DIFCO) yeast nitrogen base (#233520); and 2% glucose (as only carbon-source). For each experiment, pre-cultures were inoculated from SD plates and grown at 30°C while shaking with 300 rpm for 8 to 10 hours in 1 mL pre-culture tubes. Then, the cells were inoculated (starting optical density; OD ~0.1) in 500 mL Erlenmeyer flasks with 50 mL of growth medium. Cultivation was performed at 30 °C with stirrer bar at 300 rpm until an OD of 1.2. The YSBN.6 strains *zwf1*Δ (ΔZWF1::Kan) and *pfk1*Δ (ΔPFK1::Kan), were grown in a similar minimal defined medium with the addition of 0.02 % (v/v) of kanamycin and under the same time, temperature, and mixing conditions. To start the experiment, 1 mL of inoculum with an OD (between 0.8 to 1.0) was injected into the bioreactor for obtaining a starting OD of 0.1. When the ethanol signal decayed, 0.8 mL of 50 % glucose was injected to prolong the exponential growth phase.

During the experiment, a time-lapse camera took a picture of the bioreactor every minute. Using ImageJ, an open platform for scientific image analysis, [208] yeast concentrations of relative values were obtained by averaging grayscale level in a region of interest of the image in a video. Absolute OD values were also obtained at the beginning and at the end of each experiment with a Thermo electron corporation GENESYS 10 UV spectrophotometer.

Data analysis

The raw mass spectra were transformed into mzXML format via MSConvert (Proteowizard) [209] and imported to MATLAB (R2016b). Each sample file was interpolated linearly (106 points in the range 50-500 Da). A peak list was generated with an intensity threshold of 50 a.u. The resulting time traces (i.e. signal intensity for each m/z value as a function of time) were subjected to an agglomerative hierarchical cluster tree (Ward method; Euclidean distance; Figure 21c and 2d). To ease visualization, the time traces were smoothed (moving mean; span = 25). Principal component analysis was also used for dimensionality reduction and visualization of the mass spectra (Figure 23a-b). Generation of molecular formulae from accurate mass was performed assuming protonated ions in the positive ion mode and deprotonated ions in negative mode. The so-called seven golden rules [210] were taken into account.

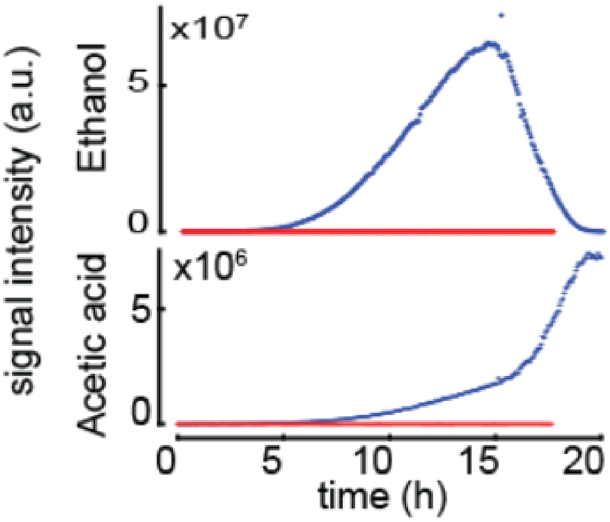

Figure S 1. Signal intensity of ethanol and acetic acid after $^{13}C_6$-glucose injection in a solution containing yeast (same as Figure 21b; blue) and a negative control (red) under exactly the same conditions, but without yeast. As expected, ethanol and acetic acid production can be attributed to yeast growth.

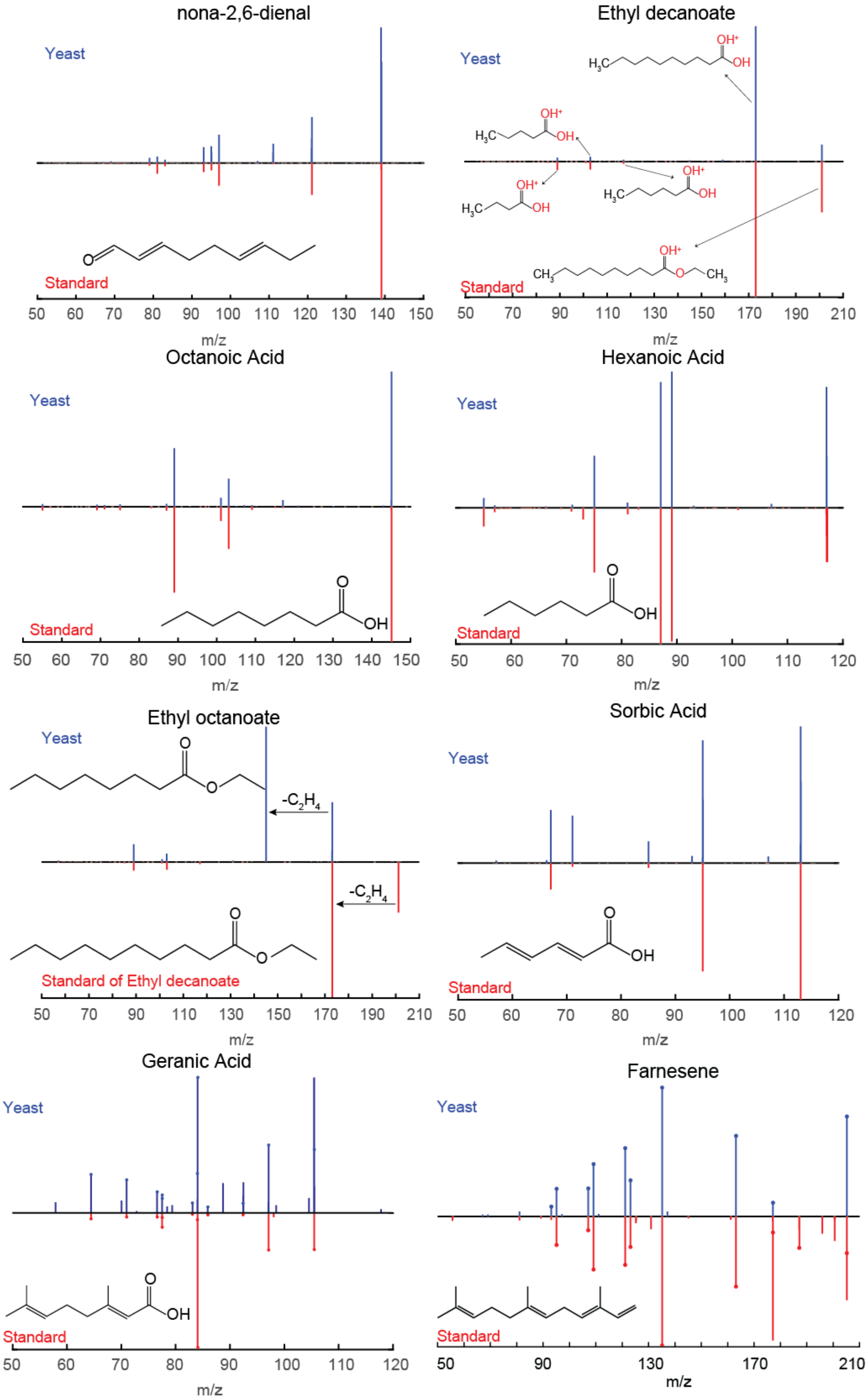

Figure S 2 Head-to-tail MS/MS mass spectra of selected yeast metabolites (top) and standards (bottom). [Article's](#) copyright: Attribution 4.0 International ([CC BY 4.0](#))

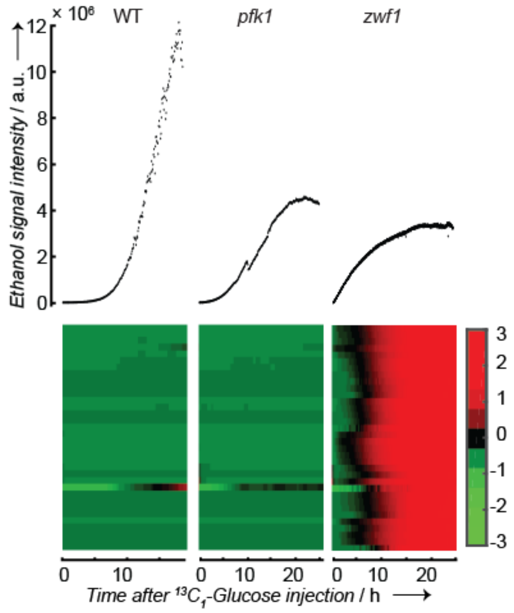

Figure S 3. Replicated experiment injecting $^{13}C_1$-glucose to the cultivations of the three yeast strains WT, pfk1, zwf1 provided a similar global picture as that shown in Figure 22 of the main text, including ethanol (top traces) and a series of odd-numbered carbon compounds (i.e., $C_9H_{18}O$, $C_{11}H_{22}O$, $C_{13}H_{26}O$ and $C_{15}H_{30}O$) characteristic of zwf1 (heatmap. [Article's] copyright: Attribution 4.0 International ([CC BY 4.0])

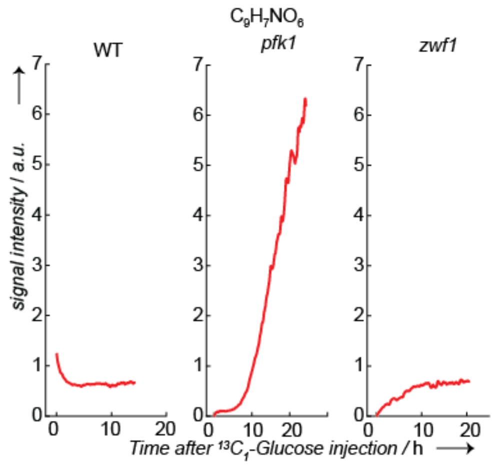

Figure S 4. One selected compound detected in excess in mutant pfk1

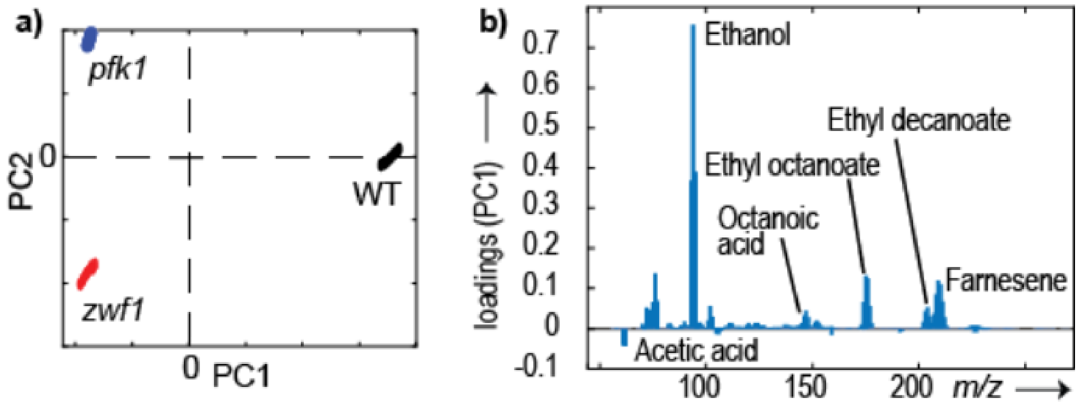

Figure S 5. PCA including ethanol and acetic acid. Article's copyright: Attribution 4.0 International (CC BY 4.0)

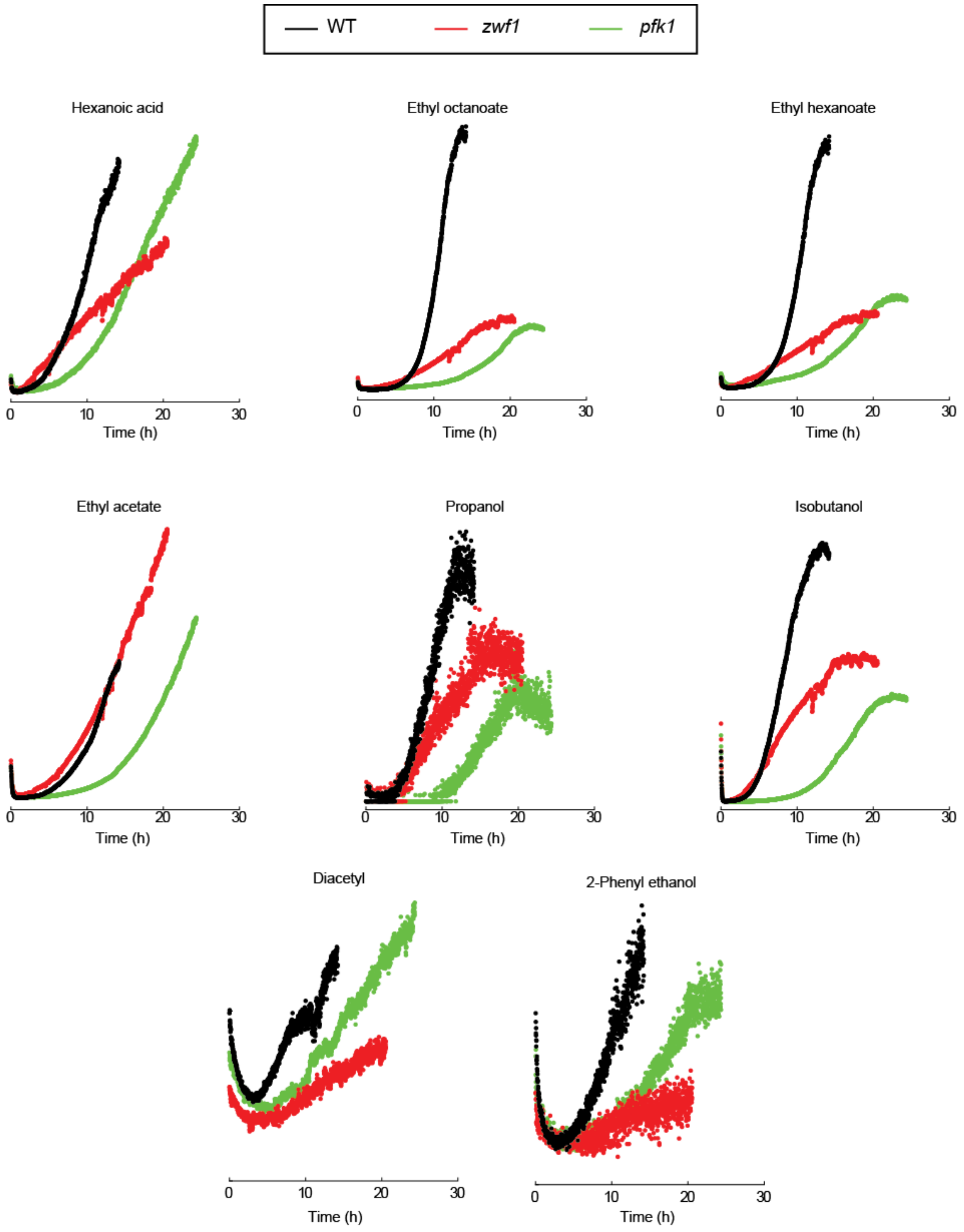

Figure S 6. Aroma-relevant compounds were produced at different rates for the three strains investigated. Note that the bottom five compounds were not confirmed via MS/MS and thus assignment is only based on accurate mass and isotopic distribution. Article's copyright: Attribution 4.0 International (CC BY 4.0)

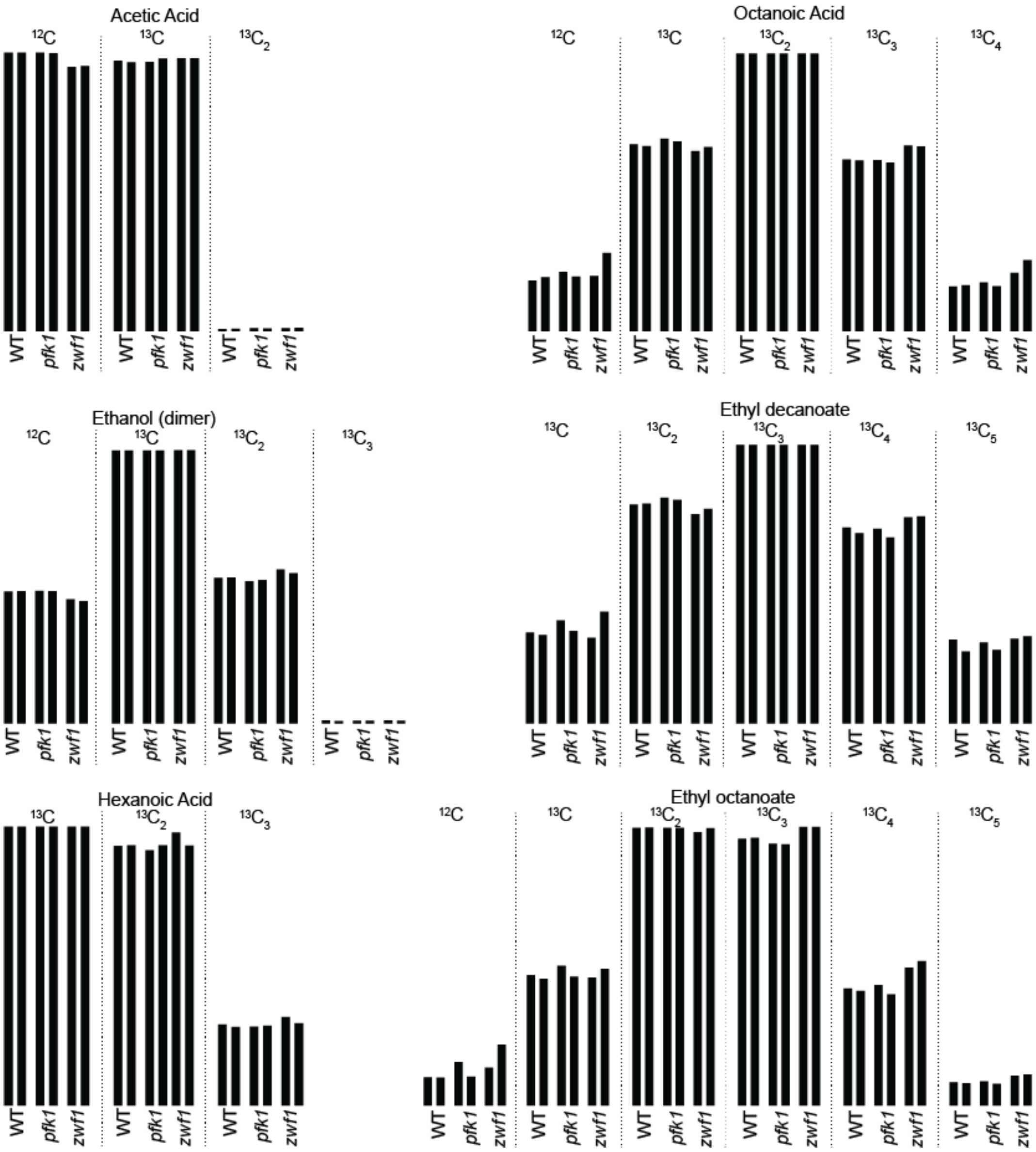

Figure S 7. Replicate experiment confirmed enhanced incorporation of ^{13}C in metabolites of zwf1 as compared to WT and pfk1. Article's copyright: Attribution 4.0 International (CC BY 4.0)

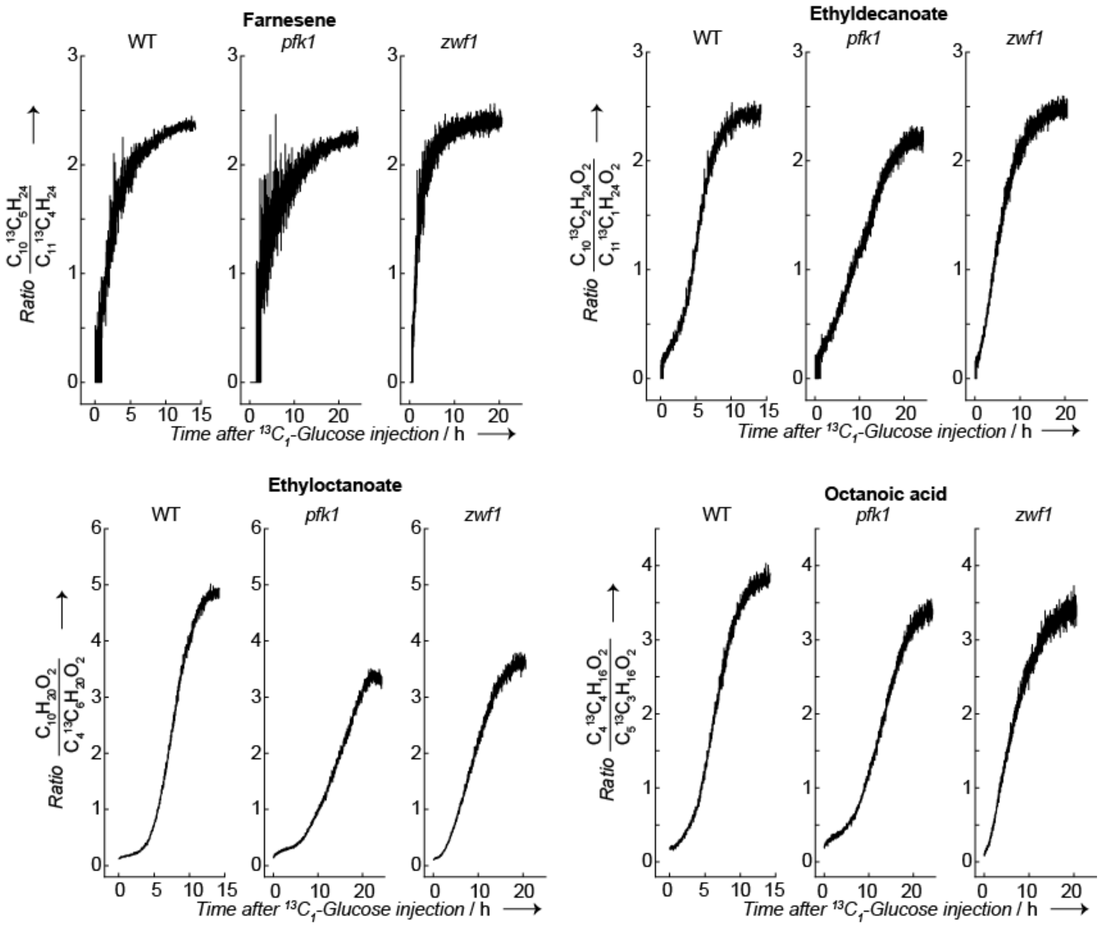

Figure S 8. $^{13}C/^{12}C$ ratios for identified compounds show the kinetics of volatiles production upon $^{13}C_1$-glucose injection. [Article's](#) copyright: Attribution 4.0 International ([CC BY 4.0](#))

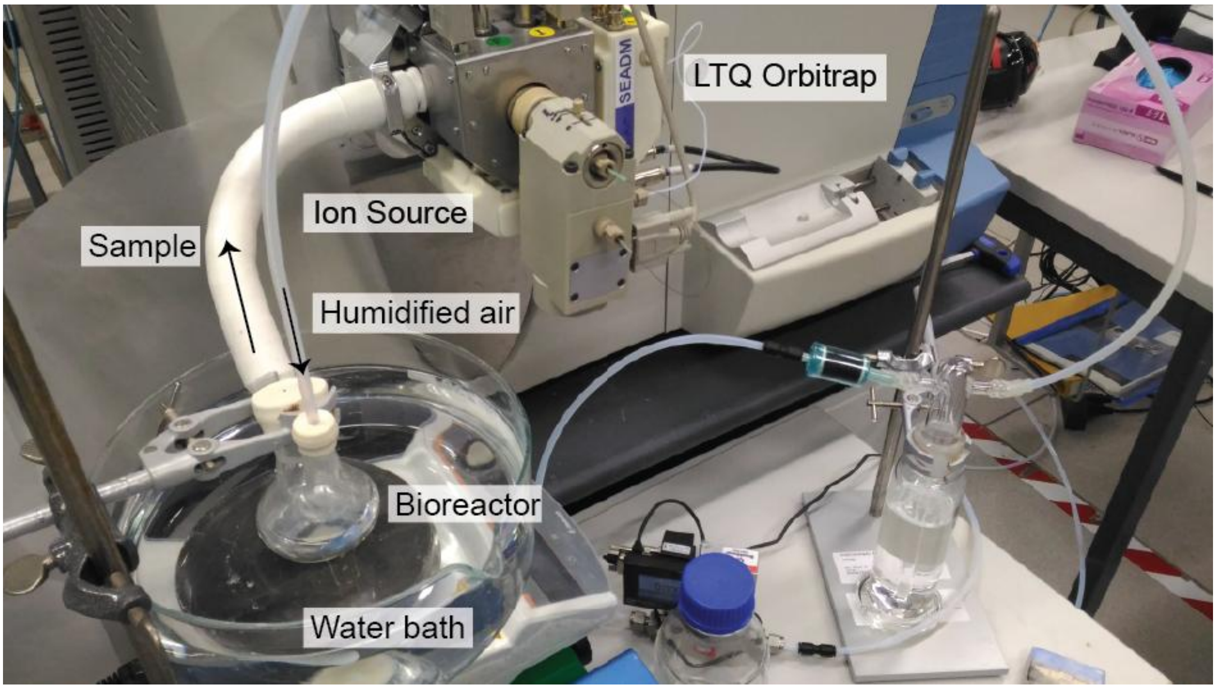

Figure S 9. Experimental set-up used to monitor yeast volatiles during growth in glucose. Article's copyright: Attribution 4.0 International (CC BY 4.0)

Table S 1. 263 signals detected upon injecting $^{13}C_6$-glucose and ^{12}C-glucose to WT. The order corresponds to the one shown in the heatmap from Figure 21b (top-to-bottom). Note how series of molecules with similar molecular formula tend to cluster together. The molecular formulae were generated assuming $[M+H]^+$ ion formation. Article's copyright: Attribution 4.0 International (CC BY 4.0)

#	Molecular formula	*m/z* measured with ^{12}C-glucose	Mass error (ppm)	*m/z* measured with $^{13}C_6$-glucose	Mass error (ppm)	RDBE
1 YMDB	C2H6O2	63.0440	-0.2	65.0506	-1.8	0
2 YMDB	C10H10O2	163.0754	0.1	173.1088	-0.4	6
3 HMDB	C8H6O	119.0486	-4.8	127.0754	-4.3	6
4 HMDB	C8H8N2	133.0759	-0.8	141.1032	2.6	6
5 YMDB	C8H8O4	169.0495	-0.4	177.0763	-0.3	5
6 HMDB	C11H10O3	191.0705	1.1	202.1074	1.5	7
7 HMDB	C8H3NO2	146.0236	-0.5	154.0500	-3.2	8
8 HMDB	C11H9NO2	188.0707	0.3	199.1076	0.8	8
9	C11H9NO	172.0757	0.1	183.1126	0.6	8
10 HMDB	C11H11NO	174.0908	-3.1	185.1286	2.5	7
11 JP	C12H9NO	184.0754	-1.6	196.1163	2.1	9
12	C11H5NO	168.0450	3.9	179.0820	4.2	10

13 [HMDB]	C8H8N2O2	165.0658	-0.1	173.0922	-2.5	6
14	C19H24	253.1951	0.3	272.2580	-2.6	8
15 [YMDB]	C8H8O3	153.0545	-0.8	161.0809	-3.4	5
16 [HMDB]	C8H7NO5	198.0396	-0.6	206.0655	-4.9	6
17	C9H6O5	195.0286	-1.2	204.0585	-2.4	7
18 [HMDB]	C14H10O3	227.0700	-1.2	241.1180	3.2	10
19 [YMDB]	C14H12O3	229.0860	0.4	243.1335	2.8	9
20 [HMDB]	C11H14	147.1167	-0.8	158.1541	2.6	5
21	C7H19N5O4	238.1517	3.2	245.1746	0.7	1
22 [HMDB]	C11H10O2	175.0755	0.9	186.1125	1.3	7
23 [YMDB]	C11H9NO3	204.0656	0.5	215.1026	0.9	8
24 [HMDB]	C11H8O5	221.0444	-0.3	232.0818	2.1	8
25	C8H11NO4	186.0762	0.4	194.1021	-4.1	4
26	C8H3NO	130.0282	-4.4	138.0550	-3.9	8
27 [YMDB]	C7H14O	115.1116	-1.7	122.1353	0.9	1
28 [HMDB]	C6H12	85.1013	2.0	91.1211	-1.6	1
29 [HMDB]	C19H28O2	289.2162	-0.1	308.2795	-1.2	6
30 [HMDB]	C10H16O3	185.1174	1.2	195.1509	0.7	3
31 [YMDB]	C10H18O3	187.1330	0.7	197.1664	0.2	2
32 [YMDB]	C10H18O	155.1431	0.2	165.1765	-0.3	2
33 [C]	C5H8	69.0701	3.3	74.0868	2.5	2
34	C7H6	91.0544	1.7	98.0777	0.0	5
35	C9H3NO3	174.0187	0.7	183.0481	-3.2	9
36 [YMDB]	C9H10O3	167.0702	-0.4	176.1001	-1.9	5
37 [YMDB]	C5H8O3	117.0545	-0.8	122.0712	-1.1	2
38 [YMDB]	C11H22O	171.1743	-0.1	182.2113	0.4	1
39 [YMDB]	C16H32O2	257.2478	1.0	273.3014	1.1	1
40 [HMDB]	C7H16O2	133.1225	1.6	140.1458	0.4	0
41 [YMDB]	C4H10O	75.0805	0.4	79.0941	3.4	0
42 [YMDB]	C4H12O2	93.0910	-0.2	97.1046	2.2	-1
43 [YMDB]	C3H8O	61.0648	-0.2	64.0749	0.8	0
44	C5H14O2	107.1067	0.2	112.1234	-0.2	-1
45 [YMDB]	C12H24O2	201.1854	2.6	213.2250	-0.5	1
46	C9H24N4O	205.2027	1.8	214.2317	-3.7	0
47 [JP]	C5H10	71.0857	1.8	76.1024	1.1	1
48	C7H18O2	135.1381	0.8	142.1614	-0.2	-1
49 [YMDB]	C14H28O2	229.2164	0.7	243.2634	1.3	1

50 [YMDB]	C6H14O2	119.1068	1.4	125.1266	-1.2	0
51 [HMDB]	C4H6N2O	99.0557	3.8	103.0689	1.6	3
52	C4H10N2O	103.0868	1.8	107.1004	3.9	1
53 [HMDB]	C4H9N	72.0807	-1.6	76.0943	1.6	1
54 [HMDB]	C17H30O	251.2374	1.8	268.2946	2.5	3
55 [HMDB]	C18H28O2	277.2165	1.0	295.2767	0.7	5
56	C10H23NO2	190.1803	0.8	200.2137	0.3	0
57 [YMDB]	C11H22O2	187.1693	0.2	198.2062	0.6	1
58 [YMDB]	C10H20O2	173.1540	2.5	183.1875	1.9	1
59 [YMDB]	C6H16O2	121.1224	0.6	127.1426	1.6	-1
60 [YMDB]	C13H26O2	215.2007	0.6	228.2438	-1.5	1
61	C12H27NO2	218.2117	1.1	230.2517	0.2	0
62	C18H31NO2	294.2427	-0.1	312.3021	-3.1	4
63	C5H15N5O2	178.1304	3.3	183.1458	-4.4	1
64 [JP]	C20H38O4	343.2845	0.5	363.3522	2.5	2
65	C13H22N2O5	287.1612	3.7	300.2034	-1.0	4
66 [HMDB]	C18H34O4	315.2531	0.2	333.3138	1.4	2
67	C12H20	165.1640	1.1	177.2040	-0.1	3
68	C5H4	65.0385	-0.5	70.0553	-1.1	4
69 [YMDB]	C8H16O2	145.1222	-0.7	153.1490	-0.5	1
70 [YMDB]	C18H34O2	283.2636	1.5	301.3238	1.3	2
71	C10H5NO5	220.0243	1.1	230.0568	-3.2	9
72	C10H5NO2	172.0394	0.7	182.0719	-4.8	9
73 [HMDB]	C13H20	177.1636	-0.7	190.2076	1.6	4
74 [YMDB]	C15H22	203.1795	0.3	218.2296	-0.3	5
75 [YMDB]	C15H24O	221.1900	0.0	236.2401	-0.5	4
76	C7H12	97.1010	-1.4	104.1248	1.6	2
77 [YMDB]	C8H14O	127.1117	-0.4	135.1385	-0.2	2
78 [HMDB]	C9H16	125.1324	-0.4	134.1628	1.1	2
79 [YMDB]	C8H14	111.1167	-0.9	119.1436	-0.6	2
80 [HMDB]	C6H10	83.0858	3.2	89.1056	-0.6	2
81 [HMDB]	C6H6	79.0542	0.1	85.0745	1.7	4
82 [HMDB]	C7H8	93.0699	0.6	100.0932	-0.9	4
83 [HMDB]	C12H18	163.1484	1.7	175.1884	0.5	4
84	C15H29NO	240.2323	0.3	255.2828	1.5	2
85	C15H27N1	222.2222	2.5	237.2719	0.0	3
86 [HMDB]	C7H10	95.0855	-0.5	102.1092	2.6	3

87 HMDB	C8H12	109.1012	0.0	117.1280	0.2	3
88 YMDB	C8H10	107.0856	0.9	115.1124	1.1	4
89 YMDB	C15H24	205.1950	-0.2	220.2461	3.3	4
90 HMDB	C11H16	149.1327	1.5	160.1696	2.0	4
91 YMDB	C9H12	121.1013	1.2	130.1312	-0.9	4
92 YMDB	C15H26O	223.2060	1.6	238.2561	1.0	3
93 HMDB	C9H14	123.1169	0.4	132.1472	1.8	3
94 YMDB	C10H14	135.1170	1.4	145.1504	0.7	4
95	C6H8	81.0698	-1.1	87.0900	0.5	3
96 YMDB	C4H10O2	91.0754	0.8	95.0886	-1.4	0
97 YMDB	C2H5NO	60.0447	4.9	62.0513	3.0	1
98 HMDB	C5H6	67.0545	4.8	72.0713	3.9	3
99	C10H5NO4	204.0289	-1.2	214.0623	-1.5	9
100	C10H5NO3	188.0344	0.8	198.0669	-4.2	9
101 HMDB	C10H7NO2	174.0550	0.1	184.0879	-2.8	8
102 HMDB	C10H7NO	158.0600	-0.2	168.0939	2.0	8
103 YMDB	C10H16	137.1326	0.7	147.1660	0.0	3
104 HMDB	C11H10O4	207.0654	1.2	218.1019	-0.5	7
105 YMDB	C9H10O	135.0803	-1.2	144.1102	-2.9	5
106 YMDB	C8H10O3	155.0701	-1.4	163.0964	-3.9	4
107 YMDB	C8H10O2	139.0751	-1.9	147.1015	-4.7	4
108 YMDB	C5H6O2	99.0440	-0.4	104.0607	-0.8	3
109 YMDB	C5H8O4	133.0495	-0.3	138.0658	-3.9	2
110 HMDB	C4H10O3	107.0704	1.1	111.0836	-0.8	0
111 HMDB	C7H15NO2	146.1177	0.7	153.1405	-3.2	1
112 HMDB	C7H14	99.1166	-2.4	106.1403	0.6	1
113 HMDB	C9H18O3	175.1329	-0.1	184.1632	1.0	1
114	C13H22	179.1796	1.2	192.2227	-1.3	3
115 HMDB	C15H26O2	239.2005	-0.2	254.2506	-0.7	3
116 YMDB	C9H16O	141.1274	0.0	150.1573	-1.7	2
117 HMDB	C15H28O	225.2216	1.2	240.2712	-1.3	2
118 HMDB	C10H18	139.1481	0.0	149.1815	-0.6	2
119 YMDB	C6H12O	101.0959	-2.3	107.1161	-1.0	1
120 YMDB	C11H20O	169.1588	0.5	180.1957	1.0	2
121 HMDB	C12H12	157.1008	-2.1	169.1413	-0.4	7
122 HMDB	C14H24	193.1953	1.4	207.2419	-0.1	3
123 YMDB	C9H10	119.0858	2.0	128.1152	-3.6	5

124 YMDB	C6H4	77.0387	1.4	83.0589	2.9	5
125	C15H26	207.2106	-0.7	222.2612	0.8	3
126 YMDB	C15H30O2	243.2321	0.9	258.2817	-1.4	1
127 HMDB	C11H18	151.1483	0.9	162.1848	-1.4	3
128 HMDB	C13H24	181.1952	0.7	194.2387	0.6	2
129 YMDB	C9H18O2	159.1379	-0.4	168.1678	-1.8	1
130 YMDB	C10H16O	153.1275	0.9	163.1609	0.3	3
131 YMDB	C9H16O2	157.1223	0.3	166.1522	-1.3	2
132 HMDB	C15H20	201.1639	0.7	216.2145	2.2	6
133 HMDB	C4H6	55.0544	3.3	59.0676	-0.6	2
134 HMDB	C12H16	161.1324	-0.5	173.1729	1.1	5
135 HMDB	C20H34O	291.2685	0.8	311.3357	1.6	4
136 HMDB	C16H26	219.2107	0.0	235.2648	2.1	4
137 HMDB	C20H32	273.2580	1.0	293.3248	0.4	5
138 HMDB	C10H16O2	169.1220	-1.6	179.1555	-2.0	3
139 HMDB	C8H12O3	157.0861	0.9	165.1129	1.0	3
140 YMDB	C10H14O	151.1115	-1.4	161.1454	0.9	4
141 YMDB	C7H14O2	131.1065	-1.1	138.1298	-2.1	1
142 YMDB	C6H8O3	129.0547	0.4	135.0749	1.3	3
143 HMDB	C8H9NO3	168.0657	0.8	176.0916	-4.2	5
144 HMDB	C8H11NO3	170.0812	0.2	178.1076	-2.2	4
145 HMDB	C16H28O	237.2217	1.7	253.2753	1.8	3
146 YMDB	C16H30O2	255.2322	1.4	271.2859	1.5	2
147 YMDB	C11H14O3	195.1016	0.1	206.1385	0.5	5
148 YMDB	C7H10O2	127.0754	0.4	134.0987	-0.7	3
149 HMDB	C11H12O3	193.0860	0.6	204.1230	1.0	6
150 YMDB	C3H8O3	93.0547	0.8	96.0648	1.5	0
151	C14H4N4O	245.0447	-4.6	259.0922	-2.0	15
152 YMDB	C18H36O2	285.2791	1.2	303.3394	0.9	1
153 YMDB	C10H18O2	171.1380	0.5	181.1715	0.0	2
154 YMDB	C7H12O2	129.0910	-0.4	136.1138	-4.8	2
155	C10H3NO4	202.0142	3.7	212.0463	-3.2	10
156 YMDB	C9H18O	143.1429	-0.7	152.1733	0.6	1
157 HMDB	C7H12O	113.0960	-0.8	120.1193	-2.0	2
158 YMDB	C10H12	133.1010	-1.3	143.1344	-1.7	5
159 YMDB	C9H14O	139.1118	0.7	148.1417	-1.1	3
160 YMDB	C6H8O	97.0648	-0.4	103.0850	0.9	3

161 YMDB	C12H22O2	199.1694	0.9	211.2090	-2.2	2
162 YMDB	C6H10O3	131.0702	-0.4	137.0905	0.6	2
163 YMDB	C6H8O2	113.0597	0.0	119.0799	1.1	3
164 HMDB	C8H13NO	140.1068	-1.1	148.1337	-0.9	3
165JP	C14H24O	209.1903	1.5	223.2374	2.1	3
166 YMDB	C14H26O2	227.2008	1.1	241.2474	-0.1	2
167	C5H13NO2	120.1018	-0.6	125.1185	-0.9	0
168 YMDB	C10H12O2	165.0909	-0.5	175.1243	-0.9	5
169 YMDB	C6H10O	99.0803	-1.4	105.1005	-0.1	2
170 HMDB	C15H22O	219.1744	0.5	234.2246	-0.1	5
171 HMDB	C15H20O	217.1589	0.9	232.2090	0.3	6
172 HMDB	C11H16O	165.1272	-1.1	176.1642	-0.5	4
173 HMDB	C13H18	175.1481	-0.2	188.1916	-0.3	5
174	C11H12	145.1012	-0.2	156.1381	0.4	6
175 YMDB	C11H16O2	181.1222	-0.7	192.1591	-0.2	4
176 YMDB	C10H14O2	167.1065	-1.0	177.1399	-1.4	4
177 HMDB	C9H14O3	171.1018	1.1	180.1316	-0.4	3
178 HMDB	C16H24	217.1952	0.4	233.2488	0.6	5
179	C6H15NO2	134.1175	-0.2	140.1378	0.7	0
180 YMDB	C4H11NO2	106.0861	-1.1	110.0998	1.1	0
181 YMDB	C5H12O2	105.0911	1.2	110.1078	0.7	0
182 YMDB	C6H12O3	133.0858	-1.1	139.1060	-0.1	1
183	C5H13NO3	136.0968	-0.2	141.1135	-0.5	0
184 YMDB	C5H10O3	119.0705	2.2	124.0868	-1.8	1
185 YMDB	C5H8O2	101.0600	3.1	106.0767	2.6	2
186 YMDB	C4H8O2	89.0599	2.0	93.0731	-0.4	1
187 HMDB	C5H6O3	115.0390	0.0	120.0557	-0.3	3
188 YMDB	C3H8O2	77.0597	0.4	80.0699	1.2	0
189 YMDB	C3H6O	59.0492	1.4	62.0593	2.4	1
190 YMDB	C2H5NO2	76.0396	4.5	78.0462	3.0	1
191 HMDB	C15H24O2	237.1850	0.2	252.2355	1.5	4
192 HMDB	C14H22	191.1793	-0.5	205.2259	-1.9	4
193 YMDB	C10H10O	147.0804	-0.2	157.1138	-0.7	6
194 HMDB	C16H26O	235.2057	0.2	251.2598	2.2	4
195 HMDB	C16H28O2	253.2162	0.0	269.2699	0.2	3
196 YMDB	C5H10O	87.0806	2.0	92.0973	1.4	1
197 YMDB	C6H6O	95.0492	0.6	101.0694	1.8	4

198 [YMDB]	C10H12O	149.0960	-0.8	159.1294	-1.3	5
199 [HMDB]	C7H10O	111.0804	0.0	118.1037	-1.2	3
200 [YMDB]	C8H14O2	143.1067	0.0	151.1335	0.1	2
201 [YMDB]	C8H14O3	159.1016	0.3	167.1284	0.4	2
202 [YMDB]	C8H12O	125.0961	0.4	133.1230	0.5	3
203 [YMDB]	C7H8O	109.0649	0.9	116.0882	-0.4	4
204 [HMDB]	C9H14O2	155.1068	0.9	164.1367	-0.7	3
205 [HMDB]	C11H14O	163.1117	-0.5	174.1486	0.1	5
206 [YMDB]	C9H12O2	153.0908	-1.4	162.1207	-2.9	4
207	C12H14	159.1168	0.1	171.1569	-1.0	6
208 [HMDB]	C15H22O2	235.1694	0.6	250.2195	0.1	5
209 [YMDB]	C9H12O	137.0958	-1.9	146.1262	-0.5	4
210	C10H10	131.0855	-0.5	141.1193	2.1	6
211 [YMDB]	C9H12O3	169.0858	-1.0	178.1161	0.1	4
212 [HMDB]	C15H20O2	233.1538	1.0	248.2044	2.3	6
213 [HMDB]	C10H12O3	181.0863	2.3	191.1193	-0.6	5
214 [YMDB]	C10H14O3	183.1014	-0.7	193.1349	-1.1	4
215 [HMDB]	C20H38O2	311.2950	1.7	331.3618	1.1	2
216	C15H31NO	242.2483	1.7	257.2984	1.1	1
217	C16H33NO2	272.2589	1.9	288.3126	1.9	1
218 [YMDB]	C18H32O2	281.2480	1.9	299.3069	-2.9	3
219 [YMDB]	C8H16O	129.1272	-1.1	137.1545	2.4	1
220 [YMDB]	C9H10O2	151.0752	-0.8	160.1051	-2.3	5
221 [YMDB]	C3H7NO2	90.0549	-0.8	93.0646	-4.9	1
222 [HMDB]	C4H4O3	101.0233	-0.4	105.0365	-2.4	3
223 [YMDB]	C10H20O3	189.1486	0.2	199.1820	-0.2	1
224	C7H3NO3	150.0184	-1.1	157.0426	3.7	7
225 [HMDB]	C3H6N2O2	103.0505	2.7	106.0606	3.3	2
226 [HMDB]	C9H16O3	173.1173	0.5	182.1472	-0.9	2
227 [YMDB]	C13H22O	195.1746	1.4	208.2177	-1.0	3
228 [HMDB]	C12H20O	181.1589	1.2	193.1985	-2.2	3
229 [YMDB]	C6H10O2	115.0753	-0.8	121.0955	0.3	2
230 [YMDB]	C5H10O2	103.0756	2.1	108.0923	1.6	1
231 [YMDB]	C3H6O2	75.0442	1.7	78.0543	2.5	1
232 [HMDB]	C5H8O	85.0651	3.2	90.0818	2.5	2
233 [YMDB]	C4H8O	73.0649	1.8	77.0781	-1.1	1
234 [YMDB]	C4H6O2	87.0443	3.1	91.0575	0.6	2

235 HMDB	C11H14O2	179.1066	-0.2	190.1436	0.3	5
236 HMDB	C15H24O3	253.1804	2.1	268.2300	-0.1	4
237 HMDB	C11H18O2	183.1377	-1.2	194.1747	-0.7	3
238 YMDB	C6H12O2	117.0913	2.2	123.1110	-0.5	1
239 YMDB	C2H4O2	61.0285	1.4	63.0351	-0.4	1
240 HMDB	C4H6O	71.0494	3.2	75.0626	0.1	2
241	C14H20	189.1638	0.0	203.2104	-1.4	5
242 HMDB	C15H22O3	251.1648	2.5	266.2140	-1.4	5
243 HMDB	C15H24O4	269.1749	0.5	284.2246	-1.5	4
244	C5H12N2	101.1071	-2.7	106.1242	1.3	1
245 HMDB	C18H32O	265.2526	0.1	283.3129	-0.1	3
246 HMDB	C11H14O4	211.0965	0.3	222.1330	-1.4	5
247 HMDB	C8H9NO4	184.0606	1.0	192.0865	-3.6	5
248	C16H31NO2	270.2434	2.2	286.2966	0.7	2
249 HMDB	C4H9NO	88.0756	-0.8	92.0893	1.8	1
250 YMDB	C14H22O	207.1743	-0.2	221.2214	0.5	4
251 YMDB	C13H16	173.1325	0.4	186.1756	-2.2	6
252 YMDB	C8H8	105.0701	1.9	113.0964	-2.1	5
253 HMDB	C11H16O3	197.1171	-0.4	208.1541	0.0	4
254 HMDB	C15H22O4	267.1593	0.9	282.2086	-2.8	5
255	C14H18	187.1482	0.6	201.1948	-0.9	6
256	C11H18O3	199.1331	1.4	210.1696	-0.4	3
257 HMDB	C15H26O4	271.1904	0.2	286.2410	1.3	3
258 HMDB	C15H29NO4	288.2158	-4.0	303.2673	0.2	2
259 HMDB	C13H24O	197.1897	-1.4	210.2332	-1.4	2
260 HMDB	C11H18O	167.1432	1.1	178.1797	-1.0	3
261 YMDB	C11H20O2	185.1537	0.7	196.1907	1.1	2
262 HMDB	C13H24O2	213.1851	1.0	226.2278	-3.1	2
263 HMDB	C17H32O	253.2529	1.4	270.3097	0.4	2

YMDB Molecular formula matches at least with one compound in yeast metabolome database

HMDB Molecular formula matches at least with one compound in human metabolome database

JP Molecular formula matches at least with one compound in Massbank database

C Molecular formula matches at least with one compound in KEGG PATHWAY database

Table S 2. Mass spectral features detected upon injecting $^{13}C_1$-glucose to WT, zwf1 and pfk1. The order corresponds to the one shown in the heatmap from Figure 22d (top-to-bottom). The molecular formulae were generated assuming $[M+H]^+$ ion formation. [Article's](#) copyright: Attribution 4.0 International ([CC BY 4.0](#))

#	M/Z	MOLECULAR FORMULA (^{12}C & ^{13}C)	UNIQUE MOLECULAR FORMULA	MASS ERROR (PPM)
1	269.0499	C11(13C)1H5N5O3	C12H5N5O3	0.04
2	270.0530	C10(13C)2H5N5O3	C12H5N5O3	-1.01
3	268.0464	C12H5N5O3	C12H5N5O3	-0.58
4	149.0870	C8(13C)2H10O	C10H10O	-0.95
5	138.1034	C3(13C)2H13NO3	C5H13NO3	-1.07
6	271.0457	C10(13C)3H5N3O4	C13H5N3O4	1.40
7	79.0663	C1(13C)2H8O2	C3H8O2	-1.07
8	148.0835	C9(13C)1H10O	C10H10O	-2.09
9	227.0386	C8(13C)1H7NO6	C9H7NO6	2.97
10	226.0356	C9H7NO6	C9H7NO6	4.24
11	228.0422	C7(13C)2H7NO6	C9H7NO6	3.69
12	228.0314	C5(13C)4H5NO6	C9H5NO6	-4.29
13	108.0197	-	-	-
14	209.0277	C8(13C)1H5NO5	C9H5NO5	1.32
15	77.0427	C1(13C)1H5NO2	C2H5NO2	0.71
16	215.1554	C10(13C)2H20O3	C12H20O3	0.92
17	192.0480	C8(13C)1H6N2O3	C9H6N2O3	-2.41
18	200.1640	C9(13C)3H20O2	C12H20O2	1.60
19	199.1605	C10(13C)2H20O2	C12H20O2	0.77
20	172.1326	C7(13C)3H16O2	C10H16O2	1.34
21	74.0317	C2(13C)1H4O2	C3H4O2	-0.79
22	176.0911	C5(13C)3H12O4	C8H12O4	1.33
23	170.0530	C7(13C)1H8O4	C8H8O4	0.55
24	168.0733	C8(13C)1H10O3	C9H10O3	-2.13
25	202.1155	C9(13C)1H16O4	C10H16O4	-0.06
26	109.0559	C5(13C)2H6O	C7H6O	0.73
27	102.0268	C3(13C)1H4O3	C4H4O3	1.26
28	192.1676	C9(13C)1H22O3	C10H22O3	0.54
29	191.1641	C10H22O3	C10H22O3	-0.33
30	201.1120	C10H16O4	C10H16O4	-0.89
31	160.0684	C6(13C)1H10O4	C7H10O4	-0.90
32	236.1129	C7(13C)3H16O6	C10H16O6	3.66
33	159.0653	C7H10O4	C7H10O4	0.88
34	167.0612	C7(13C)2H8O3	C9H8O3	-0.57
35	186.0842	C8(13C)1H12O4	C9H12O4	0.22
36	105.0459	C2(13C)2H6O3	C4H6O3	1.90
37	133.0405	C3(13C)2H6O4	C5H6O4	-0.49
38	103.0299	C2(13C)2H4O3	C4H4O3	-1.51
39	190.1337	C5(13C)5H16O3	C10H16O3	-1.53
40	201.1030	C8(13C)2H14O4	C10H14O4	-0.99
41	183.0925	C8(13C)2H12O3	C10H12O3	-0.80

42	71.0404	C2(13C)2H4O	C4H4O	2.90
43	168.1015	C7(13C)3H12O2	C10H12O2	2.53
44	154.0858	C6(13C)3H10O2	C9H10O2	2.47
45	131.0886	C3(13C)4H10O2	C7H10O2	-1.41
46	143.0887	C4(13C)4H10O2	C8H10O2	-0.31
47	107.0525	(13C)4H6O3	C4H6O3	0.77
48	126.0629	C6(13C)1H8O2	C7H8O2	-1.10
49	91.0391	C3H6O3	C3H6O3	1.93
50	148.0597	C3(13C)3H8O4	C6H8O4	0.99
51	113.0508	C4(13C)2H6O2	C6H6O2	-0.14
52	100.0475	C4(13C)1H6O2	C5H6O2	1.27
53	172.1048	C8(13C)1H14O3	C9H14O3	-0.59
54	138.0631	C7(13C)1H8O2	C8H8O2	0.02
55	104.0424	C3(13C)1H6O3	C4H6O3	0.31
56	154.0580	C7(13C)1H8O3	C8H8O3	0.31
57	76.0392	C2H5NO2	C2H5NO2	-1.49
58	171.0475	C4(13C)4H6O4	C8H6O4	1.41
59	163.0870	C9H10N2O	C9H10N2O	2.68
60	161.0710	C9H8N2O	C9H8N2O	0.52
61	70.0651	C4H7N	C4H7N	-0.27
62	188.1276	C7(13C)3H16O3	C10H16O3	1.47
63	187.1240	C8(13C)2H16O3	C10H16O3	0.59
64	186.1205	C9(13C)1H16O3	C10H16O3	-0.31
65	173.1083	C7(13C)2H14O3	C9H14O3	0.38
66	169.1135	C8(13C)2H14O2	C10H14O2	0.95
67	144.0734	C6(13C)1H10O3	C7H10O3	-1.32
68	131.0613	C4(13C)2H8O3	C6H8O3	-0.51
69	114.0632	C5(13C)1H8O2	C6H8O2	1.50
70	145.0770	C5(13C)2H10O3	C7H10O3	-0.16
71	115.0663	C4(13C)2H8O2	C6H8O2	-0.98
72	101.0506	C3(13C)2H6O2	C5H6O2	-1.56
73	89.0509	C2(13C)2H6O2	C4H6O2	1.73
74	219.0477	C8(13C)4H6O4	C12H6O4	1.61
75	133.0768	C4(13C)2H10O3	C6H10O3	-1.23
76	132.0737	C5(13C)1H10O3	C6H10O3	0.91
77	141.1184	C7(13C)2H14O	C9H14O	-0.18
78	129.0820	C5(13C)2H10O2	C7H10O2	-0.53
79	115.1026	C5(13C)2H12O	C7H12O	-1.83
80	147.0925	C5(13C)2H12O3	C7H12O3	-0.81
81	146.0894	C6(13C)1H12O3	C7H12O3	1.13
82	101.0873	C4(13C)2H10O	C6H10O	1.95
83	157.1134	C7(13C)2H14O2	C9H14O2	0.13
84	155.0978	C7(13C)2H12O2	C9H12O2	0.75
85	113.0870	C5(13C)2H10O	C7H10O	-1.01
86	99.0713	C4(13C)2H8O	C6H8O	-1.60
87	97.0558	C4(13C)2H6O	C6H6O	-0.64
88	156.0736	C7(13C)1H10O3	C8H10O3	-0.31

89	160.0962	C5(13C)3H12O3	C8H12O3	1.18
90	159.0927	C6(13C)2H12O3	C8H12O3	0.14
91	158.0891	C7(13C)1H12O3	C8H12O3	-0.92
92	146.0805	C4(13C)3H10O3	C7H10O3	0.99
93	142.0942	C7(13C)1H12O2	C8H12O2	-1.35
94	145.1043	C4(13C)4H12O2	C8H12O2	-0.97
95	144.1012	C5(13C)3H12O2	C8H12O2	0.99
96	147.1198	C4(13C)4H14O2	C8H14O2	-1.62
97	129.1093	C4(13C)4H12O	C8H12O	-1.45
98	162.1117	C5(13C)3H14O3	C8H14O3	0.57
99	161.1082	C6(13C)2H14O3	C8H14O3	-0.47
100	160.1051	C7(13C)1H14O3	C8H14O3	1.30
101	144.1102	C7(13C)1H14O2	C8H14O2	1.13
102	146.1168	C5(13C)3H14O2	C8H14O2	0.32
103	145.1132	C6(13C)2H14O2	C8H14O2	-0.83
104	127.1027	C6(13C)2H12O	C8H12O	-0.55
105	127.0664	C5(13C)2H8O2	C7H8O2	0.22
106	157.0771	C6(13C)2H10O3	C8H10O3	0.75
107	143.0977	C6(13C)2H12O2	C8H12O2	-0.17
108	141.0821	C6(13C)2H10O2	C8H10O2	0.51
109	125.0872	C6(13C)2H10O	C8H10O	0.22
110	85.0557	C3(13C)2H6O	C5H6O	-2.39
111	186.1120	C7(13C)3H14O3	C10H14O3	2.01
112	174.1119	C6(13C)3H14O3	C9H14O3	1.34
113	172.0963	C6(13C)3H12O3	C9H12O3	1.91
114	175.1235	C7(13C)2H16O3	C9H16O3	-2.75
115	167.0980	C8(13C)2H12O2	C10H12O2	1.54
116	151.1030	C8(13C)2H12O	C10H12O	1.40
117	187.0878	C7(13C)2H12O4	C9H12O4	1.11
118	185.1085	C8(13C)2H14O3	C10H14O3	1.12
119	148.0687	C5(13C)1H10O4	C6H10O4	1.12
120	162.0840	C6(13C)1H12O4	C7H12O4	-1.49
121	169.0772	C7(13C)2H10O3	C9H10O3	1.53
122	171.0928	C7(13C)2H12O3	C9H12O3	0.95
123	143.0614	C5(13C)2H8O3	C7H8O3	0.52
124	173.0721	C6(13C)2H10O4	C8H10O4	0.95
125	139.0666	C6(13C)2H8O2	C8H8O2	1.22
126	174.0756	C5(13C)3H10O4	C8H10O4	1.90
127	159.0564	C5(13C)2H8O4	C7H8O4	0.75
128	155.0611	C6(13C)2H8O3	C8H8O3	-1.52
129	141.0454	C5(13C)2H6O3	C7H6O3	-1.99
130	125.0509	C5(13C)2H6O2	C7H6O2	1.00
131	158.0528	C6(13C)1H8O4	C7H8O4	-0.30
132	142.0579	C6(13C)1H8O3	C7H8O3	-0.66
133	172.0685	C7(13C)1H10O4	C8H10O4	-0.02
134	130.0577	C5(13C)1H8O3	C6H8O3	-1.80
135	106.0579	C3(13C)1H8O3	C4H8O3	-0.61

136	120.0373	C3(13C)1H6O4	C4H6O4	0.65
137	88.0474	C3(13C)1H6O2	C4H6O2	-0.16
138	87.0349	C2(13C)2H4O2	C4H4O2	-2.32
139	134.0803	C3(13C)3H10O3	C6H10O3	0.03
140	118.0854	C3(13C)3H10O2	C6H10O2	-0.36
141	117.1096	C3(13C)4H12O	C7H12O	1.06
142	158.0811	C5(13C)3H10O3	C8H10O3	4.66
143	142.1219	C6(13C)3H14O	C9H14O	1.00
144	116.0425	C4(13C)1H6O3	C5H6O3	1.49
145	98.0683	C5(13C)1H8O	C6H8O	1.29
146	96.0527	C5(13C)1H6O	C6H6O	2.32
147	175.0876	C6(13C)2H12O4	C8H12O4	0.38
148	132.0648	C3(13C)3H8O3	C6H8O3	0.76
149	128.1058	C5(13C)3H12O	C8H12O	-2.76
150	140.0786	C7(13C)1H10O2	C8H10O2	-0.68
151	124.0837	C7(13C)1H10O	C8H10O	-1.13
152	84.0526	C4(13C)1H6O	C5H6O	0.97
153	125.0540	C4(13C)1H5N3O	C5H5N3O	1.07
154	135.0561	C3(13C)2H8O4	C5H8O4	-1.20
155	124.0505	C5H5N3O	C5H5N3O	-0.27
156	123.0474	(13C)4H6O4	C4H6O4	1.04
157	109.0595	C4(13C)1H5N3	C5H5N3	4.96
158	141.0490	C4(13C)1H5N3O2	C5H5N3O2	1.27
159	123.0385	C4(13C)1H3N3O	C5H3N3O	1.88
160	140.0455	C5H5N3O2	C5H5N3O2	0.09
161	122.0350	C5H3N3O	C5H3N3O	0.52
162	121.0319	(13C)4H4O4	C4H4O4	1.86
163	92.0422	C2(13C)1H6O3	C3H6O3	-1.19
164	108.0560	C5H5N3	C5H5N3	3.45
165	89.0420	(13C)4H4O2	C4H4O2	1.50
166	64.0476	C1(13C)1H6O2	C2H6O2	2.45
167	178.1703	C5(13C)5H20O2	C10H20O2	-0.44
168	177.1668	C6(13C)4H20O2	C10H20O2	-1.39
169	176.1637	C7(13C)3H20O2	C10H20O2	0.22
170	175.1606	C8(13C)2H20O2	C10H20O2	1.84
171	174.1571	C9(13C)1H20O2	C10H20O2	0.89
172	214.2254	C6(13C)9H24	C15H24	0.50
173	213.2219	C7(13C)8H24	C15H24	-0.28
174	155.1525	C5(13C)6H16	C11H16	-0.77
175	225.1947	C9(13C)6H22O	C15H22O	0.89
176	224.1916	C10(13C)5H22O	C15H22O	2.15
177	223.1881	C11(13C)4H22O	C15H22O	1.42
178	222.1846	C12(13C)3H22O	C15H22O	0.67
179	230.2293	C8(13C)7H26O	C15H26O	0.75
180	229.2262	C9(13C)6H26O	C15H26O	1.99
181	228.2227	C10(13C)5H26O	C15H26O	1.27
182	168.1647	C7(13C)5H18	C12H18	-1.44

183	227.2102	C9(13C)6H24O	C15H24O	0.45
184	226.2067	C10(13C)5H24O	C15H24O	-0.28
185	209.2002	C9(13C)6H22	C15H22	2.89
186	225.2036	C11(13C)4H24O	C15H24O	0.97
187	208.1966	C10(13C)5H22	C15H22	2.10
188	227.2192	C11(13C)4H26O	C15H26O	0.54
189	140.1337	C5(13C)5H14	C10H14	0.86
190	127.1301	C5(13C)4H14	C9H14	-1.48
191	126.1270	C6(13C)3H14	C9H14	0.76
192	113.1144	C4(13C)4H12	C8H12	-2.06
193	225.2121	C13(13C)2H26O	C15H26O	-0.94
194	125.1235	C7(13C)2H14	C9H14	-0.57
195	112.1113	C5(13C)3H12	C8H12	0.46
196	111.1078	C6(13C)2H12	C8H12	-1.04
197	212.2188	C8(13C)7H24	C15H24	1.06
198	154.1494	C6(13C)5H16	C11H16	1.07
199	211.2153	C9(13C)6H24	C15H24	0.27
200	153.1459	C7(13C)4H16	C11H16	-0.02
201	126.1180	C4(13C)5H12	C9H12	0.60
202	210.2122	C10(13C)5H24	C15H24	1.62
203	125.1145	C5(13C)4H12	C9H12	-0.73
204	124.1114	C6(13C)3H12	C9H12	1.55
205	111.0988	C4(13C)4H10	C8H10	-1.22
206	128.1336	C4(13C)5H14	C9H14	-0.16
207	210.2041	C10(13C)4H23N	C14H23N	1.82
208	228.2137	C8(13C)7H24O	C15H24O	1.18
209	114.1179	C3(13C)5H12	C8H12	-0.57
210	85.0834	C2(13C)4H8	C6H8	1.54
211	151.1303	C7(13C)4H14	C11H14	0.62
212	149.1237	C9(13C)2H14	C11H14	1.41
213	121.0924	C7(13C)2H10	C9H10	1.01
214	150.1358	C10(13C)1H16	C11H16	-0.35
215	122.1044	C8(13C)1H12	C9H12	-1.16
216	97.0831	C3(13C)4H8	C7H8	-1.86
217	110.0957	C5(13C)3H10	C8H10	1.35
218	96.0800	C4(13C)3H8	C7H8	1.09
219	208.2051	C12(13C)3H24	C15H24	0.03
220	207.2016	C13(13C)2H24	C15H24	-0.77
221	152.1424	C8(13C)3H16	C11H16	-1.12
222	151.1393	C9(13C)2H16	C11H16	0.75
223	209.2087	C11(13C)4H24	C15H24	0.83
224	123.1079	C7(13C)2H12	C9H12	0.21
225	223.1970	C13(13C)2H24O	C15H24O	1.50
226	206.1896	C12(13C)3H22	C15H22	0.50
227	205.1865	C13(13C)2H22	C15H22	1.89
228	224.2001	C12(13C)3H24O	C15H24O	0.23
229	207.1927	C11(13C)4H22	C15H22	-0.87

230	109.0922	C6(13C)2H10	C8H10	-0.17
231	95.0765	C5(13C)2H8	C7H8	-0.67
232	124.1204	C8(13C)1H14	C9H14	1.72
233	110.1047	C7(13C)1H12	C8H12	1.53
234	136.1201	C9(13C)1H14	C10H14	-0.72
235	96.0890	C6(13C)1H10	C7H10	1.30
236	82.0733	C5(13C)1H8	C6H8	0.98
237	138.1477	C4(13C)3H18O2	C7H18O2	-2.09
238	137.1447	C5(13C)2H18O2	C7H18O2	-0.03
239	136.1416	C6(13C)1H18O2	C7H18O2	2.06
240	93.0610	C5(13C)2H6	C7H6	0.36
241	134.0530	C4(13C)1H8O4	C5H8O4	0.91
242	119.0531	C3(13C)1H7NO3	C4H7NO3	-1.39
243	74.0958	C2(13C)3H10	C5H10	2.40
244	73.0922	C3(13C)2H10	C5H10	0.13
245	72.0887	C4(13C)1H10	C5H10	-2.20
246	218.1745	C9(13C)3H22O3	C12H22O3	1.23
247	217.1710	C10(13C)2H22O3	C12H22O3	0.47
248	167.1616	C8(13C)4H18	C12H18	0.25
249	166.1581	C9(13C)3H18	C12H18	-0.76
250	165.1550	C10(13C)2H18	C12H18	0.96
251	149.1354	C4(13C)4H16O2	C8H16O2	-2.24
252	148.1323	C5(13C)3H16O2	C8H16O2	-0.34
253	147.1288	C6(13C)2H16O2	C8H16O2	-1.48
254	146.1257	C7(13C)1H16O2	C8H16O2	0.45
255	139.1302	C6(13C)4H14	C10H14	-0.34
256	99.0991	C3(13C)4H10	C7H10	1.77
257	138.1267	C7(13C)3H14	C10H14	-1.55
258	98.0956	C4(13C)3H10	C7H10	0.08
259	97.0921	C5(13C)2H10	C7H10	-1.65
260	84.0799	C3(13C)3H8	C6H8	-0.44
261	137.1236	C8(13C)2H14	C10H14	0.51
262	83.0768	C4(13C)2H8	C6H8	2.99
263	129.1183	C6(13C)2H14O	C8H14O	-1.29
264	81.0608	C4(13C)2H6	C6H6	-1.33
265	142.1493	C5(13C)5H16	C10H16	0.16
266	141.1458	C6(13C)4H16	C10H16	-1.02
267	140.1427	C7(13C)3H16	C10H16	1.00
268	139.1392	C8(13C)2H16	C10H16	-0.19
269	135.1081	C8(13C)2H12	C10H12	1.23
270	69.0611	C3(13C)2H6	C5H6	2.96
271	68.0576	C4(13C)1H6	C5H6	0.53
272	130.1223	C5(13C)3H14O	C8H14O	3.47
273	108.0887	C7(13C)1H10	C8H10	-1.72
274	226.2161	C12(13C)3H26O	C15H26O	1.80
275	173.1536	C10H20O2	C10H20O2	-0.07
276	94.0735	C6(13C)1H8	C7H8	2.36

277	158.1169	C6(13C)3H14O2	C9H14O2	1.18
278	164.1515	C11(13C)1H18	C12H18	-0.05
279	120.0888	C8(13C)1H10	C9H10	-0.37
280	224.2091	C14(13C)1H26O	C15H26O	0.32
281	80.0578	C5(13C)1H6	C6H6	2.22
282	256.1900	C12(13C)3H24O3	C15H24O3	0.56
283	78.0418	C5(13C)1H4	C6H4	-2.29
284	145.1222	C8H16O2	C8H16O2	-0.69
285	221.1810	C13(13C)2H22O	C15H22O	-0.08
286	137.1146	C6(13C)4H12	C10H12	0.36
287	135.1381	C7H18O2	C7H18O2	0.83
288	206.1806	C10(13C)5H20	C15H20	0.41
289	205.1771	C11(13C)4H20	C15H20	-0.41
290	220.1686	C12(13C)3H20O	C15H20O	-0.93
291	222.1756	C10(13C)5H20O	C15H20O	0.58
292	221.1725	C11(13C)4H20O	C15H20O	1.86
293	204.1740	C12(13C)3H20	C15H20	0.98
294	131.1253	C4(13C)4H14O	C8H14O	1.28
295	123.0990	C5(13C)4H10	C9H10	0.04
296	156.0933	C6(13C)2H11NO2	C8H11NO2	2.09
297	155.0898	C7(13C)1H11NO2	C8H11NO2	1.03
298	153.0823	C7(13C)2H10O2	C9H10O2	1.39
299	137.0873	C7(13C)2H10O	C9H10O	1.23
300	139.1029	C7(13C)2H12O	C9H12O	0.51
301	111.0715	C5(13C)2H8O	C7H8O	-0.16
302	150.1183	C6(13C)5H12	C11H12	2.38
303	221.1631	C9(13C)6H18O	C15H18O	-0.26
304	180.1652	C8(13C)5H18	C13H18	1.94
305	236.1635	C12(13C)3H20O2	C15H20O2	-0.67
306	218.1530	C12(13C)3H18O	C15H18O	-0.49
307	169.1409	C7(13C)4H16O	C11H16O	0.25
308	219.1655	C13(13C)2H20O	C15H20O	0.36
309	161.1234	C10(13C)2H14	C12H14	-0.62
310	160.1114	C9(13C)3H12	C12H12	1.03
311	129.1371	C3(13C)6H14	C9H14	1.13
312	167.1343	C9(13C)2H16O	C11H16O	0.95
313	179.1613	C9(13C)4H18	C13H18	-1.50
314	225.2319	C10(13C)6H26	C16H26	4.45
315	178.1587	C10(13C)3H18	C13H18	2.61
316	219.1565	C11(13C)4H18O	C15H18O	0.27
317	152.1339	C6(13C)5H14	C11H14	1.72
318	220.1600	C10(13C)5H18O	C15H18O	1.02
319	205.1682	C9(13C)6H18	C15H18	-0.50
320	141.1368	C4(13C)6H14	C10H14	-1.16
321	127.1215	C3(13C)6H12	C9H12	1.91
322	166.1491	C7(13C)5H16	C12H16	-0.88
323	112.1023	C3(13C)5H10	C8H10	0.28

324	203.1620	C11(13C)4H18	C15H18	2.28
325	198.1484	C9(13C)3H18O2	C12O18O2	2.10
326	138.0908	C6(13C)3H10O	C9H10O	2.43
327	136.1120	C9H13N	C9H13N	-0.41
328	150.1273	C8(13C)3H14	C11H14	2.52
329	122.0959	C6(13C)3H10	C9H10	2.37
330	238.1795	C12(13C)3H22O2	C15H22O2	0.82
331	183.1565	C8(13C)4H18O	C12H18O	0.48
332	181.1500	C10(13C)2H18O	C12H18O	1.12
333	226.2349	C9(13C)7H26	C16H26	3.17
334	163.1390	C10(13C)2H16	C12H16	-1.20
335	207.1842	C9(13C)6H20	C15H20	1.21
336	204.1651	C10(13C)5H18	C15H18	0.88
337	148.1113	C8(13C)3H12	C11H12	0.16
338	223.1791	C9(13C)6H20O	C15H20O	1.33
339	147.1077	C9(13C)2H12	C11H12	-0.98
340	203.1705	C13(13C)2H20	C15H20	0.16
341	202.1585	C12(13C)3H18	C15H18	1.47
342	139.0939	C5(13C)4H10O	C9H10O	0.37
343	211.1884	C3(13C)12H18	C152H18	-0.01
344	143.1528	C4(13C)6H16	C10H16	1.33
345	181.1773	C9(13C)4H20	C13H20	0.47
346	180.1742	C10(13C)3H20	C13H20	2.05
347	226.1977	C8(13C)7H22O	C15H22O	-0.37
348	179.1738	C4(13C)6H20O2	C10H20O2	0.49
349	169.1682	C6(13C)6H18	C12H18	-0.44
350	100.1022	C2(13C)5H10	C7H10	-1.10
351	214.1434	C2(13C)11H14O2	C131H14O2	-0.78
352	182.1808	C8(13C)5H20	C13H20	1.39
353	183.1292	C9(13C)2H16O2	C11H16O2	1.12
354	224.1826	C1(13C)15H16	C16H16	-0.74
355	184.1601	C7(13C)5H18O	C12H18O	1.38
356	181.1410	C8(13C)4H16O	C12H16O	1.01
357	197.1449	C10(13C)2H18O2	C12H18O2	1.26
358	138.1182	C5(13C)5H12	C10H12	1.57
359	124.1325	C3(13C)3H16O2	C6H16O2	0.96
360	121.1224	C6H16O2	C6H16O2	0.57
361	127.0938	C4(13C)4H10O	C8H10O	-0.71
362	108.1008	C2(13C)3H12O2	C5H12O2	-2.60
363	123.1290	C4(13C)2H16O2	C6H16O2	-0.39
364	122.1259	C5(13C)1H16O2	C6H16O2	1.93
365	59.0766	C2(13C)2H8	C4H8	-0.60
366	58.0735	C3(13C)1H8	C4H8	4.34
367	155.1614	C7(13C)4H18	C11H18	-0.64
368	212.2273	C10(13C)5H26	C15H26	-0.97
369	154.1579	C8(13C)3H18	C11H18	-1.73
370	232.2453	C8(13C)7H28O	C15H28O	2.27

371	211.2229	C3(13C)6H24N4O	C9H24N4O	2.20
372	130.1491	C4(13C)5H16	C9H16	-0.90
373	229.2347	C11(13C)4H28O	C15H28O	0.12
374	231.2413	C9(13C)6H28O	C15H28O	-0.39
375	230.2378	C10(13C)5H28O	C15H28O	-1.12
376	115.1304	C4(13C)4H14	C8H14	1.06
377	242.2106	C12(13C)3H26O2	C15H26O2	0.01
378	227.2281	C13(13C)2H28O	C15H28O	0.63
379	129.1461	C5(13C)4H16	C9H16	1.29
380	128.1425	C6(13C)3H16	C9H16	-0.01
381	114.1268	C5(13C)3H14	C8H14	-0.40
382	113.1233	C6(13C)2H14	C8H14	-1.88
383	76.0750	C1(13C)3H8O	C4H8O	2.35
384	73.0833	C1(13C)4H8	C5H8	-0.15
385	210.0397	C9H7NO5	C9H7NO5	0.06
386	195.0483	C8(13C)1H7NO4	C9H7NO4	0.69
387	244.2100	C10(13C)4H25NO2	C14H25NO2	3.39
388	196.1960	C9(13C)5H22	C14H22	-0.78
389	195.1930	C10(13C)4H22	C14H22	0.66
390	194.1895	C11(13C)3H22	C14H22	-0.19
391	87.0990	C2(13C)4H10	C6H10	0.39
392	242.2017	C10(13C)5H24O2	C15H24O2	-0.08
393	240.1951	C12(13C)3H24O2	C15H24O2	0.41
394	239.1915	C13(13C)2H24O2	C15H24O2	-0.29
395	127.1390	C7(13C)2H16	C9H16	-1.32
396	86.0955	C3(13C)3H10	C6H10	-1.56
397	100.1112	C4(13C)3H12	C7H12	-0.89
398	99.1081	C5(13C)2H12	C7H12	1.97
399	101.1147	C3(13C)4H12	C7H12	0.77
400	85.0924	C4(13C)2H10	C6H10	1.78
401	61.0558	C1(13C)2H6O	C3H6O	-0.55
402	212.0557	C9H9NO5	C9H9NO5	1.73
403	205.1977	C8(13C)4H24O2	C12H24O2	-2.96
404	238.0429	C10(13C)1H8O6	C11H8O6	0.66
405	213.0588	C8(13C)1H9NO5	C9H9NO5	0.39
406	197.0638	C8(13C)1H9NO4	C9H9NO4	0.19
407	169.0687	C7(13C)1H9NO3	C8H9NO3	-0.88
408	196.0603	C9H9NO4	C9H9NO4	-0.66
409	168.0657	C8H9NO3	C8H9NO3	0.80
410	234.2331	C9(13C)5H28O2	C14H28O2	0.42
411	233.2296	C10(13C)4H28O2	C14H28O2	-0.29
412	232.2265	C11(13C)3H28O2	C14H28O2	0.92
413	231.2230	C12(13C)2H28O2	C14H28O2	0.21
414	206.2012	C7(13C)5H24O2	C12H24O2	-2.14
415	204.1951	C9(13C)3H24O2	C12H24O2	0.62
416	203.1916	C10(13C)2H24O2	C12H24O2	-0.20
417	202.1881	C11(13C)1H24O2	C12H24O2	-1.03

418	75.0988	C1(13C)4H10	C5H10	-1.44
419	78.0906	C1(13C)3H10O	C4H10O	1.05
420	96.1011	C1(13C)3H12O2	C4H12O2	0.32
421	95.0976	C2(13C)2H12O2	C4H12O2	-1.44
422	77.0871	C2(13C)2H10O	C4H10O	-1.12
423	93.0910	C4H12O2	C4H12O2	-0.22
424	94.0945	C3(13C)1H12O2	C4H12O2	1.57
425	76.0840	C3(13C)1H10O	C4H10O	2.62
426	75.0805	C4H10O	C4H10O	0.41
427	109.1133	C3(13C)2H14O2	C5H14O2	-0.85
428	108.1102	C4(13C)1H14O2	C5H14O2	1.77
429	107.1067	C5H14O2	C5H14O2	0.23
430	62.0683	C2(13C)1H8O	C3H8O	2.50
431	61.0648	C3H8O	C3H8O	-0.22
432	61.0478	C1(13C)1H5NO	C2H5NO	0.15
433	371.1017	C20(13C)3H13NO4	C23H13NO4	-0.28
434	194.0448	C9H7NO4	C9H7NO4	-0.17
435	90.0907	C2(13C)3H10O	C5H10O	2.48
436	72.0802	C2(13C)3H8	C5H8	3.82
437	71.0767	C3(13C)2H8	C5H8	1.50
438	70.0732	C4(13C)1H8	C5H8	-0.88
439	237.0394	C11H8O6	C11H8O6	-0.04
440	60.0810	C3H9N	C3H9N	3.27
441	229.0345	C9H8O7	C9H8O7	0.89
442	123.0716	C6(13C)2H8O	C8H8O	1.01
443	170.1256	C9(13C)1H16O2	C10H16O2	-0.60
444	103.0751	C5H10O2	C5H10O2	-2.27
445	106.0852	C2(13C)3H10O2	C5H10O2	-1.73
446	105.0822	C3(13C)2H10O2	C5H10O2	0.96
447	104.0786	C4(13C)1H10O2	C5H10O2	-0.64
448	77.0508	C1(13C)2H6O2	C3H6O2	0.16
449	134.1166	C4(13C)3H14O2	C7H14O2	-0.71
450	133.1136	C5(13C)2H14O2	C7H14O2	1.42
451	132.1100	C6(13C)1H14O2	C7H14O2	0.17
452	118.0581	C4(13C)1H8O3	C5H8O3	0.65
453	120.1009	C3(13C)3H12O2	C6H12O2	-1.16
454	119.0979	C4(13C)2H12O2	C6H12O2	1.22
455	118.0943	C5(13C)1H12O2	C6H12O2	-0.19
456	117.0456	C3(13C)2H6O3	C5H6O3	-0.95
457	119.0616	C3(13C)2H8O3	C5H8O3	2.05
458	87.0717	C3(13C)2H8O	C5H8O	1.75
459	86.0681	C4(13C)1H8O	C5H8O	-0.18
460	190.1431	C7(13C)3H18O3	C10H18O3	0.95
461	189.1396	C8(13C)2H18O3	C10H18O3	0.07
462	188.1361	C9(13C)1H18O3	C10H18O3	-0.82
463	158.1442	C5(13C)5H16O	C10H16O	0.44
464	176.1547	C5(13C)5H18O2	C10H18O2	0.10

465	175.1512	C6(13C)4H18O2	C10H18O2	-0.85
466	157.1407	C6(13C)4H16O	C10H16O	-0.62
467	156.1376	C7(13C)3H16O	C10H16O	1.19
468	172.1411	C9(13C)1H18O2	C10H18O2	-1.16
469	171.1291	C8(13C)2H16O2	C10H16O2	0.38
470	173.1446	C8(13C)2H18O2	C10H18O2	-0.19
471	174.1482	C7(13C)3H18O2	C10H18O2	0.77
472	155.1341	C8(13C)2H16O	C10H16O	0.12
473	59.0403	C1(13C)2H4O	C3H4O	1.08
474	211.1973	C5(13C)10H20	C150H20	0.08
475	192.1587	C7(13C)3H20O3	C10H20O3	0.44
476	191.1556	C8(13C)2H20O3	C10H20O3	1.92
477	137.0999	C4(13C)1H13NO3	C5H13NO3	-2.30
478	122.0802	C2(13C)3H10O3	C5H10O3	-1.13
479	104.0697	C2(13C)3H8O2	C5H8O2	-0.83
480	101.0596	C5H8O2	C5H8O2	-1.36
481	119.0701	C5H10O3	C5H10O3	-1.58
482	120.0736	C4(13C)1H10O3	C5H10O3	-0.17
483	121.0771	C3(13C)2H10O3	C5H10O3	1.21
484	103.0666	C3(13C)2H8O2	C5H8O2	1.92
485	102.0631	C4(13C)1H8O2	C5H8O2	0.30
486	78.0633	C2(13C)1H8O2	C3H8O2	2.57
487	212.2004	C11(13C)3H24O	C14H24O	1.71
488	232.2175	C9(13C)5H26O2	C14H26O2	0.84
489	204.1852	C7(13C)5H22O2	C12H22O2	-3.89
490	230.2109	C11(13C)3H26O2	C14H26O2	1.35
491	229.2074	C12(13C)2H26O2	C14H26O2	0.63
492	202.1795	C9(13C)3H22O2	C12H22O2	1.10
493	201.1760	C10(13C)2H22O2	C12H22O2	0.28
494	132.1011	C4(13C)3H12O2	C7H12O2	0.02
495	93.0820	C2(13C)2H10O2	C4H10O2	-0.43
496	92.0790	C3(13C)1H10O2	C4H10O2	2.66
497	91.0754	C4H10O2	C4H10O2	0.84
498	89.0872	C3(13C)2H10O	C5H10O	0.62
499	88.0837	C4(13C)1H10O	C5H10O	-1.28
500	77.0597	C3H8O2	C3H8O2	0.42
501	60.0527	C2(13C)1H6O	C3H6O	4.21
502	107.0977	C3(13C)2H12O2	C5H12O2	0.04
503	106.0942	C4(13C)1H12O2	C5H12O2	-1.54
504	105.0911	C5H12O2	C5H12O2	1.15
505	230.0380	C7(13C)4H3N3O3	C11H3N3O3	-0.59
506	75.0715	C2(13C)2H8O	C4H8O	0.15
507	74.0680	C3(13C)1H8O	C4H8O	-2.12
508	57.0610	C2(13C)2H6	C4H6	1.10
509	56.0575	C3(13C)1H6	C4H6	-1.90
510	160.1325	C6(13C)3H16O2	C9H16O2	0.57
511	159.1289	C7(13C)2H16O2	C9H16O2	-0.48

512	143.1340	C7(13C)2H16O	C9H16O	-0.85
513	153.1186	C8(13C)2H14O	C10H14O	0.75
514	117.0819	C4(13C)2H10O2	C6H10O2	-1.79
515	185.1721	C8(13C)4H20O	C12H20O	-0.05
516	184.1690	C9(13C)3H20O	C12H20O	1.49
517	183.1655	C10(13C)2H20O	C12H20O	0.58
518	130.0945	C6(13C)1H12O2	C7H12O2	0.91
519	131.0976	C5(13C)2H12O2	C7H12O2	-1.26
520	116.0788	C5(13C)1H10O2	C6H10O2	0.64
521	186.1756	C7(13C)5H20O	C12H20O	0.85
522	163.1238	C6(13C)2H16O3	C8H16O3	-1.05
523	149.1081	C5(13C)2H14O3	C7H14O3	-1.45
524	148.1050	C6(13C)1H14O3	C7H14O3	0.46
525	213.2035	C10(13C)4H24O	C14H24O	0.37
526	135.0928	C4(13C)2H12O3	C6H12O3	1.41
527	134.0893	C5(13C)1H12O3	C6H12O3	0.18
528	107.0897	C3(13C)1H11NO2	C4H11NO2	0.43
529	158.1254	C8(13C)1H16O2	C9H16O2	-1.54
530	76.0473	C2(13C)1H6O2	C3H6O2	-2.05
531	89.0599	C4H8O2	C4H8O2	1.96
532	92.0700	C1(13C)3H8O2	C4H8O2	2.44
533	91.0665	C2(13C)2H8O2	C4H8O2	0.62
534	90.0630	C3(13C)1H8O2	C4H8O2	-1.23
535	73.0560	C2(13C)2H6O	C4H6O	1.48
536	72.0524	C3(13C)1H6O	C4H6O	-0.83
537	141.1104	C7(13C)1H13NO	C8H13NO	0.12
538	107.0767	C6(13C)2H8	C8H8	0.73
539	106.0731	C7(13C)1H8	C8H8	-0.84
540	62.0347	H3N3O	H3N3O	-3.10
541	108.0735	C3(13C)1H10O3	C4H10O3	-1.50
542	63.0351	(13C)2H4O2	C2H4O2	-0.51
543	62.0320	C1(13C)1H4O2	C2H4O2	4.10
544	61.0285	C2H4O2	C2H4O2	1.40
545	105.0611	C6(13C)2H6	C8H6	1.67
546	164.1273	C5(13C)3H16O3	C8H16O3	-0.03
547	150.1116	C4(13C)3H14O3	C7H14O3	-0.33
548	145.1410	C5(13C)4H16O	C9H16O	1.46
549	142.1139	C6(13C)2H13NO	C8H13NO	1.29
550	104.0576	C7(13C)1H6	C8H6	0.07
551	188.1643	C8(13C)3H20O2	C11H20O2	3.34
552	109.0765	C2(13C)2H10O3	C4H10O3	-4.09
553	71.0494	C4H6O	C4H6O	3.18
554	162.1207	C7(13C)1H16O3	C8H16O3	0.69
555	152.1150	C9(13C)1H14O	C10H14O	-0.34
556	105.0701	C8H8	C8H8	1.86
557	182.1620	C11(13C)1H20O	C12H20O	-0.33
558	56.0212	C2(13C)1H2O	C3H2O	-0.13

559	262.2560	C9(13C)7H30O2	C16H30O2	2.35
560	288.2803	C13(13C)5H34O2	C18H34O2	1.29
561	242.2384	C11(13C)5H28O	C16H28O	1.38
562	258.2419	C13(13C)3H30O2	C16H30O2	-0.20
563	257.2388	C14(13C)2H30O2	C16H30O2	0.90
564	241.2349	C12(13C)4H28O	C16H28O	0.69
565	260.2489	C11(13C)5H30O2	C16H30O2	1.09
566	259.2463	C5(13C)12H26O	C17H26O	1.50
567	261.2529	C3(13C)14H26O	C17H26O	1.04
568	256.2263	C13(13C)3H28O2	C16H28O2	0.18
569	255.2237	C7(13C)10H24O	C17H24O	0.59
570	187.1603	C9(13C)2H20O2	C11H20O2	0.06
571	216.1952	C10(13C)3H24O2	C13H24O2	1.24
572	201.2038	C9(13C)4H24O	C13H24O	1.93
573	239.2193	C12(13C)4H26O	C16H26O	1.10
574	262.2918	C10(13C)7H34O	C17H34O	0.26
575	257.2746	C15(13C)2H34O	C17H34O	-1.22
576	202.2069	C8(13C)5H24O	C13H24O	0.52
577	199.1972	C4(13C)10H20	C14H20	-0.62
578	197.1996	C8(13C)6H22	C14H22	0.07
579	198.2031	C7(13C)7H22	C14H22	0.91
580	203.2104	C7(13C)6H24O	C13H24O	1.34
581	182.1898	C10(13C)3H22	C13H22	1.50
582	183.1928	C9(13C)4H22	C13H22	-0.06
583	215.1917	C11(13C)2H24O2	C13H24O2	0.47
584	171.1654	C9(13C)2H20O	C11H20O	-0.20
585	214.2070	C9(13C)5H24O	C14H24O	1.15
586	241.2071	C13(13C)2H26O2	C15H26O2	-0.68
587	193.1864	C12(13C)2H22	C14H22	1.28
588	117.0371	C1(13C)4H4O3	C5H4O3	2.74
589	177.1395	C7(13C)2H18O3	C9H18O3	-0.72
590	178.1430	C6(13C)3H18O3	C9H18O3	0.22
591	176.1364	C8(13C)1H18O3	C9H18O3	0.89
592	108.0932	C2(13C)2H11NO2	C4H11NO2	1.98
593	245.2118	C7(13C)8H24O2	C15H24O2	0.13
594	244.2168	C10(13C)5H26O2	C15H26O2	-2.31
595	126.1359	C8(13C)1H16	C9H16	0.92
596	84.0889	C5(13C)1H10	C6H10	-0.20
597	228.2402	C14(13C)1H30O	C15H30O	-0.53
598	98.1046	C6(13C)1H12	C7H12	0.28
599	58.0367	C2(13C)1H4O	C3H4O	-1.81
600	260.2762	C10(13C)7H32O	C17H32O	0.63
601	246.2328	C10(13C)5H28O2	C15H28O2	-0.86
602	243.2231	C13(13C)2H28O2	C15H28O2	0.77
603	177.1946	C5(13C)6H22O	C11H22O	0.49
604	260.2852	C12(13C)5H34O	C17H34O	0.71
605	259.2817	C13(13C)4H34O	C17H34O	0.07

606	261.2887	C11(13C)6H34O	C17H34O	1.35
607	258.2782	C14(13C)3H34O	C17H34O	-0.57
608	148.1596	C4(13C)5H18O	C9H18O	-1.14
609	147.1566	C5(13C)4H18O	C9H18O	0.78
610	146.1531	C6(13C)3H18O	C9H18O	-0.35
611	145.1495	C7(13C)2H18O	C9H18O	-1.51
612	87.1079	C4(13C)2H12	C6H12	0.62
613	172.1778	C10(13C)1H22O	C11H22O	0.89
614	144.1465	C8(13C)1H18O	C9H18O	0.45
615	116.1151	C6(13C)1H14O	C7H14O	-0.20
616	204.2229	C8(13C)5H26O	C13H26O	2.25
617	203.2194	C9(13C)4H26O	C13H26O	1.44
618	202.2154	C10(13C)3H26O	C13H26O	-1.61
619	201.2123	C11(13C)2H26O	C13H26O	-0.21
620	255.2591	C15(13C)2H32O	C17H32O	-0.86
621	205.2259	C7(13C)6H26O	C13H26O	0.85
622	176.1915	C6(13C)5H22O	C11H22O	2.10
623	175.1880	C7(13C)4H22O	C11H22O	1.16
624	174.1844	C8(13C)3H22O	C11H22O	0.21
625	173.1809	C9(13C)2H22O	C11H22O	-0.75
626	259.2732	C11(13C)6H32O	C17H32O	1.73
627	258.2701	C12(13C)5H32O	C17H32O	2.83
628	234.2609	C8(13C)7H30O	C15H30O	1.84
629	119.1252	C3(13C)4H14O	C7H14O	0.23
630	118.1217	C4(13C)3H14O	C7H14O	-1.19
631	117.1186	C5(13C)2H14O	C7H14O	1.23
632	233.2569	C9(13C)6H30O	C15H30O	-0.80
633	229.2437	C13(13C)2H30O	C15H30O	0.20
634	232.2538	C10(13C)5H30O	C15H30O	0.42
635	231.2503	C11(13C)4H30O	C15H30O	-0.30
636	230.2472	C12(13C)3H30O	C15H30O	0.93

Table S 3. Compounds contributing to PC1 (i.e., absolute value loading > 0.01). Article's copyright: Attribution 4.0 International (CC BY 4.0)

#	M/Z	MOLECULAR FORMULA (^{12}C & ^{13}C)	UNIQUE MOLECULAR FORMULA	ID	LOADING VALUE
1	159.0653241	C7H10O4	C7H10O4		-0.02
2	145.1132461	C6(13C)2H14O2	C8H14O2		0.01
3	178.1703032	C5(13C)5H20O2	C10H20O2	Ethyl octanoate	0.01
3	177.1667822	C6(13C)4H20O2	C10H20O2	Ethyl octanoate	0.06
3	176.1637092	C7(13C)3H20O2	C10H20O2	Ethyl octanoate	0.12
3	175.1606362	C8(13C)2H20O2	C10H20O2	Ethyl octanoate	0.13
3	174.1571152	C9(13C)1H20O2	C10H20O2	Ethyl octanoate	0.07
4	112.1112931	C5(13C)3H12	C8H12		0.01
4	111.1077721	C6(13C)2H12	C8H12		0.01
5	212.2187852	C8(13C)7H24	C15H24	Farnesene	0.03
5	211.2152642	C9(13C)6H24	C15H24	Farnesene	0.07
5	210.2121912	C10(13C)5H24	C15H24	Farnesene	0.11
5	208.2051492	C12(13C)3H24	C15H24	Farnesene	0.08
5	207.2016282	C13(13C)2H24	C15H24	Farnesene	0.04
5	209.2086702	C11(13C)4H24	C15H24	Farnesene	0.12
6	153.1458941	C7(13C)4H16	C11H16		0.02
6	152.1423731	C8(13C)3H16	C11H16		0.02
6	151.1393001	C9(13C)2H16	C11H16		0.02
7	124.1114331	C6(13C)3H12	C9H12		0.01
7	123.1079121	C7(13C)2H12	C9H12		0.01
8	96.08900509	C6(13C)1H10	C7H10		0.01
8	97.09207809	C5(13C)2H10	C7H10		0.01
9	82.07331107	C5(13C)1H8	C6H8		0.01
9	83.07683208	C4(13C)2H8	C6H8		0.01
10	74.0957671	C2(13C)3H10	C5H10		0.01
10	73.09224609	C3(13C)2H10	C5H10		0.05
10	72.08872509	C4(13C)1H10	C5H10		0.05
11	148.1323211	C5(13C)3H16O2	C8H16O2	Octanoic Acid	0.03
11	147.1288001	C6(13C)2H16O2	C8H16O2	Octanoic Acid	0.04
11	146.1257271	C7(13C)1H16O2	C8H16O2	Octanoic Acid	0.03
12	205.1977222	C8(13C)4H24O2	C12H24O2	Ethyl decanoate	0.03
12	206.2012432	C7(13C)5H24O2	C12H24O2	Ethyl decanoate	0.01
12	204.1950972	C9(13C)3H24O2	C12H24O2	Ethyl decanoate	0.05
12	203.1915762	C10(13C)2H24O2	C12H24O2	Ethyl decanoate	0.04
12	202.1880552	C11(13C)1H24O2	C12H24O2	Ethyl decanoate	0.02
13	95.0975801	C2(13C)2H12O2	C4H12O2	Ethanol	0.39
13	93.09098609	C4H12O2	C4H12O2	Ethanol	0.37
13	94.09450709	C3(13C)1H12O2	C4H12O2	Ethanol	0.76
14	77.08706609	C2(13C)2H10O	C4H10O		0.07
14	76.08399308	C3(13C)1H10O	C4H10O		0.14
14	75.08047208	C4H10O	C4H10O		0.07
15	71.07669208	C3(13C)2H8	C5H8		0.01

15	70.07317107	C4(13C)1H8	C5H8		0.01
16	101.0595701	C5H8O2	C5H8O2		0.02
16	103.0666121	C3(13C)2H8O2	C5H8O2		0.03
16	102.0630911	C4(13C)1H8O2	C5H8O2		0.06
17	120.0736051	C4(13C)1H10O3	C5H10O3		0.01
18	90.06295106	C3(13C)1H8O2	C4H8O2		0.02
19	106.0731431	C7(13C)1H8	C8H8		-0.02
19	105.0700701	C8H8	C8H8		-0.01
20	62.03201103	C1(13C)1H4O2	C2H4O2	Acetic acid	-0.04
20	61.02849003	C2H4O2	C2H4O2	Acetic acid	-0.04

Table S 4. Compounds contributing to PC2 (i.e., absolute value loading > 0.01)

#	*M/Z*	MOLECULAR FORMULA (^{12}C & ^{13}C)	UNIQUE MOLECULAR FORMULA	ID	LOADING VALUE
1	227.0386	C9(13C)1H3N5O2	C10H3N5O2		0.13
1	226.0356	C10H3N5O2	C10H3N5O2		0.12
1	228.0422	C8(13C)2H3N5O2	C10H3N5O2		0.02
2	228.0314	C9(13C)2H3N3O3	C11H3N3O3		0.01
3	192.0480	C8(13C)1H6N2O3	C9H6N2O3		0.07
4	172.1326	C7(13C)3H16O2	C10H16O2	Geranic acid	0.03
4	170.1256	C9(13C)1H16O2	C10H16O2	Geranic acid	0.03
4	171.1291	C8(13C)2H16O2	C10H16O2	Geranic acid	0.05
5	102.0268	C3(13C)1H4O3	C4H4O3		0.01
6	192.1676	C9(13C)1H22O3	C10H22O3		0.02
6	191.1641	C10H22O3	C10H22O3		0.17
7	201.1120	C10H16O4	C10H16O4		0.02
8	160.0684	C6(13C)1H10O4	C7H10O4		0.03
8	159.0653	C7H10O4	C7H10O4		0.34
9	236.1129	C7(13C)3H16O6	C10H16O6		0.03
10	113.0508	C4(13C)2H6O2	C6H6O2		0.01
11	100.0475	C4(13C)1H6O2	C5H6O2		0.05
11	101.0506	C3(13C)2H6O2	C5H6O2		0.04
12	104.0424	C3(13C)1H6O3	C4H6O3		0.01
13	76.0392	C2H5NO2	C2H5NO2		0.02
14	188.1276	C7(13C)3H16O3	C10H16O3		0.04
14	187.1240	C8(13C)2H16O3	C10H16O3		0.04
14	186.1205	C9(13C)1H16O3	C10H16O3		0.02
15	169.1135	C8(13C)2H14O2	C10H14O2		0.01
16	144.0734	C6(13C)1H10O3	C7H10O3		0.03
16	145.0770	C5(13C)2H10O3	C7H10O3		0.03
17	131.0613	C4(13C)2H8O3	C6H8O3		0.03
17	130.0577	C5(13C)1H8O3	C6H8O3		0.04
18	114.0632	C5(13C)1H8O2	C6H8O2	Sorbic acid	0.06
18	115.0663	C4(13C)2H8O2	C6H8O2	Sorbic acid	0.05

19	89.0509	C2(13C)2H6O2	C4H6O2		0.01
19	88.0474	C3(13C)1H6O2	C4H6O2		0.03
20	133.0768	C4(13C)2H10O3	C6H10O3		0.02
20	132.0737	C5(13C)1H10O3	C6H10O3		0.03
21	129.0820	C5(13C)2H10O2	C7H10O2		0.03
22	115.1026	C5(13C)2H12O	C7H12O		0.01
23	101.0873	C4(13C)2H10O	C6H10O		0.01
24	157.1134	C7(13C)2H14O2	C9H14O2		0.01
25	113.0870	C5(13C)2H10O	C7H10O		0.01
26	99.0713	C4(13C)2H8O	C6H8O		0.01
26	98.0683	C5(13C)1H8O	C6H8O		0.01
27	160.0962	C5(13C)3H12O3	C8H12O3		0.02
27	159.0927	C6(13C)2H12O3	C8H12O3		0.04
27	158.0891	C7(13C)1H12O3	C8H12O3		0.03
28	142.0942	C7(13C)1H12O2	C8H12O2		0.04
28	144.1012	C5(13C)3H12O2	C8H12O2		0.03
28	143.0977	C6(13C)2H12O2	C8H12O2		0.06
29	147.1198	C4(13C)4H14O2	C8H14O2		0.02
29	144.1102	C7(13C)1H14O2	C8H14O2		0.07
29	146.1168	C5(13C)3H14O2	C8H14O2		0.06
29	145.1132	C6(13C)2H14O2	C8H14O2		0.10
30	162.1117	C5(13C)3H14O3	C8H14O3		0.01
30	161.1082	C6(13C)2H14O3	C8H14O3		0.02
30	160.1051	C7(13C)1H14O3	C8H14O3		0.02
31	127.1027	C6(13C)2H12O	C8H12O		0.06
31	128.1058	C5(13C)3H12O	C8H12O		0.02
32	127.0664	C5(13C)2H8O2	C7H8O2		0.01
33	157.0771	C6(13C)2H10O3	C8H10O3		0.01
34	141.0821	C6(13C)2H10O2	C8H10O2		0.01
34	140.0786	C7(13C)1H10O2	C8H10O2		0.01
35	125.0872	C6(13C)2H10O	C8H10O		0.01
36	143.0614	C5(13C)2H8O3	C7H8O3		0.01
36	142.0579	C6(13C)1H8O3	C7H8O3		0.01
37	116.0425	C4(13C)1H6O3	C5H6O3		0.04
37	117.0456	C3(13C)2H6O3	C5H6O3		0.01
38	178.1703	C5(13C)5H20O2	C10H20O2	Ethyl octanoate	0.01
38	177.1668	C6(13C)4H20O2	C10H20O2	Ethyl octanoate	0.06
38	176.1637	C7(13C)3H20O2	C10H20O2	Ethyl octanoate	0.16
38	175.1606	C8(13C)2H20O2	C10H20O2	Ethyl octanoate	0.20
38	174.1571	C9(13C)1H20O2	C10H20O2	Ethyl octanoate	0.12
39	126.1270	C6(13C)3H14	C9H14		0.01
39	125.1235	C7(13C)2H14	C9H14		0.01
40	112.1113	C5(13C)3H12	C8H12		0.01
40	111.1078	C6(13C)2H12	C8H12		0.01
41	212.2188	C8(13C)7H24	C15H24	Farnesene	0.01
41	211.2153	C9(13C)6H24	C15H24	Farnesene	0.04
41	210.2122	C10(13C)5H24	C15H24	Farnesene	0.08

41	208.2051	C12(13C)3H24	C15H24	Farnesene	0.09
41	207.2016	C13(13C)2H24	C15H24	Farnesene	0.04
41	209.2087	C11(13C)4H24	C15H24	Farnesene	0.11
42	124.1114	C6(13C)3H12	C9H12		0.01
42	123.1079	C7(13C)2H12	C9H12		0.01
43	152.1424	C8(13C)3H16	C11H16		0.02
43	151.1393	C9(13C)2H16	C11H16		0.01
44	96.0890	C6(13C)1H10	C7H10		0.01
44	98.0956	C4(13C)3H10	C7H10		0.01
44	97.0921	C5(13C)2H10	C7H10		0.02
45	74.0958	C2(13C)3H10	C5H10		0.03
45	73.0922	C3(13C)2H10	C5H10		0.13
45	72.0887	C4(13C)1H10	C5H10		0.15
46	149.1354	C4(13C)4H16O2	C8H16O2	Octanoic acid	0.01
46	148.1323	C5(13C)3H16O2	C8H16O2	Octanoic acid	0.07
46	147.1288	C6(13C)2H16O2	C8H16O2	Octanoic acid	0.13
46	146.1257	C7(13C)1H16O2	C8H16O2	Octanoic acid	0.11
46	145.1222	C8H16O2	C8H16O2	Octanoic acid	0.03
47	139.1302	C6(13C)4H14	C10H14		0.01
47	138.1267	C7(13C)3H14	C10H14		0.02
47	137.1236	C8(13C)2H14	C10H14		0.02
48	83.0768	C4(13C)2H8	C6H8		0.02
49	140.1427	C7(13C)3H16	C10H16		0.01
50	108.0887	C7(13C)1H10	C8H10		-0.02
51	59.0766	C2(13C)2H8	C4H8		0.01
51	58.0735	C3(13C)1H8	C4H8		0.02
52	229.2347	C11(13C)4H28O	C15H28O		-0.01
53	204.1951	C9(13C)3H24O2	C12H24O2	Ethyl decanoate	0.04
53	203.1916	C10(13C)2H24O2	C12H24O2	Ethyl decanoate	0.04
53	202.1881	C11(13C)1H24O2	C12H24O2	Ethyl decanoate	0.01
54	95.0976	C2(13C)2H12O2	C4H12O2		-0.14
54	94.0945	C3(13C)1H12O2	C4H12O2		-0.14
55	77.0871	C2(13C)2H10O	C4H10O		-0.02
55	76.0840	C3(13C)1H10O	C4H10O		-0.02
56	371.1017	C20(13C)3H13NO4	C23H13NO4		0.01
57	229.0345	C9H8O7	C9H8O7		0.01
58	103.0751	C5H10O2	C5H10O2		0.03
58	105.0822	C3(13C)2H10O2	C5H10O2		0.04
58	104.0786	C4(13C)1H10O2	C5H10O2		0.07
59	133.1136	C5(13C)2H14O2	C7H14O2		0.01
60	118.0581	C4(13C)1H8O3	C5H8O3		0.01
61	120.1009	C3(13C)3H12O2	C6H12O2	Hexanoic acid	0.01
61	119.0979	C4(13C)2H12O2	C6H12O2	Hexanoic acid	0.04
61	118.0943	C5(13C)1H12O2	C6H12O2	Hexanoic acid	0.05
62	87.0717	C3(13C)2H8O	C5H8O		0.02
62	86.0681	C4(13C)1H8O	C5H8O		0.03
63	190.1431	C7(13C)3H18O3	C10H18O3		0.02

63	189.1396	C8(13C)2H18O3	C10H18O3		0.02
63	188.1361	C9(13C)1H18O3	C10H18O3		0.01
64	176.1547	C5(13C)5H18O2	C10H18O2		0.01
64	175.1512	C6(13C)4H18O2	C10H18O2		0.05
64	172.1411	C9(13C)1H18O2	C10H18O2		0.06
64	173.1446	C8(13C)2H18O2	C10H18O2		0.12
64	174.1482	C7(13C)3H18O2	C10H18O2		0.11
65	157.1407	C6(13C)4H16O	C10H16O	Citral	0.03
65	156.1376	C7(13C)3H16O	C10H16O	Citral	0.07
65	155.1341	C8(13C)2H16O	C10H16O	Citral	0.08
66	104.0697	C2(13C)3H8O2	C5H8O2		0.02
66	101.0596	C5H8O2	C5H8O2		0.20
66	103.0666	C3(13C)2H8O2	C5H8O2		0.22
66	102.0631	C4(13C)1H8O2	C5H8O2		0.47
67	120.0736	C4(13C)1H10O3	C5H10O3		0.06
67	121.0771	C3(13C)2H10O3	C5H10O3		0.05
68	202.1795	C9(13C)3H22O2	C12H22O2		0.02
68	201.1760	C10(13C)2H22O2	C12H22O2		0.01
69	77.0597	C3H8O2	C3H8O2		-0.02
70	74.0680	C3(13C)1H8O	C4H8O		0.01
71	160.1325	C6(13C)3H16O2	C9H16O2		0.01
71	159.1289	C7(13C)2H16O2	C9H16O2		0.01
72	153.1186	C8(13C)2H14O	C10H14O		0.02
73	117.0819	C4(13C)2H10O2	C6H10O2		0.03
73	116.0788	C5(13C)1H10O2	C6H10O2		0.03
74	130.0945	C6(13C)1H12O2	C7H12O2		0.01
74	131.0976	C5(13C)2H12O2	C7H12O2		0.02
75	89.0599	C4H8O2	C4H8O2		0.09
75	91.0665	C2(13C)2H8O2	C4H8O2		0.06
75	90.0630	C3(13C)1H8O2	C4H8O2		0.19
76	73.0560	C2(13C)2H6O	C4H6O		0.01
76	72.0524	C3(13C)1H6O	C4H6O		0.03
77	107.0767	C6(13C)2H8	C8H8		0.12
77	106.0731	C7(13C)1H8	C8H8		0.21
77	105.0701	C8H8	C8H8		0.09
78	62.0320	C1(13C)1H4O2	C2H4O2		-0.02
78	61.0285	C2H4O2	C2H4O2		0.04
79	84.0889	C5(13C)1H10	C6H10		-0.02
80	98.1046	C6(13C)1H12	C7H12		-0.01
81	58.0367	C2(13C)1H4O	C3H4O		-0.01
82	147.1566	C5(13C)4H18O	C9H18O		-0.01
82	146.1531	C6(13C)3H18O	C9H18O		-0.02
82	145.1495	C7(13C)2H18O	C9H18O		-0.02
82	144.1465	C8(13C)1H18O	C9H18O		-0.02
83	172.1778	C10(13C)1H22O	C11H22O		-0.01
83	175.1880	C7(13C)4H22O	C11H22O		-0.02
83	174.1844	C8(13C)3H22O	C11H22O		-0.02

83	173.1809	C9(13C)2H22O	C11H22O	-0.02
84	203.2194	C9(13C)4H26O	C13H26O	-0.02
84	202.2154	C10(13C)3H26O	C13H26O	-0.02
85	118.1217	C4(13C)3H14O	C7H14O	-0.02
85	117.1186	C5(13C)2H14O	C7H14O	-0.02
86	233.2569	C9(13C)6H30O	C15H30O	-0.01
86	229.2437	C13(13C)2H30O	C15H30O	-0.01
86	232.2538	C10(13C)5H30O	C15H30O	-0.03
86	231.2503	C11(13C)4H30O	C15H30O	-0.03
86	230.2472	C12(13C)3H30O	C15H30O	-0.03

Table S 5. Compounds detected in negative ion mode during yeast growth in $^{13}C_1$-glucose. All the analytes were detected in $[M\text{-}H]^-$ form. [Article's](#) copyright: Attribution 4.0 International ([CC BY 4.0](#))

#	*M/Z*	MOLECULAR FORMULA (^{12}C & ^{13}C)	UNIQUE MOLECULAR FORMULA	RDBE	MASS ERROR (PPM)	ID
1	58.03793	C2(13C)1H6O	C3H6O	1	-0.23	
2	59.01383	C2H4O2	C2H4O2	1	-0.38	Acetic acid
2	60.0172	C1(13C)1H4O2	C2H4O2	1	-0.13	Acetic acid
2	61.02057	(13C)2H4O2	C2H4O2	1	0.11	Acetic acid
3	73.02951	C3H6O2	C3H6O2	1	0.09	Propionic acid
3	74.03288	C2(13C)1H6O2	C3H6O2	1	0.29	Propionic acid
4	86.0693	C4(13C)1H10O	C5H10O	1	0.65	
4	87.07252	C3(13C)2H10O	C5H10O	1	-0.89	
5	87.0452	C4H8O2	C4H8O2	1	0.53	Butanoic acid
5	88.04857	C3(13C)1H8O2	C4H8O2	1	0.70	Butanoic acid
5	89.05194	C2(13C)2H8O2	C4H8O2	1	0.85	Butanoic acid
5	90.05516	C1(13C)3H8O2	C4H8O2	1	-0.64	Butanoic acid
6	104.0708	C2(13C)3H10O2	C5H10O2	1	-0.65	Pentanoic acid
7	113.0973	C7H14O	C7H14O	1	0.98	Heptanoic acid
7	114.1005	C6(13C)1H14O	C7H14O	1	-0.38	Heptanoic acid
7	115.1039	C5(13C)2H14O	C7H14O	1	0.01	Heptanoic acid
7	116.1073	C4(13C)3H14O	C7H14O	1	0.40	Heptanoic acid
8	115.0766	C6H12O2	C6H12O2	1	1.26	Hexanoic acid
8	116.0799	C5(13C)1H12O2	C6H12O2	1	0.78	Hexanoic acid
8	117.0832	C4(13C)2H12O2	C6H12O2	1	0.31	Hexanoic acid
8	118.0865	C3(13C)3H12O2	C6H12O2	1	-0.15	Hexanoic acid
9	119.0349	C4H8O4	C4H8O4	1	-0.69	
9	120.0383	C3(13C)1H8O4	C4H8O4	1	-0.31	
9	121.0417	C2(13C)2H8O4	C4H8O4	1	0.06	
10	134.054	C4(13C)1H10O4	C5H10O4	1	0.09	
10	135.0574	C3(13C)2H10O4	C5H10O4	1	0.42	
11	142.1317	C8(13C)1H18O	C9H18O	1	-1.00	
11	143.1354	C7(13C)2H18O	C9H18O	1	1.40	

11	144.1388	C6(13C)3H18O	C9H18O	1	1.70	
11	145.1426	C5(13C)4H18O	C9H18O	1	4.73	
12	143.1076	C8H16O2	C8H16O2	1	-1.06	Octanoic acid
12	144.1112	C7(13C)1H16O2	C8H16O2	1	0.63	Octanoic acid
12	145.1144	C6(13C)2H16O2	C8H16O2	1	-0.43	Octanoic acid
12	146.1179	C5(13C)3H16O2	C8H16O2	1	0.56	Octanoic acid
12	147.1211	C4(13C)4H16O2	C8H16O2	1	-0.50	Octanoic acid
12	148.1243	C3(13C)5H16O2	C8H16O2	1	-1.53	Octanoic acid
13	147.0665	C6H12O4	C6H12O4	1	1.47	
13	148.0695	C5(13C)1H12O4	C6H12O4	1	-0.92	
14	162.0854	C6(13C)1H14O4	C7H14O4	1	0.69	
15	172.1427	C9(13C)1H20O2	C10H20O2	1	1.68	Decanoic acid
15	173.1459	C8(13C)2H20O2	C10H20O2	1	0.78	Decanoic acid
15	174.149	C7(13C)3H20O2	C10H20O2	1	-0.68	Decanoic acid
15	175.1522	C6(13C)4H20O2	C10H20O2	1	-1.55	Decanoic acid
15	176.1556	C5(13C)5H20O2	C10H20O2	1	-1.29	Decanoic acid
16	175.0971	C8H16O4	C8H16O4	1	-2.74	
16	176.1006	C7(13C)1H16O4	C8H16O4	1	-1.91	
16	177.1043	C6(13C)2H16O4	C8H16O4	1	0.04	
17	188.1373	C9(13C)1H20O3	C10H20O3	1	-0.12	
17	189.1408	C8(13C)2H20O3	C10H20O3	1	0.64	
17	190.1441	C7(13C)3H20O3	C10H20O3	1	0.35	
17	191.1474	C6(13C)4H20O3	C10H20O3	1	0.06	
18	189.1134	C9H18O4	C9H18O4	1	0.88	
18	190.1164	C8(13C)1H18O4	C9H18O4	1	-0.98	
18	191.1203	C7(13C)2H18O4	C9H18O4	1	1.86	
18	192.1233	C6(13C)3H18O4	C9H18O4	1	0.01	
18	193.1266	C5(13C)4H18O4	C9H18O4	1	-0.27	
19	200.1734	C11(13C)1H24O2	C12H24O2	1	-1.53	Dodecanoic acid
19	201.1773	C10(13C)2H24O2	C12H24O2	1	1.17	Dodecanoic acid
19	202.1803	C9(13C)3H24O2	C12H24O2	1	-0.58	Dodecanoic acid
19	203.184	C8(13C)4H24O2	C12H24O2	1	1.11	Dodecanoic acid
19	204.1868	C7(13C)5H24O2	C12H24O2	1	-1.60	Dodecanoic acid
19	205.1908	C6(13C)6H24O2	C12H24O2	1	1.53	Dodecanoic acid
20	206.1392	C7(13C)3H20O4	C10H20O4	1	1.22	
21	218.1477	C10(13C)1H22O4	C11H22O4	1	-0.86	
21	219.1513	C9(13C)2H22O4	C11H22O4	1	0.26	
21	220.1547	C8(13C)3H22O4	C11H22O4	1	0.46	
22	229.2086	C12(13C)2H28O2	C14H28O2	1	1.03	Tetradecanoic acid
22	230.212	C11(13C)3H28O2	C14H28O2	1	1.22	Tetradecanoic acid
22	232.2186	C9(13C)5H28O2	C14H28O2	1	0.73	Tetradecanoic acid
23	234.1693	C9(13C)3H24O4	C12H24O4	1	-4.03	
24	246.1795	C12(13C)1H26O4	C13H26O4	1	1.26	Tridecanoic acid
24	247.1828	C11(13C)2H26O4	C13H26O4	1	1.04	Tridecanoic acid
24	248.1861	C10(13C)3H26O4	C13H26O4	1	0.81	Tridecanoic acid
24	249.189	C9(13C)4H26O4	C13H26O4	1	-1.01	Tridecanoic acid
25	101.0519	C3(13C)2H8O2	C5H8O2	2	0.36	

26	103.0312	C2(13C)2H6O3	C4H6O3	2	0.70
27	114.0641	C5(13C)1H10O2	C6H10O2	2	-0.51
28	119.026	C2(13C)2H6O4	C4H6O4	2	-0.35
29	131.0624	C4(13C)2H10O3	C6H10O3	2	-0.21
29	132.0656	C3(13C)3H10O3	C6H10O3	2	-1.37
30	142.0956	C7(13C)1H14O2	C8H14O2	2	0.99
30	143.0991	C6(13C)2H14O2	C8H14O2	2	1.99
30	144.1022	C5(13C)3H14O2	C8H14O2	2	0.22
31	145.0781	C5(13C)2H12O3	C7H12O3	2	0.15
31	146.0818	C4(13C)3H12O3	C7H12O3	2	2.50
32	158.0904	C7(13C)1H14O3	C8H14O3	2	0.17
32	159.0938	C6(13C)2H14O3	C8H14O3	2	0.45
32	160.0968	C5(13C)3H14O3	C8H14O3	2	-1.76
32	161.1005	C4(13C)4H14O3	C8H14O3	2	0.38
33	169.1236	C10H18O2	C10H18O2	2	1.16
33	170.1268	C9(13C)1H18O2	C10H18O2	2	0.24
33	171.1303	C8(13C)2H18O2	C10H18O2	2	1.08
33	172.1334	C7(13C)3H18O2	C10H18O2	2	-0.40
33	173.1374	C6(13C)4H18O2	C10H18O2	2	3.31
34	175.0887	C6(13C)2H14O4	C8H14O4	2	0.33
34	176.0919	C5(13C)3H14O4	C8H14O4	2	-0.55
35	186.1218	C9(13C)1H18O3	C10H18O3	2	0.68
35	187.1251	C8(13C)2H18O3	C10H18O3	2	0.38
35	188.1282	C7(13C)3H18O3	C10H18O3	2	-0.97
35	189.132	C6(13C)4H18O3	C10H18O3	2	1.38
36	216.1596	C9(13C)3H22O3	C12H22O3	2	-0.38
36	217.1628	C8(13C)4H22O3	C12H22O3	2	-1.09
37	221.067	C8H14O7	C8H14O7	2	1.46
37	222.0699	C7(13C)1H14O7	C8H14O7	2	-0.59
38	177.1088	(13C)6H12N4O2	C6H12N4O2	3	-0.44
39	206.1426	C1(13C)7H16N4O2	C8H16N4O2	3	-4.51
39	207.1466	(13C)8H16N4O2	C8H16N4O2	3	-1.39
40	174.0897	C1(13C)5H10N4O2	C6H10N4O2	4	-0.99
41	203.125	C2(13C)6H14N4O2	C8H14N4O2	4	2.31
41	204.1281	C1(13C)7H14N4O2	C8H14N4O2	4	1.05
41	205.1312	(13C)8H14N4O2	C8H14N4O2	4	-0.19
42	231.2154	C3(13C)12H24O	C15H24O	4	-1.29
43	215.1567	C3(13C)10H18O2	C13H18O2	5	-1.17

ANNEX 3. Supporting information – “Real-Time Monitoring of Tricarboxylic Acid Metabolites in Exhaled Breath”

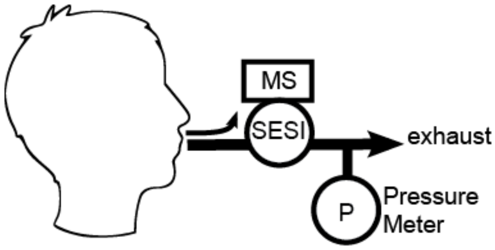

*Figure S 10. **Schematic description of the experimental set-up**. The subjects exhaled through a heated tube connected to the ionization source. A fraction of the flow was sampled by the mass spectrometer, and the rest was discharged to the laboratory fume hood (i.e. exhaust). The subjects were asked to control the exhalation pressure by monitoring a digital manometer during the exhalation maneuver. Clean nitrogen flushed the ionization source and the sampling tube to avoid cross contamination in between measurements. Article’s copyright © 2018, American Chemical Society*

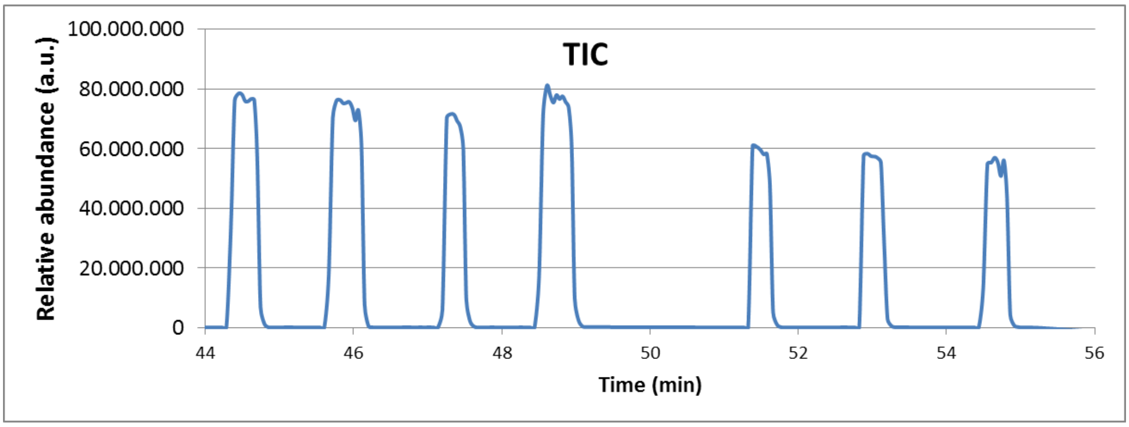

*Figure S 11. **Total ion current (TIC) as a function of time during the exhalation maneuvers**. Between 44 and 50 min, one subject exhaled four times, resulting in a repeatable signal intensity of ~ 8x107. Between 50 – 56 min another subject exhaled three consecutive times, resulting in equally repeatable signals, but of lower intensity (~ 6x10^7). Article’s copyright © 2018, American Chemical Society*

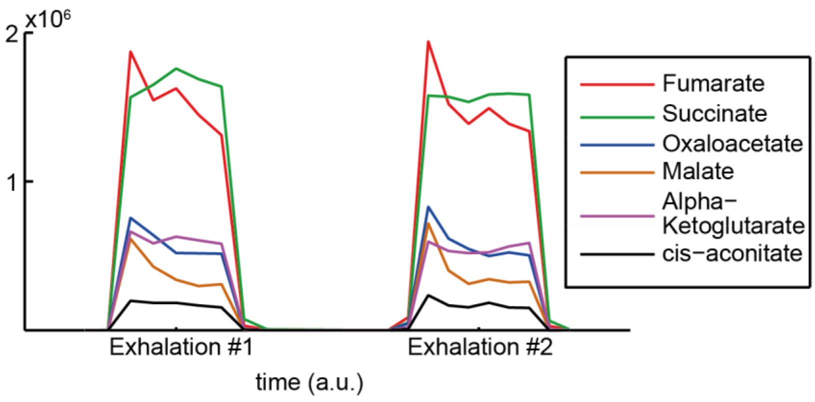

Figure S 12. ***Signal intensities vs time during two consecutives exhalations from the same subject.*** *Article's copyright © 2018, American Chemical Society*

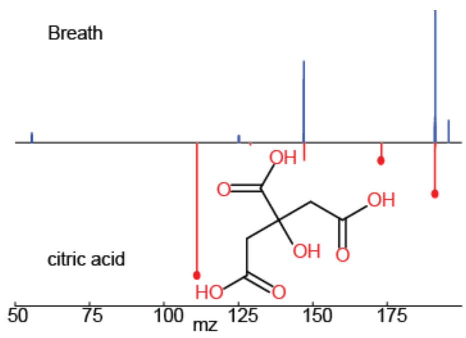

Figure S 13. ***SESI-MS/MS fragmentation spectra of citric acid standard (bottom) and breath (top).*** *The mismatch in the pattern suggest that the exhaled compound does not correspond to citric acid, but to an isomeric molecule. Article's copyright © 2018, American Chemical Society*

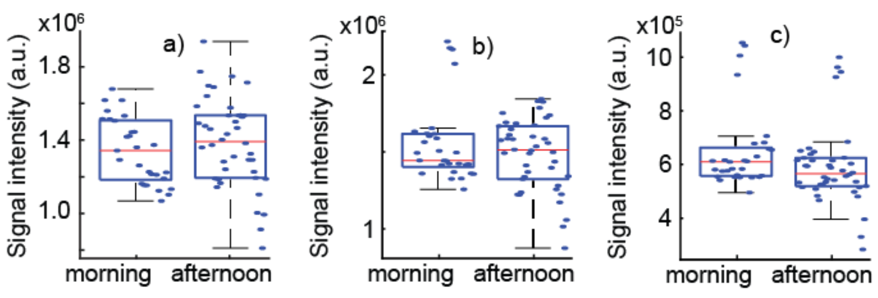

Figure S 14. ***TCA cycle metabolites a) fumaric acid; b) succinic acid and c) alpha-ketoglutaric acid showed no significant time-of-day dependence in exhaled breath abundance****. Article's copyright © 2018, American Chemical Society*

Table S 6. Lock masses employed in negative ion mode to ensure high mass accuracy during the experiments. Article's copyright © 2018, American Chemical Society

Formula	m/z
$C_2H_3O_2^-$	59.01385
$C_4H_7O_2^-$	87.04515
$C_6H_{11}O_2^-$	115.07645
$C_8H_{15}O_2^-$	143.10775
$C_{10}H_{19}O_2^-$	171.13905
$C_{12}H_{23}O_2^-$	199.17035
$C_{14}H_{27}O_2^-$	227.20165
$C_{16}H_{31}O_2^-$	255.23295

Table S 7. List of chemicals used for running MS/MS experiments and collision energies used to compare the fragmentation pattern of the standards and the exhaled breath. Article's copyright © 2018, American Chemical Society

	Supplier	Product No.	Collision energy (%)
Cis-aconitic acid	ABCR	AB113312	14
Alpha-ketoglutaric acid	TCI	K0005	18
Succinic acid	Acros	21955	20
Fumaric acid	Sigma-Aldrich	47910	20
Malic acid	Sigma-Aldrich	02310	18
Oxaloacetic acid	Acros	41660	20

Table S 8. ***Estimation of gas-phase concentrations in breath for healthy humans****. Article's copyright © 2018, American Chemical Society*

Metabolite	Molecular weight	octanol:water partition coefficient (Log K_{ow})	Vapor Pressure (Pa at 25 °C)	Log (blood:air partition coefficient)*	Typical Concen-tration in blood (µM)	Predicted-Concen-tration in breath (ppq)
Malic acid	134	-1.26 [Ref [250]]	4.37E-06 [Ref [251]]	12.54	10 [Ref [252]]	0.1
Fumaric acid	116	0.46 [Ref [250]]	2.05E-02 [Ref [251]]	7.90	1.5 [Ref [252]]	485
Succinic acid	118	-0.59 [Ref [250]]	2.55E-05 [Ref [251]]	11.47	16 [Ref [253]]	1
Alpha-ketoglutaric acid	146	-2.08‡	9.57E-03§	9.45	7 [Ref [252]]	64
cis-Aconitic acid	174	-0.14‡	1.11E-04§	10.28	1.2 [Ref [219]]	2
Oxaloacetic acid	132	-2.58‡	6.27E-03§	9.97	7.14Ŧ	19

*Predicted by the Buist *et al.*[242] method: Log(PBA) = 6.96-1.04 Log(VP)-0.533 Log(K_{OW})-0.00495 MW.

‡Predicted by KOWWIN v1.67 estimate.

§Modified Grain method.

ŦAs no references were found, we computed the mean of the other five metabolites.

Table S 9. Retention times and fragmentation spectra data from Figure 28 for EBC. Article's copyright © 2018, American Chemical Society

Fumaric acid			**Succinic acid**			**Malic acid**		
Retention time (min)	*m/z*	*int*	*Retention time (min)*	*m/z*	*int*	*Retention time (min)*	*m/z*	*int*
2.76	115.0023	100	3.02	117.0312	3.4818	1.82	133.0283	2.9695
	71.0128	58.2385		117.0177	100		133.0127	100
				116.6577	2.2875		132.5941	2.2926
				99.0078	17.4765		115.0192	2.1325
				73.0446	2.976		115.0026	99.7345
				73.0292	62.042		114.6414	1.3964
				72.8056	1.2898		89.0245	5.8868
				55.0232	1.6885		87.0087	1.583
							73.0056	1.0304
							72.9927	5.6229
							71.014	22.0675
							59.0137	1.265
							45.0021	0.9565
							43.022	2.0663

Table S 10. Mean values, mean differences, corresponding 95% confidence interval and p-value resulting from running an unpaired t-test to compare morning vs afternoon levels of the TCA cycle metabolites identified in exhaled breath. Article's copyright © 2018, American Chemical Society

	mean morning values (a.u.)	**mean afternoon values (a.u.)**	**Mean difference (a.u.)**	**95% confidence interval (a.u.)**		**p-value**
malic acid	400e+3	348e+3	53e+3	24e+3	82e+3	0.0005
oxaloacetic acid	690e+3	602e+3	89e+3	28e+3	149e+3	0.0048
cis-aconitic acid	212e+3	179e+3	33e+3	13e+3	54e+3	0.0021
α-Ketoglutaric acid	653e+3	589e+3	64e+3	-8e+3	135e+3	0.0812
succinic acid	1558e+3	1481e+3	78e+3	-41e+3	196e+3	0.1978
fumaric acid	1340e+3	1387e+3	-46e+3	-153e+3	60e+3	0.3858

References

Photography of the ETH-Bibliothek taken from https://www.kulturzueri.ch website

[1] C. D. Keeling, “The Concentration and Isotopic Abundances of Carbon Dioxide in the Atmosphere,” *Tellus*, vol. 12, no. 2, pp. 200–203, Aug. 2018.
[2] D. P. Tans, “CO2 data from Mauna Loa,” *NOAA/ESRL*. [Online]. Available: www.esrl.noaa.gov/gmd/ccgg/trends/.
[3] S. Arrhenius, “XXXI. On the influence of carbonic acid in the air upon the temperature of the ground,” *London, Edinburgh, Dublin Philos. Mag. J. Sci.*, vol. 41, no. 251, pp. 237–276, Apr. 1896.
[4] EEA, “European Union emission inventory report 1990-2016,” Copenhagen, 2018.
[5] W. H. A. (WHA), “Health and the environment: addressing the health impact of air pollution,” Geneva, 2014.
[6] W. H. O. O. and E. H. Team, “WHO Air quality guidelines for particulate matter, ozone, nitrogen dioxide and sulfur dioxide : global update 2005 : summary of risk assessment,” Geneva, 2006.
[7] K. Donaldson *et al.*, “Combustion-derived nanoparticles: A review of their toxicology following inhalation exposure,” *Part. Fibre Toxicol.*, vol. 2, no. 1, p. 10, 2005.
[8] N. L. Mills *et al.*, “Adverse cardiovascular effects of air pollution,” *Nat. Clin. Pract. Cardiovasc. Med.*, vol. 6, p. 36, Nov. 2008.
[9] M. R. Miller *et al.*, “Inhaled Nanoparticles Accumulate at Sites of Vascular Disease.,” *ACS Nano*, vol. 11, no. 5, pp. 4542–4552, May 2017.
[10] M. R. Miller, C. A. Shaw, and J. P. Langrish, “From particles to patients: oxidative stress and the cardiovascular effects of air pollution,” *Future Cardiol.*, vol. 8, no. 4, pp. 577–602, Jul. 2012.
[11] Y. H. Shaib, M. Rugge, D. Y. Graham, and R. M. Genta, “PERSPECTIVES IN CLINICAL GASTROENTEROLOGY AND HEPATOLOGY: Management of Gastric Polyps: An Endoscopy-Based Approach,” *Clin. Gastroenterol. Hepatol.*, vol. 11, no. 11, pp. 1374–1384, Nov. 2013.
[12] O. Lawal, W. M. Ahmed, T. M. E. Nijsen, R. Goodacre, and S. J. Fowler, “Exhaled breath analysis: a review of ‘breath-taking’ methods for off-line analysis,” *Metabolomics*, vol. 13, no. 10, p. 110, Aug. 2017.
[13] B. R. Winters, J. D. Pleil, M. M. Angrish, M. A. Stiegel, T. H. Risby, and M. C. Madden, “Standardization of the collection of exhaled breath condensate and exhaled breath aerosol using a feedback regulated sampling device.,” *J. Breath Res.*, vol. 11, no. 4, p. 47107, Nov. 2017.
[14] C. Lourenço and C. Turner, “Breath Analysis in Disease Diagnosis: Methodological Considerations and Applications,” *Metabolites*, vol. 4, no. 2, pp. 465–498, Jun. 2014.
[15] S. T. Chambers, A. Scott-Thomas, and M. Epton, “Developments in novel breath tests for bacterial and fungal pulmonary infection.,” *Curr. Opin. Pulm. Med.*, vol. 18, no. 3, pp. 228–232, May 2012.
[16] L. D. J. Bos, P. J. Sterk, and M. J. Schultz, “Volatile Metabolites of Pathogens: A Systematic Review,” *PLoS Pathog.*, vol. 9, 2013.
[17] N. Karami *et al.*, “Identification of bacteria using volatile organic compounds.,” *Cell. Mol. Biol. (Noisy-le-grand).*, vol. 63, no. 2, pp. 112–121, Feb. 2017.
[18] J. Zhu, H. D. Bean, Y.-M. Kuo, and J. E. Hill, “Fast detection of volatile organic compounds from bacterial cultures by secondary electrospray ionization-mass spectrometry.,” *J. Clin. Microbiol.*, vol. 48, no. 12, pp. 4426–4431, Dec. 2010.
[19] E. Tait, J. D. Perry, S. P. Stanforth, and J. R. Dean, “Identification of volatile organic compounds produced by bacteria using HS-SPME-GC-MS.,” *J. Chromatogr. Sci.*, vol. 52, no. 4, pp. 363–373, Apr. 2014.

[20] M. Bunge *et al.*, “On-Line Monitoring of Microbial Volatile Metabolites by Proton Transfer Reaction-Mass Spectrometry ,” *Appl. Environ. Microbiol.*, vol. 74, no. 7, pp. 2179–2186, Apr. 2008.
[21] A. Fleming, “On the Antibacterial Action of Cultures of a Penicillium, with Special Reference to their Use in the Isolation of B. influenzæ,” *Br. J. Exp. Pathol.*, vol. 10, no. 3, pp. 226–236, Jun. 1929.
[22] D. J. Spakowicz and S. A. Strobel, “Biosynthesis of hydrocarbons and volatile organic compounds by fungi: bioengineering potential,” *Appl. Microbiol. Biotechnol.*, vol. 99, no. 12, pp. 4943–4951, Jun. 2015.
[23] B. Okaikwei, “Simultaneous analysis of trace gases in ambient air by FTIR-spectroscopy,” University of Bremen, 2008.
[24] J. Mohn and L. Emmenegger, Determination of Sulphur Dioxide by Pulsed UV-Fluorescence. 2018.
[25] A. B. Bluhme, J. L. Ingemar, C. Meusinger, and M. S. Johnson, “Water vapor inhibits hydrogen sulfide detection in pulsed fluorescence sulfur monitors,” *Atmos. Meas. Tech.*, vol. 9, no. 6, pp. 2669–2673, Jun. 2016.
[26] D. A. Long, “Introductory Raman Spectroscopy. John R. Ferraro, Kazuo Nakamoto and Chris W. Brown. Academic Press, Amsterdam, Second Edition, 2003. xiii + 434,” *J. Raman Spectrosc.*, vol. 36, no. 10, p. 1012.
[27] Y. Dellaa, C. Rahmoune, J. Kister, and N. Dupuy, “Analysis of Air Pollution Aerosols by Raman Spectroscopy and Spectral Resolution Methods,” *AIP Conf. Proc.*, vol. 1267, no. 1, pp. 529–530, Aug. 2010.
[28] M. Uhl, “Determination of drugs in hair using GC/MS/MS,” *Forensic Sci. Int.*, vol. 84, no. 1, pp. 281–294, 1997.
[29] B. A. Eckenrode, “Environmental and forensic applications of field-portable GC-MS: an overview,” *J. Am. Soc. Mass Spectrom.*, vol. 12, no. 6, pp. 683–693, 2001.
[30] M. Grapp, H. H. Maurer, and H. Desel, “Systematic forensic toxicological analysis by GC-MS in serum using automated mass spectral deconvolution and identification system.,” *Drug Test. Anal.*, vol. 8, no. 8, pp. 816–825, Aug. 2016.
[31] M. Blomquist, R. Bonnichsen, C.-G. Fri, Y. Mårde, and R. Ryhage, “Gas chromatography-mass spectrometry in forensic chemistry for identification of substances isolated from tissue,” *Zeitschrift für Rechtsmedizin*, vol. 69, no. 1, pp. 52–61, 1971.
[32] D. L. Lin, S. M. Wang, C. H. Wu, B. G. Chen, and R. H. Liu, “Chemical derivatization for forensic drug analysis by GC- and LC-MS.,” *Forensic Sci. Rev.*, vol. 28, no. 1, pp. 17–35, Jan. 2016.
[33] W. M. Haynes, D. R. Lide, and T. J. Bruno, *CRC handbook of chemistry and physics : a ready-reference book of chemical and physical data*, 2016–2017, 97th Edition / Editor–in–Chief: W. M. Haynes ed. Boca Raton, Florida : CRC Press, 2017.
[34] M. Hamden, “Gas Phase Ion-Molecule Reaction Rate Constants Through 1986. Yasumasa Ikezoe, Shingo Matsuoka, Masahiro Takebe and Albert Viggiano (eds). Maruzen Company Ltd, Tokyo. 1987. (viii) + 244 pp. US$ 150.00,” *Rapid Commun. Mass Spectrom.*, vol. 3, no. 3, pp. iii–iii, Sep. 2018.
[35] F. T. Mackenzie and J. A. Mackenzie, “Our changing planet : an introduction to earth system science and global environmental change.” Macmillan College Pub. ; Toronto : Maxwell Macmillan Canada ; New York : Maxwell Macmillan International, New York, 1995.
[36] C. Barrios-Collado, “Capturing in Vivo Plant Metabolism by Real-Time Analysis

of Low to High Molecular Weight Volatiles," *Anal. Chem.*, vol. 88, 2016.
[37] J. J. Thomson, "XL. Cathode Rays," *London, Edinburgh, Dublin Philos. Mag. J. Sci.*, vol. 44, no. 269, pp. 293–316, Oct. 1897.
[38] "Experiments on a new cathode dark space in helium and hydrogen," *Proc. R. Soc. London. Ser. A*, vol. 80, no. 535, p. 45 LP-49, Dec. 1907.
[39] A. J. Dempster, "Positive Ray Analysis of Lithium and Magnesium," *Phys. Rev.*, vol. 18, no. 6, pp. 415–422, Dec. 1921.
[40] W. Bleakney, "A New Method of Positive Ray Analysis and Its Application to the Measurement of Ionization Potentials in Mercury Vapor," *Phys. Rev.*, vol. 34, no. 1, pp. 157–160, Jul. 1929.
[41] A. O. Nier and J. Bardeen, "The Production of Concentrated Carbon (13) by Thermal Diffusion," *J. Chem. Phys.*, vol. 9, no. 9, pp. 690–692, Sep. 1941.
[42] A. O. Nier, "The Concentration of Carbon 13 by Thermal Diffusion," *Phys. Rev.*, vol. 57, no. 1, pp. 30–34, Jan. 1940.
[43] A. O. Nier, R. W. Thompson, and B. F. Murphey, "The Isotopic Constitution of Lead and the Measurement of Geological Time. III," *Phys. Rev.*, vol. 60, no. 2, pp. 112–116, Jul. 1941.
[44] A. O. Nier, "Variations in the Relative Abundances of the Isotopes of Common Lead from Various Sources," *J. Am. Chem. Soc.*, vol. 60, no. 7, pp. 1571–1576, Jul. 1938.
[45] A. O. Nier, E. T. Booth, J. R. Dunning, and A. V Grosse, "Nuclear Fission of Separated Uranium Isotopes," *Phys. Rev.*, vol. 57, no. 6, p. 546, Mar. 1940.
[46] A. O. Nier, "The Isotopic Constitution of Uranium and the Half-Lives of the Uranium Isotopes. I," *Phys. Rev.*, vol. 55, no. 2, pp. 150–153, Jan. 1939.
[47] A. O. Nier, E. T. Booth, J. R. Dunning, and A. V Grosse, "Further Experiments on Fission of Separated Uranium Isotopes," *Phys. Rev.*, vol. 57, no. 8, p. 748, Apr. 1940.
[48] E. T. Booth, J. R. Dunning, A. V Grosse, and A. O. Nier, "Neutron Capture by Uranium (238)," *Phys. Rev.*, vol. 58, no. 5, pp. 475–476, Sep. 1940.
[49] R. Gomer and M. G. Inghram, "Applications of Field Ionization to Mass Spectrometry," *J. Am. Chem. Soc.*, vol. 77, no. 2, p. 500, Jan. 1955.
[50] H. D. Beckey, "Field desorption mass spectrometry: A technique for the study of thermally unstable substances of low volatility," *Int. J. Mass Spectrom. Ion Phys.*, vol. 2, no. 6, pp. 500–502, 1969.
[51] M. S. B. Munson and F. H. Field, "Chemical Ionization Mass Spectrometry. I. General Introduction," *J. Am. Chem. Soc.*, vol. 88, no. 12, pp. 2621–2630, Jun. 1966.
[52] D. I. Carroll, I. Dzidic, R. N. Stillwell, K. D. Haegele, and E. C. Horning, "Atmospheric pressure ionization mass spectrometry. Corona discharge ion source for use in a liquid chromatograph-mass spectrometer-computer analytical system," *Anal. Chem.*, vol. 47, no. 14, pp. 2369–2373, Dec. 1975.
[53] E. C. Horning, M. G. Horning, D. I. Carroll, I. Dzidic, and R. N. Stillwell, "New picogram detection system based on a mass spectrometer with an external ionization source at atmospheric pressure," *Anal. Chem.*, vol. 45, no. 6, pp. 936–943, May 1973.
[54] K. Tanaka *et al.*, "Protein and polymer analyses up to m/z 100 000 by laser ionization time-of-flight mass spectrometry," *Rapid Commun. Mass Spectrom.*, vol. 2, no. 8, pp. 151–153, Aug. 2018.
[55] M. Dole, L. L. Mack, R. L. Hines, R. C. Mobley, L. D. Ferguson, and M. B. Alice, "Molecular Beams of Macroions," *J. Chem. Phys.*, vol. 49, no. 5, pp. 2240–2249, Sep. 1968.

[56] M. Yamashita and J. B. Fenn, "Electrospray ion source. Another variation on the free-jet theme," *J. Phys. Chem.*, vol. 88, no. 20, pp. 4451–4459, Sep. 1984.
[57] C. M. Whitehouse, R. N. Dreyer, M. Yamashita, and J. B. Fenn, "Electrospray interface for liquid chromatographs and mass spectrometers," *Anal. Chem.*, vol. 57, no. 3, pp. 675–679, Mar. 1985.
[58] J. B. Fenn, M. Mann, C. K. Meng, S. F. Wong, and C. M. Whitehouse, "Electrospray ionization for mass spectrometry of large biomolecules," *Science (80-.).*, vol. 246, no. 4926, p. 64 LP-71, Oct. 1989.
[59] J. B. Whitehouse, C. M.; Levin, F.; Meng, C. K.; Fenn, "In Further Adventures With An Electrospray Ion Source," in *Proceedings of the 34th ASMS Conference*, 1986.
[60] P. K. and J. B. F. S. Fuerstenau, "ESIMS in the Analysis of Trace Species in Gases," in *Proceedings of the 47th ASMS Conference on Mass Spectrometry Dallas (TX)*, 1999.
[61] C. Wu, W. F. Siems, and H. H. Hill, "Secondary Electrospray Ionization Ion Mobility Spectrometry/Mass Spectrometry of Illicit Drugs," *Anal. Chem.*, vol. 72, no. 2, pp. 396–403, Jan. 2000.
[62] P. Martínez-Lozano and J. Rus, "Fernández de la Mora, G., Hernández, M. & Fernández de la Mora, J. Secondary Electrospray Ionization (SESI) of Ambient Vapors for Explosive Detection at Concentrations Below Parts Per Trillion," *J. Am. Soc. Mass Spectrom.*, vol. 20, 2009.
[63] L. Meier, C. Berchtold, S. Schmid, and R. Zenobi, "Sensitive detection of drug vapors using an ion funnel interface for secondary electrospray ionization mass spectrometry," *J. Mass Spectrom.*, vol. 47, no. 5, pp. 555–559, May 2012.
[64] M. Tam and H. H. Hill, "Secondary Electrospray Ionization-Ion Mobility Spectrometry for Explosive Vapor Detection," *Anal. Chem.*, vol. 76, no. 10, pp. 2741–2747, May 2004.
[65] P. Martínez-Lozano and J. Fernandez de la Mora, "On-line Detection of Human Skin Vapors," *J. Am. Soc. Mass Spectrom.*, vol. 20, 2009.
[66] P. Martínez-Lozano and J. Fernández de la Mora, "Direct Analysis of Fatty Acid Vapors in Breath by Electrospray Ionization and Atmospheric Pressure Ionization-Mass Spectrometry," *Anal. Chem.*, vol. 80, no. 21, pp. 8210–8215, Nov. 2008.
[67] X. Li *et al.*, "Drug Pharmacokinetics Determined by Real-Time Analysis of Mouse Breath," *Angew. Chemie Int. Ed.*, vol. 54, no. 27, pp. 7815–7818, May 2015.
[68] J. He, P. M.-L. Sinues, M. Hollmen, X. Li, M. Detmar, and R. Zenobi, "Fingerprinting breast cancer vs. normal mammary cells by mass spectrometric analysis of volatiles.," *Sci. Rep.*, vol. 4, p. 5196, Jun. 2014.
[69] P. Martínez-Lozano Sinues *et al.*, "Mass spectrometry fingerprinting coupled to National Institute of Standards and Technology Mass Spectral search algorithm for pattern recognition," *Anal. Chim. Acta*, vol. 755, pp. 28–36, 2012.
[70] H. D. Bean, T. R. Mellors, J. Zhu, and J. E. Hill, "Profiling Aged Artisanal Cheddar Cheese Using Secondary Electrospray Ionization Mass Spectrometry," *J. Agric. Food Chem.*, vol. 63, no. 17, pp. 4386–4392, May 2015.
[71] C. Ballabio *et al.*, "Rapid identification of bacteria in blood cultures by mass-spectrometric analysis of volatiles.," *Journal of clinical pathology*, vol. 67, no. 8. England, pp. 743–746, Aug-2014.
[72] J. Zhu *et al.*, "Robust detection of P. aeruginosa and S. aureus acute lung infections by secondary electrospray ionization-mass spectrometry (SESI-MS)

breathprinting: from initial infection to clearance.," *J. Breath Res.*, vol. 7, no. 3, p. 37106, Sep. 2013.
[73] J. Zhu, H. D. Bean, J. Jimenez-Diaz, and J. E. Hill, "Secondary electrospray ionization-mass spectrometry (SESI-MS) breathprinting of multiple bacterial lung pathogens, a mouse model study.," *J. Appl. Physiol.*, vol. 114, no. 11, pp. 1544–1549, Jun. 2013.
[74] G. Vidal-de-Miguel, M. Macía, P. Pinacho, and J. Blanco, "Low-Sample Flow Secondary Electrospray Ionization: Improving Vapor Ionization Efficiency," *Anal. Chem.*, vol. 84, no. 20, pp. 8475–8479, Oct. 2012.
[75] K. Tang, J. S. Page, and R. D. Smith, "Charge competition and the linear dynamic range of detection in electrospray ionization mass spectrometry," *J. Am. Soc. Mass Spectrom.*, vol. 15, no. 10, pp. 1416–1423, 2004.
[76] A. Schmidt, M. Karas, and T. Dülcks, "Effect of different solution flow rates on analyte ion signals in nano-ESI MS, or: when does ESI turn into nano-ESI?," *J. Am. Soc. Mass Spectrom.*, vol. 14, no. 5, pp. 492–500, 2003.
[77] G. Hopfgartner, K. Bean, J. Henion, and R. Henry, "Ion spray mass spectrometric detection for liquid chromatography: A concentration- or a mass-flow-sensitive device?," *J. Chromatogr. A*, vol. 647, no. 1, pp. 51–61, 1993.
[78] M. T. Davis, D. C. Stahl, S. A. Hefta, and T. D. Lee, "A Microscale Electrospray Interface for Online, Capillary Liquid Chromatography/Tandem Mass Spectrometry of Complex Peptide Mixtures," *Anal. Chem.*, vol. 67, no. 24, pp. 4549–4556, Dec. 1995.
[79] D. C. Gale and R. D. Smith, "Small volume and low flow-rate electrospray lonization mass spectrometry of aqueous samples," *Rapid Commun. Mass Spectrom.*, vol. 7, no. 11, pp. 1017–1021, Aug. 2018.
[80] M. R. Emmett and R. M. Caprioli, "Micro-electrospray mass spectrometry: ultra-high-sensitivity analysis of peptides and proteins," *J. Am. Soc. Mass Spectrom.*, vol. 5, no. 7, pp. 605–613, 1994.
[81] M. S. Wilm and M. Mann, "Electrospray and Taylor-Cone theory, Dole's beam of macromolecules at last?," *Int. J. Mass Spectrom. Ion Process.*, vol. 136, no. 2, pp. 167–180, 1994.
[82] X. Tang, J. E. Bruce, and H. H. Hill, "Characterizing Electrospray Ionization Using Atmospheric Pressure Ion Mobility Spectrometry," *Anal. Chem.*, vol. 78, no. 22, pp. 7751–7760, Nov. 2006.
[83] S. Geromanos, G. Freckleton, and P. Tempst, "Tuning of an Electrospray Ionization Source for Maximum Peptide-Ion Transmission into a Mass Spectrometer," *Anal. Chem.*, vol. 72, no. 4, pp. 777–790, Feb. 2000.
[84] A. M. G.-C. and N. R.-M. and J. M. Montanero, "The minimum or natural rate of flow and droplet size ejected by Taylor cone–jets: physical symmetries and scaling laws," *New J. Phys.*, vol. 15, no. 3, p. 33035, 2013.
[85] M. A. Herrada, J. M. López-Herrera, A. M. Gañán-Calvo, E. J. Vega, J. M. Montanero, and S. Popinet, "Numerical simulation of electrospray in the cone-jet mode," *Phys. Rev. E*, vol. 86, no. 2, p. 26305, Aug. 2012.
[86] B. R. Reschke and A. T. Timperman, "A Study of Electrospray Ionization Emitters with Differing Geometries with Respect to Flow Rate and Electrospray Voltage," *J. Am. Soc. Mass Spectrom.*, vol. 22, no. 12, pp. 2115–2124, 2011.
[87] G. A. Valaskovic, J. P. Murphy, and M. S. Lee, "Automated orthogonal control system for electrospray ionization," *J. Am. Soc. Mass Spectrom.*, vol. 15, no. 8, pp. 1201–1215, 2004.
[88] T. Kien Nguyen, V. D. Nguyen, B. Seong, N. Hoang, J. Park, and D. Byun, "Control and improvement of jet stability by monitoring liquid meniscus in

electrospray and electrohydrodynamic jet," *J. Aerosol Sci.*, vol. 71, pp. 29–39, 2014.
[89] A. Suhendi, M. M. Munir, A. Bagus Suryamas, A. Nandiyanto, T. Ogi, and K. Okuyama, *Control of cone-jet geometry during electrospray by an electric current*, vol. 24. 2013.
[90] A. Gomez and K. Tang, "Charge and fission of droplets in electrostatic sprays," *Phys. Fluids*, vol. 6, no. 1, pp. 404–414, Jan. 1994.
[91] M. R. Morad, A. Rajabi, M. Razavi, and S. R. P. Sereshkeh, "A Very Stable High Throughput Taylor Cone-jet in Electrohydrodynamics," *Sci. Rep.*, vol. 6, p. 38509, Dec. 2016.
[92] C. N. Ryan, K. L. Smith, and J. P. W. Stark, "Characterization of multi-jet electrospray systems," *J. Aerosol Sci.*, vol. 51, pp. 35–48, 2012.
[93] V. I. K. and N. A. Fuks, "Electrohydrodynamic Atomisation of Liquids," *Russ. Chem. Rev.*, vol. 45, no. 12, p. 1179, 1976.
[94] M. G. Ikonomou, A. T. Blades, and P. Kebarle, "Electrospray mass spectrometry of methanol and water solutions suppression of electric discharge with SF6 gas.," *J. Am. Soc. Mass Spectrom.*, vol. 2, no. 6, pp. 497–505, Dec. 1991.
[95] F. M. Wampler, A. T. Blades, and P. Kebarle, "Negative ion electrospray mass spectrometry of nucleotides: ionization from water solution with SF6 discharge suppression," *J. Am. Soc. Mass Spectrom.*, vol. 4, no. 4, pp. 289–295, 1993.
[96] R. T. Collins, J. J. Jones, M. T. Harris, and O. A. Basaran, "Electrohydrodynamic tip streaming and emission of charged drops from liquid cones," *Nat. Phys.*, vol. 4, p. 149, Dec. 2007.
[97] R. T. Collins, K. Sambath, M. T. Harris, and O. A. Basaran, "Universal scaling laws for the disintegration of electrified drops," *Proc. Natl. Acad. Sci.*, vol. 110, no. 13, p. 4905 LP-4910, Mar. 2013.
[98] A. M. Gañán-Calvo, J. M. López-Herrera, N. Rebollo-Muñoz, and J. M. Montanero, "The onset of electrospray: the universal scaling laws of the first ejection," *Sci. Rep.*, vol. 6, p. 32357, Sep. 2016.
[99] Lord Rayleigh, "XX. On the equilibrium of liquid conducting masses charged with electricity," *London, Edinburgh, Dublin Philos. Mag. J. Sci.*, vol. 14, no. 87, pp. 184–186, Sep. 1882.
[100] J. V Iribarne and B. A. Thomson, "On the evaporation of small ions from charged droplets," *J. Chem. Phys.*, vol. 64, no. 6, pp. 2287–2294, Mar. 1976.
[101] B. A. Thomson and J. V Iribarne, "Field induced ion evaporation from liquid surfaces at atmospheric pressure," *J. Chem. Phys.*, vol. 71, no. 11, pp. 4451–4463, Dec. 1979.
[102] L. A. Dillon, V. N. Stone, L. A. Croasdell, P. R. Fielden, N. J. Goddard, and C. L. Paul Thomas, "Optimisation of secondary electrospray ionisation (SESI) for the trace determination of gas-phase volatile organic compounds," *Analyst*, vol. 135, no. 2, pp. 306–314, 2010.
[103] J. F. De La Mora, "The effect of charge emission from electrified liquid cones," *J. Fluid Mech.*, vol. 243, pp. 561–574, 1992.
[104] C. Barrios-Collado, G. Vidal-de-Miguel, and P. Martinez-Lozano Sinues, "Numerical modeling and experimental validation of a universal secondary electrospray ionization source for mass spectrometric gas analysis in real-time," *Sensors Actuators B Chem.*, vol. 223, pp. 217–225, 2016.
[105] P. Martinez-Lozano Sinues *et al.*, "Circadian Variation of the Human Metabolome Captured by Real-Time Breath Analysis," *PLoS One*, vol. 9, no. 12, p. e114422, Dec. 2015.

[106] D. Garcia-Gomez *et al.*, "Real-Time Quantification of Amino Acids in the Exhalome by Secondary Electrospray Ionization-Mass Spectrometry: A Proof-of-Principle Study.," *Clin. Chem.*, vol. 62, no. 9, pp. 1230–1237, Sep. 2016.
[107] P. Sinues *et al.*, "119 Exhaled breath analysis by real-time mass spectrometry in patients with pulmonary fibrosis," *Chest*, vol. 151, no. 5, p. A16, May 2017.
[108] P. Martinez-Lozano Sinues *et al.*, "Breath analysis in real time by mass spectrometry in chronic obstructive pulmonary disease.," *Respiration.*, vol. 87, no. 4, pp. 301–310, 2014.
[109] M. T. Gaugg *et al.*, "Metabolic effects of inhaled salbutamol determined by exhaled breath analysis.," *J. Breath Res.*, vol. 11, no. 4, p. 46004, Sep. 2017.
[110] E. R. 3rd Miller, L. J. Appel, L. Jiang, and T. H. Risby, "Association between cigarette smoking and lipid peroxidation in a controlled feeding study.," *Circulation*, vol. 96, no. 4, pp. 1097–1101, Aug. 1997.
[111] P. Gaugg, M. T.; Garcia Gomez, D.; Barrios Collado, C.; Vidal de Miguel, G.; Kohler, M.; Zenobi, R.; Martinez-Lozano Sinues, "Expanding metabolite coverage of real-time breath analysis by coupling a universal secondary electrospray ionization source and high resolution mass spectrometry – a pilot study on tobacco smokers," *J. Breath Res.*, vol. 10, 2016.
[112] L. Bregy *et al.*, "Differentiation of oral bacteria in in vitro cultures and human saliva by secondary electrospray ionization – mass spectrometry," *Sci. Rep.*, vol. 5, p. 15163, Oct. 2015.
[113] M. E. Monge, G. A. Harris, P. Dwivedi, and F. M. Fernández, "Mass Spectrometry: Recent Advances in Direct Open Air Surface Sampling/Ionization," *Chem. Rev.*, vol. 113, no. 4, pp. 2269–2308, Apr. 2013.
[114] M.-Z. Huang, S.-C. Cheng, Y.-T. Cho, and J. Shiea, "Ambient ionization mass spectrometry: a tutorial.," *Anal. Chim. Acta*, vol. 702, no. 1, pp. 1–15, Sep. 2011.
[115] F. M. Benoit, W. R. Davidson, A. M. Lovett, S. Nacson, and A. Ngo, "Breath analysis by API/MS—human exposure to volatile organic solvents," *Int. Arch. Occup. Environ. Health*, vol. 55, no. 2, pp. 113–120, 1985.
[116] F. M. Benoit, W. R. Davidson, A. M. Lovett, S. Nacson, and A. Ngo, "Breath analysis by atmospheric pressure ionization mass spectrometry," *Anal. Chem.*, vol. 55, no. 4, pp. 805–807, Apr. 1983.
[117] B. A. Thomson, W. R. Davidson, and A. M. Lovett, "Applications of a Versatile Technique for Trace Analysis: Atmospheric Pressure Negative Chemical Ionization," *Environ. Health Perspect.*, vol. 36, pp. 77–84, 1980.
[118] A. M. Lovett, N. M. Reid, J. A. Buckley, J. B. French, and D. M. Cameron, "Real-time analysis of breath using an atmospheric pressure ionization mass spectrometer," *Biomed. Mass Spectrom.*, vol. 6, no. 3, pp. 91–97, Aug. 2018.
[119] D. A. Lane and B. A. Thomson, "Monitoring a Chlorine Spill from a Train Derailment," *J. Air Pollut. Control Assoc.*, vol. 31, no. 2, pp. 122–127, Feb. 1981.
[120] S. Fuerstenau, "Aggregation and Fragmentation in an electrospray ion source," Yale University, New Haven (CT), 1994.
[121] Y. H. Chen, H. H. Hill, and D. P. Wittmer, "Analytical merit of electrospray ion mobility spectrometry as a chromatographic detector," *J. Microcolumn Sep.*, vol. 6, no. 5, pp. 515–524, Aug. 2018.
[122] C.-M. Hong, F.-C. Tsai, and J. Shiea, "A Multiple Channel Electrospray Source Used To Detect Highly Reactive Ketenes from a Flow Pyrolyzer," *Anal. Chem.*, vol. 72, no. 6, pp. 1175–1178, Mar. 2000.
[123] C. Y. Lee and J. Shiea, "Gas chromatography connected to multiple channel

electrospray ionization mass spectrometry for the detection of volatile organic compounds.," *Anal. Chem.*, vol. 70, no. 13, pp. 2757–2761, Jul. 1998.
[124] X. Li, L. Huang, H. Zhu, and Z. Zhou, "Direct human breath analysis by secondary nano-electrospray ionization ultrahigh-resolution mass spectrometry: Importance of high mass resolution and mass accuracy," *Rapid Commun. Mass Spectrom.*, vol. 31, no. 3, pp. 301–308, Nov. 2016.
[125] J.-C. Wolf, M. Schaer, P. Siegenthaler, and R. Zenobi, "Direct Quantification of Chemical Warfare Agents and Related Compounds at Low ppt Levels: Comparing Active Capillary Dielectric Barrier Discharge Plasma Ionization and Secondary Electrospray Ionization Mass Spectrometry," *Anal. Chem.*, vol. 87, no. 1, pp. 723–729, Jan. 2015.
[126] M. J. Aernecke, T. Mendum, G. Geurtsen, A. Ostrinskaya, and R. R. Kunz, "Vapor Pressure of Hexamethylene Triperoxide Diamine (HMTD) Estimated Using Secondary Electrospray Ionization Mass Spectrometry," *J. Phys. Chem. A*, vol. 119, no. 47, pp. 11514–11522, Nov. 2015.
[127] J. C. R. and M. A. J. and C. G.-H. and C. S. C. and S. S. and C. L. P. Thomas, "Analysis of human breath samples using a modified thermal desorption: gas chromatography electrospray ionization interface," *J. Breath Res.*, vol. 8, no. 3, p. 37105, 2014.
[128] L. Meier, C. Berchtold, S. Schmid, and R. Zenobi, "High mass resolution breath analysis using secondary electrospray ionization mass spectrometry assisted by an ion funnel," *J. Mass Spectrom.*, vol. 47, no. 12, pp. 1571–1575, Dec. 2012.
[129] N. Brenner, M. Haapala, K. Vuorensola, and R. Kostiainen, "Simple Coupling of Gas Chromatography to Electrospray Ionization Mass Spectrometry," *Anal. Chem.*, vol. 80, no. 21, pp. 8334–8339, Nov. 2008.
[130] A. J. Ingram, C. L. Boeser, and R. N. Zare, "Going beyond electrospray: mass spectrometric studies of chemical reactions in and on liquids," *Chem. Sci.*, vol. 7, no. 1, pp. 39–55, 2016.
[131] P. Martinez-Lozano Sinues, E. Criado, and G. Vidal, "Mechanistic study on the ionization of trace gases by an electrospray plume," *Int. J. Mass Spectrom.*, vol. 313, pp. 21–29, 2012.
[132] J. Fernandez de la Mora, "Ionization of vapor molecules by an electrospray cloud," *Int. J. Mass Spectrom.*, vol. 300, no. 2, pp. 182–193, 2011.
[133] D. F. Hunt, C. N. McEwen, and R. A. Upham, "Chemical ionization mass spectrometry II. Diferentiation of primary, secondary, and tertiary amines," *Tetrahedron Lett.*, vol. 12, no. 47, pp. 4539–4542, 1971.
[134] D. F. Hunt, C. N. McEwen, and R. A. Upham, "Determination of active hydrogen in organic compounds by chemical ionization mass spectrometry," *Anal. Chem.*, vol. 44, no. 7, pp. 1292–1294, Jun. 1972.
[135] W. Blum, E. Schlumpf, J. G. Liehr, and W. J. Richter, "On-line hydrogen/deuterium exchange in capillary gas chromatography - chemical ionization mass spectrometry (GC-CIMS) as a means of structure analysis in complex mixtures," *Tetrahedron Lett.*, vol. 17, no. 7, pp. 565–568, 1976.
[136] A. K. Meher and Y.-C. Chen, "Analysis of volatile compounds by open-air ionization mass spectrometry," *Anal. Chim. Acta*, vol. 966, pp. 41–46, 2017.
[137] B. O. Keller, J. Sui, A. B. Young, and R. M. Whittal, "Interferences and contaminants encountered in modern mass spectrometry," *Anal. Chim. Acta*, vol. 627, no. 1, pp. 71–81, 2008.
[138] X. Guo, A. P. Bruins, and T. R. Covey, "Characterization of typical chemical background interferences in atmospheric pressure ionization liquid

chromatography-mass spectrometry," *Rapid Commun. Mass Spectrom.*, vol. 20, no. 20, pp. 3145–3150, Sep. 2006.
[139] A. Schlosser and R. Volkmer-Engert, "Volatile polydimethylcyclosiloxanes in the ambient laboratory air identified as source of extreme background signals in nanoelectrospray mass spectrometry," *J. Mass Spectrom.*, vol. 38, no. 5, pp. 523–525, Mar. 2003.
[140] J. C. Reynolds *et al.*, "Detection of Volatile Organic Compounds in Breath Using Thermal Desorption Electrospray Ionization-Ion Mobility-Mass Spectrometry," *Anal. Chem.*, vol. 82, no. 5, pp. 2139–2144, Mar. 2010.
[141] K. M. Verge and G. R. Agnes, "Plasticizer contamination from vacuum system o-rings in a quadrupole ion trap mass spectrometer," *J. Am. Soc. Mass Spectrom.*, vol. 13, no. 8, pp. 901–905, 2002.
[142] M. H. Amad, N. B. Cech, G. S. Jackson, and C. G. Enke, "Importance of gas-phase proton affinities in determining the electrospray ionization response for analytes and solvents," *J. Mass Spectrom.*, vol. 35, no. 7, pp. 784–789, Jul. 2000.
[143] J. V Iribarne, P. J. Dziedzic, and B. A. Thomson, "Atmospheric pressure ion evaporation-mass spectrometry," *Int. J. Mass Spectrom. Ion Phys.*, vol. 50, no. 3, pp. 331–347, 1983.
[144] V. Znamenskiy, I. Marginean, and A. Vertes, "Solvated Ion Evaporation from Charged Water Nanodroplets," *J. Phys. Chem. A*, vol. 107, no. 38, pp. 7406–7412, Sep. 2003.
[145] J. Sunner, G. Nicol, and P. Kebarle, "Factors determining relative sensitivity of analytes in positive mode atmospheric pressure ionization mass spectrometry," *Anal. Chem.*, vol. 60, no. 13, pp. 1300–1307, Jul. 1988.
[146] J. Sunner, M. G. Ikonomou, and P. Kebarle, "Sensitivity enhancements obtained at high temperatures in atmospheric pressure ionization mass spectrometry," *Anal. Chem.*, vol. 60, no. 13, pp. 1308–1313, Jul. 1988.
[147] G. Nicol, J. Sunner, and P. Kebarle, "Kinetics and thermodynamics of protonation reactions: H3O+ (H2O)h + B = BH+ (H2O)b + (h − b + 1) H2O, where B is a nitrogen, oxygen or carbon base," *Int. J. Mass Spectrom. Ion Process.*, vol. 84, no. 1, pp. 135–155, 1988.
[148] P. Kebarle and U. H. Verkerk, "Electrospray: from ions in solution to ions in the gas phase, what we know now.," *Mass Spectrom. Rev.*, vol. 28, no. 6, pp. 898–917, 2009.
[149] W. S. Law *et al.*, "On the Mechanism of Extractive Electrospray Ionization," *Anal. Chem.*, vol. 82, no. 11, pp. 4494–4500, Jun. 2010.
[150] R. Wang *et al.*, "On the mechanism of extractive electrospray ionization (EESI) in the dual-spray configuration.," *Anal. Bioanal. Chem.*, vol. 402, no. 8, pp. 2633–2643, Mar. 2012.
[151] J. M. López-Herrera, A. Barrero, A. Boucard, I. G. Loscertales, and M. Márquez, "An experimental study of the electrospraying of water in air at atmospheric pressure," *J. Am. Soc. Mass Spectrom.*, vol. 15, no. 2, pp. 253–259, 2004.
[152] J. D. Beauchamp and J. D. Pleil, "Breath: An Often Overlooked Medium in Biomarker Discovery," *Biomarker Validation*. 27-Feb-2015.
[153] P. Španěl and D. Smith, "Chapter 4 - Recent SIFT-MS Studies of Volatile Compounds in Physiology, Medicine and Cell Biology," A. Amann and D. B. T.-V. B. Smith, Eds. Boston: Elsevier, 2013, pp. 48–76.
[154] R. S. Blake, P. S. Monks, and A. M. Ellis, "Proton-Transfer Reaction Mass Spectrometry," *Chem. Rev.*, vol. 109, no. 3, pp. 861–896, Mar. 2009.

[155] D. S. and P. Š. and J. H. and J. Beauchamp, “Mass spectrometry for real-time quantitative breath analysis,” *J. Breath Res.*, vol. 8, no. 2, p. 27101, 2014.
[156] P. Martínez-Lozano and J. F. de la Mora, “Electrospray ionization of volatiles in breath,” *Int. J. Mass Spectrom.*, vol. 265, no. 1, pp. 68–72, 2007.
[157] H. Chen, A. Wortmann, W. Zhang, and R. Zenobi, “Rapid In Vivo Fingerprinting of Nonvolatile Compounds in Breath by Extractive Electrospray Ionization Quadrupole Time-of-Flight Mass Spectrometry,” *Angew. Chemie Int. Ed.*, vol. 46, no. 4, pp. 580–583, Jan. 2007.
[158] G. R. Johnson and L. Morawska, “The Mechanism of Breath Aerosol Formation,” *J. Aerosol Med. Pulm. Drug Deliv.*, vol. 22, no. 3, pp. 229–237, May 2009.
[159] W. Miekisch, J. K. Schubert, and G. F. E. Noeldge-Schomburg, “Diagnostic potential of breath analysis—focus on volatile organic compounds,” *Clin. Chim. Acta*, vol. 347, no. 1, pp. 25–39, 2004.
[160] P. Martinez-Lozano Sinues, M. Kohler, S. A. Brown, R. Zenobi, and R. Dallmann, “Gauging circadian variation in ketamine metabolism by real-time breath analysis,” *Chem. Commun.*, vol. 53, no. 14, pp. 2264–2267, 2017.
[161] H. P. H. Arp *et al.*, “More of EPA’s SPARC Online Calculator−The Need for High-Quality Predictions of Chemical Properties,” *Environ. Sci. Technol.*, vol. 44, no. 12, pp. 4400–4401, Jun. 2010.
[162] D. García-Gómez, P. Martínez-Lozano Sinues, C. Barrios-Collado, G. Vidal-de-Miguel, M. Gaugg, and R. Zenobi, “Identification of 2-Alkenals, 4-Hydroxy-2-alkenals, and 4-Hydroxy-2,6-alkadienals in Exhaled Breath Condensate by UHPLC-HRMS and in Breath by Real-Time HRMS,” *Anal. Chem.*, vol. 87, no. 5, pp. 3087–3093, Mar. 2015.
[163] G. J. Patti, O. Yanes, and G. Siuzdak, “Metabolomics: the apogee of the omics trilogy,” *Nat. Rev. Mol. Cell Biol.*, vol. 13, 2012.
[164] K. Skogerson, G. Wohlgemuth, D. K. Barupal, and O. Fiehn, “The volatile compound BinBase mass spectral database.,” *BMC Bioinformatics*, vol. 12, p. 321, Aug. 2011.
[165] G. Bergström, M. Rothschild, I. Groth, and C. Crighton, “Oviposition by butterflies on young leaves: Investigation of leaf volatiles,” *Chemoecology*, vol. 5, 1994.
[166] M. C. Lemfack, J. Nickel, M. Dunkel, R. Preissner, and B. Piechulla, “mVOC: a database of microbial volatiles,” *Nucleic Acids Res*, vol. 42, 2014.
[167] “Indoor air quality: organic pollutants. Report on a WHO meeting.,” *EURO Rep. Stud.*, no. 111, pp. 1–70, 1989.
[168] J. Kesselmeier and M. Staudt, “Biogenic volatile organic compounds (VOC): An overview on emission, physiology and ecology,” *J. Atmos. Chem.*, vol. 33, 1999.
[169] B. E. Ebert, C. Halbfeld, and L. M. Blank, “Exploration and Exploitation of the Yeast Volatilome,” *Curr. Metabolomics*, vol. 4, 2016.
[170] A. Amann *et al.*, “The human volatilome: volatile organic compounds (VOCs) in exhaled breath, skin emanations, urine, feces and saliva.,” *J. Breath Res.*, vol. 8, no. 3, p. 34001, Sep. 2014.
[171] C. Bicchi and M. Maffei, “The plant volatilome: methods of analysis.,” *Methods Mol. Biol.*, vol. 918, pp. 289–310, 2012.
[172] A. E. Boukouris, S. D. Zervopoulos, and E. D. Michelakis, “Metabolic Enzymes Moonlighting in the Nucleus: Metabolic Regulation of Gene Transcription,” *Trends Biochem. Sci.*, vol. 41, 2016.
[173] S. D. Copley, “Enzymes with extra talents: moonlighting functions and catalytic

promiscuity," *Curr. Opin. Chem. Biol.*, vol. 7, 2003.
[174] W. Schwab, "14 - Role of metabolome diversity in fruit and vegetable quality: multifunctional enzymes and volatiles," in *Woodhead Publishing Series in Food Science, Technology and Nutrition*, B. Brückner and S. G. B. T.-F. and V. F. Wyllie, Eds. Woodhead Publishing, 2008, pp. 272–286.
[175] N. D. Mallette, W. B. Knighton, G. A. Strobel, R. P. Carlson, and B. M. Peyton, "Resolution of volatile fuel compound profiles from Ascocoryne sarcoides: a comparison by proton transfer reaction-mass spectrometry and solid phase microextraction gas chromatography-mass spectrometry," *AMB Express*, vol. 2, 2012.
[176] B. Calenic, "Oxidative stress and volatile organic compounds: interplay in pulmonary, cardio-vascular, digestive tract systems and cancer," *Open Chem*, vol. 13, 2015.
[177] D. Sun *et al.*, "Effects of Growth Parameters on the Analysis of Aspergillus flavus Volatile Metabolites," *Separations* , vol. 3, no. 2. 2016.
[178] M. Caldeira, "Profiling allergic asthma volatile metabolic patterns using a headspace-solid phase microextraction/gas chromatography based methodology," *J. Chromatogr.*, vol. 1218, 2011.
[179] K. Krogerus and B. R. Gibson, "Influence of valine and other amino acids on total diacetyl and 2,3-pentanedione levels during fermentation of brewer's wort," *Appl. Microbiol. Biotechnol.*, vol. 97, 2013.
[180] V. Capozzi, "PTR-MS Characterization of VOCs Associated with Commercial Aromatic Bakery Yeasts of Wine and Beer Origin," *Molecules*, vol. 21, 2016.
[181] G. Vas and K. Vékey, "Solid-phase microextraction: a powerful sample preparation tool prior to mass spectrometric analysis," *J. Mass Spectrom.*, vol. 39, 2004.
[182] C. L. Arthur and J. Pawliszyn, "Solid phase microextraction with thermal desorption using fused silica optical fibers," *Anal. Chem.*, vol. 62, 1990.
[183] M. D. Krebs, "Detection of biological and chemical agents using differential mobility spectrometry (DMS) technology," *IEEE Sens. J.*, vol. 5, 2005.
[184] G. R. Lambertus, "Silicon Microfabricated Column with Microfabricated Differential Mobility Spectrometer for GC Analysis of Volatile Organic Compounds," *Anal. Chem.*, vol. 77, 2005.
[185] W. Vautz and J. I. Baumbach, "Analysis of bio-processes using ion mobility spectrometry," *Eng. Life Sci.*, vol. 8, 2008.
[186] W. Vautz and J. I. Baumbach, "Exemplar application of multi-capillary column ion mobility spectrometry for biological and medical purpose," *Int. J. Ion Mobil. Spectrom.*, vol. 11, 2008.
[187] J. M. Scotter, V. S. Langford, P. F. Wilson, M. J. McEwan, and S. T. Chambers, "Real-time detection of common microbial volatile organic compounds from medically important fungi by Selected Ion Flow Tube-Mass Spectrometry (SIFT-MS)," *J. Microbiol. Methods*, vol. 63, 2005.
[188] H. Link, T. Fuhrer, L. Gerosa, N. Zamboni, and U. Sauer, "Real-time metabolome profiling of the metabolic switch between starvation and growth," *Nat. Methods*, vol. 12, 2015.
[189] C. Berchtold, L. Meier, R. Steinhoff, and R. Zenobi, "A new strategy based on real-time secondary electrospray ionization and high-resolution mass spectrometry to discriminate endogenous and exogenous compounds in exhaled breath," *Metabolomics*, vol. 10, 2013.
[190] L. Huang, X. Li, M. Xu, Z. Huang, and Z. Zhou, "Identification of Relatively High Molecular Weight Compounds in Human Breath Using Secondary Nano

Electrospray Ionization Ultrahigh Resolution Mass Spectrometry," *Gaodeng Xuexiao Huaxue Xuebao/Chemical J. Chinese Univ.*, vol. 38, 2017.
[191] J. B. Kiselev, P.; Fenn, "ESIMS Analysis of Vapors at Trace Levels," in *Proceedings of the 49th ASMS Conference on Mass Spectrometry and Allied Topics*, 2001.
[192] S. Saad, M. Peter, and R. Dechant, "In scarcity and abundance: metabolic signals regulating cell growth," *Physiol.*, vol. 28, 2013.
[193] Y. Joblin, "Detection of moulds by volatile organic compounds: Application to heritage conservation," *Int. Biodeterior. Biodegrad.*, vol. 64, 2010.
[194] G. A. Strobel, "Bioprospecting-fuels from fungi," *Biotechnol. Lett.*, vol. 37, 2015.
[195] A. Korpi, J. Jarnberg, and A.-L. Pasanen, "Microbial volatile organic compounds.," *Crit. Rev. Toxicol.*, vol. 39, no. 2, pp. 139–193, 2009.
[196] H. H. Jelen and J. Grabarkiewicz-Szczesna, "Volatile compounds of Aspergillus strains with different abilities to produce ochratoxin A," *J. Agric. Food Chem.*, vol. 53, 2005.
[197] T. A. Gianoulis *et al.*, "Genomic analysis of the hydrocarbon-producing, cellulolytic, endophytic fungus Ascocoryne sarcoides.," *PLoS Genet.*, vol. 8, no. 3, p. e1002558, 2012.
[198] S. Makhoul, "Proton-transfer-reaction mass spectrometry for the study of the production of volatile compounds by bakery yeast starters," *J. Mass Spectrom.*, vol. 49, 2014.
[199] S. M. G. Saerens, F. R. Delvaux, K. J. Verstrepen, and J. M. Thevelein, "Production and biological function of volatile esters in Saccharomyces cerevisiae," *Microb Biotechnol*, vol. 3, 2010.
[200] K. Nordstrom, "Formation of Esters from Acids by Brewer's Yeast: Formation from Unsaturated Acids," *Nature*, vol. 210, 1966.
[201] P. Molimard and H. E. Spinnler, "Review: Compounds involved in the flavor of surface mold-ripened cheeses: Origins and properties," *J. Dairy Sci.*, vol. 79, 1996.
[202] L. M. Blank, L. Kuepfer, and U. Sauer, "Large-scale 13C-flux analysis reveals mechanistic principles of metabolic network robustness to null mutations in yeast.," *Genome Biol.*, vol. 6, no. 6, p. R49, 2005.
[203] A. Arvanitidis and J. J. Heinisch, "Studies on the function of yeast phosphofructokinase subunits by in vitro mutagenesis," *J. Biol. Chem.*, vol. 269, 1994.
[204] A. Klinder, J. Kirchberger, A. Edelmann, and G. Kopperschlager, "Assembly of phosphofructokinase-1 from Saccharomyces cerevisiae in extracts of single-deletion mutants," *Yeast*, vol. 14, 1998.
[205] S. M. G. Saerens, "Parameters affecting ethyl ester production by Saccharomyces cerevisiae during fermentation," *Appl. Environ. Microbiol.*, vol. 74, 2008.
[206] M. Ramirez-Gaona, "YMDB 2.0: a significantly expanded version of the yeast metabolome database," *Nucleic Acids Res.*, vol. 45, 2017.
[207] L. M. Blank and U. Sauer, "TCA cycle activity in Saccharomyces cerevisiae is a function of the environmentally determined specific growth and glucose uptake rates," *Microbiol.-Sgm*, vol. 150, 2004.
[208] C. A. Schneider, W. S. Rasband, and K. W. Eliceiri, "NIH Image to ImageJ: 25 years of image analysis," *Nat. Methods*, vol. 9, 2012.
[209] D. Kessner, M. Chambers, R. Burke, D. Agus, and P. Mallick, "ProteoWizard: Open source software for rapid proteomics tools development," *Bioinformatics*, vol. 24, 2008.

[210] T. Kind and O. Fiehn, “Seven Golden Rules for heuristic filtering of molecular formulas obtained by accurate mass spectrometry.,” *BMC Bioinformatics*, vol. 8, p. 105, Mar. 2007.
[211] L. Berg, J. M.; Tymoczko, J. L.; Stryer, *Biochemistry 5th ed.*, 5th editio. New York, 2002.
[212] S. Cardaci and M. R. Ciriolo, “TCA Cycle Defects and Cancer When Metabolism Tunes Redox State,” in *International journal of cell biology*, 2012.
[213] M. Carbonneau *et al.*, “The oncometabolite 2-hydroxyglutarate activates the mTOR signalling pathway,” *Nat. Commun.*, vol. 7, p. 12700, Sep. 2016.
[214] J. A. Menendez, T. Alarcon, and J. Joven, “Gerometabolites: the pseudohypoxic aging side of cancer oncometabolites.,” *Cell Cycle*, vol. 13, no. 5, pp. 699–709, 2014.
[215] F. A. Gallagher *et al.*, “Production of hyperpolarized [1,4-13C2]malate from [1,4-13C2]fumarate is a marker of cell necrosis and treatment response in tumors.,” *Proc. Natl. Acad. Sci. U. S. A.*, vol. 106, no. 47, pp. 19801–19806, Nov. 2009.
[216] L. Abela *et al.*, “Plasma metabolomics reveals a diagnostic metabolic fingerprint for mitochondrial aconitase (ACO2) deficiency,” *PLoS One*, vol. 12, no. 5, p. e0176363, May 2017.
[217] R. Gao *et al.*, “Serum Metabolomics to Identify the Liver Disease-Specific Biomarkers for the Progression of Hepatitis to Hepatocellular Carcinoma.,” *Sci. Rep.*, vol. 5, p. 18175, Dec. 2015.
[218] Z.-G. Gong *et al.*, “Metabolomics and eicosanoid analysis identified serum biomarkers for distinguishing hepatocellular carcinoma from hepatitis B virus-related cirrhosis.,” *Oncotarget*, vol. 8, no. 38, pp. 63890–63900, Sep. 2017.
[219] N. Yoshimi *et al.*, “Blood metabolomics analysis identifies abnormalities in the citric acid cycle, urea cycle, and amino acid metabolism in bipolar disorder.,” *BBA Clin.*, vol. 5, pp. 151–158, Jun. 2016.
[220] D. S. Wishart *et al.*, “HMDB: the Human Metabolome Database.,” *Nucleic Acids Res.*, vol. 35, no. Database issue, pp. D521-6, Jan. 2007.
[221] D. S. Wishart *et al.*, “HMDB 3.0--The Human Metabolome Database in 2013.,” *Nucleic Acids Res.*, vol. 41, no. Database issue, pp. D801-7, Jan. 2013.
[222] A. Hansel, A. Jordan, R. Holzinger, P. Prazeller, W. Vogel, and W. Lindinger, “Proton transfer reaction mass spectrometry: on-line trace gas analysis at the ppb level,” *Int. J. Mass Spectrom. Ion Process.*, vol. 149–150, pp. 609–619, 1995.
[223] W. Lindinger, A. Hansel, and A. Jordan, “On-line monitoring of volatile organic compounds at pptv levels by means of proton-transfer-reaction mass spectrometry (PTR-MS) medical applications, food control and environmental research,” *Int. J. Mass Spectrom. Ion Process.*, vol. 173, no. 3, pp. 191–241, 1998.
[224] D. Smith and P. Spanel, “The Novel Selected-ion Flow Tube Approach to Trace Gas Analysis of Air and Breath,” *Rapid Commun. Mass Spectrom.*, vol. 10, no. 10, pp. 1183–1198, Aug. 1996.
[225] P. Spanel and D. Smith, “On the features, successes and challenges of selected ion flow tube mass spectrometry.,” *Eur. J. Mass Spectrom. (Chichester, Eng).*, vol. 19, no. 4, pp. 225–246, 2013.
[226] K. Dryahina, D. Smith, and P. Spanel, “Quantification of methane in humid air and exhaled breath using selected ion flow tube mass spectrometry.,” *Rapid Commun. Mass Spectrom.*, vol. 24, no. 9, pp. 1296–1304, May 2010.
[227] P. Spanel and D. Smith, “Selected ion flow tube mass spectrometry for on-line

trace gas analysis in biology and medicine.," *Eur. J. Mass Spectrom. (Chichester, Eng).*, vol. 13, no. 1, pp. 77–82, 2007.
[228] H. D. Bean, J. Zhu, and J. E. Hill, "Characterizing Bacterial Volatiles using Secondary Electrospray Ionization Mass Spectrometry (SESI-MS)," in *Journal of visualized experiments : JoVE*, 2011.
[229] C. Cruickshank-Quinn, M. Armstrong, R. Powell, J. Gomez, M. Elie, and N. Reisdorph, "Determining the presence of asthma-related molecules and salivary contamination in exhaled breath condensate," *Respir. Res.*, vol. 18, no. 1, p. 57, 2017.
[230] A. T. Rioseras, M. T. Gaugg, and P. Martinez-Lozano Sinues, "Secondary electrospray ionization proceeds via gas-phase chemical ionization," *Anal. Methods*, vol. 9, no. 34, pp. 5052–5057, 2017.
[231] P. Sukul *et al.*, "FEV manoeuvre induced changes in breath VOC compositions: an unconventional view on lung function tests.," *Sci. Rep.*, vol. 6, p. 28029, Jun. 2016.
[232] T. Lomonaco *et al.*, "A breath sampling system assessing the influence of respiratory rate on exhaled breath composition.," *Conf. Proc. ... Annu. Int. Conf. IEEE Eng. Med. Biol. Soc. IEEE Eng. Med. Biol. Soc. Annu. Conf.*, vol. 2015, pp. 7618–7621, 2015.
[233] R. G. Carroll, "Pulmonary System," in *Elsevier's Integrated Physiology*, 1st ed., Philadelphia: Elsevier, 2007, pp. 99–115.
[234] M. T. Gaugg *et al.*, "Mass-Spectrometric Detection of Omega-Oxidation Products of Aliphatic Fatty Acids in Exhaled Breath.," *Anal. Chem.*, vol. 89, no. 19, pp. 10329–10334, Oct. 2017.
[235] M. A. Fernandez-Peralbo, M. Calderon Santiago, F. Priego-Capote, and M. D. Luque de Castro, "Study of exhaled breath condensate sample preparation for metabolomics analysis by LC-MS/MS in high resolution mode.," *Talanta*, vol. 144, pp. 1360–1369, Nov. 2015.
[236] M. C. Chambers *et al.*, "A cross-platform toolkit for mass spectrometry and proteomics.," *Nature biotechnology*, vol. 30, no. 10. United States, pp. 918–920, Oct-2012.
[237] P. Martinez-Lozano Sinues, M. Kohler, and R. Zenobi, "Human Breath Analysis May Support the Existence of Individual Metabolic Phenotypes," *PLoS One*, vol. 8, no. 4, p. e59909, Apr. 2013.
[238] K. Dryahina, D. Smith, M. Bortlik, N. Machkova, M. Lukas, and P. Spanel, "Pentane and other volatile organic compounds, including carboxylic acids, in the exhaled breath of patients with Crohn's disease and ulcerative colitis.," *J. Breath Res.*, vol. 12, no. 1, p. 16002, Nov. 2017.
[239] D. Smith, K. Sovova, K. Dryahina, T. Dousova, P. Drevinek, and P. Spanel, "Breath concentration of acetic acid vapour is elevated in patients with cystic fibrosis.," *J. Breath Res.*, vol. 10, no. 2, p. 21002, May 2016.
[240] K. Dryahina *et al.*, "Quantification of pentane in exhaled breath, a potential biomarker of bowel disease, using selected ion flow tube mass spectrometry.," *Rapid Commun. Mass Spectrom.*, vol. 27, no. 17, pp. 1983–1992, Sep. 2013.
[241] J. H. and M. M. and S. S. and T. T. and M. G. and A. Hansel, "On-line breath analysis with PTR-TOF," *J. Breath Res.*, vol. 3, no. 2, p. 27004, 2009.
[242] H. E. Buist, L. de Wit-Bos, T. Bouwman, and W. H. J. Vaes, "Predicting blood:air partition coefficients using basic physicochemical properties," *Regul. Toxicol. Pharmacol.*, vol. 62, no. 1, pp. 23–28, 2012.
[243] D. Zamora, M. Amo-Gonzalez, M. Lanza, G. Fernandez de la Mora, and J. Fernandez de la Mora, "Reaching a Vapor Sensitivity of 0.01 Parts Per

Quadrillion in the Screening of Large Volume Freight.," *Anal. Chem.*, vol. 90, no. 4, pp. 2468–2474, Feb. 2018.

[244] R. Dallmann, A. U. Viola, L. Tarokh, C. Cajochen, and S. A. Brown, "The human circadian metabolome.," *Proc. Natl. Acad. Sci. U. S. A.*, vol. 109, no. 7, pp. 2625–2629, Feb. 2012.

[245] K. D. Singh *et al.*, "Translating secondary electrospray ionization-high-resolution mass spectrometry to the clinical environment," *J. Breath Res.*, vol. 12, no. 2, 2018.

[246] D. Sachse, A. L. Solevåg, J. P. Berg, and B. Nakstad, "The Role of Plasma and Urine Metabolomics in Identifying New Biomarkers in Severe Newborn Asphyxia: A Study of Asphyxiated Newborn Pigs following Cardiopulmonary Resuscitation," *PLoS One*, vol. 11, no. 8, p. e0161123, Aug. 2016.

[247] X. Jian, N. Li, C. Zhang, and Q. Hua, "In silico profiling of cell growth and succinate production in Escherichia coli NZN111.," *Bioresour. Bioprocess.*, vol. 3, no. 1, p. 48, 2016.

[248] P. M.-L. Sinues, M. Kohler, and R. Zenobi, "Monitoring Diurnal Changes in Exhaled Human Breath," *Anal. Chem.*, vol. 85, no. 1, pp. 369–373, Jan. 2013.

[249] D. Smith and P. Spanel, "Pitfalls in the analysis of volatile breath biomarkers: suggested solutions and SIFT-MS quantification of single metabolites.," *J. Breath Res.*, vol. 9, no. 2, p. 22001, Apr. 2015.

[250] C. Hansch, A. Leo, and D. Hoekman, "Exploring QSAR: Hydrophobic, electronic, and steric constants," *ACS Professional Reference Book*, vol. 2. American Chemical Society, Washington, DC.

[251] C. L. Yaws, "Handbook of Vapor Pressure C1-C4 Compounds," in *In Handbook of Vapor Pressure*, Gulf Publishing, 1994, p. Vol 1. p 347.

[252] G. F. Hoffmann, W. Meier-Augenstein, S. Stockler, R. Surtees, D. Rating, and W. L. Nyhan, "Physiology and pathophysiology of organic acids in cerebrospinal fluid.," *J. Inherit. Metab. Dis.*, vol. 16, no. 4, pp. 648–669, 1993.

[253] M. J. Magera, J. K. Helgeson, D. Matern, and P. Rinaldo, "Methylmalonic acid measured in plasma and urine by stable-isotope dilution and electrospray tandem mass spectrometry.," *Clin. Chem.*, vol. 46, no. 11, pp. 1804–1810, Nov. 2000.